Electronic Supplementary Information (ESI) to accompany:

In Silico Screening of Metal-Organic Frameworks in Separation Applications

Rajamani Krishna* and Jasper M. van Baten

Van ‘t Hoff Institute for Molecular Sciences, University of Amsterdam, Science Park 904,

1098 XH Amsterdam, The Netherlands

Tel +31 20 6270990; Fax: + 31 20 5255604;

email: r.krishna@uva.nl

Structures investigated, molecular simulation techniques employed, and simulation data

1. Zeolite Structures

1.1. All-silica zeolites

Tables 1 and 2 gives salient information on the variety of all-silica zeolite structures discussed in the article. The crystallographic data are available on the zeolite atlas website of the International Zeolite Association (IZA) [1]. The unit cell dimensions, and pore volumes are summarized in Tables 3 and 4.

CH_4 molecules are described with a united atom model, in which each molecule is treated as a single interaction center [2].The interaction between adsorbed molecules is described with Lennard-Jones terms. The Lennard-Jones parameters for CH_4-zeolite interactions are taken from Dubbeldam et al.[3]. The force field for H_2 corresponds to that given by Kumar et al.[4] In implementing this force field, quantum effects for H_2 have been ignored because the work of Kumar et al.[4] has shown that quantum effects are of negligible importance for temperatures above 200 K; all our simulations were performed at 300 K. The Lennard-Jones parameters for CO_2-zeolite and N_2-zeolite are essentially those of Makrodimitris et al.[5]; see also García-Pérez et al.[6]. For simulations with linear alkanes with two or more C atoms, the beads in the chain are connected by harmonic bonding potentials. A harmonic cosine bending potential models the bond bending between three neighboring beads, a Ryckaert-Bellemans potential controls the torsion angle. The force fields of Dubbeldam et al.[3] was used for the variety of potentials. The Lennard-Jones potentials are shifted and cut at 12 Å. The zeolite frameworks were considered to be rigid in all the simulation results reported in the article.

The pore volumes were determined using the helium insertion technique of Talu and Myers [7]. Table 8 gives the force field for interaction of He with the O atoms in the zeolite structure required in these simulations.

1.2. Additional zeolite structures

Besides all-silica zeolites that are discussed in the manuscript of our Perspective, we also carried out CBMC simulations to determine the adsorption selectivities of three different mixtures in the following seven zeolites using information in the IZA atlas: AFT, BIK, EPI, JBW, LEV, LOV and SIV. These are named "Additional all-silica zeolites". The CBMC mixture simulation data are presented right at the end of the accompanying Figures along with the selectivity values. The unit cell dimensions of these structures of these Additional all-silica zeolites are summarized in Table 5. Some of these structures such as JBW and BIK do yield extremely high selectivities, in the 100-1000 range. However, a closer examination of the pore topologies reveals that the channel dimensions are extremely constrained and the selectivities are most likely to be due to exclusion on basis of size. To verify this further we determined the effective pore diameters following the method of Delaunay triangulation, described in the work by Foster et al.[8] The values are listed in Table 5. We note that the effective pore diameters range from 3.3 Å to 3.7 Å. We consider the channel sizes to be too small to be of any technological use in practice. Diffusional limitations will be so severe as to preclude them.

This will serve as an illustration that CBMC simulations alone cannot give guidelines as the efficacy of any zeolite or MOF; it has to have a reasonable degree of mobility. A further point to note is that all the 7 additional zeolites have low working capacities. The low working capacities are due to low pore volumes and surface areas. Table 24 presents the pore volume and surface area data for these additional zeolites. We note that JBW and BIK have surface areas of 25 and 1.4 m^2/g, several orders of magnitude below those of MOFs.

1.3. Zeolite structures with cations present

Simulations were performed to determine the adsorption selectivity for CO_2/CH_4 mixtures in cation exchanged zeolites. The following structures were investigated

NaX (106 Si, 86 Al, 86 Na^+, Si/Al=1.23),

NaY (138 Si, 54 Al, 54 Na^+, Si/Al=2.55),

The structural details, including pore volume data are given in Tables 6, and 7. We note that the presence of cations reduces the accessible pore volume.

The force field information for the simulations with cations are taken from García-Sanchez et al.[9]. In the MC simulations, the cations were allowed to move within the framework and both Lennard-Jones and Coulombic interactions are taken into consideration.

For determination of the pore volumes, the Lennard-Jones parameters for interactions of the He probe atoms with Na^+ are specified in Table 8. The cations were maintained in their preferred locations.

2. MOFs and ZIFs

The structural information for the metal organic frameworks (MOFs) and ZIFs (zeolitic imidazolate frameworks) have been taken from various publications.

For IRMOF-1 (= MOF 5 = $Zn_4O(BDC)_3$ with BDC^{2-} = 1-4 benzenedicarboxylate), we used the structural data published by Dubbeldam et al. [10, 11].

The structural information for CuBTC (= $Cu_3(BTC)_2$ with BTC = 1,3,5-benzenetricarboxylate) have been taken from Chui et al. [12] and Yang and Zhong [13]. The crystal structure of Chui et al. [12] includes axial oxygen atoms weakly bonded to the Cu atoms, which correspond to water ligands. Our simulations have been performed on the dry CuBTC with these oxygen atoms removed.

The structural information for Zn(bdc)dabco is from Bárcia et al.[14] and Lee et al. [15].

MIL-47 structural data was taken from Alaerts et al. [16], Finsy et al. [17], and Barthelet et al. [18].

The structural data for MIL-53 (Cr) = $Cr(OH)(O_2C\text{-}C_6H_4\text{-}CO_2)$ was taken from Coombes et al [19] (the simulations were carried out with the large-pore (-lp) structure).

The ZIF-8 = Zn(methylimidazole)$_2$ structure was constructed on the basis of the structural data from Banerjee et al.[20]. The original structural data files (cif file) contain solvent molecules; these were removed and the solvent-free structures were simulated.

The structural information on MgMOF-74 (= Mg_2(dobdc) = Mg\(dobdc) with dobdc = (dobdc^{4-} = 1,4-dioxido-2,5-benzenedicarboxylate)), ZnMOF-74 (= Zn_2(dobdc) = Zn\(dobdc)), CoMOF-74 = (Co_2(dobdc) = Co\(dobdc)), NiMOF-74 = (Ni_2(dobdc) = Ni\(dobdc)), were obtained from a variety of references [21-26].

The structural information for Na-rhoZMOF is provided by Babarao and Jiang [27].

The structural information for MOF-177 (= $Zn_4O(BTB)_2$ with (BTB^{3-} = 1,3,5-benzenetribenzoate)) is provided by Chae et al.[28].

The structural information for Co(BDP) with (BDP^{2-} = 1,4-benzenedipyrazolate) is from Choi et al. [29] and Salles et al. [30].

The structural information for BeBTB = $Be_{12}(OH)_{12}(BTB)_4$ with (BTB^{3-} = 1,3,5-benzenetribenzoate) is from Sumida et al. [31].

The structural information for CuBTT is from Demessence et al. [32]

The salient information on MOF and ZIF structures are summarized in Table 9.

Table 10 gives information on the unit cell dimensions, and pore volumes.

The metal organic framework structures were considered to be rigid in the simulations. For the atoms in the host metal organic framework, the generic UFF [33] and DREIDING [34] force fields were used. The Lennard-Jones parameters for MOF and ZIF atoms are summarized in Tables 11, 12, 13, 14, 15, 16, 17, 18, 19, 20, 21, and 22. The Lorentz-Berthelot mixing rules were applied for calculating σ and ε/k_B for guest-host interactions.

For CO_2 and N_2 adsorption in MOFs, the charges of the host framework need to be accounted for.

Our force field implementation for CO_2 in CuBTC correspond to those of Martín-Calvo et al.[35]

Our force field implementation for CO_2 in IRMOF-1 correspond to those of Walton et al.[36] and Dubbeldam et al.[11].

For MIL-47 (V) and MIL-53 (Cr) –lp simulations, the same CO_2-CO_2 interaction parameters were used as for zeolites and correspond to those of García-Pérez et al.[6]. The charges on the host framework were taken from the works of Rosenbach et al.[37], and Salles et al.[38].

For ZIF-8, the Lennard-Jones potentials for the framework atoms of ZIF-8 were taken from the combined works of Mayo et al.[34], Yang and Zhong [39], and Jorgensen et al.[40] as was reported in the computational study of Zhou et al.[41] The framework charges of ZIF-8 were estimated using the group-contribution procedure based on quantum mechanical calculations described in the paper by Xu and Zhong [42]. See Table 15.

The simulations for Na-rhoZMOF were carried out with the force field information provided by Babarao and Jiang [27]. See Table 16.

The simulations for ZnMOF-74 and MgMOF-74 were carried out with the force field information provided by Yazaydin et al.[26]. See Tables 17 and 18.

The force field information for MOF-177 is summarized in Table 19.

The force field information for BeBTB, Co(BDP) and CuBTT are presented in Tables 20, 21, and 22. For these structures only CH_4/H_2 mixtures simulations were carried out. Consequently, the information on the charges of the framework atoms is not required.

For Zn(bdc)dabco only hexane isomers separations were investigated. For this purpose the force field information used is that provided in our earlier paper [43].

3. Graphite (Carbon) slits

In order to highlight the principle of separation of alkane isomers, we also carried out simulations with graphite slits of four different widths: 0.74 nm, 0.94 nm, 1.14 nm, and 1.34 nm. These widths are obtained by correcting the centre-to-centre distance of C atoms on the surface for the Lennard-Jones sigma parameter. The force field for the graphite layers are essentially the same as described in the work of Severson and Snurr.[44]

4. Determination of pore volume

The pore volume is determined using a simulation of a single helium molecule at the reference temperature T [45-47]

$$V_p = \frac{1}{m}\int_0^{V_{pore}} \exp\left(-\frac{U(\mathbf{r})}{k_B T}\right) d\mathbf{r} \qquad (1)$$

where U is the interaction energy between a single helium atom and the framework, and m is the mass of the framework. The pore volume can be readily computed from Monte Carlo sampling using Widom particle insertion [48]. Basically, the average Boltzmann factor associated with the random insertion of a probe molecule is computed. This value is averaged over all generated trial positions. In equation (1) the integration is over the entire volume of the sample and yields the value of the accessible pore volume per unit mass of the framework; the units of V_p are m^3/kg, or in more commonly used units mL/(g framework). The volume fraction, ϕ, is then given by V_p/V_{total} where V_{total} is the total volume of the unit cell. Usually, a reference temperature of 298.15 K is chosen for the experimental determination of the helium void volume; this value is also used in the simulations.

The force field for He-He interactions are taken from Table 1 of Talu and Myers [7]; these are listed also in Table 8. For zeolites the He-O interaction parameters were also taken from their Table 1. For determination of the pore volume fraction we have switched to the Talu and Myers force field parameters that has been tuned to represent experimental data on pore volumes in MFI.

For MOFs, the interaction between He and the atoms of the MOF structures were then determined using the Lorentz-Berthelot mixing rules.

For determination of the accessible pore volumes of FAU, NaX, NaY, TSC, ITQ-29, and LTA the sodalite cages were blocked and no He probe atoms could enter these cages. Only the supercage volumes are determined for these structures. For DDR, NaRhoZMOF, CHA, AWW, CuBTT, the appropriate blocking strategy was used for the inaccessible pockets.

The pore volume data are included in Table 4 (all-silca zeolites), Tables 7 (zeolites with cations), and Table 10 (MOFs and ZIFs).

5. Determination of pore surface area

The surface area of various structures were determined using the method described by Düren et al.[49]. The information is summarized in Table 23.

6. Heat of adsorption

We determined the isosteric heats of adsorption, ΔH_{st}, from CBMC simulations using the fluctuation formula

$$\Delta H_{st} = RT - \frac{< U_i n_i > - < U_i >< n_i >}{\langle n_i^2 \rangle - \langle n_i \rangle^2} \qquad (2)$$

where n_{i} represents the number of molecules in the simulation box and $\langle \ldots \rangle$ denotes ensemble averaging. In this connection the reader is referred to the paper of Karavias and Myers [50], who point out that the conventional definition of the isosteric heat of *adsorption* is in reality the heat of *desorption*.

7. Characteristic diameter using Delaunay triangulation

In many cases, the characteristic size of the channels or windows of microporous structures were determined following the method of Delaunay triangulation, described in the work by Foster et al.[8] These values represent the maximum hard-sphere diameter that can pass through the structure. The values quoted are obtained by substracting the Lennard-Jones sigma parameter of the framework atom.

8. MD simulation methodology

Diffusion is simulated using Newton's equations of motion until the system properties, on average, no longer change in time. The Verlet algorithm is used for time integration. A time step of 1 fs was used in all simulations. For each simulation, *initializing* CBMC moves are used to place the molecules in the domain, minimizing the energy. Next, follows an *equilibration* stage. These are essentially the same as the production cycles, only the statistics are not yet taken into account. This removes any initial large disturbances in the system that do not affect statistics on molecular displacements. After a fixed number of initialization and equilibrium steps, the MD simulation *production* cycles start. For every cycle, the statistics for determining the mean square displacements (MSDs) are updated. The MSDs are determined for time intervals ranging from 2 fs to 1 ns. In order to do this, an order-*N* algorithm, as detailed in Chapter 4 of Frenkel and Smit[48] is implemented. The Nosé-Hoover thermostat is applied to all the diffusing particles.

The DLPOLY code[51] was used along with the force field implementation as described in the previous section. DL_POLY is a molecular dynamics simulation package written by W. Smith, T.R. Forester and I.T. Todorov and has been obtained from CCLRCs Daresbury Laboratory via the website.[51]

The MD simulations were carried out for a variety of loadings within the various structures. All simulations were carried out on the LISA clusters of PCs equipped with Intel Xeon processors running at 3.4 GHz on the Linux operating system[52]. Each MD simulation, for a specified loading, was run for 120 h, determined to be long enough to obtain reliable statistics for determination of the diffusivities. In several cases the campaigns were replicated and the results averaged.

The self-diffusivities $D_{\mathrm{i,self}}$ for each species in binary mixtures are computed from MD simulations by analyzing the mean square displacement of each species *i* for each coordinate direction

$$D_{i,self} = \frac{1}{2n_i} \lim_{\Delta t \to \infty} \frac{1}{\Delta t} \left\langle \left(\sum_{l=1}^{n_i} \left(\mathbf{r}_{l,i}(t+\Delta t) - \mathbf{r}_{l,i}(t) \right)^2 \right) \right\rangle \tag{3}$$

For three-dimensional pore networks (MFI, BOG, FAU, NaX, NaY, BEA, LTA, TSC, ERI, LTA-5A, LTA-4A, CHA, ISV, IRMOF-1, CuBTC, ZIF-8, MOF-177, BeBTB, CuBTT) the arithmetic average of the diffusivities in the three coordinate directions were used in further analysis and reported in the Figures accompanying this Supplementary material. For one-dimensional pore structures (AFI, MTW, TON, LTL, MIL-47, MIL-53(Cr), MgMOF-74, ZnMOF-74, NiMOF-74, CoMOF-74, Co(BDP)) the diffusivities along the direction of diffusion are reported and analyzed. For DDR the reported diffusivities are the averages in x- and y- directions.

9. Determination of diffusion selectivities and permeabilities for membrane permeation

The Maxwell-Stefan (M-S) equations for binary mixture diffusion across a microporous membrane layer can be written as

$$-\phi \frac{c_i}{RT}\nabla \mu_i = \sum_{\substack{j=1 \\ j \neq i}}^{2} \frac{x_j N_i - x_i N_j}{Đ_{ij}} + \frac{N_i}{Đ_i}; \quad i = 1,2 \tag{4}$$

In equation (4) the $Đ_i$ are the M-S diffusivities of species 1 and 2, respectively, portraying the interaction between component *i* in the mixture with the surface, or wall of the structure. The fluxes N_i defined in equation (4) are expressed in terms of the number of moles of species *i* transported per m^2 of *membrane cross sectional area* per second. The $Đ_{ij}$ are M-S exchange coefficients representing interaction between component *i* with component j. The c_i are the loadings, defined in terms of moles per m^3 of *accessible* pore volume, within the pore and x_i represent the component mole fractions

$$x_i = c_i / (c_1 + c_2 + ...c_n); \quad i = 1, n \tag{5}$$

ϕ represents the fractional pore volume of the microporous crystalline material. It is to be noted that the ϕ appears in the M-S equations because the c_i are defined in terms of pore volume and not the total volume of the crystals. The Onsager reciprocal relations require

$$Đ_{ij} = Đ_{ji} \tag{6}$$

For binary mixtures we can define a square 2×2 matrix [*B*]

$$-\phi \frac{c_i}{RT}\nabla \mu_i = \sum_{j=1}^{2} B_{ij} N_j; \quad i = 1,2 \tag{7}$$

The four elements of the matrix [*B*] are given explicitly by

$$B_{11} = \frac{1}{Đ_1} + \frac{x_2}{Đ_{12}} \tag{8}$$

$$B_{22} = \frac{1}{Đ_2} + \frac{x_1}{Đ_{12}} \tag{9}$$

$$B_{12} = -\frac{x_1}{Đ_{12}} \tag{10}$$

$$B_{21} = -\frac{x_2}{Đ_{12}} \tag{11}$$

Furthermore, we define a matrix [Δ] as the inverse of [B]

$$[\Delta] \equiv [B]^{-1} = \begin{bmatrix} \frac{1}{Đ_1} + \frac{x_2}{Đ_{12}} & -\frac{x_1}{Đ_{12}} \\ -\frac{x_2}{Đ_{12}} & \frac{1}{Đ_2} + \frac{x_1}{Đ_{12}} \end{bmatrix}^{-1} \tag{12}$$

The inversion can be carried out explicitly to give the following expressions

$$\Delta_{11} = \frac{Đ_1 \left(1 + \frac{x_1 Đ_2}{Đ_{12}} \right)}{1 + \frac{x_1 Đ_2 + x_2 Đ_1}{Đ_{12}}} \tag{13}$$

$$\Delta_{22} = \frac{Đ_2 \left(1 + \frac{x_2 Đ_1}{Đ_{12}} \right)}{1 + \frac{x_2 Đ_1 + x_1 Đ_2}{Đ_{12}}} \tag{14}$$

$$\Delta_{12} = \frac{Đ_1 \frac{x_1 Đ_2}{Đ_{12}}}{1 + \frac{x_1 Đ_2 + x_2 Đ_1}{Đ_{12}}} \tag{15}$$

$$\Delta_{21} = \frac{x_2}{x_1} \Delta_{12} = \frac{Đ_2 \frac{x_2 Đ_1}{Đ_{12}}}{1 + \frac{x_1 Đ_2 + x_2 Đ_1}{Đ_{12}}} \tag{16}$$

The elements Δ_{ij} can be determined from MD simulations in each of the three coordinate directions using the formula

$$\Delta_{ij} = \frac{1}{2}\lim_{\Delta t\to\infty}\frac{1}{n_j}\frac{1}{\Delta t}\left\langle\left(\sum_{l=1}^{n_i}\left(\mathbf{r}_{l,i}(t+\Delta t)-\mathbf{r}_{l,i}(t)\right)\right)\bullet\left(\sum_{k=1}^{n_j}\left(\mathbf{r}_{k,j}(t+\Delta t)-\mathbf{r}_{k,j}(t)\right)\right)\right\rangle \tag{17}$$

In this expression n_i and n_j represent the number of molecules of species *i* and *j* respectively, and $\mathbf{r}_{l,i}(t)$ is the position of molecule *l* of species *i* at any time *t*. For unary systems eq (17) yields the M-S diffusivity $Đ_i$.

The Onsager reciprocal relations (6) translate to

$$\Delta_{ij}c_j = \Delta_{ji}c_i \tag{18}$$

For *n*-component mixtures the following expression for self-diffusivities $D_{i,self}$ can be derived following earlier work [53, 54]

$$\frac{1}{D_{i,self}} = \frac{1}{Đ_i} + \sum_{j=1}^{n}\frac{x_j}{Đ_{ij}} = \frac{1}{Đ_i} + \frac{x_i}{Đ_{ii}} + \sum_{\substack{j=1\\ j\neq i}}^{n}\frac{x_j}{Đ_{ij}}; \quad i = 1,2,...n \tag{19}$$

For the special case of a binary mixture we get

$$\frac{1}{D_{1,self}} = \frac{1}{Đ_1} + \frac{x_1}{Đ_{11}} + \frac{x_2}{Đ_{12}} \tag{20}$$

$$\frac{1}{D_{2,self}} = \frac{1}{Đ_2} + \frac{x_2}{Đ_{22}} + \frac{x_1}{Đ_{12}} \tag{21}$$

Let ℓ be the thickness of the crystalline layer on the membrane. If the downstream compartments of the membrane are evacuated we may approximate the concentration differences as follows

$$\begin{aligned}\frac{\Delta c_1}{\ell} &\approx \frac{c_1}{\ell}\\ \frac{\Delta c_2}{\ell} &\approx \frac{c_2}{\ell}\end{aligned} \tag{22}$$

where c_i are the pore concentrations in equilibrium with the partial fugacities in the upstream face of the membrane.

Let us further assume that the M-S diffusivities vary with the fractional occupancies according to

$$Đ_i = Đ_i(0)(1-\theta_i) \tag{23}$$

where $Đ_i(0)$ are the zero-loading diffusivities. For multicomponent Langmuir isotherm, the M-S equations can be integrated analytically to obtain [55]

$$\begin{aligned} N_1 &= \phi\Delta_{11}\frac{c_1}{\ell} + \phi\Delta_{12}\frac{c_2}{\ell} \\ N_2 &= \phi\Delta_{21}\frac{c_1}{\ell} + \phi\Delta_{22}\frac{c_2}{\ell} \end{aligned} \tag{24}$$

where the elements of the matrix [Δ] are evaluated at the upstream loadings. Equation (24) corresponds to eq. (44) of Krishna and Baur [55], re-written in the notation used here.

It is convenient to define the effective diffusivities, $D_{i,eff}$,

$$\begin{aligned} D_{1,eff} &= \Delta_{11} + \Delta_{12}\frac{c_2}{c_1} \\ D_{2,eff} &= \Delta_{22} + \Delta_{21}\frac{c_1}{c_2} \end{aligned} \tag{25}$$

From equations (13), (14), (15), and (16) we derive the following explicit expressions

$$D_{1,eff} = \Delta_{11} + \Delta_{12}\frac{c_2}{c_1} = \frac{Đ_1\left(1+\frac{x_1Đ_2}{Đ_{12}}\right)}{1+\frac{x_1Đ_2}{Đ_{12}}+\frac{x_2Đ_1}{Đ_{12}}} + \frac{Đ_1\frac{x_1Đ_2}{Đ_{12}}}{1+\frac{x_1Đ_2}{Đ_{12}}+\frac{x_2Đ_1}{Đ_{12}}}\frac{c_2}{c_1} = \frac{Đ_1\left(1+\frac{Đ_2}{Đ_{12}}\right)}{1+\frac{x_1Đ_2}{Đ_{12}}+\frac{x_2Đ_1}{Đ_{12}}} \tag{26}$$

$$D_{2,eff} = \Delta_{22} + \Delta_{21}\frac{c_1}{c_2} = \frac{Đ_2\left(1+\frac{x_2Đ_1}{Đ_{12}}\right)}{1+\frac{x_1Đ_2}{Đ_{12}}+\frac{x_2Đ_1}{Đ_{12}}} + \frac{Đ_2\frac{x_2Đ_1}{Đ_{12}}}{1+\frac{x_1Đ_2}{Đ_{12}}+\frac{x_2Đ_1}{Đ_{12}}}\frac{c_1}{c_2} = \frac{Đ_2\left(1+\frac{Đ_1}{Đ_{12}}\right)}{1+\frac{x_1Đ_2}{Đ_{12}}+\frac{x_2Đ_1}{Đ_{12}}} \tag{27}$$

The effective diffusivities can be determined from MD mixture simulations.

For separation of a binary mixture, the permeation selectivity is

$$S_{Perm} = \frac{N_1/f_1}{N_2/f_2} \tag{28}$$

In view of eqs (24) and (25), the permeation selectivity can be expressed as

$$S_{perm} = \frac{N_1/f_1}{N_2/f_2} = \frac{D_{1,eff}}{D_{2,eff}} \frac{c_1/f_1}{c_2/f_2} \tag{29}$$

For separation of a binary mixture, the diffusion selectivity can be defined as follows

$$S_{diff} = \frac{D_{1,eff}}{D_{2,eff}} \tag{30}$$

From equations (26) and (27) we get

$$\frac{D_{1,eff}}{D_{2,eff}} = \frac{\left(\frac{1}{Đ_2} + \frac{1}{Đ_{12}}\right)}{\left(\frac{1}{Đ_1} + \frac{1}{Đ_{12}}\right)} = \frac{Đ_1}{Đ_2} \frac{\left(1 + \frac{Đ_2}{Đ_{12}}\right)}{\left(1 + \frac{Đ_1}{Đ_{12}}\right)} \tag{31}$$

For separation of a binary mixture, the adsorption selectivity is

$$S_{ads} = \frac{c_1/f_1}{c_2/f_2} \tag{32}$$

From equations (29), and (32) we get

$$S_{perm} = S_{ads} \times S_{diff} \tag{33}$$

We now show that S_{diff} can be ***approximated*** by the ratio of self-diffusivities. From equations (20) and (21) the ratio of self-diffusivities can be written as follows

$$\frac{D_{1,self}}{D_{2,self}} = \frac{\frac{1}{Đ_2} + \frac{x_2}{Đ_{22}} + \frac{x_1}{Đ_{12}}}{\frac{1}{Đ_1} + \frac{x_1}{Đ_{11}} + \frac{x_2}{Đ_{12}}} \tag{34}$$

$$\frac{D_{1,self}}{D_{2,self}} = \frac{Đ_1}{Đ_2} \frac{1 + \frac{x_2 Đ_2}{Đ_{22}} + \frac{x_1 Đ_2}{Đ_{12}}}{1 + \frac{x_1 Đ_1}{Đ_{11}} + \frac{x_2 Đ_1}{Đ_{12}}} \tag{35}$$

In view of the Vignes interpolation formula[56]

$$Đ_{12} = \left(Đ_{11}\right)^{x_1} \left(Đ_{22}\right)^{x_2}$$

we conclude that the ratio of the self-diffusivities is a good approximation for the diffusion selectivities

$$\frac{D_{1,self}}{D_{2,self}} \approx \frac{Đ_1}{Đ_2} \frac{1 + \frac{Đ_2}{Đ_{12}}}{1 + \frac{Đ_1}{Đ_{12}}} = \frac{D_{1,eff}}{D_{2,eff}} = S_{diff} \tag{36}$$

In our previous screening study of zeolite membranes, the diffusion selectivity was estimated using the ratio of the self-diffusivities using equation (36). This is a reasonable approximation for many cases, when the pore concentrations are not near the saturation concentrations. In cases where the adsorption strength of CO_2 is strong, as is the case for MgMOF-74 and ZnMOF-74, the pore concentrations can be near saturation values at pressures in excess of 1 MPa. In such cases, eq. (31) gives a more correct estimate of the diffusion selectivities. In this Perspective, we used eq. (31) to determine the S_{diff} for the MgMOF-74 and ZnMOF-74 for CO_2/CH_4, CO_2/H_2, CO_2/N_2, and CH_4/H_2 mixtures. More specifically, the differences in the diffusion selectivity calculations for CO_2/H_2 mixtures using the two different sets of formulas lead to significantly different results at high pore concentrations. In this Perspective, we used eq. (31) to determine the S_{diff} for the various MOFs in Figure 11a of the perspective. The calculations presented in Figure 13 of the manuscript were also carried out using eq. (31). In all other cases, the S_{diff} was calculated using eq. (36); these values are nearly the same as those obtained using equation (31).

The permeability Π_i of component *i* is ,

$$\Pi_i = \frac{N_i}{\Delta f_i/\ell} \approx \frac{\frac{\rho D_{i,self}}{\ell} q_i}{f_i/\ell} \approx \frac{\rho D_{i,self} q_i}{f_i} \qquad (37)$$

The detailed derivation of eq. (37) is available in ref [57]. Here, $D_{i,self}$ is the self-diffusivity of the species i in the mixture, q_i is the molar loading of species i at the upstream face of the membrane, ρ is the framework density, for which the tabulated information is available in the accompanying pages. In the calculation of we assume that the partial fugacity f_i of component i has a vanishingly small value in the downstream compartment, i.e. $\Delta f_i \approx f_i$. Eq. (37) can also be written using different measures of component concentrations within the pores

$$\Pi_i = \frac{N_i}{\Delta f_i/\ell} \approx \frac{\frac{\phi D_{i,self}}{\ell} c_i}{f_i/\ell} \approx \frac{\phi D_{i,self} c_i}{f_i} \qquad (38)$$

where the pore concentrations c_i are defined in terms of accessible pore volume of the crystalline microporous layer, and ϕ represents the fractional pore volume of the microporous crystalline material. We have the following conversion relationship for the two concentration measures

$$c_i = \frac{q_i}{V_p} \qquad (39)$$

where V_p is the m^3 accessible pore volume per kg framework.

The SI units for the permeability Π_i is mol m m^{-2} s^{-1} Pa^{-1}. The more commonly used engineering unit for permeability is the Barrer expressed in cm^3 (STP) cm cm^{-2} s^{-1} $(cm\ Hg)^{-1}$. To convert to the commonly used engineering units of Barrers we divide the value in mol m m^{-2} s^{-1} Pa^{-1} by 3.348×10^{-16}.

10. Simulation results

The CBMC simulation results for mixture adsorption are presented in graphical form in the accompanying Figures. The information is presented per structure, in the following order: (1) all-zeolites, in alphabetical order (2) additional all-silica zeolites not considered in the manuscript, (3) Zeolites NaY and NaX with cations, (4) MOFs in alphabetical order, and (5) Graphite slits of varying widths. In some cases validation data for pure component adsorption isotherms is presented, where available for MOFs, by comparing with experimental data.

11. Acknowledgements

We are grateful to T.J.H. Vlugt, Delft, for providing the BIGMAC code. This code was modified to handle rigid molecular structures and charges, with generous assistance and technical inputs from S. Calero, Seville.

The calculation of the accessible pore volume using the Widom insertion of He probe atoms is implemented within the BIGMAC code.

12. Notation

$[B]$	matrix of inverse Maxwell-Stefan coefficients, m^{-2} s
c_i	concentration of species *i*, mol m^{-3}
c_t	total concentration in mixture, mol m^{-3}
$D_{i,self}$	self-diffusivity of species *i* within pore, $m^2\ s^{-1}$
Đ_{ii}	self-exchange diffusivity, $m^2\ s^{-1}$
Đ_{i}	M-S diffusivity of species *i*, $m^2\ s^{-1}$
Đ_{ij}	M-S exchange coefficient, $m^2\ s^{-1}$
f_i	fugacity of species *i*, Pa
f_t	total bulk fluid phase fugacity of mixture, Pa
k_B	Boltzmann constant, 1.38×10^{-23} J $molecule^{-1}\ K^{-1}$
ℓ	thickness of microporous membrane layer, m
N_i	molar flux of species *i*, based on membrane area, mol $m^{-2}\ s^{-1}$
n_i	number of molecules of species *i* in simulation box, dimensionless
n	number of species in mixture, dimensionless
q_i	component molar loading of species *i*, mol kg^{-1}
$\mathbf{r}_{l,i}(t)$	position vector for molecule *l* of species *i* at any time *t*, m
R	gas constant, 8.314 J $mol^{-1}\ K^{-1}$
S_{ads}	adsorption selectivity, dimensionless
S_{diff}	diffusion selectivity, dimensionless
S_{perm}	permeation selectivity, dimensionless
t	time, s
T	absolute temperature, K
V_p	accessible pore volume, $m^3\ kg^{-1}$
x_i	mole fraction of species *i* based on loading within pore, dimensionless

Greek letters

ε	Lennard-Jones interaction energy parameter, J molecule^{-1}
$[\Gamma]$	matrix of thermodynamic factors, dimensionless
Γ_{ij}	thermodynamic factors, dimensionless
$[\Delta]$	matrix of Maxwell-Stefan diffusivities, m^2 s^{-1}
ϕ	fractional pore volume, dimensionless
θ_i	fractional occupancy of component *i*, dimensionless
μ_i	molar chemical potential, J mol^{-1}
Π_i	permeability of species *i* across membrane, mol m m^{-2} s^{-1} Pa^{-1}.
ϕ	fractional pore volume, dimensionless
ρ	framework density, kg m^{-3}
σ	Lennard-Jones size parameter, m

Subscripts

i	referring to component *i*
p	referring to pore
t	referring to total mixture

Vector and Matrix Notation

∇	gradient operator

13. References

[1] C. Baerlocher, L.B. McCusker, Database of Zeolite Structures, International Zeolite Association, http://www.iza-structure.org/databases/, 10 January 2002.

[2] J.P. Ryckaert, A. Bellemans, Molecular dynamics of liquid alkanes, Faraday Discuss. Chem. Soc. 66 (1978) 95-106.

[3] D. Dubbeldam, S. Calero, T.J.H. Vlugt, R. Krishna, T.L.M. Maesen, B. Smit, United Atom Forcefield for Alkanes in Nanoporous Materials, J. Phys. Chem. B 108 (2004) 12301-12313.

[4] A.V.A. Kumar, H. Jobic, S.K. Bhatia, Quantum effects on adsorption and diffusion of hydrogen and deuterium in microporous materials, J. Phys. Chem. B 110 (2006) 16666-16671.

[5] K. Makrodimitris, G.K. Papadopoulos, D.N. Theodorou, Prediction of permeation properties of CO_2 and N_2 through silicalite via molecular simulations, J. Phys. Chem. B 105 (2001) 777-788.

[6] E. García-Pérez, J.B. Parra, C.O. Ania, A. García-Sánchez, J.M. Van Baten, R. Krishna, D. Dubbeldam, S. Calero, A computational study of CO_2, N_2 and CH_4 adsorption in zeolites, Adsorption 13 (2007) 469-476.

[7] O. Talu, A.L. Myers, Molecular Simulation of Adsorption: Gibbs Dividing Surface and Comparison with Experiment, A.I.Ch.E.J. 47 (2001) 1160-1168.

[8] M.D. Foster, I. Rivin, M.M.J. Treacy, O.D. Friedrichs, A geometric solution to the largest-free-sphere problem in zeolite frameworks, Microporous Mesoporous Mater. 90 (2006) 32-38.

[9] A. García-Sánchez, C.O. Ania, J.B. Parra, D. Dubbeldam, T.J.H. Vlugt, R. Krishna, S. Calero, Development of a Transferable Force Field for Carbon Dioxide Adsorption in Zeolites, J. Phys. Chem. C 113 (2009) 8814-8820.

[10] D. Dubbeldam, K.S. Walton, D.E. Ellis, R.Q. Snurr, Exceptional Negative Thermal Expansion in Isoreticular Metal–Organic Frameworks, Angew. Chem. Int. Ed. 46 (2007) 4496-4499.

[11] D. Dubbeldam, H. Frost, K.S. Walton, R.Q. Snurr, Molecular simulation of adsorption sites of light gases in the metal-organic framework IRMOF-1, Fluid Phase Equilib. 261 (2007) 152-161.

[12] S.S.Y. Chui, S.M.F. Lo, J.P.H. Charmant, A.G. Orpen, I.D. Williams, A chemically functionalizable nanoporous material $[Cu_3(TMA)_2(H2O)_3]_n$, Science 283 (1999) 1148-1150.

[13] Q. Yang, C. Zhong, Electrostatic-Field-Induced Enhancement of Gas Mixture Separation in Metal-Organic Frameworks: A Computational Study, ChemPhysChem 7 (2006) 1417-1421.

[14] P.S. Bárcia, F. Zapata, J.A.C. Silva, A.E. Rodrigues, B. Chen, Kinetic Separation of Hexane Isomers by Fixed-Bed Adsorption with a Microporous Metal-Organic Framework, J. Phys. Chem. B 111 (2008) 6101-6103.

[15] J.Y. Lee, D.H. Olson, L. Pan, T.J. Emge, J. Li, Microporous Metal–Organic Frameworks with High Gas Sorption and Separation Capacity, Adv. Funct. Mater. 17 (2007) 1255-1262.

[16] L. Alaerts, C.E.A. Kirschhock, M. Maes, M. van der Veen, V. Finsy, A. Depla, J.A. Martens, G.V. Baron, P.A. Jacobs, J.F.M. Denayer, D. De Vos, Selective Adsorption and Separation of Xylene Isomers and Ethylbenzene with the Microporous Vanadium(IV) Terephthalate MIL-47, Angew. Chem. Int. Ed. 46 (2007) 4293-4297.

[17] V. Finsy, H. Verelst, L. Alaerts, D. De Vos, P.A. Jacobs, G.V. Baron, J.F.M. Denayer, Pore-Filling-Dependent Selectivity Effects in the Vapor-Phase Separation of Xylene Isomers on the Metal-Organic Framework MIL-47, J. Am. Chem. Soc. 130 (2008) 7110-7118.

[18] K. Barthelet, J. Marrot, D. Riou, G. Férey, A Breathing Hybrid Organic - Inorganic Solid with Very Large Pores and High Magnetic Characteristics, Angew. Chem. Int. Ed. 41 (2007) 281-284.

[19] D.S. Coombes, F. Corà, C. Mellot-Draznieks, R.G. Bell, Sorption-Induced Breathing in the Flexible Metal Organic Framework CrMIL-53: Force-Field Simulations and Electronic Structure Analysis, J. Phys. Chem. C 113 (2009) 544-552.

[20] R. Banerjee, A. Phan, B. Wang, C. Knobler, H. Furukawa, M. O'Keeffe, O.M. Yaghi, High-Throughput Synthesis of Zeolitic Imidazolate Frameworks and Application to CO_2 Capture, Science 319 (2008) 939-943.

[21] D. Britt, H. Furukawa, B. Wang, T.G. Glover, O.M. Yaghi, Highly efficient separation of carbon dioxide by a metal-organic framework replete with open metal sites, Proc. Nat. Acad. Sci. U.S.A. 106 (2009) 20637-20640.

[22] N.L. Rosi, J. Kim, M. Eddaoudi, B. Chen, M. O'Keeffe, O.M. Yaghi, Rod Packings and Metal-Organic Frameworks Constructed from Rod-Shaped Secondary Building Units, J. Am. Chem. Soc. 127 (2005) 1504-1518.

[23] P.D.C. Dietzel, B. Panella, M. Hirscher, R. Blom, H. Fjellvåg, Hydrogen adsorption in a nickel based coordination polymer with open metal sites in the cylindrical cavities of the desolvated framework, Chem. Commun. (2006) 959-961.

[24] P.D.C. Dietzel, V. Besikiotis, R. Blom, Application of metal–organic frameworks with coordinatively unsaturated metal sites in storage and separation of methane and carbon dioxide, J. Mater. Chem. 19 (2009) 7362-7370.

[25] S.R. Caskey, A.G. Wong-Foy, A.J. Matzger, Dramatic Tuning of Carbon Dioxide Uptake via Metal Substitution in a Coordination Polymer with Cylindrical Pores, J. Am. Chem. Soc. 130 (2008) 10870-10871.

[26] A.Ö. Yazaydın, R.Q. Snurr, T.H. Park, K. Koh, J. Liu, M.D. LeVan, A.I. Benin, P. Jakubczak, M. Lanuza, D.B. Galloway, J.J. Low, R.R. Willis, Screening of Metal-Organic Frameworks for Carbon Dioxide Capture from Flue Gas using a Combined Experimental and Modeling Approach, J. Am. Chem. Soc. 131 (2009) 18198-18199.

[27] R. Babarao, J. Jiang, Unprecedentedly High Selective Adsorption of Gas Mixtures in rho Zeolite-like Metal-Organic Framework: A Molecular Simulation Study, J. Am. Chem. Soc. 131 (2009) 11417-11425.

[28] H.K. Chae, D.Y. Siberio-Pérez, J. Kim, Y.B. Go, M. Eddaoudi, A.J. Matzger, M. O'Keeffe, O.M. Yaghi, A route to high surface area, porosity and inclusion of large molecules in crystals, Nature 427 (2004) 523-527.

[29] H.J. Choi, M. Dincă, J.R. Long, Broadly Hysteretic H_2 Adsorption in the Microporous Metal-Organic Framework Co(1,4-benzenedipyrazolate), J. Am. Chem. Soc. 130 (2008) 7848-7850.

[30] F. Salles, G. Maurin, C. Serre, P.L. Llewellyn, C. Knöfel, H.J. Choi, Y. Filinchuk, L. Oliviero, A. Vimont, J.R. Long, G. Férey, Multistep N_2 Breathing in the Metal-Organic Framework Co(1,4-benzenedipyrazolate), J. Am. Chem. Soc. 132 (2010) 13782-13788.

[31] K. Sumida, M.R. Hill, S. Horike, A. Dailly, J.R. Long, Synthesis and Hydrogen Storage Properties of $Be_{12}(OH)_{12}(1,3,5\text{-benzenetribenzoate})_4$, J. Am. Chem. Soc. 131 (2009) 15120-15121.

[32] A. Demessence, D.M. D'Alessandro, M.W. Foo, J.R. Long, Strong CO_2 Binding in a Water-Stable, Triazolate-Bridged Metal-Organic Framework Functionalized with Ethylenediamine, J. Am. Chem. Soc. 131 (2009) 8784-8786.

[33] A.K. Rappé, C.J. Casewit, K.S. Colwel, W.A. Goddard, W.M. Skiff, UFF, a Full Periodic Table Force Field for Molecular Mechanics and Molecular Dynamics Simulations, J. Am. Chem. Soc. 114 (1992) 10024-10035.

[34] S.L. Mayo, B.D. Olafson, W.A. Goddard, DREIDING: A Generic Force Field for Molecular Simulations, J. Phys. Chem. 94 (1990) 8897-8909.

[35] A. Martín-Calvo, E. García-Pérez, S. Calero, Molecular simulations for adsorption and separation of natural gas in IRMOF-1 and Cu-BTC metal-organic frameworks, Phys. Chem. Chem. Phys. 10 (2008) 7085-7091.

[36] K.S. Walton, A.R. Millward, D. Dubbeldam, H. Frost, J.J. Low, O.M. Yaghi, R.Q. Snurr, Understanding Inflections and Steps in Carbon Dioxide Adsorption Isotherms in Metal-Organic Frameworks, J. Am. Chem. Soc. 130 (2008) 406-407.

[37] N. Rosenbach, H. Jobic, A. Ghoufi, F. Salles, G. Maurin, S. Bourrelly, P.L. Llewellyn, T. Devic, C. Serre, G. Férey, Quasi-Elastic Neutron Scattering and Molecular Dynamics Study of Methane Diffusion in Metal Organic Frameworks MIL-47(V) and MIL-53(Cr), Angew. Chem. Int. Ed. 47 (2008) 6611-6615.

[38] F. Salles, A. Ghoufi, G. Maurin, R.G. Bell, C. Mellot-Draznieks, G. Férey, Molecular Dynamics Simulations of Breathing MOFs: Structural Transformations of MIL-53(Cr) upon Thermal Activation and CO2 Adsorption, Angew. Chem. Int. Ed. 47 (2008) 8487-8491.

[39] Q. Yang, C. Zhong, Understanding Hydrogen Adsorption in Metal-Organic Frameworks with Open Metal Sites: A Computational Study, J. Phys. Chem. B 110 (2006) 655-658.

[40] W.L. Jorgensen, D.S. Maxwell, J. Tirado-Rives, Development and Testing of the OPLS All-Atom Force Field on Conformational Energetics and Properties of Organic Liquids, J. Am. Chem. Soc. 118 (1996) 11225-11236.

[41] M. Zhou, Q. Wang, L. Zhang, Y.C. Liu, Y. Kang, Adsorption Sites of Hydrogen in Zeolitic Imidazolate Frameworks, J. Phys. Chem. B 113 (2009) 11049-11053.

[42] Q. Xu, C. Zhong, A General Approach for Estimating Framework Charges in Metal-Organic Frameworks, J. Phys. Chem. C 114 (2010) 5035-5042.

[43] R. Krishna, J.M. van Baten, A molecular simulation study of commensurate – incommensurate adsorption of n-alkanes in cobalt formate frameworks, Mol. Simulation 35 (2009) 1098-1104.

[44] B.L. Severson, R.Q. Snurr, Monte Carlo simulation of n-alkane adsorption isotherms in carbon slit pores, J. Chem. Phys. 126 (2007) 134708.

[45] A.L. Myers, P.A. Monson, Adsorption in Porous Materials at High Pressure: Theory and Experiment, Langmuir 18 (2002) 10261-10273.

[46] R. Babarao, Z. Hu, J. Jiang, S. Chempath, S.I. Sandler, Storage and separation of CO_2 and CH_4 in silicalite, C_{168} schwarzite, and IRMOF-1: A comparative study from Monte Carlo simulation, Langmuir 23 (2007) 659-666.

[47] R. Babarao, J. Jiang, Exceptionally high CO_2 storage in covalent-organic frameworks: Atomistic simulation study, Energy Environ. Sci. 1 (2008) 139-143.

[48] D. Frenkel, B. Smit, Understanding molecular simulations: from algorithms to applications, Academic Press, 2nd Edition, San Diego, 2002.

[49] T. Düren, F. Millange, G. Férey, K.S. Walton, R.Q. Snurr, Calculating Geometric Surface Areas as a Characterization Tool for Metal-Organic Frameworkss, J. Phys. Chem. C 111 (2007) 15350-15356.

[50] F. Karavias, A.L. Myers, Isosteric Heats of Multicomponent Adsorption: Thermodynamics and Computer Simulations, Langmuir 7 (1991) 3118-3126.

[51] W. Smith, T.R. Forester, I.T. Todorov, The DL_POLY Molecular Simulation Package, Warrington, England, http://www.cse.clrc.ac.uk/msi/software/DL_POLY/index.shtml, March 2006.

[52] SARA, Computing & Networking Services, Amsterdam, https://subtrac.sara.nl/userdoc/wiki/lisa/description, 16 January 2008.

[53] A.I. Skoulidas, D.S. Sholl, R. Krishna, Correlation effects in diffusion of CH_4/CF_4 mixtures in MFI zeolite. A study linking MD simulations with the Maxwell-Stefan formulation, Langmuir 19 (2003) 7977-7988.

[54] R. Krishna, J.M. van Baten, Diffusion of alkane mixtures in zeolites. Validating the Maxwell-Stefan formulation using MD simulations, J. Phys. Chem. B 109 (2005) 6386-6396.

[55] R. Krishna, R. Baur, Analytic solution of the Maxwell-Stefan equations for multicomponent permeation across a zeolite membrane, Chem. Eng. J. 97 (2004) 37-45.

[56] R. Krishna, Describing the diffusion of guest molecules inside porous structures, J. Phys. Chem. C 113 (2009) 19756-19781.

[57] R. Krishna, J.M. van Baten, In Silico Screening of Zeolite Membranes for CO_2 Capture, J. Membr. Sci. 360 (2010) 323-333.

[58] A. Corma, F. Rey, J. Rius, M.J. Sabater, S. Valencia, Supramolecular self-assembled molecules as organic directing agent for synthesis of zeolites, Nature 431 (2004) 287-290.

[59] S. Calero, D. Dubbeldam, R. Krishna, B. Smit, T.J.H. Vlugt, J.F.M. Denayer, J.A. Martens, T.L.M. Maesen, Understanding the role of sodium during adsorption. A force field for alkanes in sodium exchanged faujasites, J. Am. Chem. Soc. 126 (2004) 11377-11386.

[60] E. García-Pérez, D. Dubbeldam, T.L.M. Maesen, S. Calero, Influence of cation Na/Ca ratio on adsorption in LTA 5A: A systematic molecular simulations study of alkane chain length, J. Phys. Chem. B 110 (2006) 23968-23976.

[61] A. García-Sánchez, E. García-Pérez, D. Dubbeldam, R. Krishna, S. Calero, A Simulation Study of Alkanes in Linde Type A Zeolites, Adsorpt. Sci. Technol. 25 (2007) 417-427.

Table 1. Salient information on zeolite structures.

Zeolite	**Channel or window size/ Å**
AFI	12-ring 1D channels of 7.3 Å size
AFX	490 Å^3 size cages connected to pockets of 98 Å^3 in size. Cages are separated by 3.4 Å × 3.9 Å size windows.
AWW	1D connectivity. Cages separated by 8-ring windows of 3.9 Å size. There are 2 cages per unit cell. The volume of each cage is 221 Å^3.
BEA	Intersecting channels of two sizes: 12-ring of 7.1 Å - 7.3 Å and 10-ring of 5.6 – 5.6 Å
BOG	Intersecting channels: 12-ring 7.0 Å -7.0 Å and 10-ring of 5.5 Å - 5.8 Å
CHA	316.4 Å^3 size cages separated by 3.77 Å × 4.23 Å size windows.
DDR	277.8 Å^3 size cages separated by 3.65 Å × 4.37 Å size windows
ERI	408.7 Å^3 size cages separated by 3.8 Å × 4.9 Å size windows
FAU	785.7 Å^3 size cages separated by 7.4 Å size windows. The sodalite cages are blocked in simulations and are not accessible to guest molecules; these are excluded for pore volume determination. Cage size is calculated on the basis of the equivalent sphere volume.
FER	10-ring 1D main channels of 4.2 Å -5.4 Å size, connected with 8-ring side pockets of 3.5 Å -4.8 Å size
GME	The main 12-ring channels are interconnected at right angles by a two-dimensional system of eight-ring channels, and thus form a three-dimensional channel system

Table 2. Salient information on zeolite structures (continued)

Zeolite	**Channel or window size/ Å**
ISV	Intersecting channels of two sizes: 12-ring of 6.1 Å -6.5 Å and 12-ring of 5.9 Å - 6.6 Å
ITQ-29	678 $Å^3$ sized cages separated by 4 Å × 4.22 Å sized windows. The sodalite cages are blocked in simulations and are not accessible to guest molecules. The structural information is from Corma [58].
LTA-Si	743.05 $Å^3$ size cages separated by 4.11 Å × 4.47 Å size windows. The sodalite cages are blocked in simulations and are not accessible to guest molecules.
LTL	12-ring 1D channels of 7.1 Å size
MOR	12-ring 1D main channels of 6.5 Å -7 Å size, connected with 8-ring side pockets of 2.6 Å -5.7 Å size
MFI	10-ring intersecting channels of 5.1 Å – 5.5 Å and 5.3 Å – 5.6 Å size
MTW	12-ring 1D channels of 5.6 Å -6 Å size
TON	10-ring 1D channels of 4.6 Å -5.7 Å size
TSC	Two types of cages: LTA-type of 743.05 $Å^3$ and TSC-supercage of 2552.6 $Å^3$size. Two types of 8-ring windows: 4.02 Å × 4.17 Å and 3.1 Å × 5.41 Å. The sodalite cages are blocked in simulations and are not accessible to guest molecules; these are excluded for pore volume determination.

Table 3. Unit cell dimensions, unit cell volumes, pore volumes of various all-silica zeolites. Also indicated are the framework density, ρ, (expressed as kg per m^3 framework), the factor to convert from molecules per unit cell to kmol/m^3 of accessible pore volume.

Structure	*a* / Å	*b* / Å	*c* / Å	Unit cell volume/ $Å^3$	Pore volume per unit cell/ $Å^3$	Fractional pore volume	Pore volume/ cm^3/g	Framework density/ kg/m^3	Conversion factor
AFI	23.77	13.73	8.48	2768.52	759.42	0.274	0.159	1729.88	2.1866
AFX	23.836	13.762	19.949	6543.89	2352.45	0.359	0.246	1463.71	0.7059
AWW	13.634	13.634	7.627	1417.75	441.31	0.311	0.184	1689.00	3.7628
BEA	12.66	12.66	26.41	4232.91	1728.05	0.408	0.271	1508.56	0.9609
BOG	20.24	23.80	12.80	6163.21	2305.42	0.374	0.241	1995.52	0.7203
CHA	15.08	23.91	13.80	4974.57	1898.40	0.382	0.264	1444.10	0.8747
DDR	24.01	13.86	40.89	13605.72	3333.53	0.245	0.139	1759.99	0.4981
ERI	22.95	13.25	14.81	4504.80	1635.01	0.363	0.228	1594.69	1.0156
FAU	24.28	24.28	24.28	14313.51	6285.60	0.439	0.328	1338.37	0.2642
FER	19.16	14.13	7.49	2026.65	573.24	0.283	0.160	1772.33	2.8968
GME	23.83	13.76	10.06	3298.48	1268.59	0.385	0.265	1451.94	1.3090

Table 4. Unit cell dimensions, unit cell volumes, pore volumes of various all-silica zeolites. Also indicated are the framework density, ρ, (expressed as kg per m^3 framework), the factor to convert from molecules per unit cell to kmol/m^3 of accessible pore volume.

Structure	*a* / Å	*b* / Å	*c* / Å	Unit cell volume/ Å^3	Pore volume per unit cell/ Å^3	Fractional pore volume	Pore volume/ cm^3/g	Framework density/ kg/m^3	Conversion factor
ISV	12.85	12.85	25.214	4165.34	1773.87	0.426	0.278	1533.03	0.9361
ITQ-29	11.87	11.87	11.87	1671.18	677.57	0.405	0.283	1442.03	2.4508
LTA	24.61	24.61	24.61	14905.10	5944.38	0.399	0.310	1285.25	0.2794
LTL	31.98	18.47	7.48	4415.45	1221.27	0.277	0.170	1626.97	1.3597
MFI	20.02	19.90	13.38	5332.03	1584.94	0.297	0.165	1796.39	1.0477
MOR	18.09	20.52	7.52	2793.03	795.41	0.285	0.166	1714.69	2.0877
MTW	24.86	5.01	24.33	2887.49	620.55	0.215	0.111	1935.03	2.6759
TON	13.86	17.42	5.04	1216.29	231.39	0.190	0.097	1968.76	7.1763
TSC	30.74	30.74	30.74	29053.36	13182.60	0.454	0.344	1318.73	0.1260

Table 5. Unit cell dimensions, unit cell volumes, pore volumes of **Additional** all-silica zeolites, not discussed in the main manuscript. Also indicated are the framework density, ρ, (expressed as kg per m^3 framework), the factor to convert from molecules per unit cell to kmol/m^3 of accessible pore volume.

Structure	*a* / Å	*b* / Å	*c* / Å	Unit cell volume/ Å^3	Pore volume per unit cell/ Å^3	Fractional pore volume	Pore volume/ cm^3/g	Framework density/ kg/m^3	Conversion factor	Foster diameter, from Delaunay triangulation Å
AFT	13.691	13.691	29.449	4780.48	1886.66	0.395	0.263	1502.73	0.8802	3.62
BIK	19.16	14.13	7.49	2026.65	97.01	0.151	0.081	1772.33	2.8968	3.49
EPI	9.13	17.48	10.38	1357.15	374.72	0.276	0.156	1764.42	4.4315	3.42
JBW	5.26	7.45	8.16	319.48	51.57	0.161	0.086	1714.69	32.202	3.66
LEV	23.10	13.34	23.01	7091.41	2496.33	0.352	0.232	1519.54	0.6652	3.61
LOV	7.16	7.16	20.88	1071.12	277.11	0.259	0.154	1796.39	5.992	3.71
SIV	9.88	14.08	28.13	3910.74	1195.61	0.306	0.187	1729.88	1.389	3.31

Table 6. Data on zeolite structures with cations (data on all-silica structures also included for comparison purposes). The number of atoms per unit cell of these structures are specified.

Zeolite	**Si**	**Al**	**Si/Al**	**Na++**
NaX	106	86	1.23	86
NaY	138	54	2.55	54

Table 7. Unit cell dimensions, unit cell volumes, pore volumes of cation-exchanged zeolites. Also indicated are the framework density, ρ, (expressed as kg per m^3 of (framework +cations)), the factor to convert from molecules per unit cell to kmol/m^3 of accessible pore volume).

Structure	*a* / Å	*b* / Å	*c* / Å	Unit cell volume/ Å^3	Pore volume per unit cell/ Å^3	Fractional pore volume	Pore volume/ cm^3/g	Framework density/ kg/m^3	Conversion factor
NaY	25.03	25.03	25.03	15677.56	6396.63	0.41	0.303	1347.1	0.2596
NaX	25.03	25.03	25.03	15677.56	6248.00	0.40	0.280	1421.28	0.2658

Table 8. Lennard-Jones parameters used to determine the pore volume in zeolites in which cations are present. The Na^+ - Na^+ parameters are from Calero et al. [59-61]. The He-He parameters are from Table 1 of the paper.by Talu and Myers [7]. The interaction parameters for interaction of He with the O atoms of zeolite frameworks is from Table 1 of Talu and Myers [7]

(pseudo-) atom	**Atom-atom** σ **/ Å**	**Atom-atom** ε/k_B **/ K**
He - He	2.64	10.9
He - Na^+	2.4	36.8
He - O	2.952	28
Na^+ - Na^+	2.16	124.4

Table 9. Salient structural information on MOFs and ZIFs.

MOF	**Channel dimensions**
CuBTC	The CuBTC structure consists of two types of “cages” and two types of “windows” separating these cages. Large cages are inter-connected by 9 Å windows of square cross-section. The large cages are also connected to tetrahedral-shaped pockets of ca. 6 Å size through triangular-shaped windows of ca. 4.6 Å size
IRMOF-1	Two alternating, inter-connected, cavities of 10.9 Å and 14.3 Å with window size of 8 Å.
MOF-177	Tetrahedral $[Zn_4O]^{6+}$ units are linked by large, triangular tricarboxylate ligands. Six diamond-shaped channels (upper) with diameter of 10.8 Å surround a pore containing eclipsed BTB^{3-} moieties.
MIL-47	One-dimensional diamond-shaped channels with free internal diameter of ca 8.5 Å
MIL-53 (Cr)-lp	One-dimensional lozenge-shaped channels with free internal diameter of ca 8.5 Å
Zn(bdc)dabco	There exist two types of intersecting channels of about 7.5 Å × 7.5 Å along the *x*-axis and channels of 3.8 Å × 4.7 Å along *y* and *z* axes.
ZIF-8	SOD topology consisting of cages separated by narrow windows of about 0.34 nm size. The volume of each cage is 1168 $Å^3$.
MgMOF-74	One-dimensional hexagonal-shaped channels with free internal diameter of ca. 11 Å
ZnMOF-74	One-dimensional hexagonal-shaped channels with free internal diameter of ca. 11 Å
NiMOF-74	One-dimensional hexagonal-shaped channels with free internal diameter of ca. 11 Å
CoMOF-74	One-dimensional hexagonal-shaped channels with free internal diameter of ca. 11 Å

Table 10. Unit cell dimensions, unit cell volumes, pore volumes of various MOFs and ZIFs. Also indicated are the framework density, ρ, (expressed as kg per m^3 of framework), the factor to convert from molecules per unit cell to kmol/m^3 of accessible pore volume.

Structure	*a* / Å	*b* / Å	*c* / Å	Unit cell volume/ Å^3	Pore volume per unit cell/Å^3	Fractional pore volume	Pore volume/ cm^3/g	Framework density/ kg/m^3	Conversion factor
CuBTC	26.34	26.34	26.34	18280.82	13871.82	0.759	0.863	878.83	0.1218
IRMOF1	25.83	25.83	25.83	17237.49	13996.27	0.812	1.369	593.21	0.1186
MOF-177	37.072	37.072	30.033	35745.50	3001090	0.840	1.968	426.60	0.0553
MIL-47	6.81	16.12	13.92	1527.32	929.34	0.608	0.606	1004.48	1.7868
MIL-53 (Cr)-lp	16.73	13.04	6.81	1486.14	801.60	0.539	0.518	1041.53	2.0716
Zn(bdc)dabco	10.93	10.93	9.61	1147.61	759.39	0.662	0.801	826.20	2.1867
ZIF-8	16.99	16.99	16.99	4905.20	2336.97	0.476	0.515	924.25	0.711
ZnMOF-74	25.93	25.93	6.84	3981.47	2867.85	0.709	0.582	1219.30	0.5881
MgMOF-74	25.86	25.86	6.91	4005.02	2835.86	0.708	0.782	905.37	0.5856
NiMOF-74	25.79	25.79	6.77	3898.34	2707.62	0.695	0.582	1193.81	0.6133
CoMOF-74	25.89	25.89	6.80	3949.17	2793.08	0.707	0.599	1180.26	0.5945
Na-rhoZMOF	31.06	31.06	31.062	29970.10	15165.37	0.506	0.427	1185.79	0.1095
BeBTB	24.3013	24.3013	54.57	32226.49	26013.82	0.807	1.908	423.09	0.0638
Co(BDP)	13.2529	13.253	13.995	2458.09	1643.88	0.669	0.927	721.55	1.0102
CuBTT	18.595	18.595	18.595	6429.67	3652.12	0.568	0.709	801.08	0.4547

Table 11. Lennard-Jones parameters for atoms in CuBTC. The information on charges is taken from the work of Martín-Calvo et al.[35].

(pseudo-) atom	σ / Å	ε/k_B / K	charge
Cu	3.114	2.518	1.098
O	3.03	48.2	-0.665
Ca	3.47	47.9	0.778
Cb	3.47	47.9	-0.092
Cc	3.47	47.9	-0.014
H	2.85	7.65	0.109

See Cartoon below for further explanation:

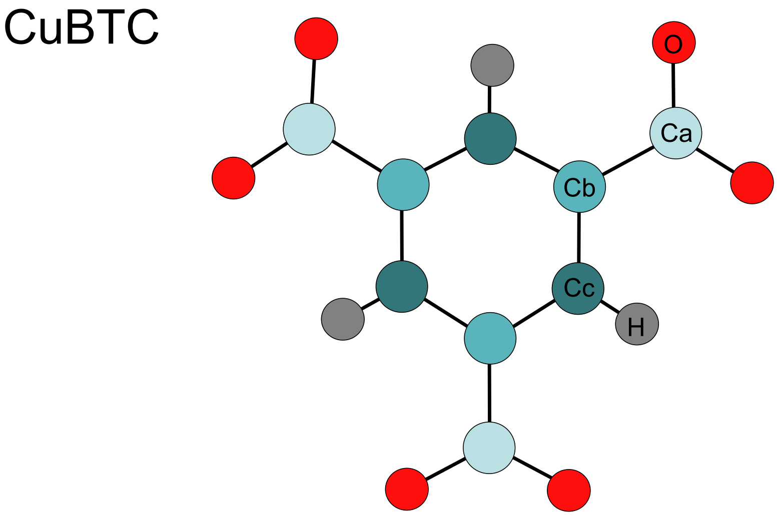

Table 12. Lennard-Jones parameters for atoms in IRMOF-1. The force field corresponds to that presented in the papers by Walton et al.[36] and Dubbeldam et al.[11].

(pseudo-) atom	σ / Å	ε/k_B / K	charge
Zn	2.69	0.41	1.275
Oa	2.98	700	-1.5
Ob	3.11	70.5	-0.6
Ca	3.74	47	0.475
Cb	3.47	47.9	0.125
Cc	3.47	47.9	-0.15
H	2.85	7.65	0.15

See Cartoon below for further explanation:

IRMOF-1

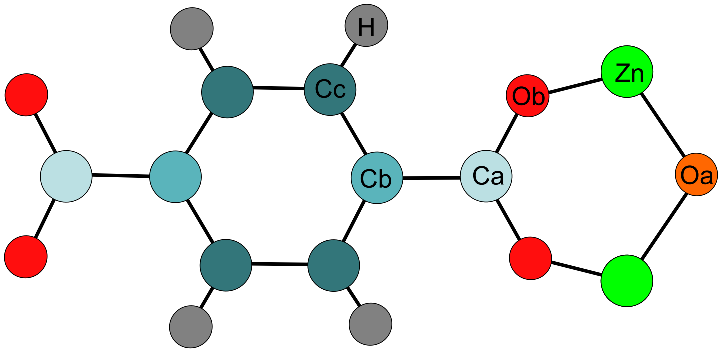

Table 13. Lennard-Jones parameters for atoms in MIL-53(Cr)-lp. The information on charges is taken from the work of Salles et al.[38].

(pseudo-) atom	σ / Å	ε/k_B / K	charge
Cr	2.69	7.55	1.032
Oa	3.03	48.2	-0.506
Ob	3.03	48.2	-0.637
Ca	3.47	47.9	-0.074
Cb	3.47	47.9	0.613
Ha	2.85	7.65	0.139
Hb	2.85	7.65	0.291

See Cartoon below for further explanation:

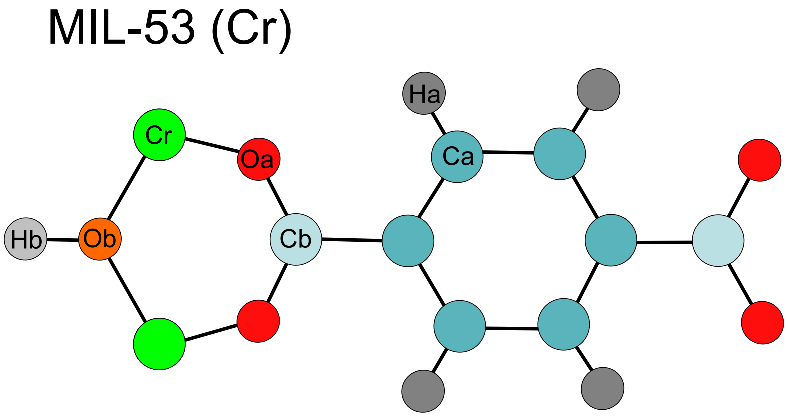

Table 14. Lennard-Jones parameters for atoms in MIL-47. The information on charges is taken from the work of Rosenbach et al.[37].

(pseudo-) atom	σ / Å	ε/k_B / K	charge
V	2.8	8.05	1.208
Oa	3.03	48.2	-0.596
Ob	3.03	48.2	-0.496
Ca	3.47	47.9	0.604
Cb	3.47	47.9	-0.071
Cc	3.47	47.9	-0.068
H	2.85	7.65	0.146

See Cartoon below for further explanation:

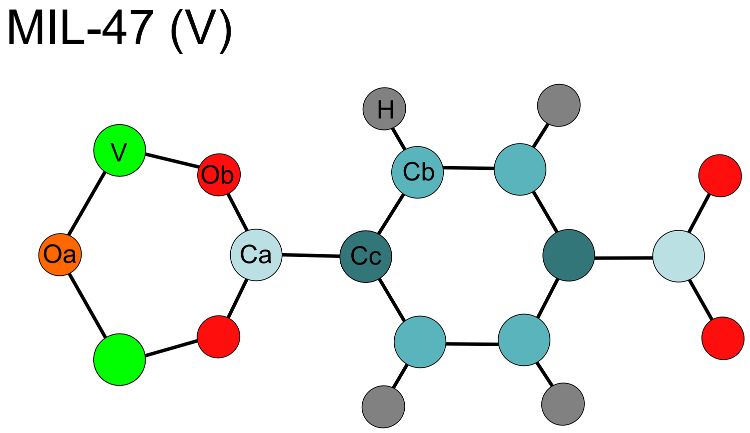

Table 15. The Lennard-Jones potentials for the framework atoms of ZIF-8 were taken from the combined works of Mayo et al.[34], Yang and Zhong [39], and Jorgensen et al.[40] as was reported in the computational study of Zhou et al.[41]The framework charges of ZIF-8 were estimated using the group-contribution procedure based on quantum mechanical calculations described by Xu and Zhong. [42]

(pseudo-) atom	σ / Å	ε/k_B / K	charge
Zn	4.54	27.59	0.749
N	3.25	85.29	-0.387
Ca	2.25	25.08	0.698
Cb	3.55	35.12	-0.0093
Cc	3.5	20.03	0.0117
Ha	2.5	15.05	-0.139
Hb	3.19	7.53	0.0627

See Cartoon below for further explanation:

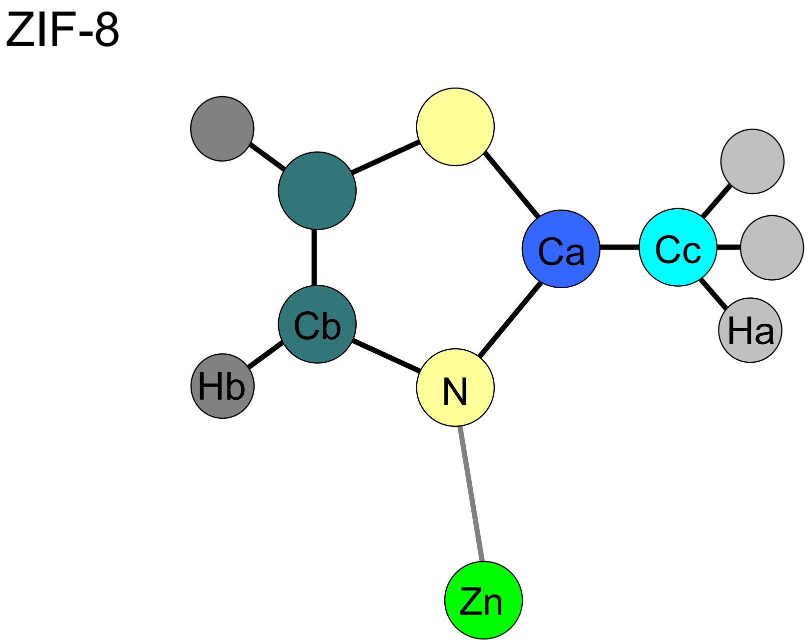

Table 16. Lennard-Jones parameters for atoms in NaRhoZMOF. The entire force field information is from Babarao and Jiang [27].

(pseudo-) atom	σ / Å	ε/k_B / K	charge
In	3.976	301.16	2.84
N	3.26	34.64	-0.381
O1	3.118	30.19	-0.751
O2	3.118	30.19	-0.813
C1	3.431	52.78	0.95
C2	3.431	52.78	-0.257
C3	3.431	52.78	-0.525
H1	2.571	22.13	0.426
H2	2.571	22.13	0.683

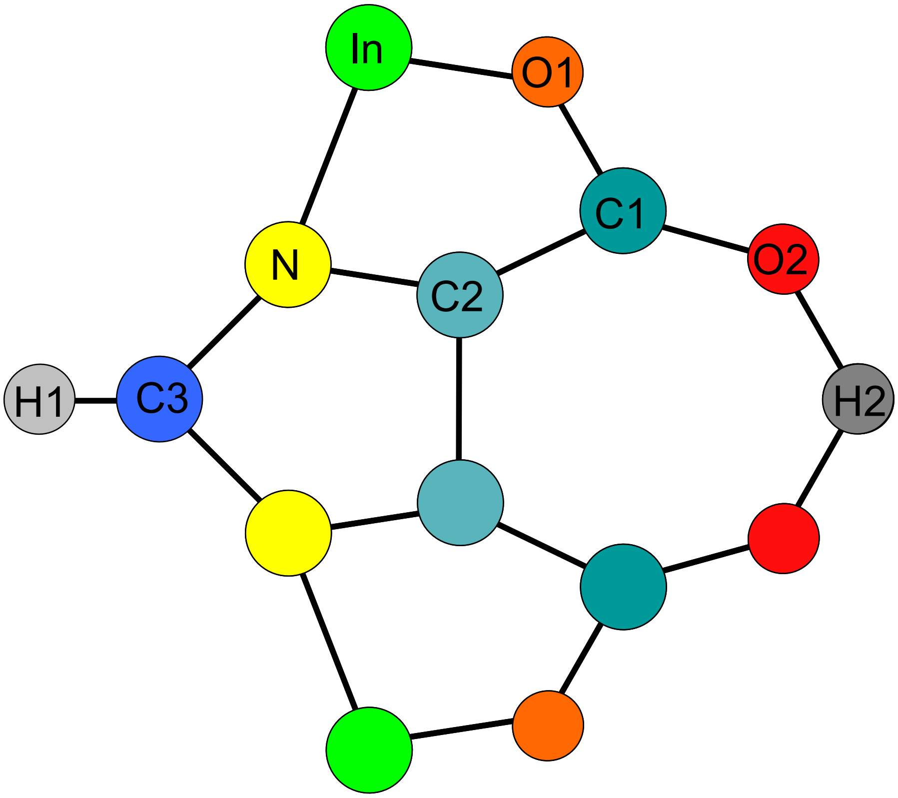

Table 17. Lennard-Jones parameters for atoms in MgMOF-74 based on the data from Yazaydin et al. [26].

(pseudo-) atom	σ / Å	ε/k_B / K	charge
Mg	2.691	55.86	1.458
OA	3.033	48.16	-0.909
OB	3.033	48.16	-0.714
OC	3.033	48.16	-0.784
CA	3.473	47.86	0.800
CB	3.473	47.86	-0.260
CC	3.473	47.86	0.492
CD	3.473	47.86	-0.280
H	2.846	7.650	0.197

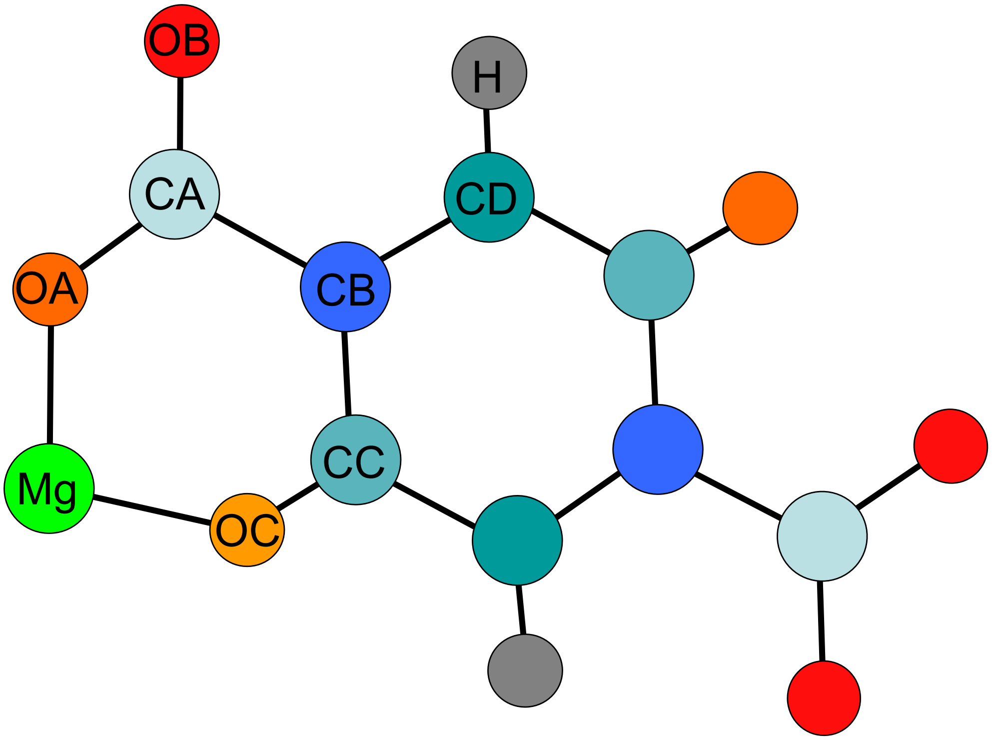

Table 18. Lennard-Jones parameters for atoms in ZnMOF-74 based on the data from Yazaydin et al[26].

(pseudo-) atom	σ / Å	ε/k_B / K	charge
Zn	4.045	27.68	1.206
OA	3.033	48.16	-0.670
OB	3.033	48.16	-0.659
OC	3.033	48.16	-0.702
CA	3.473	47.86	0.767
CB	3.473	47.86	-0.292
CC	3.473	47.86	0.325
CD	3.473	47.86	-0.147
H	2.846	7.650	0.172

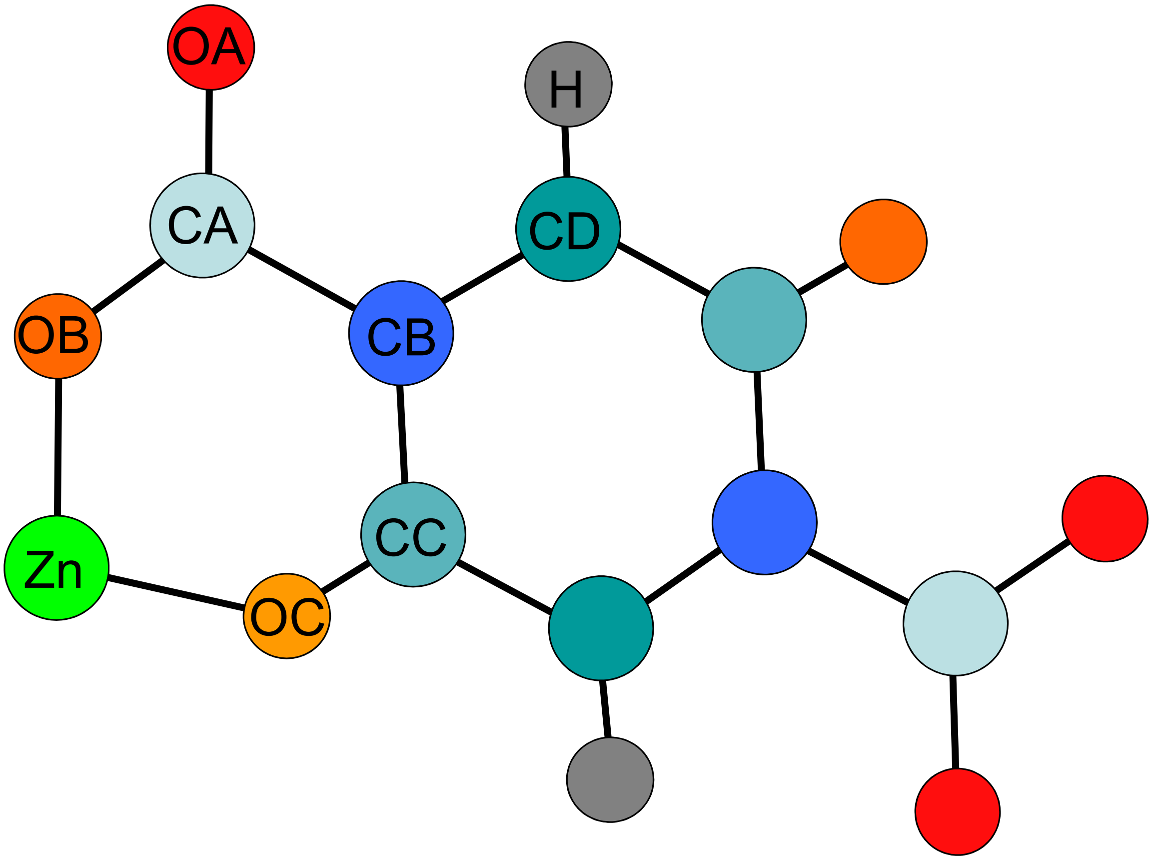

Table 19. Lennard-Jones parameters for the framework atoms of MOF-177. The framework charges of MOF-177 were estimated using the group-contribution procedure based on quantum mechanical calculations described by Xu and Zhong. [42]

(pseudo-) atom	σ / Å	ε/k_B / K	charge
CA	3.473	47.86	0.8056
CB	3.473	47.86	0.0496
CC	3.473	47.86	-0.1304
H	2.846	7.650	0.1086
OA	3.033	48.16	-1.9214
OB	3.033	48.16	-0.7934
Zn	4.044	27.68	1.5916

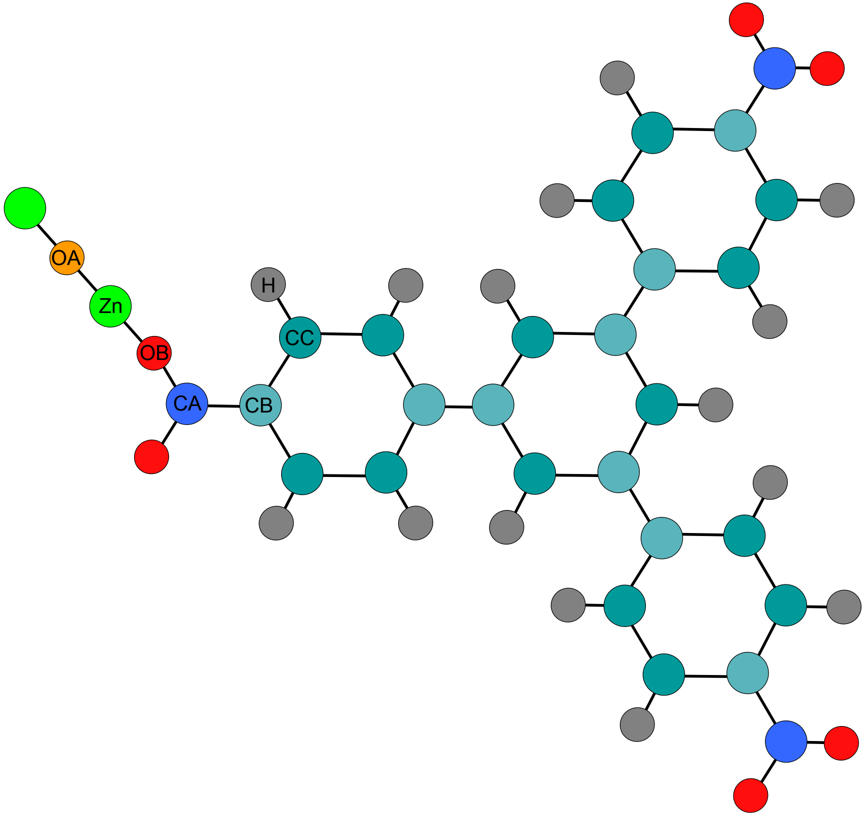

Table 20. Lennard-Jones parameters for framework atoms of BeBTB

(pseudo-) atom	σ / Å	ε/k_B / K
Be	2.446	42.78
C	3.473	47.86
O	3.033	48.16
H	2.846	7.650

Table 21. Lennard-Jones parameters for framework atoms of Co(BDP)

(pseudo-) atom	σ / Å	ε/k_B / K
Co	2.559	7.046
C	3.473	47.86
H	2.846	7.650
N	3.263	38.95

Table 22. Lennard-Jones parameters for framework atoms of CuBTT

(pseudo-) atom	σ / Å	ε/k_B / K
Cl	3.519	142.58
Cu	3.114	2.516
C	3.473	47.86
H	2.846	7.650
N	3.263	38.95

Table 23. Molecular simulations of pore volumes and surface areas for the structures investigated.

Structure	**Pore volume** / cm^3 g^{-1}	**Surface area** / m^2 g^{-1}
MFI	0.165	487.2
ISV	0.278	911.4
BEA	0.271	922.7
BOG	0.241	758.4
GME	0.265	717.6
LTL	0.170	520.6
MOR	0.166	416.7
FER	0.160	402.5
FAUSI	0.328	986.4
ITQ-29	0.283	773.3
LTASI	0.310	894.1
TSC	0.344	858.2
CHA	0.264	757.5
ERI	0.228	635.3
DDR	0.139	181.9
AFX	0.246	674.5
ZIF-8	0.515	1164.4
BeBTB	1.908	4706.4
MOF-177	1.968	4780.8
CoBDP	0.927	2148.8
ZnMOF-74	0.582	1175.5
MgMOF-74	0.782	1642.6
NiMOF-74	0.582	1239.3
CoMOF-74	0.599	1273.8
CuBTT(blocked)	0.709	1564.6
IRMOF1	1.369	3522.2
MIL47	0.606	1472.8
MIL53(Cr)-lp	0.518	1280.5
Zn(bdc)dabco	0.801	2022.5

Table 24. Molecular simulations of pore volumes, surface areas, and Delaunay diameters for the Additional Zeolites investigated.

Structure	**Pore volume** / $cm^3\ g^{-1}$	**Surface area** / $m^2\ g^{-1}$	**Delaunay diameter**/ Å
AFT	0.263	819.6	3.62
BIK	0.081	1.4	3.49
EPI	0.156	243.7	3.42
JBW	0.086	25.1	3.66
LEV	0.232	612.8	3.61
LOV	0.154	93.5	3.71
SIV	0.187	270.6	3.31

All-silica
Zeolites
(in alphabetical order)

AFI landscapes

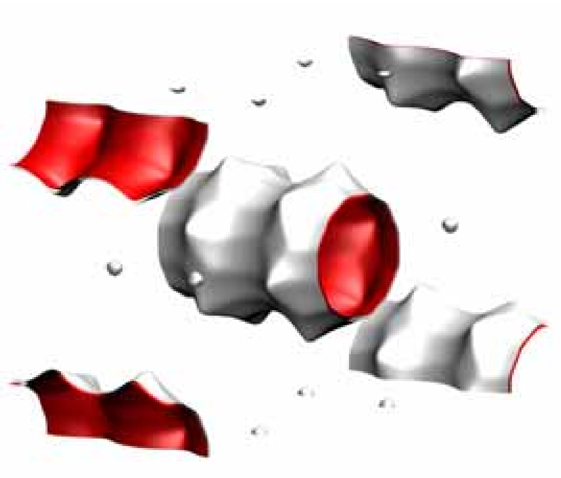

12-ring
channel of AFI

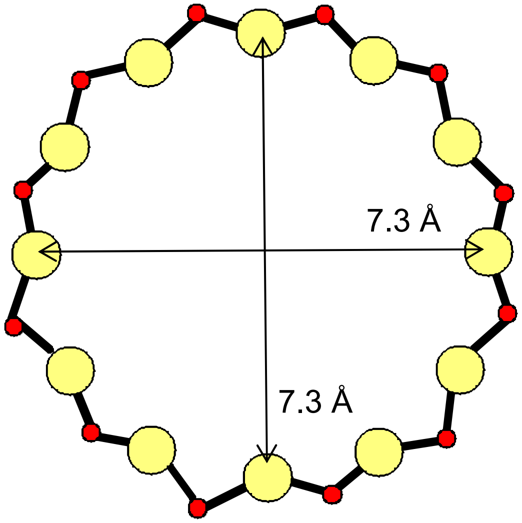

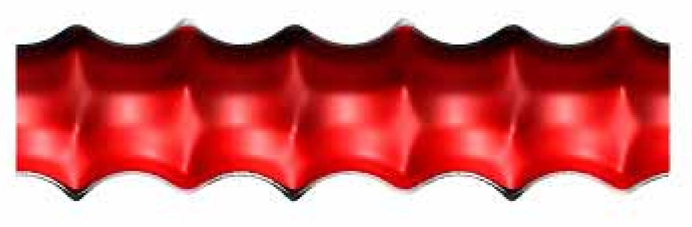

Snapshots showing location of CH_4 and CO_2

To convert from molecules per unit cell to mol kg^{-1}, multiply by 0.3467.
The pore volume is 0.159 cm^3/g.

AFI CBMC mixture simulations for CO_2 capture

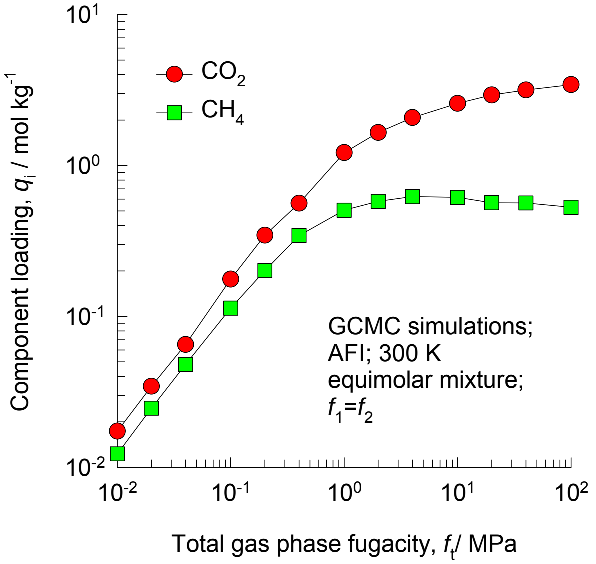

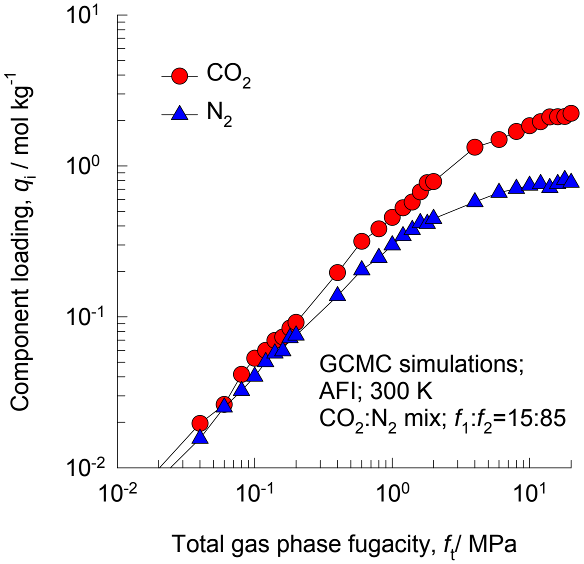

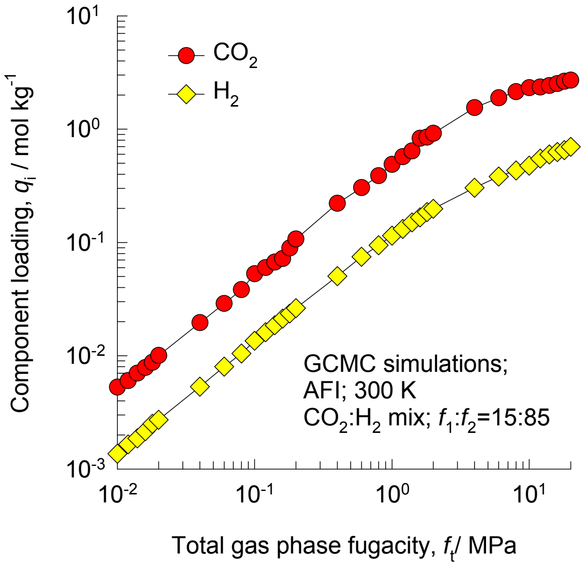

AFI CBMC nC6/3MP/22DMB mixture simulations

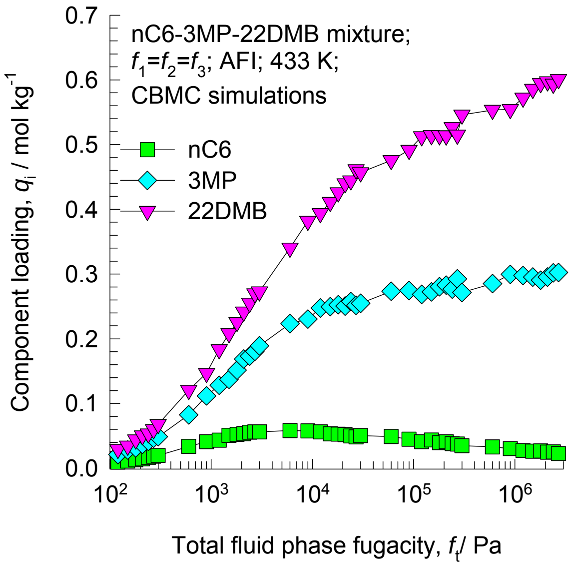

$$S_{ads} = \frac{\dfrac{q_{22DMB}}{f_{22DMB}}}{\dfrac{q_{nC6}}{f_{nC6}} + \dfrac{q_{3MP}}{f_{3MP}}}$$

Capacity is the total loading of 22DMB.

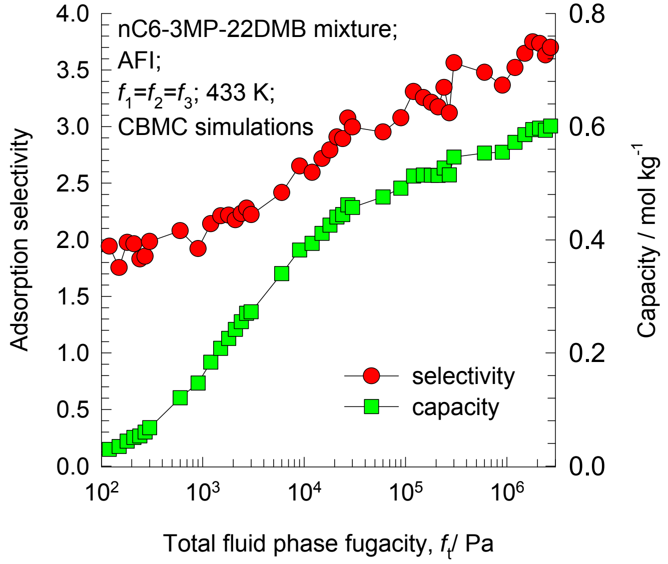

AFI snapshot of hexane isomers

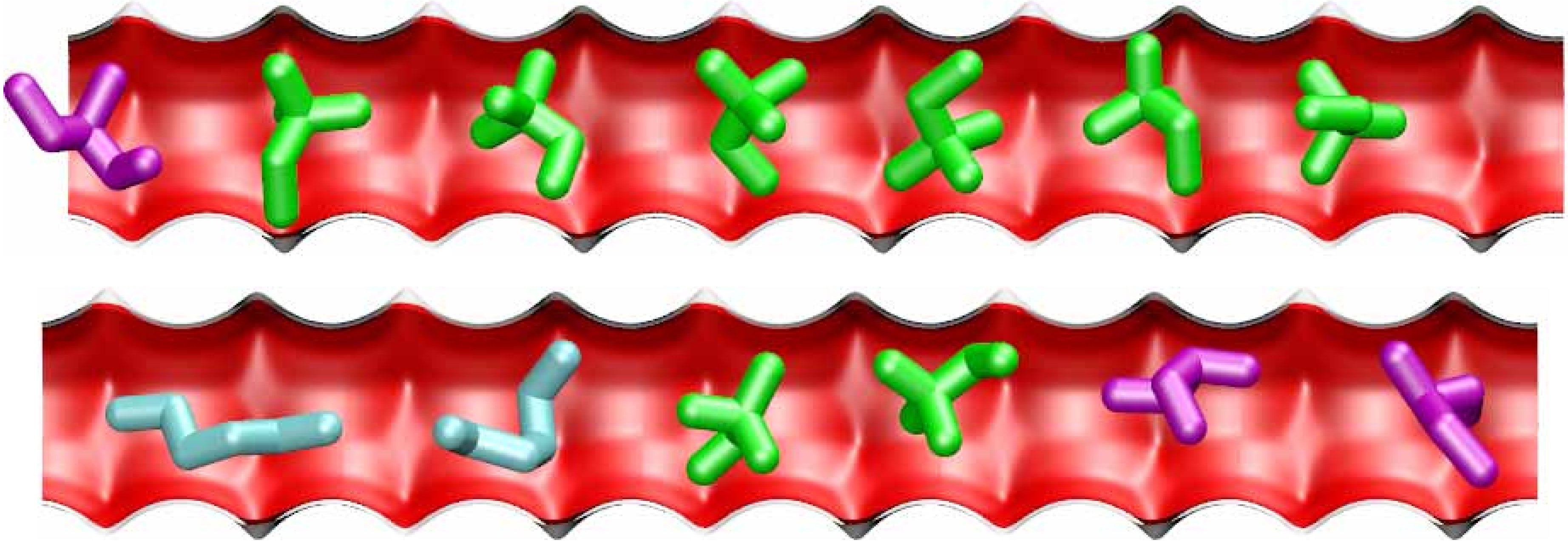

AFX pore landscape

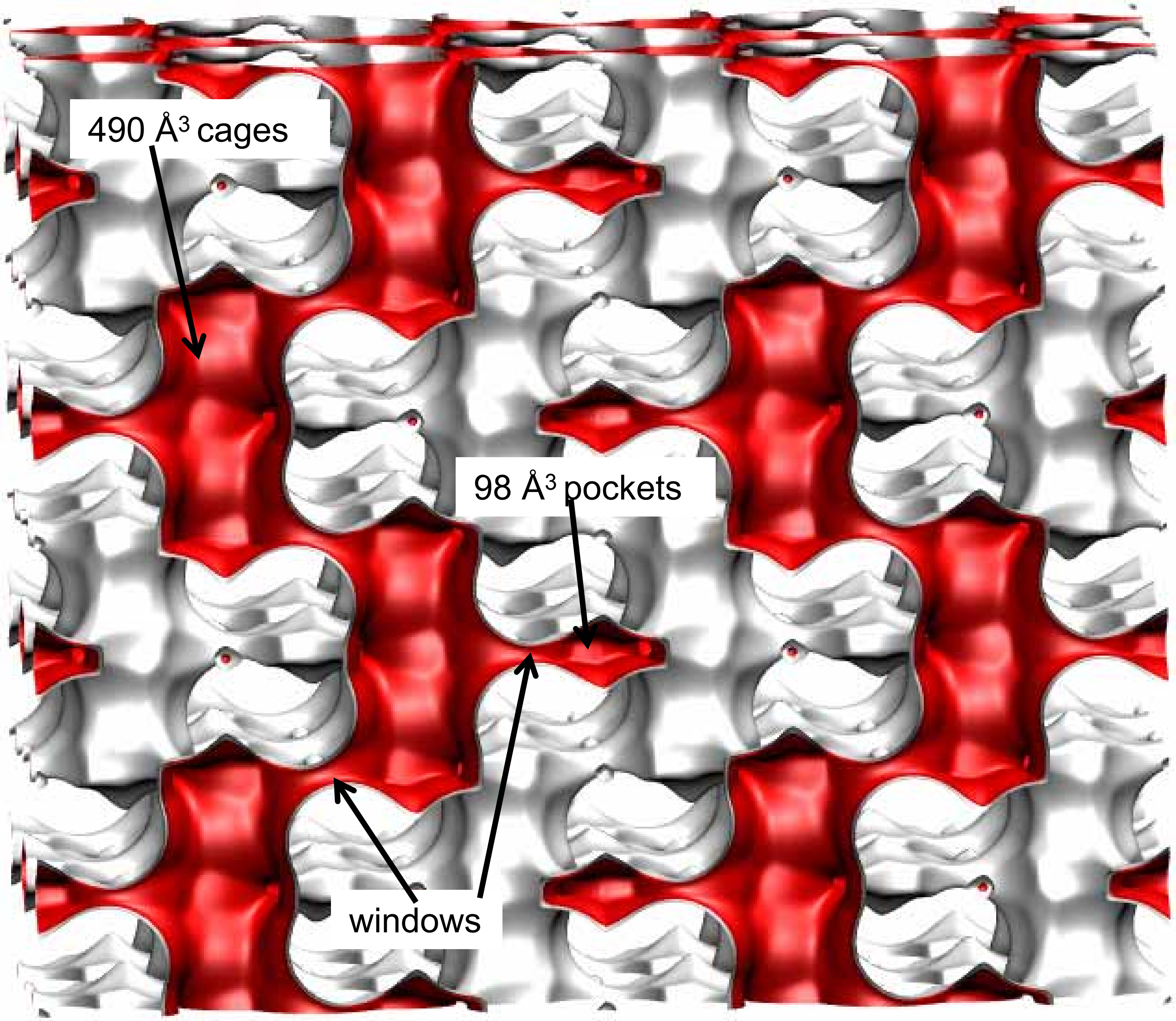

To convert from molecules per unit cell to mol kg^{-1}, multiply by 0.1734.
The pore volume is 0.2456 cm^3/g.

AFX window sizes

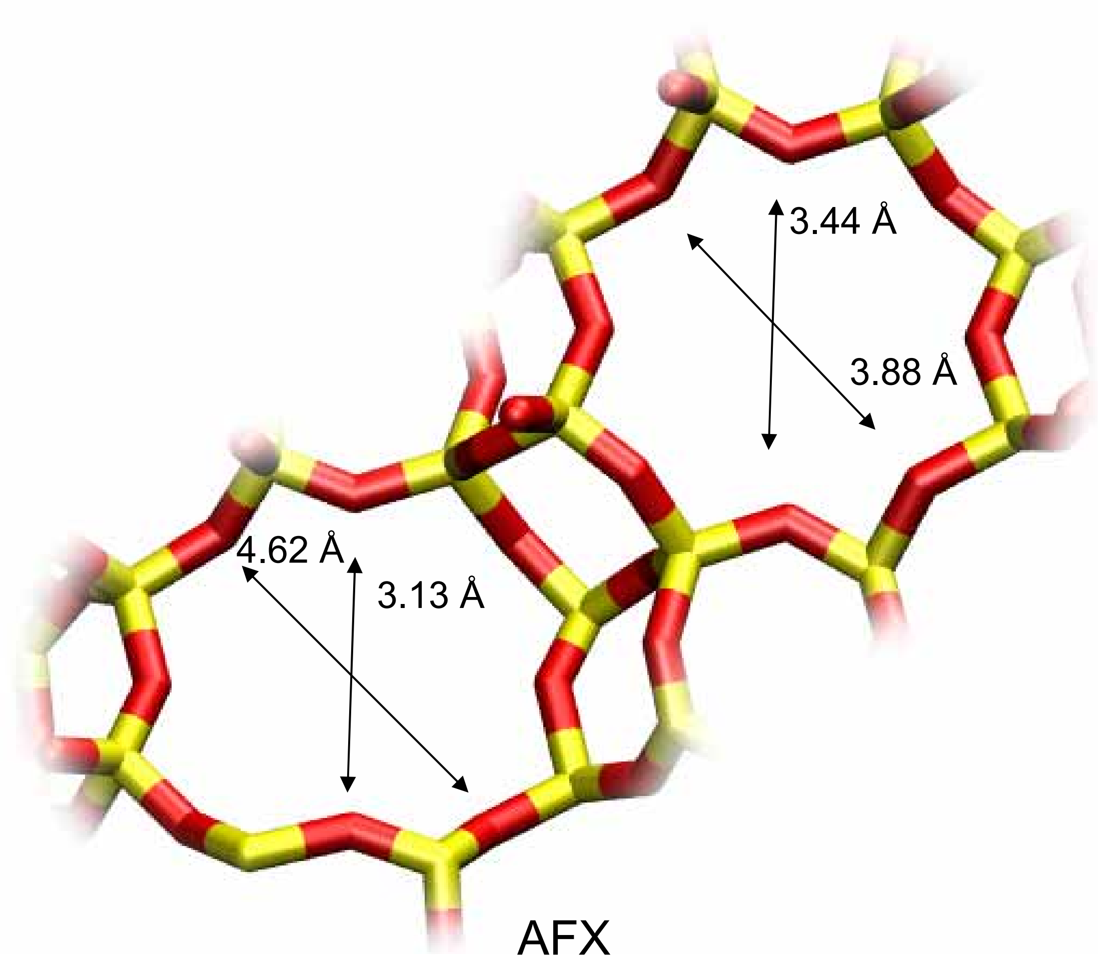

The window dimension calculated using the van der Waals diameter of framework atoms = 2.7 Å are indicated above by the arrows.

AFX CO_2/CH_4 mixture

CO_2 preferentially locates in the side pockets and this is the reason for the high selectivity. The situation is quite similar to that for MOR zeolite.

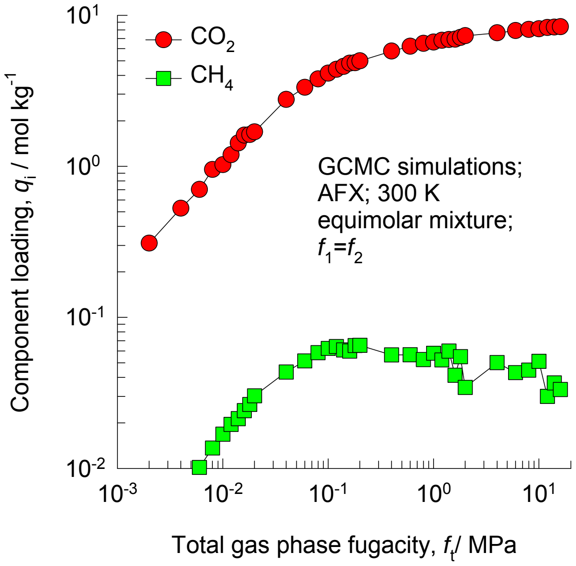

GCMC simulations;
AFX; 300 K
equimolar mixture;
$f_1=f_2$

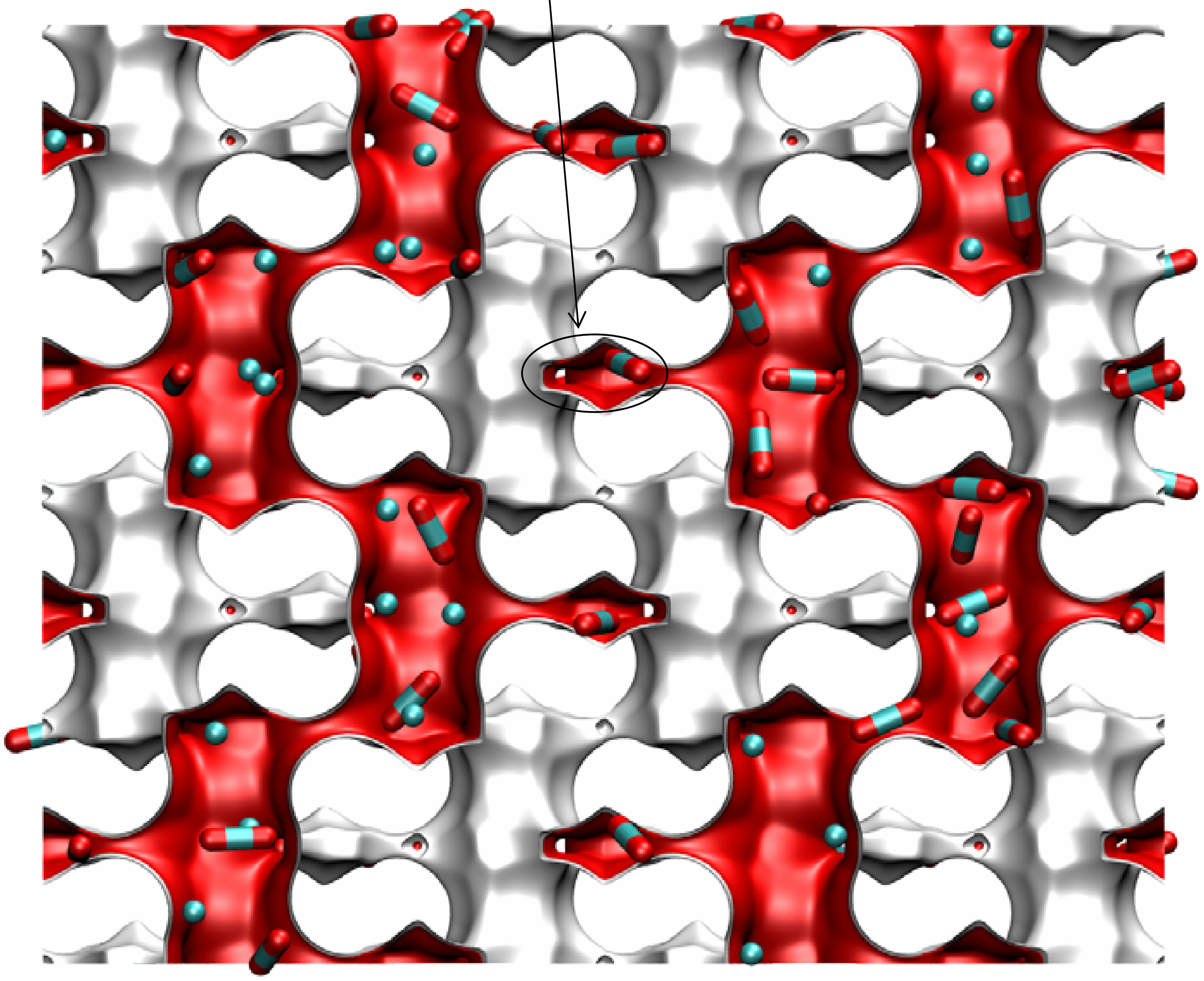

AFX CO_2/N_2 mixture

CO_2 preferentially locates in the side pockets and this is the reason for the high selectivity. The situation is quite similar to that for MOR zeolite.

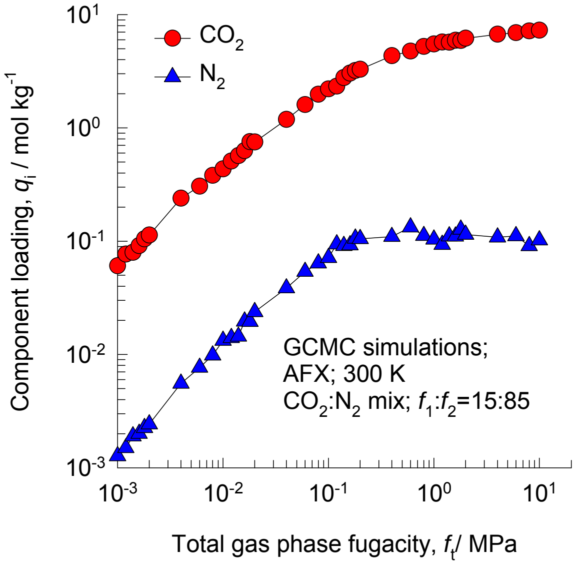

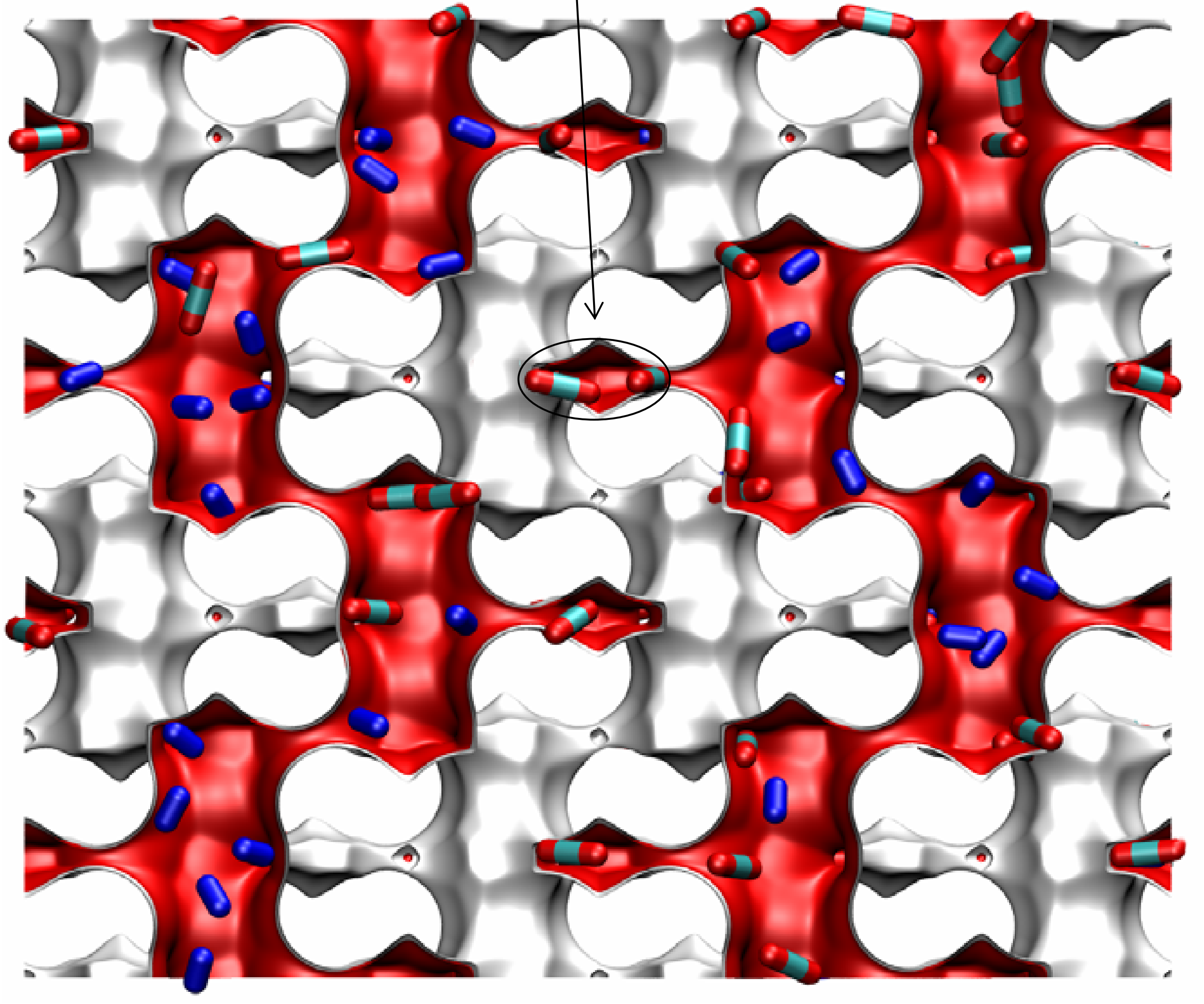

AFX CO_2/H_2 mixture

CO_2 preferentially locates in the side pockets and this is the reason for the high selectivity. The situation is quite similar to that for MOR zeolite.

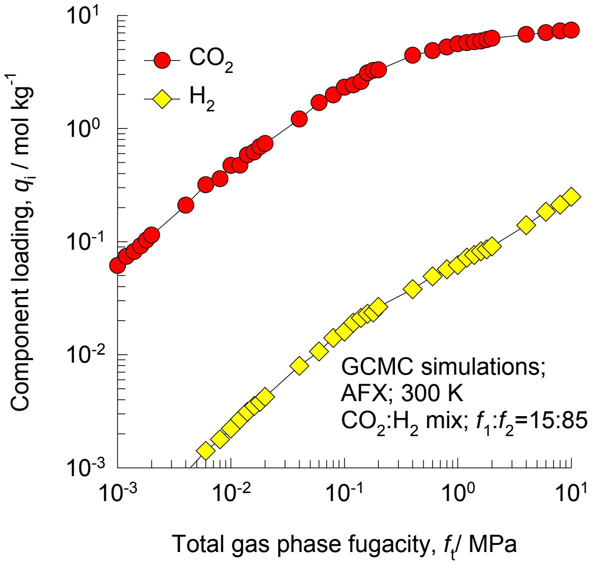

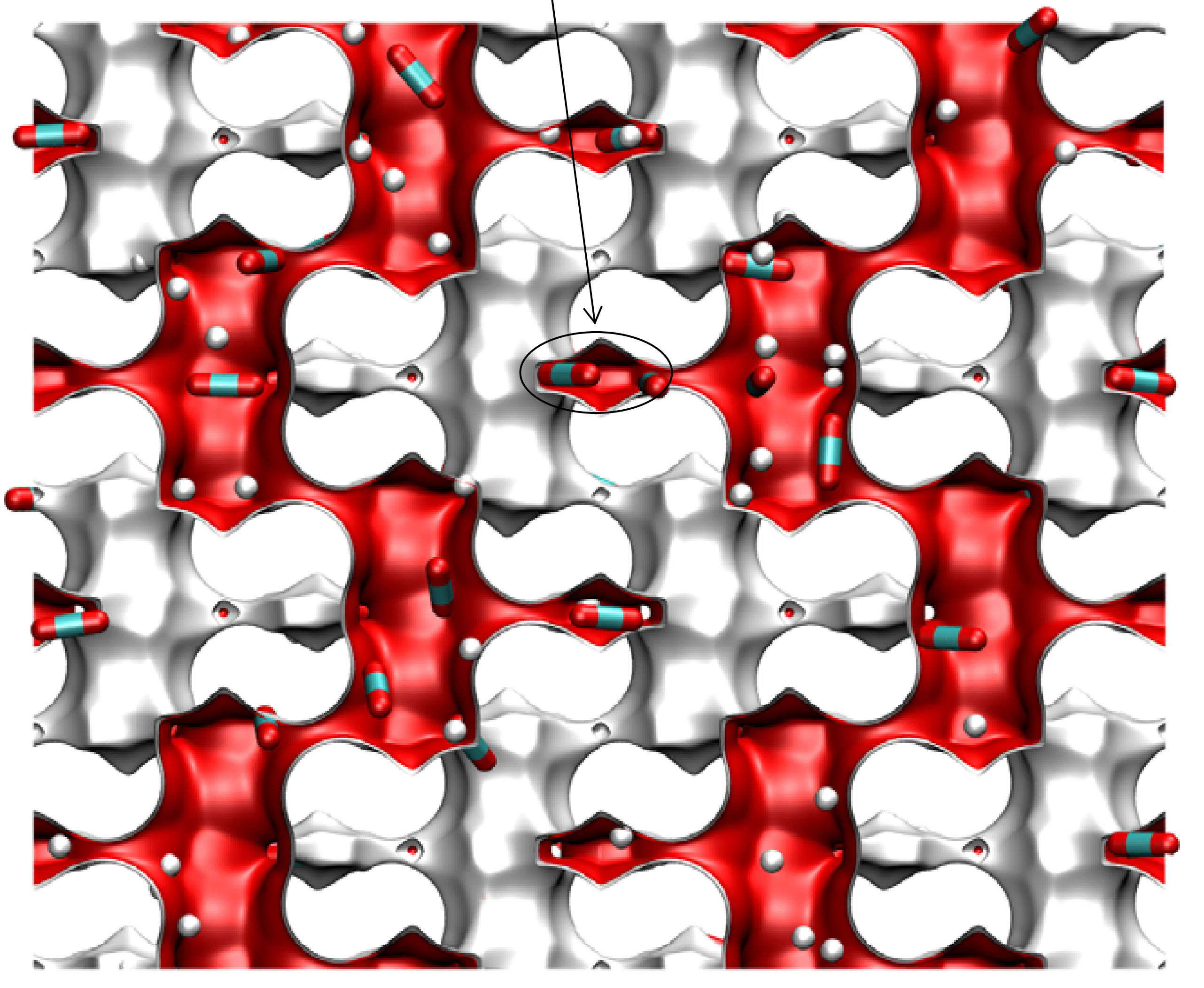

AWW landscapes

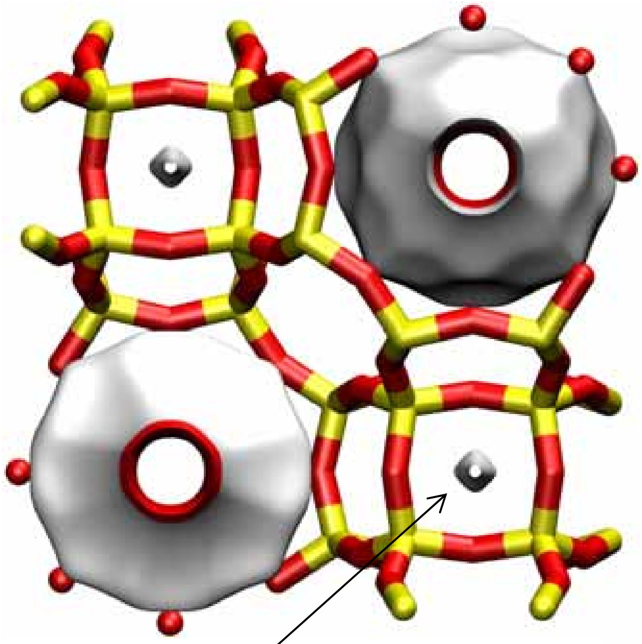

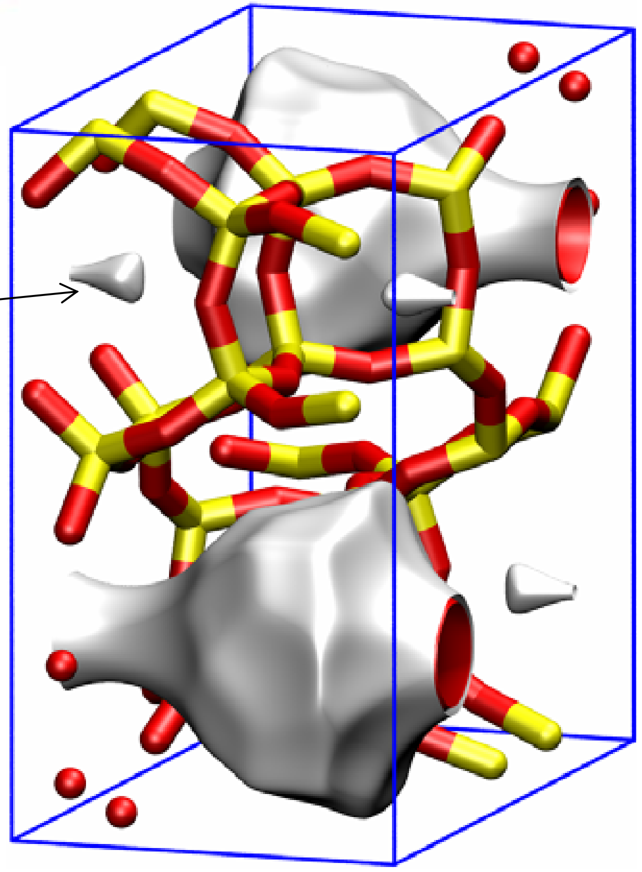

These inaccessible pockets are blocked in the simulations

To convert from molecules per unit cell to mol kg^{-1}, multiply by 0.69346.
The pore volume is 0.184 cm^{3}/g.

AWW snapshots

Mixture of CH_4 and CO_2

Mixture of N_2 and CO_2

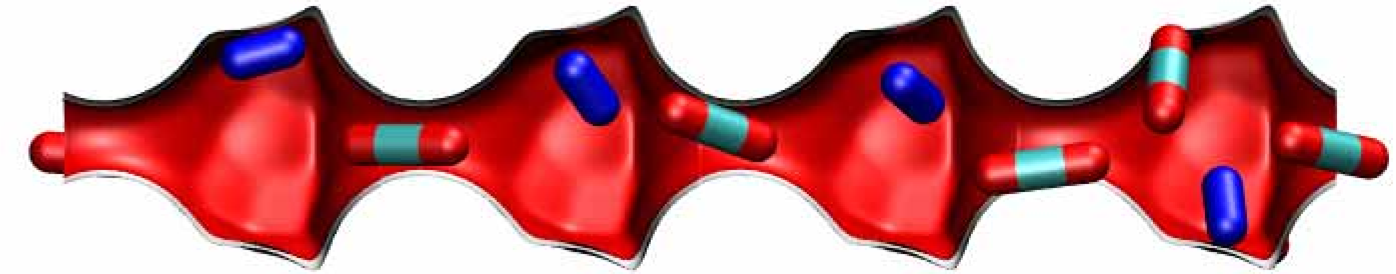

Mixture of H_2 and CO_2

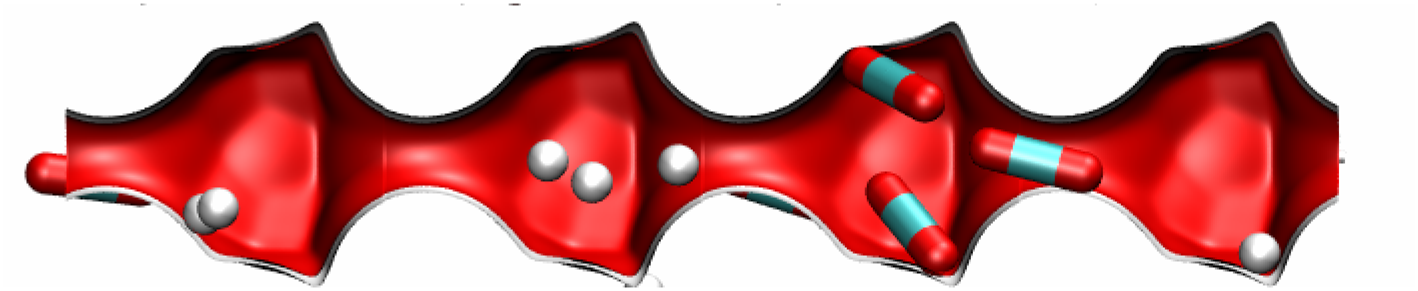

AWW CBMC mixture simulations for CO_2 capture

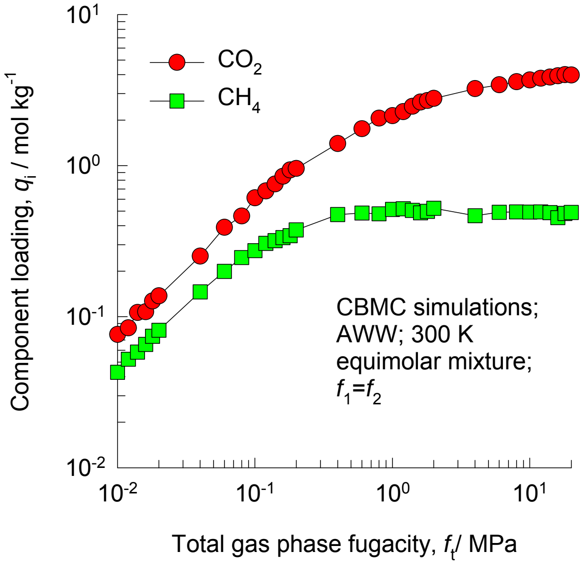

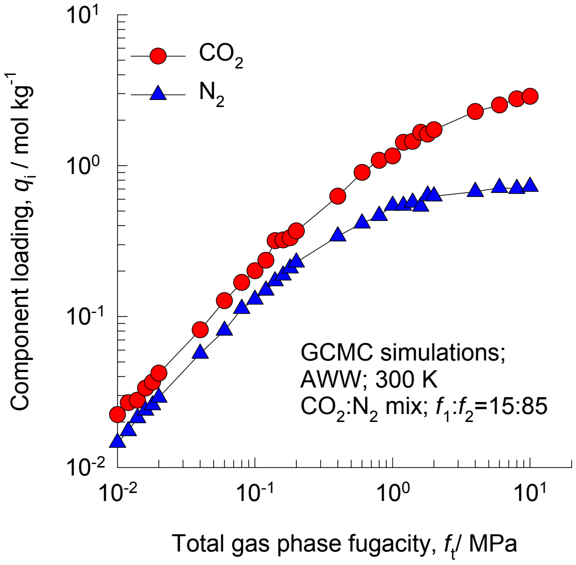

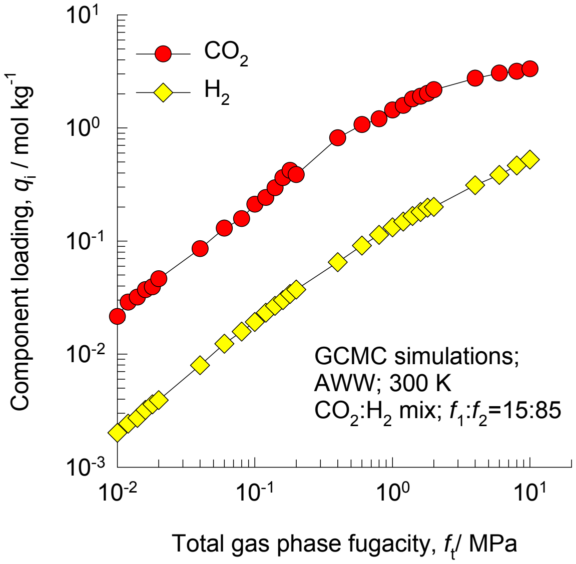

BEA pore landscape

To convert from molecules per unit cell to mol kg^{-1}, multiply by 0.26.
The pore volume is 0.271 cm^3/g.

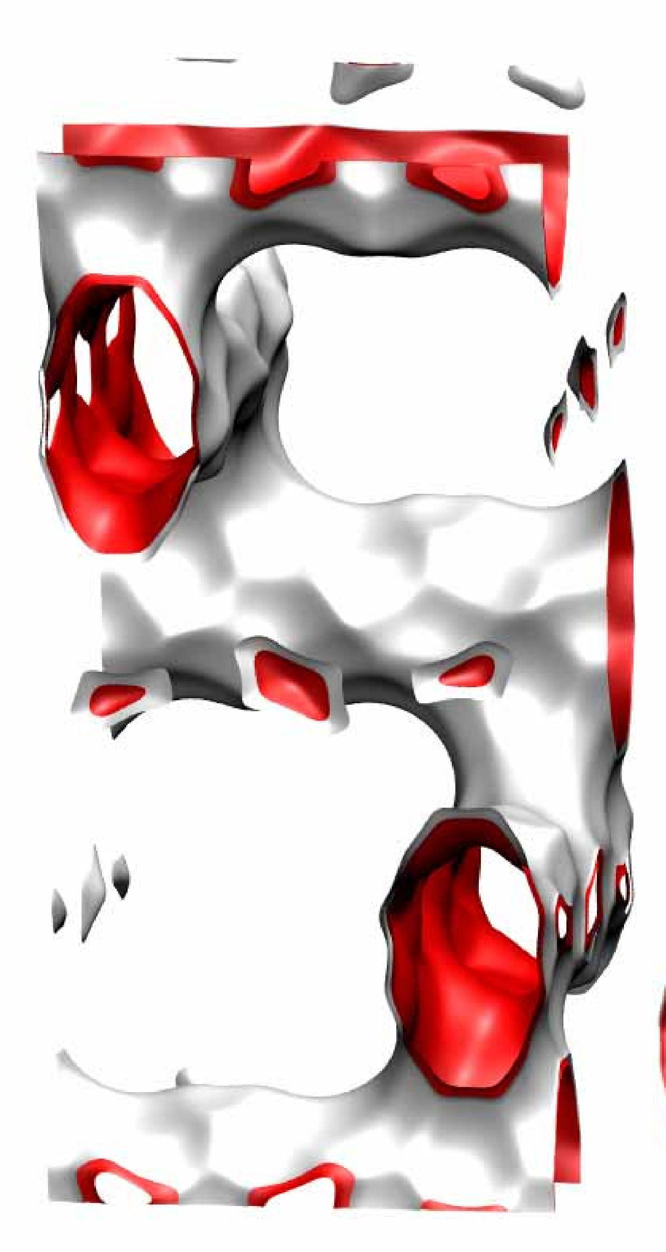

BOG has an intersecting channel system:
12-ring channels of 7.0 x 7.0 Å intersecting with
10-ring channels of 5.5 x 5.8 Å

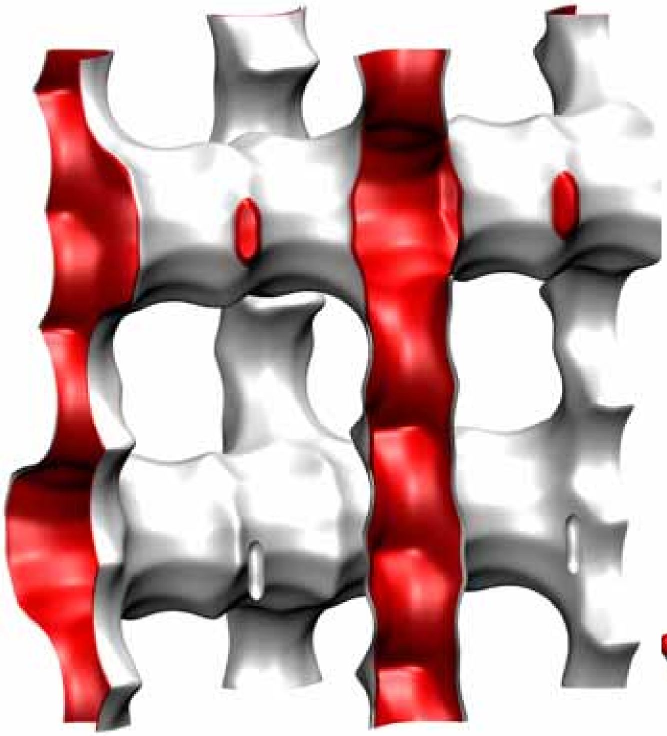

Snapshots showing location of CH_4 and CO_2

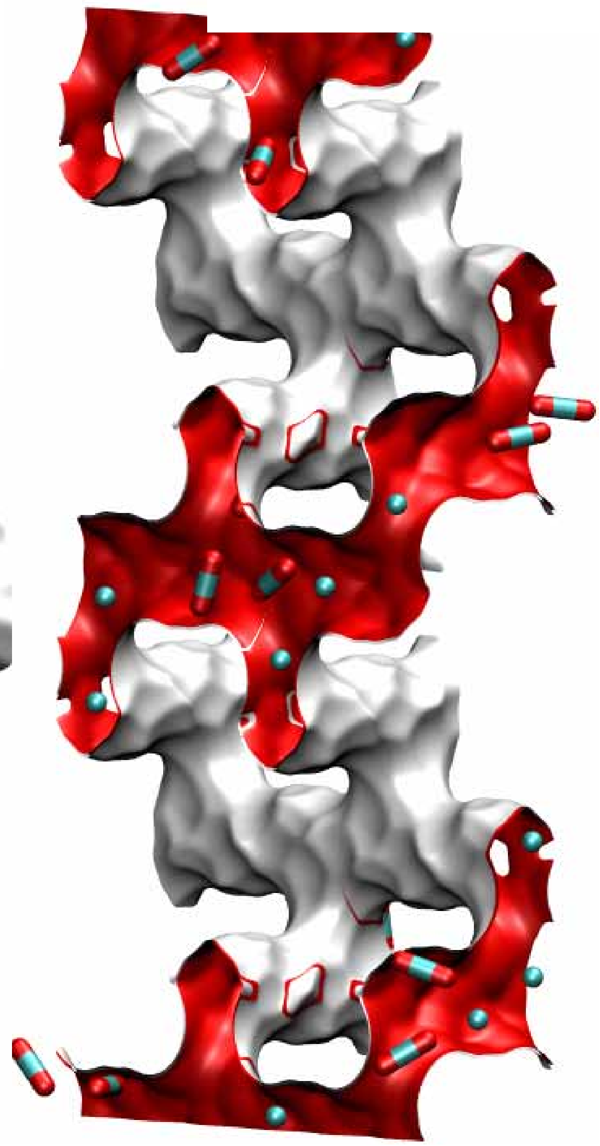

BEA CBMC mixture simulations for CO_2 capture

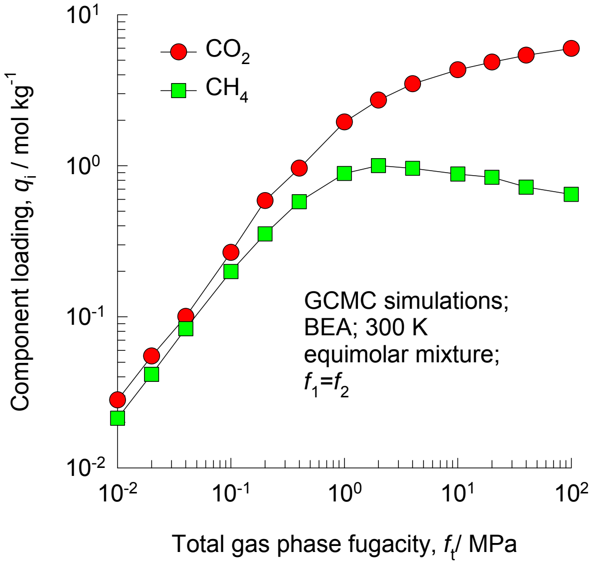

Snapshots showing location of CH_4 and CO_2

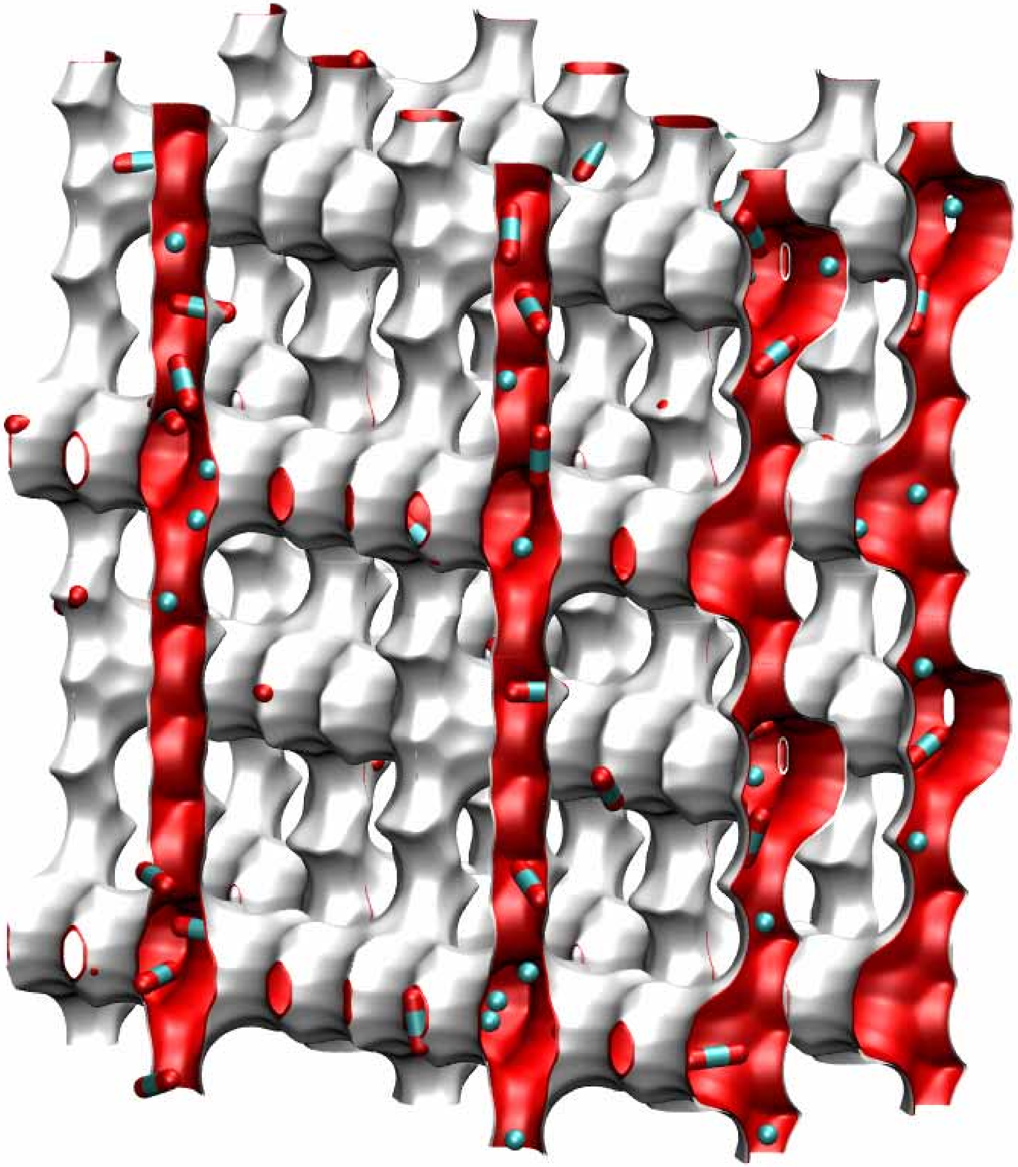

BEA CBMC nC6/3MP/22DMB mixture simulations

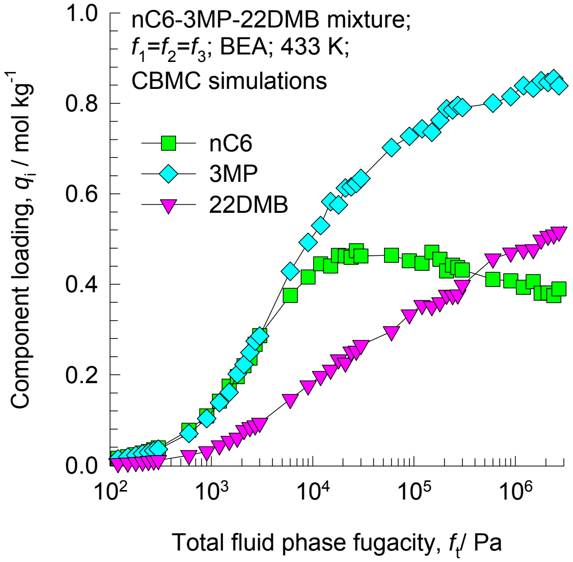

$$S_{ads} = \frac{\dfrac{q_{nC6}}{f_{nC6}} + \dfrac{q_{3MP}}{f_{3MP}}}{\dfrac{q_{22DMB}}{f_{22DMB}}}$$

Capacity is the total loading of nC6 + 3MP

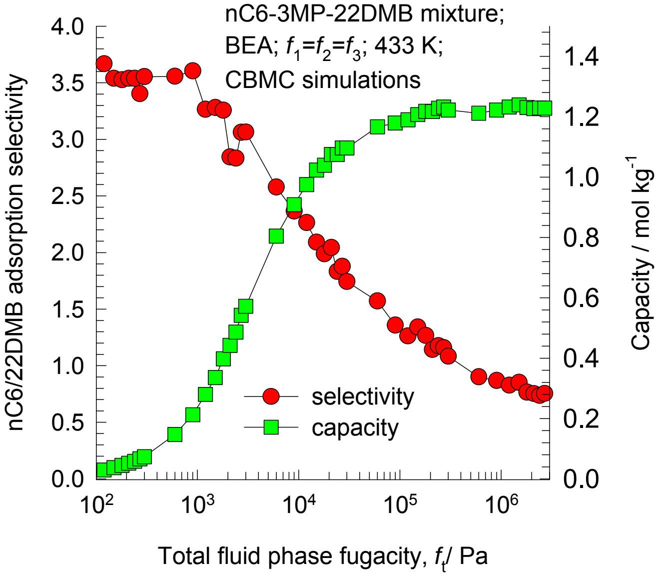

BEA snapshots of hexane isomers

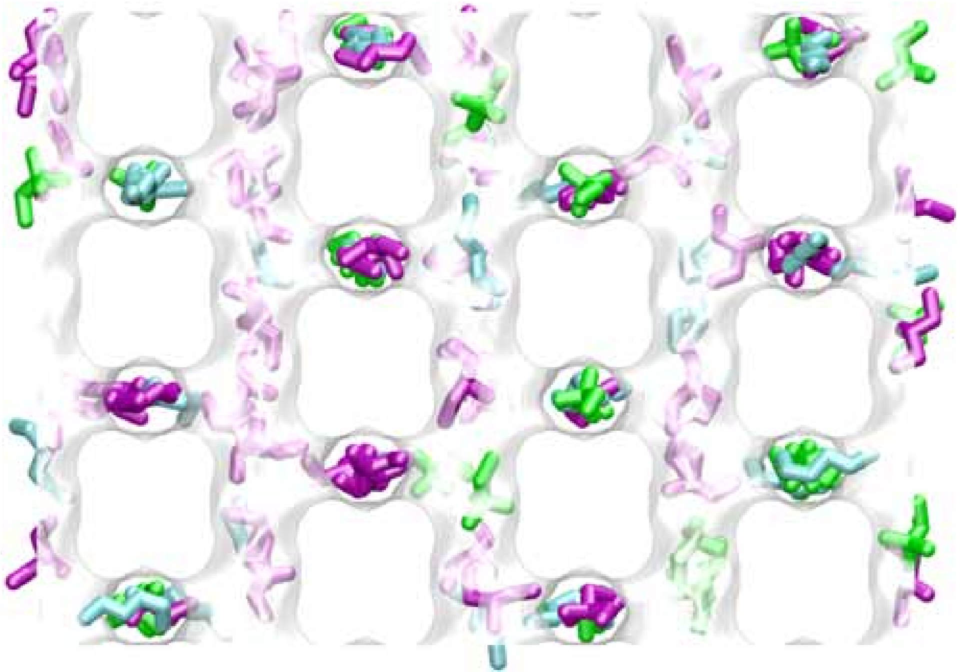

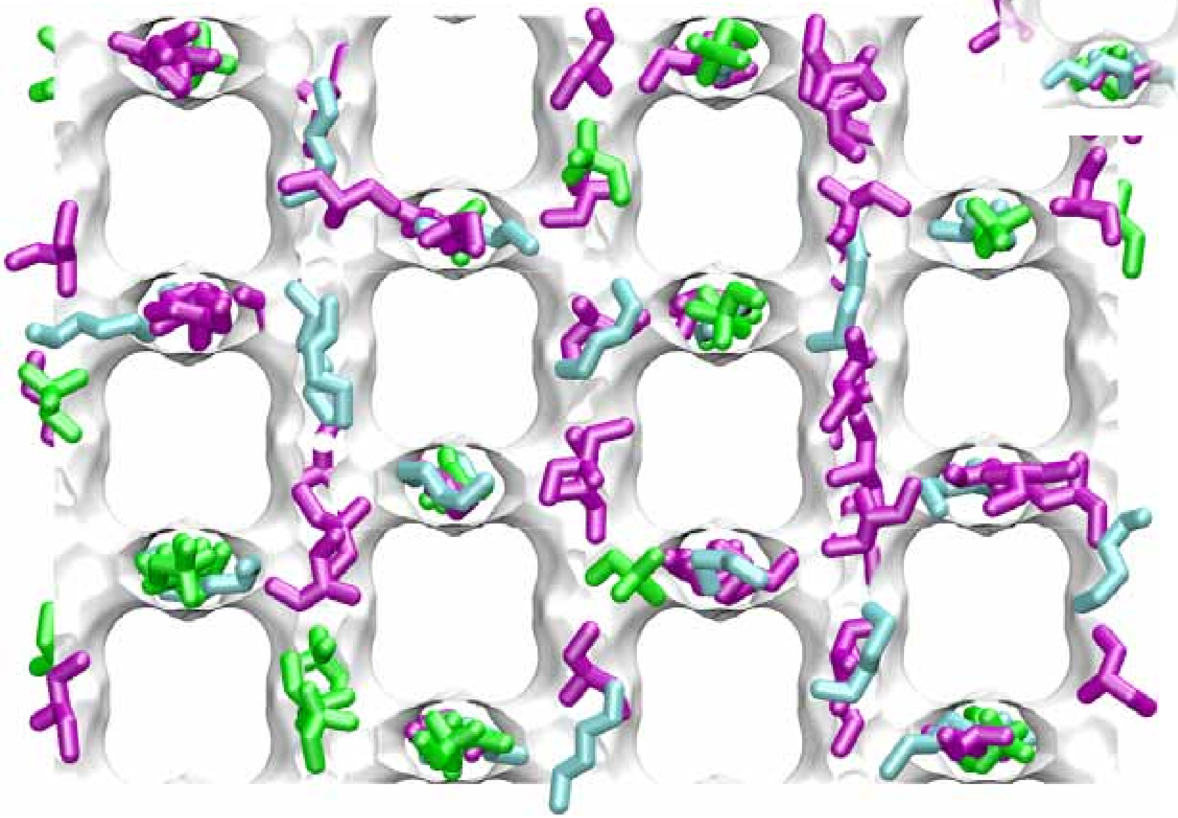

BEA snapshots of hexane isomers

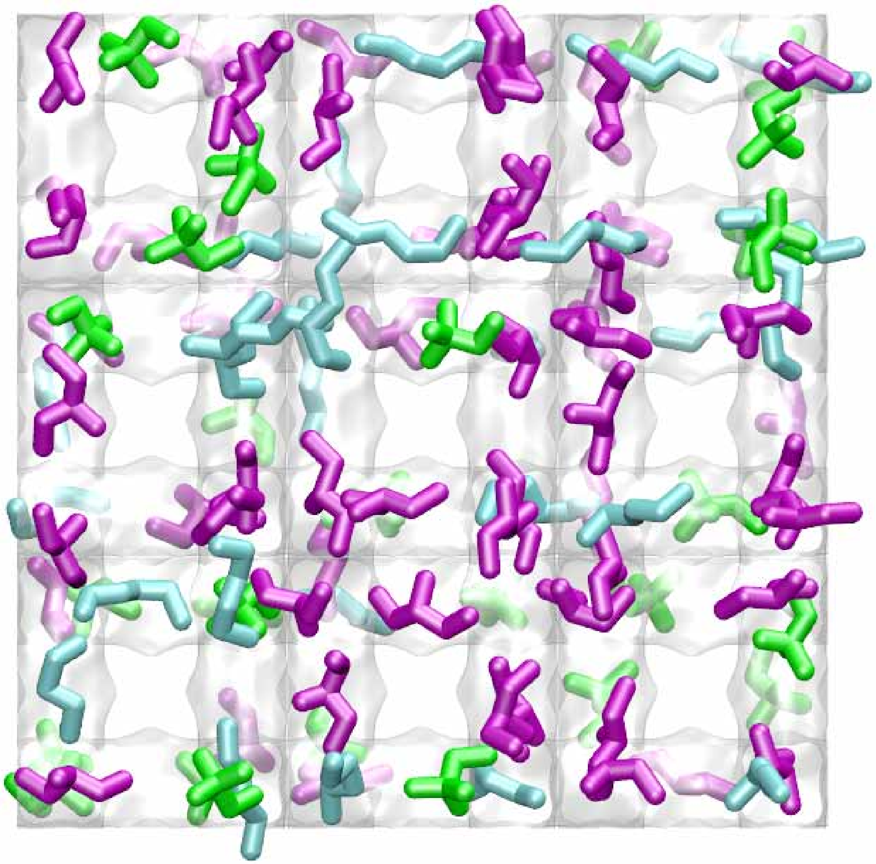

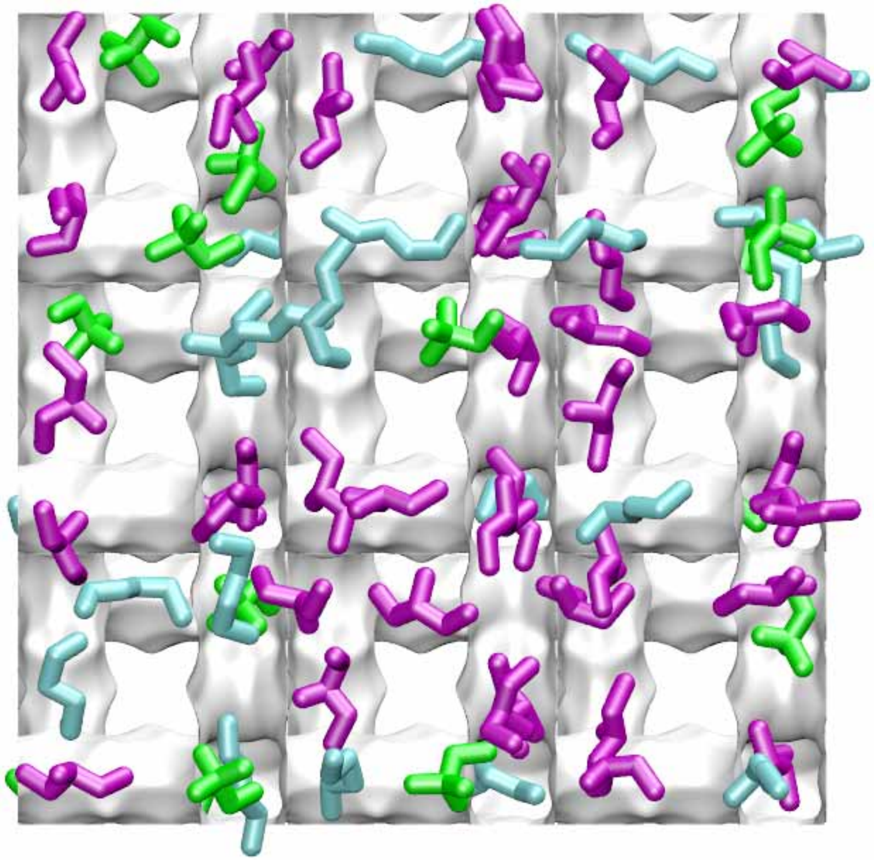

BOG pore landscape and snapshot of CO_2/CH_4 mixture

To convert from molecules per unit cell to mol kg^{-1}, multiply by 0.173366.
The pore volume is 0.241 cm^3/g.

BOG has an intersecting channel system:
12-ring channels of 7.0 x 7.0 Å intersecting with
10-ring channels of 5.5 x 5.8 Å

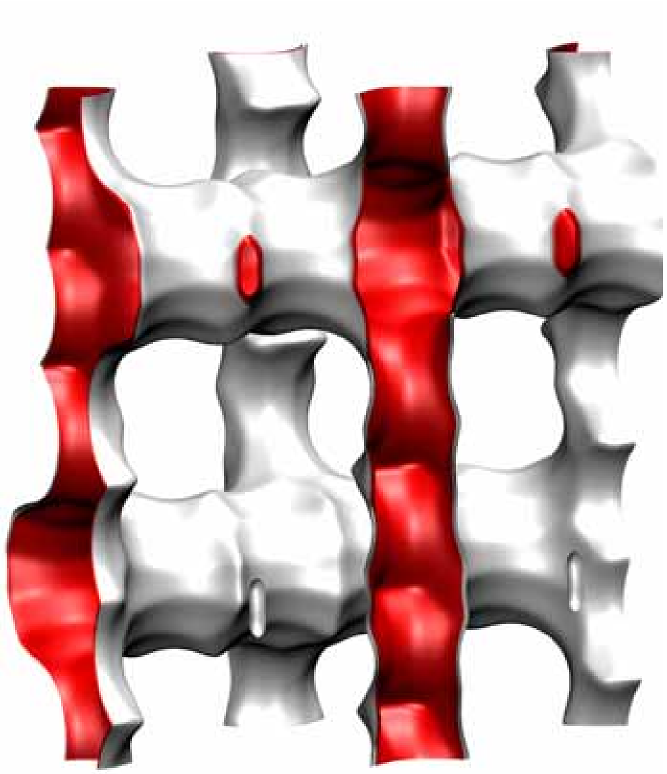

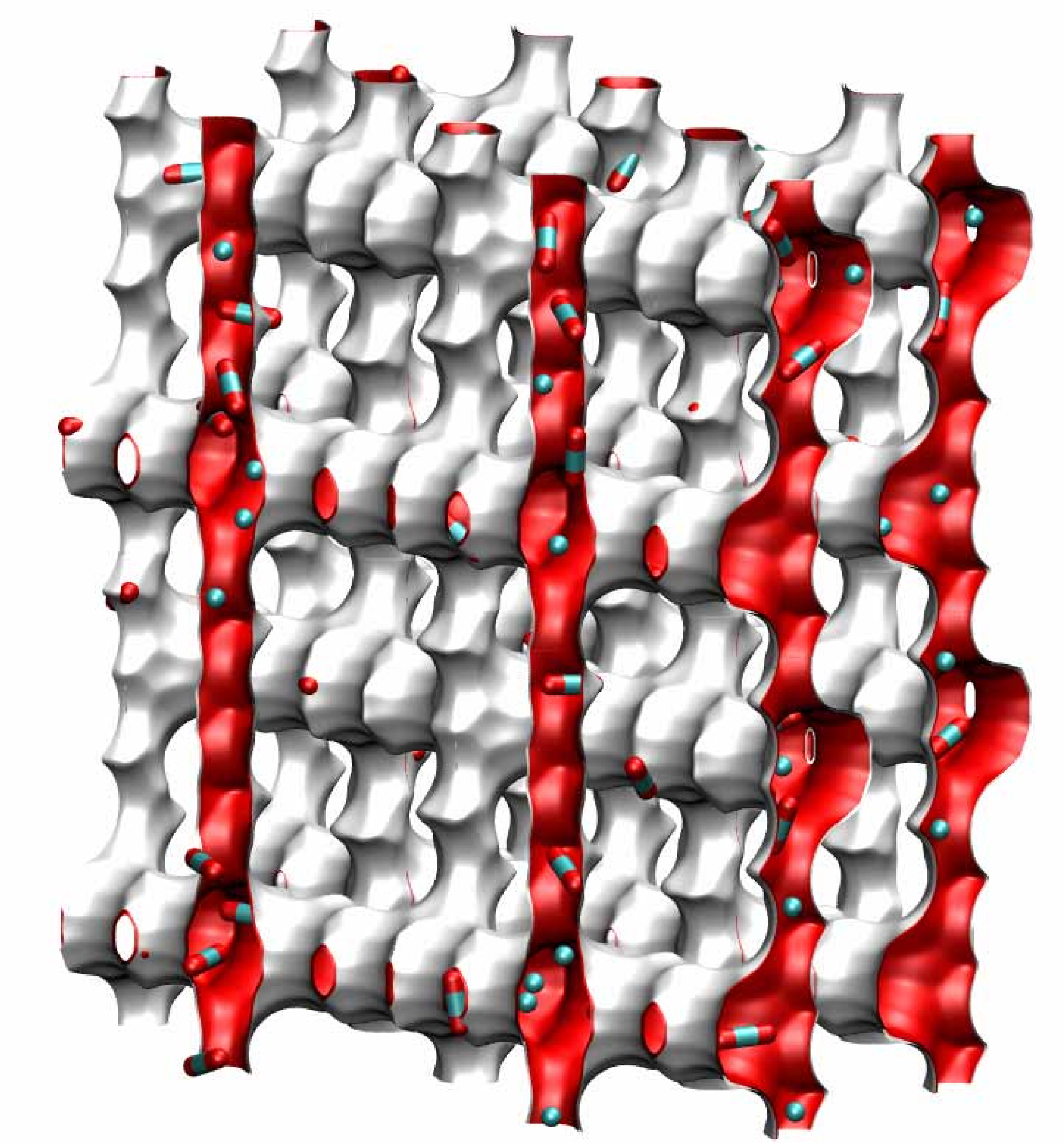

BOG CBMC mixture simulations for CO_2 capture

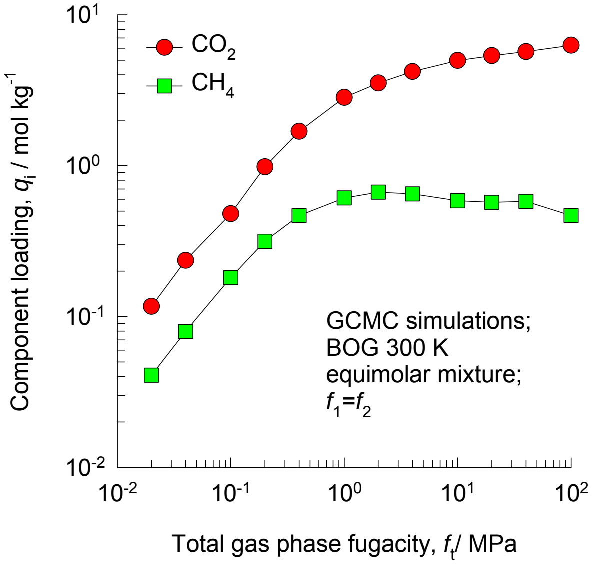

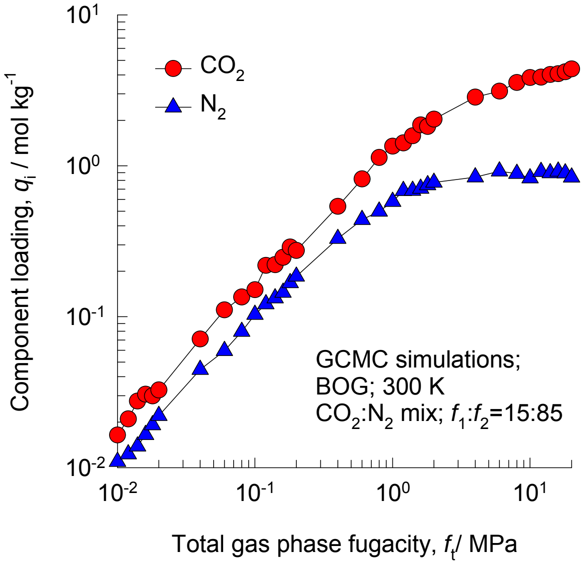

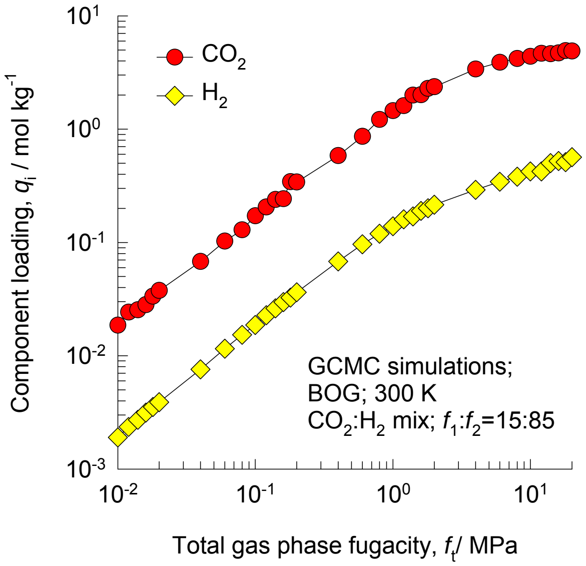

CHA (all silica)

To convert from molecules per unit cell to mol kg^{-1}, multiply by 0.2311.
The pore volume is 0.264 cm^3/g.

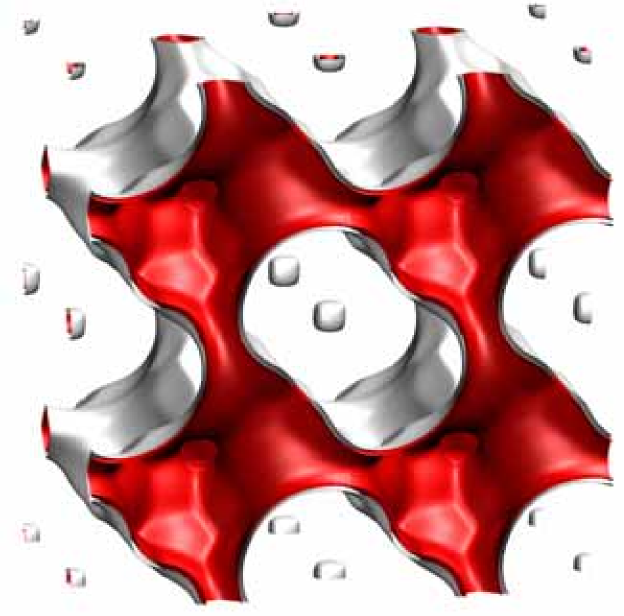

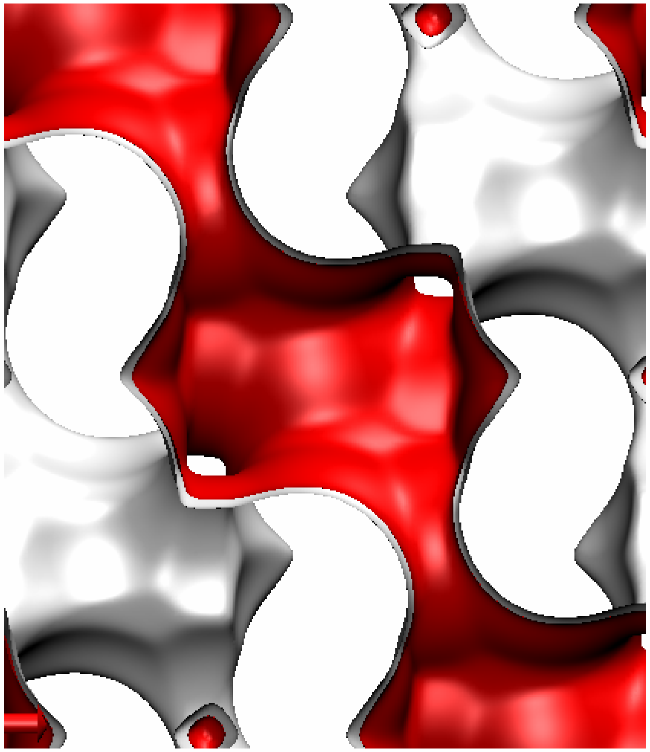

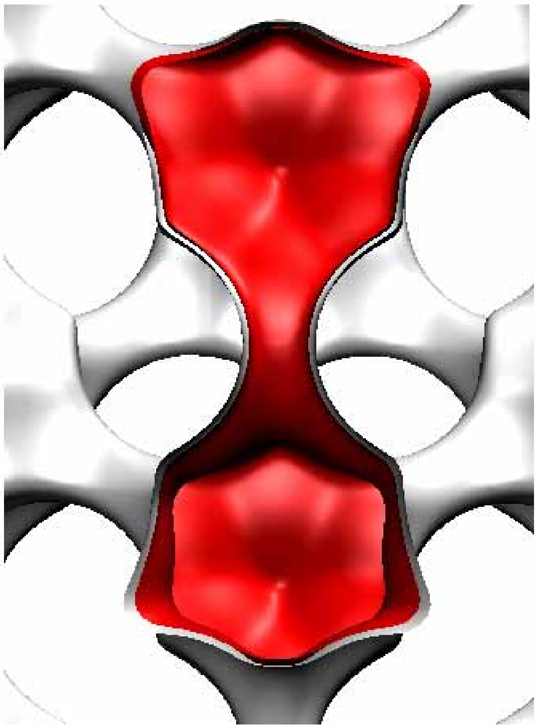

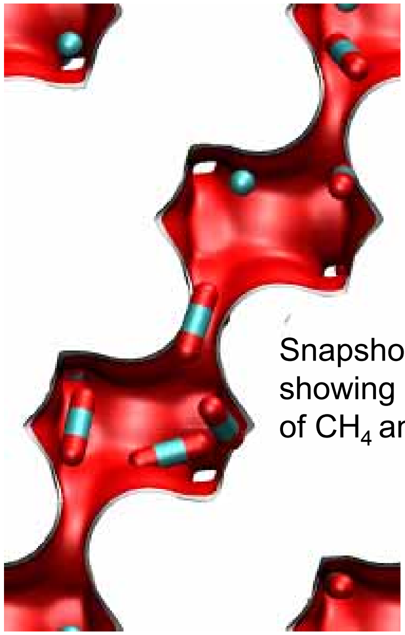

Snapshots showing location of CH_4 and CO_2

Snapshots showing location of CH_4

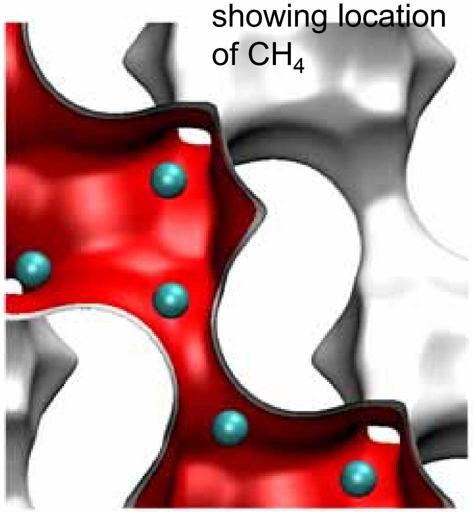

CHA CBMC mixture simulations for CO_2 capture

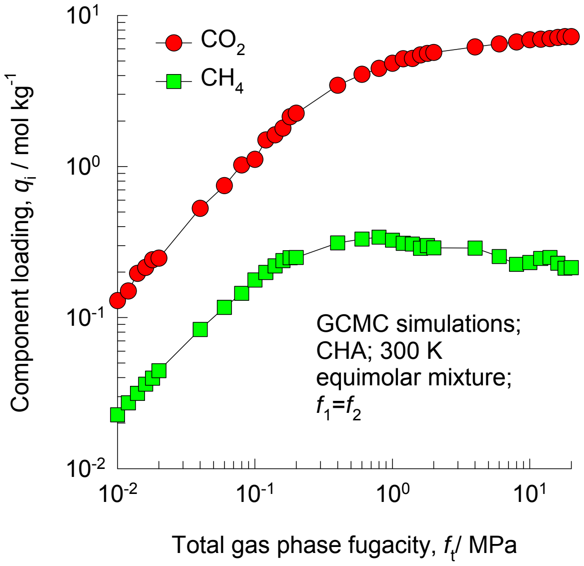

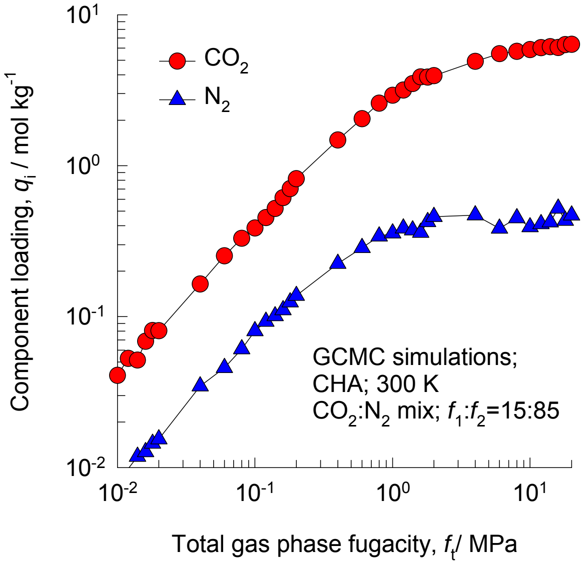

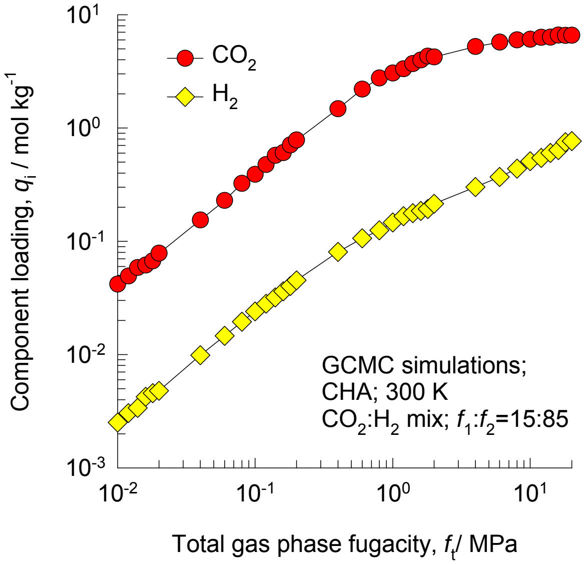

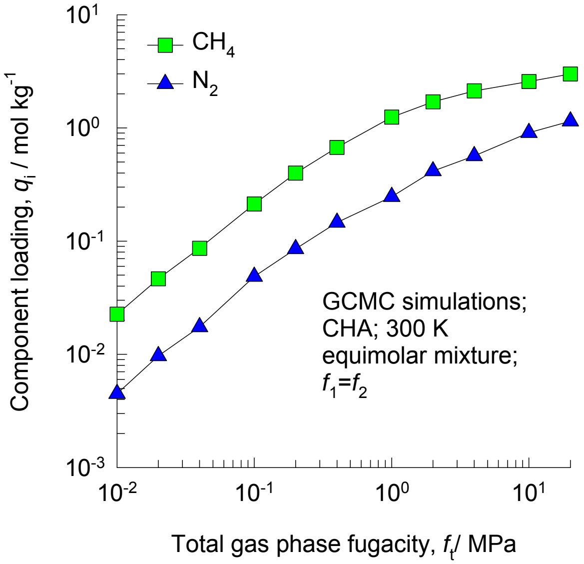

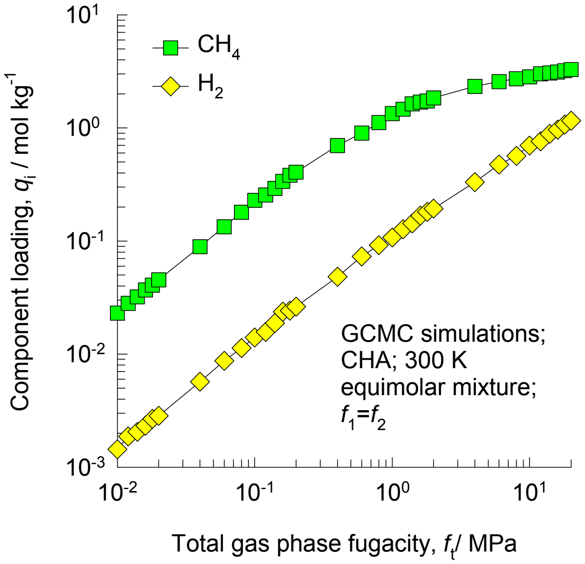

DDR

To convert from molecules per unit cell to mol kg^{-1}, multiply by 0.06936.
The pore volume is 0.139 cm^3/g.

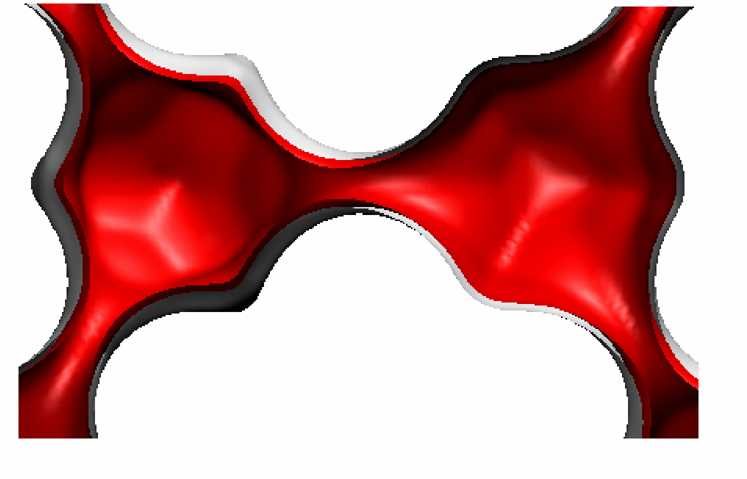

Snapshots showing location of CH_4 and CO_2

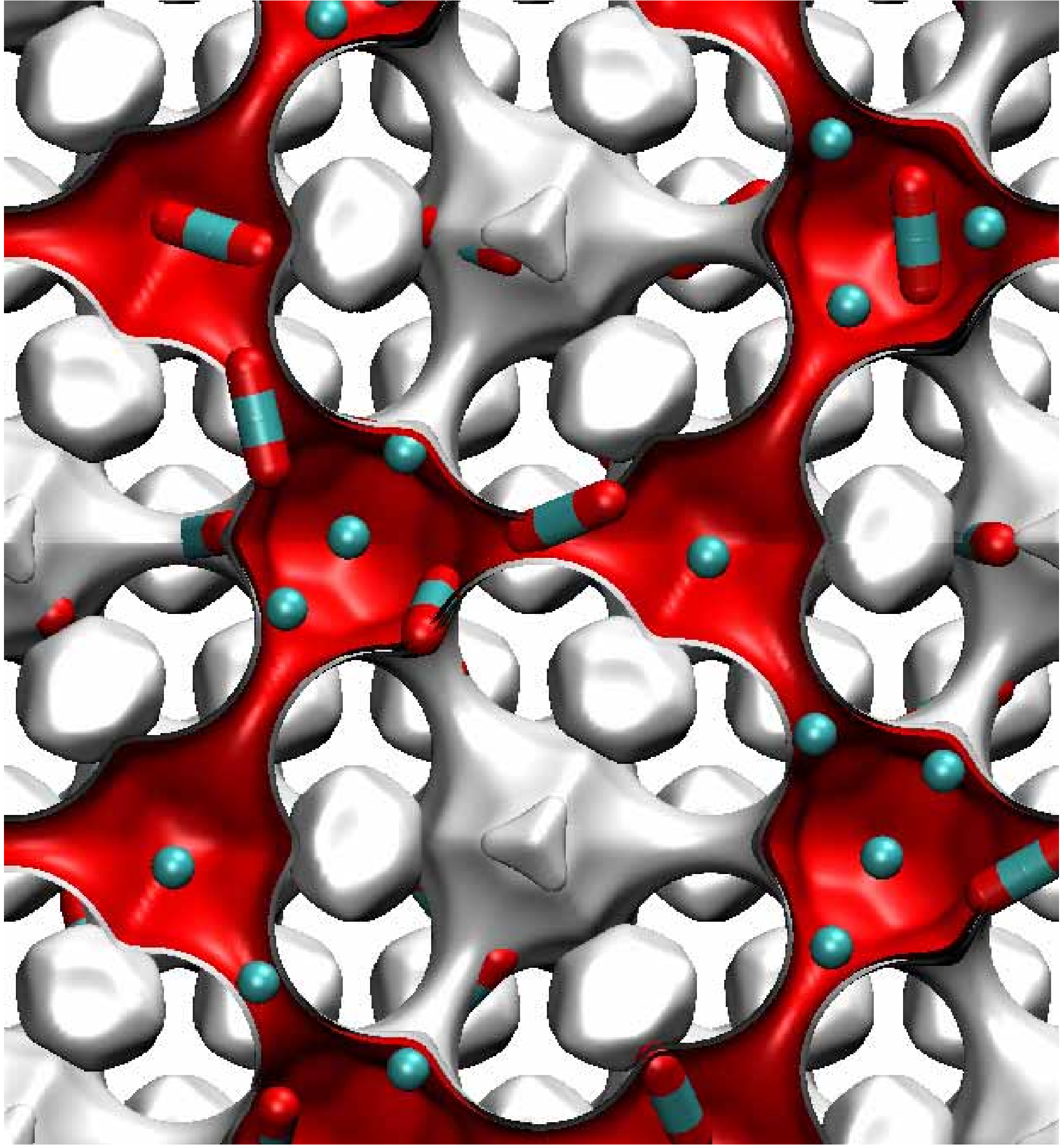

DDR CBMC mixture simulations for CO_2 capture

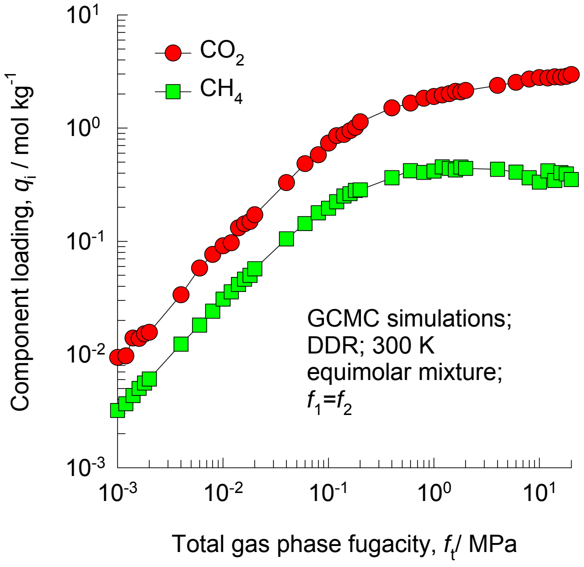

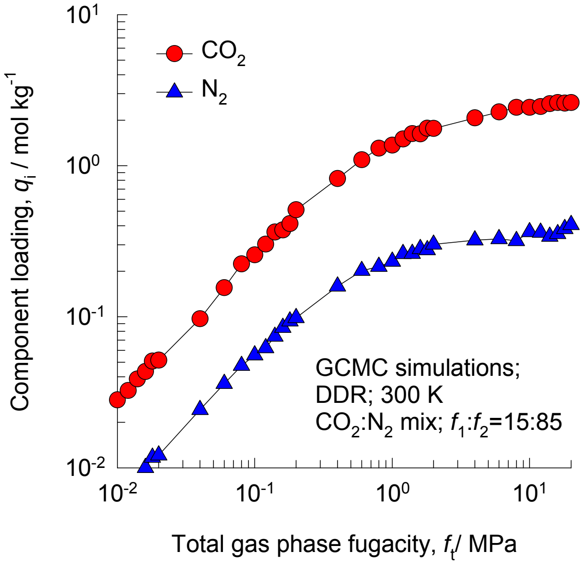

Inaccessible pockets have been blocked in these simulations

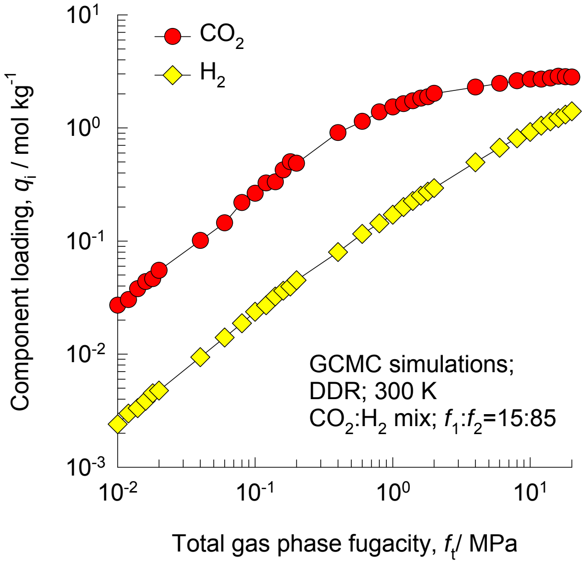

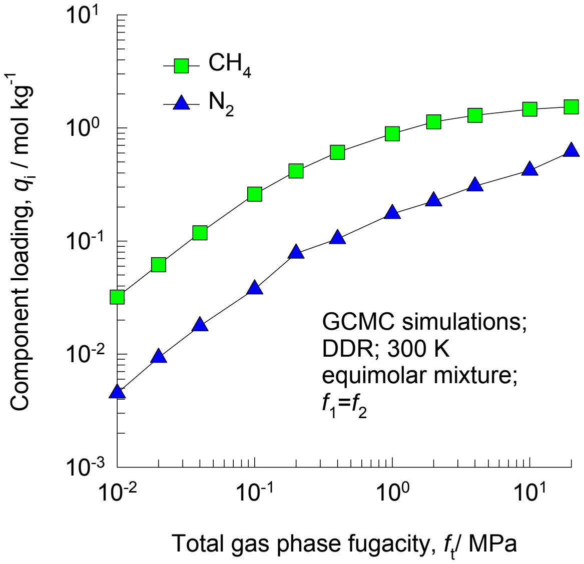

ERI pore landscape

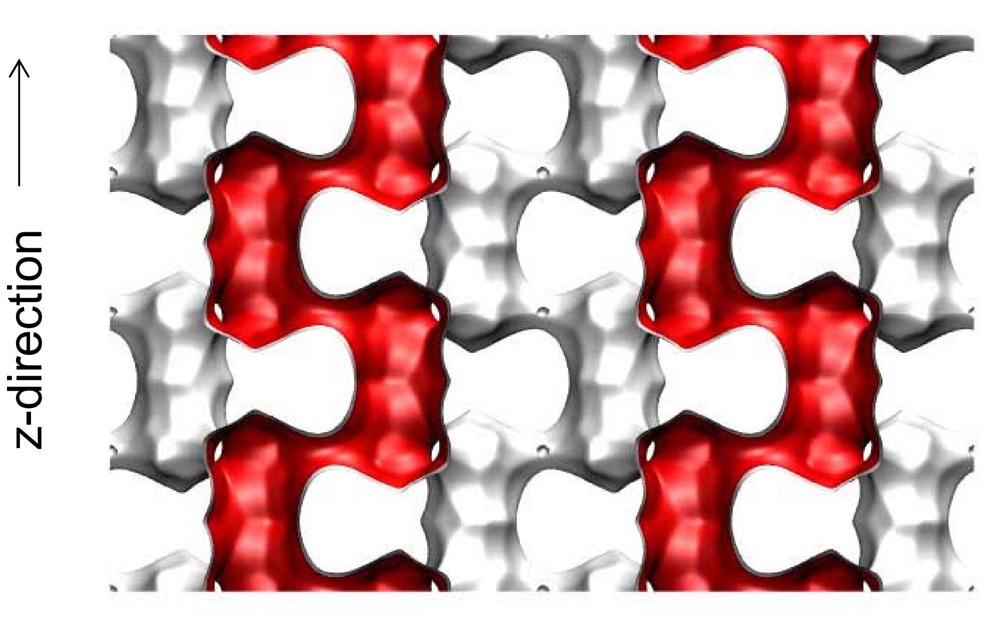

To convert from molecules per unit cell to mol kg^{-1}, multiply by 0.23115.
The pore volume is 0.2275 cm^3/g.

x-y projection

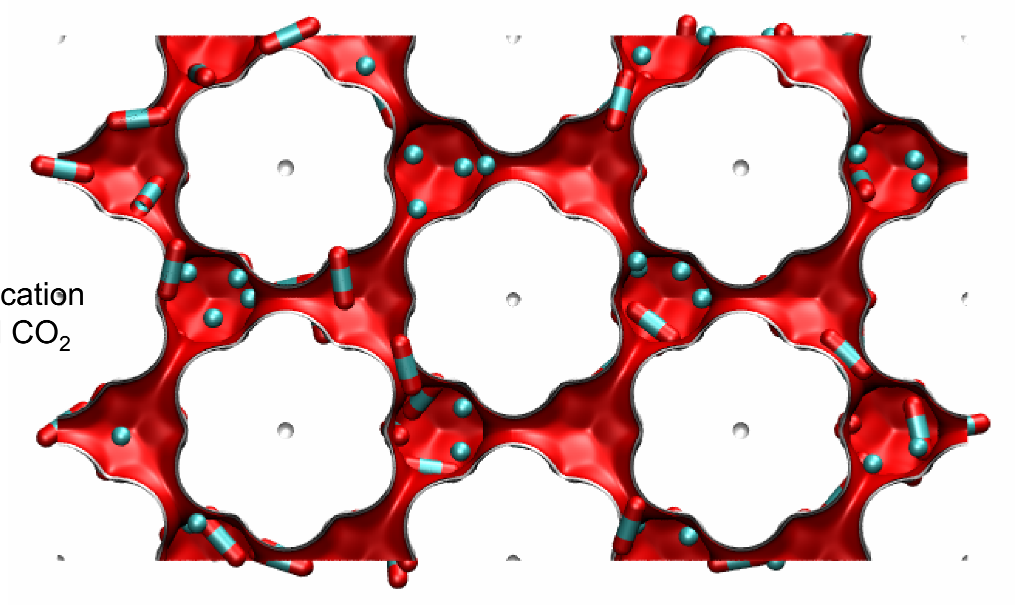

Snapshots showing location of CH_4 and CO_2

ERI CBMC mixture simulations for CO2 capture

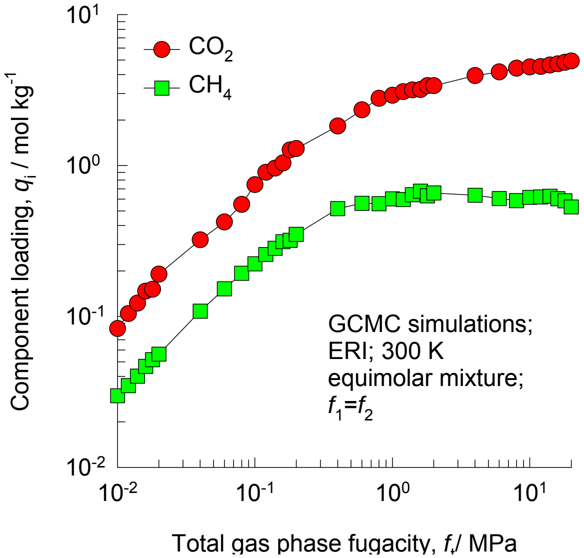

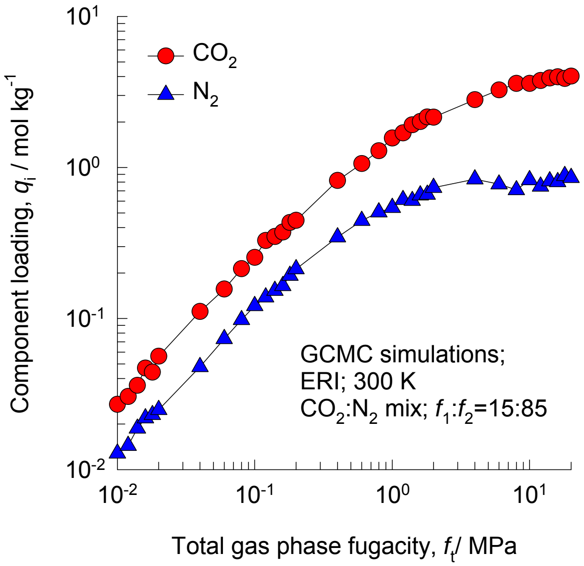

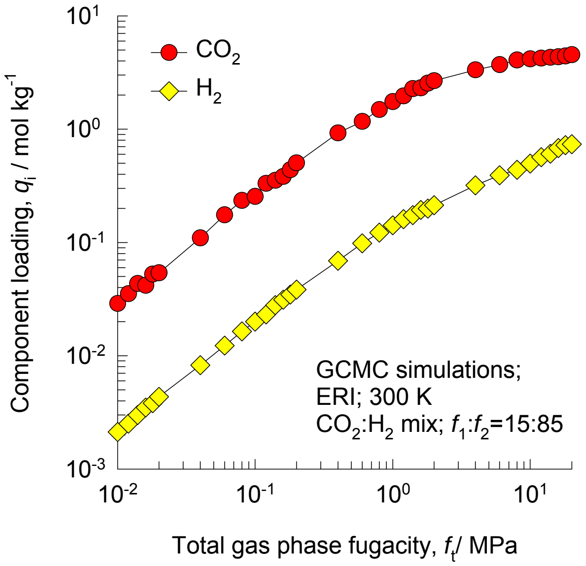

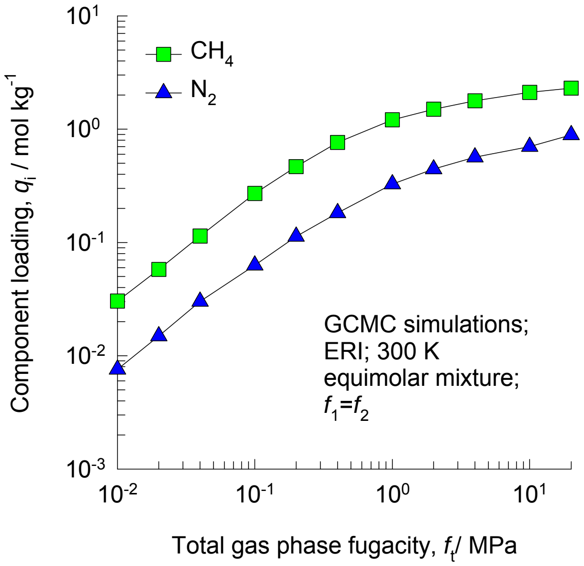

FAU pore landscape (the sodalite cages are blocked)

To convert from molecules per unit cell to mol kg^{-1}, multiply by 0.086683.
The pore volume is 0.328 cm^3/g.

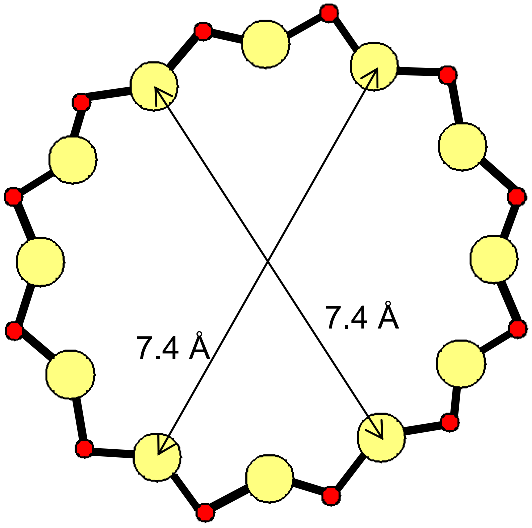

12-ring
window of FAU

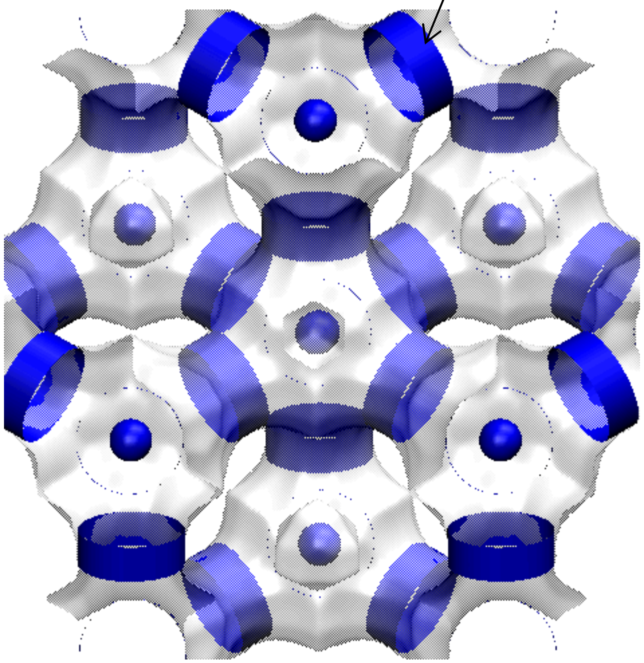

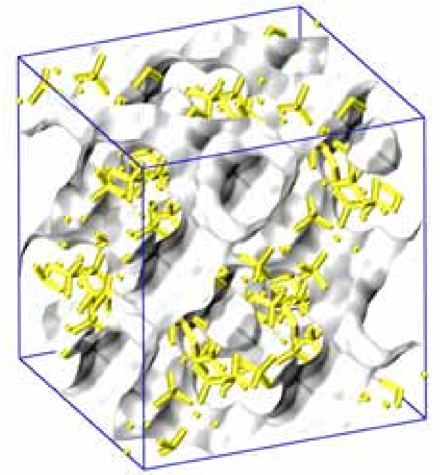

The volume of one FAU cage is 786 Å^3, larger in size than that of LTA (743 Å^3) and DDR (278 Å^3).

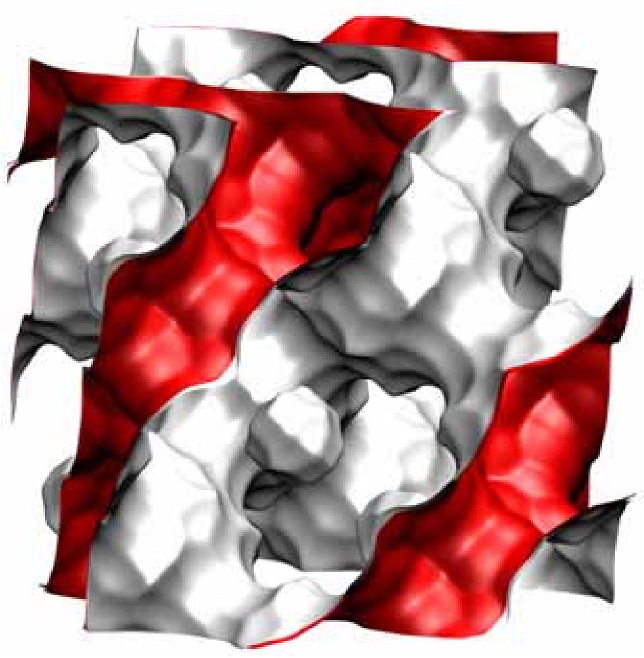

FAU CBMC mixture simulations for CO_2 capture

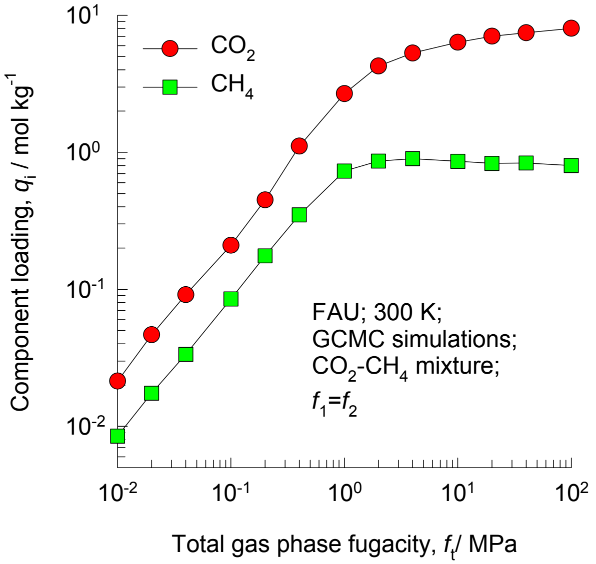

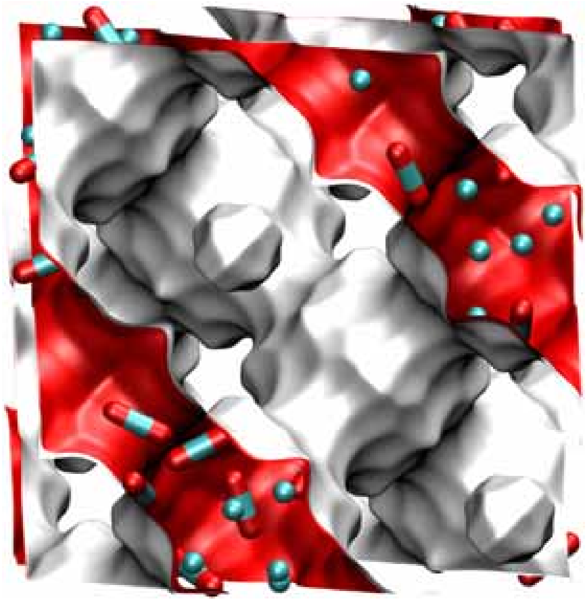

Snapshots showing location of CH_4 and CO_2

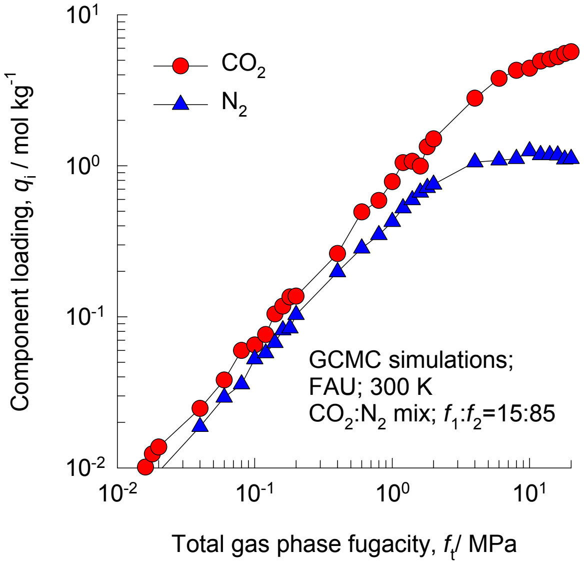

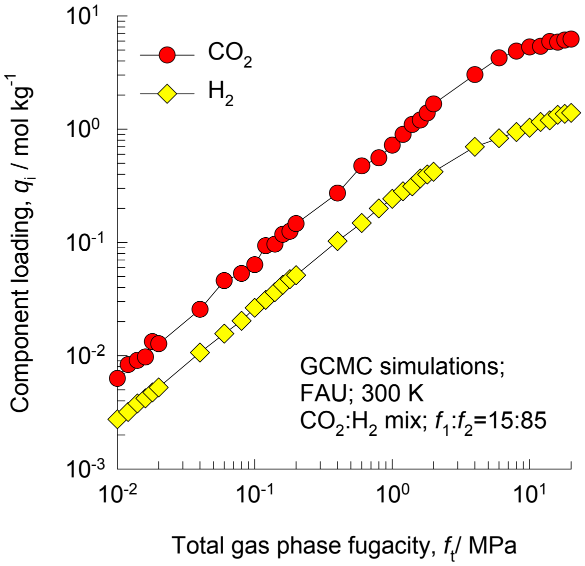

FAU-Si CBMC nC6/3MP/22DMB mixture simulations

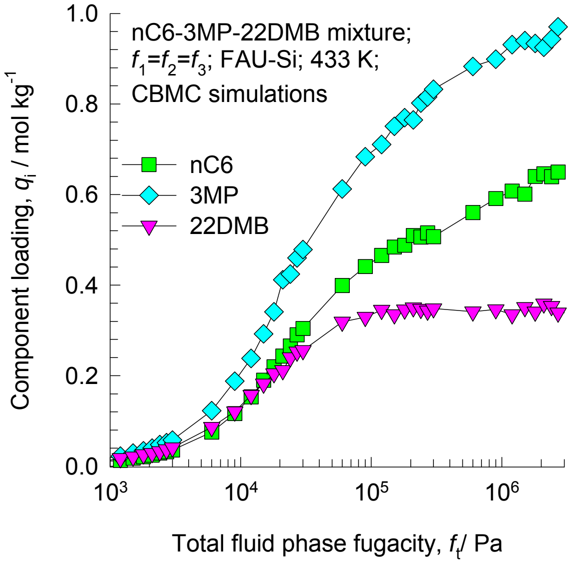

$$S_{ads} = \frac{\frac{q_{nC6}}{f_{nC6}} + \frac{q_{3MP}}{f_{3MP}}}{\frac{q_{22DMB}}{f_{22DMB}}}$$

Capacity is the total loading of nC6 + 3MP

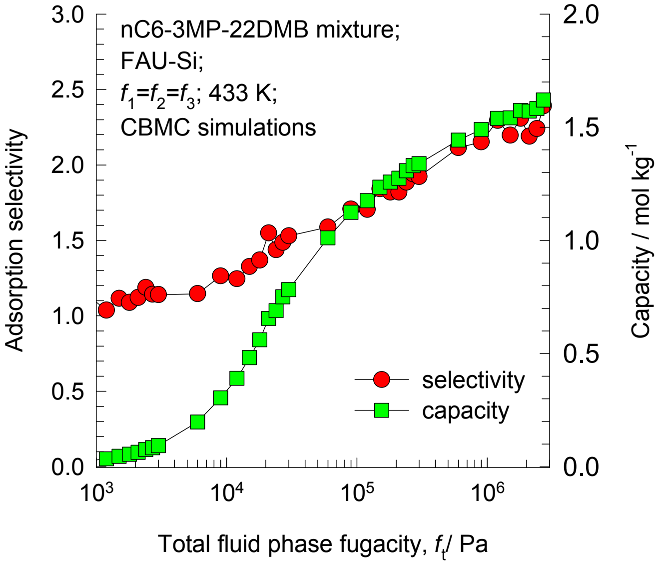

FAU-Si snapshot of hexane isomers

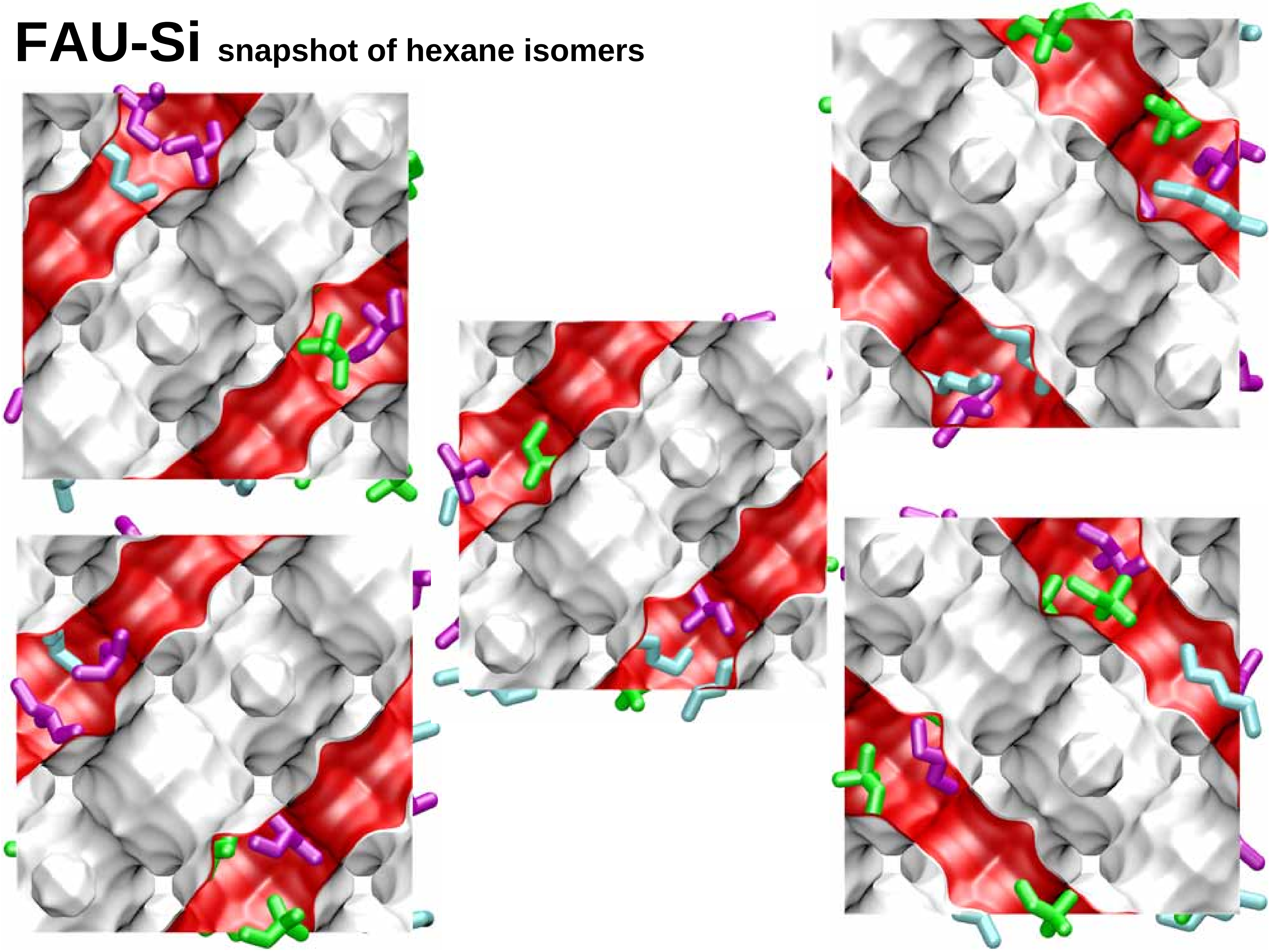

FER pore landscape

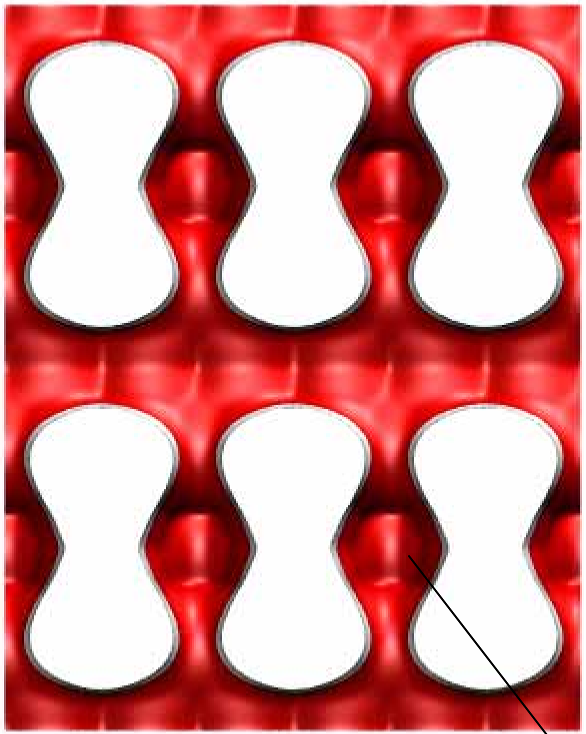

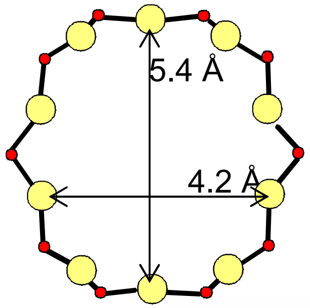

10-ring
main channels

Snapshots
showing
location of CH_4
and CO_2

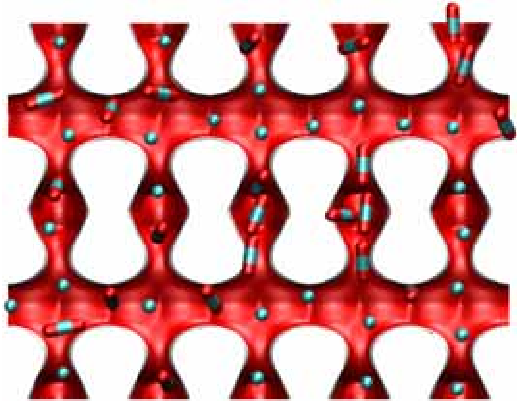

8-ring
side pockets

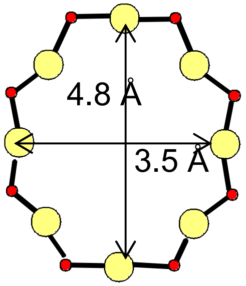

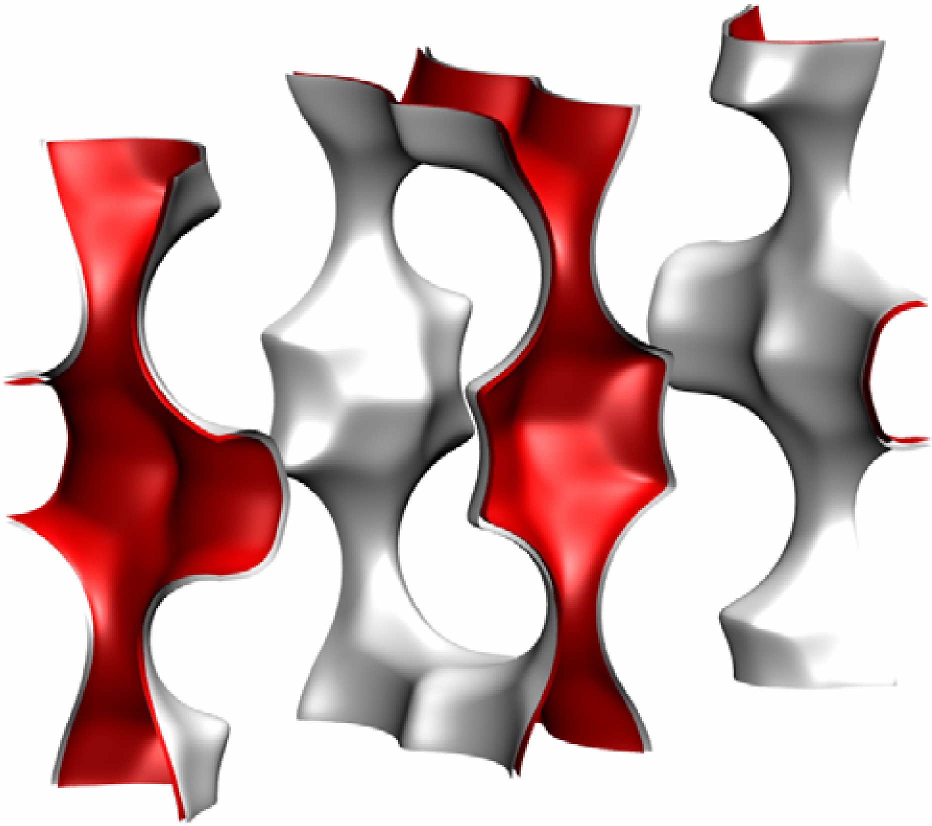

To convert from molecules per unit cell to mol kg^{-1}, multiply by 0.4623.
The pore volume is 0.16 cm^3/g.

FER CBMC mixture simulations for CO_2 capture

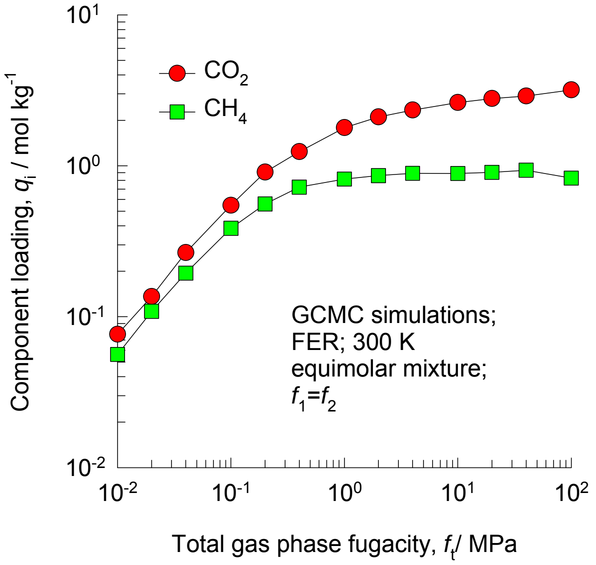

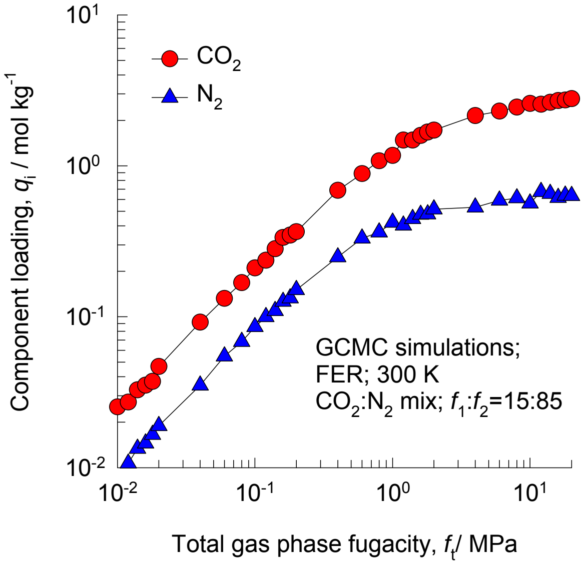

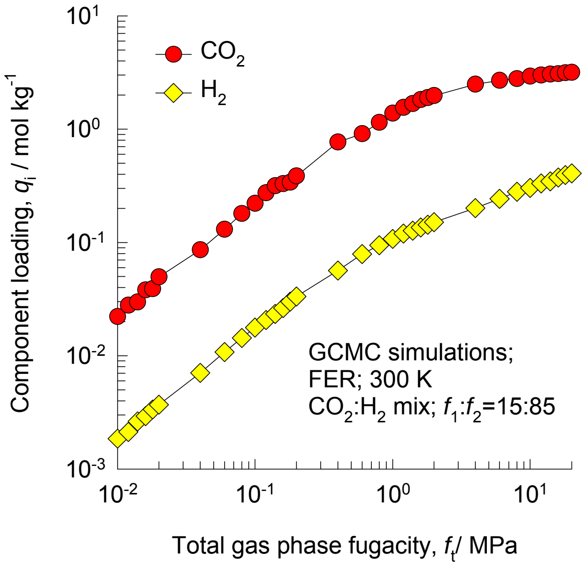

GME landscapes

To convert from molecules per unit cell to mol kg^{-1}, multiply by 0.3467.
The pore volume is 0.265 cm^3/g.

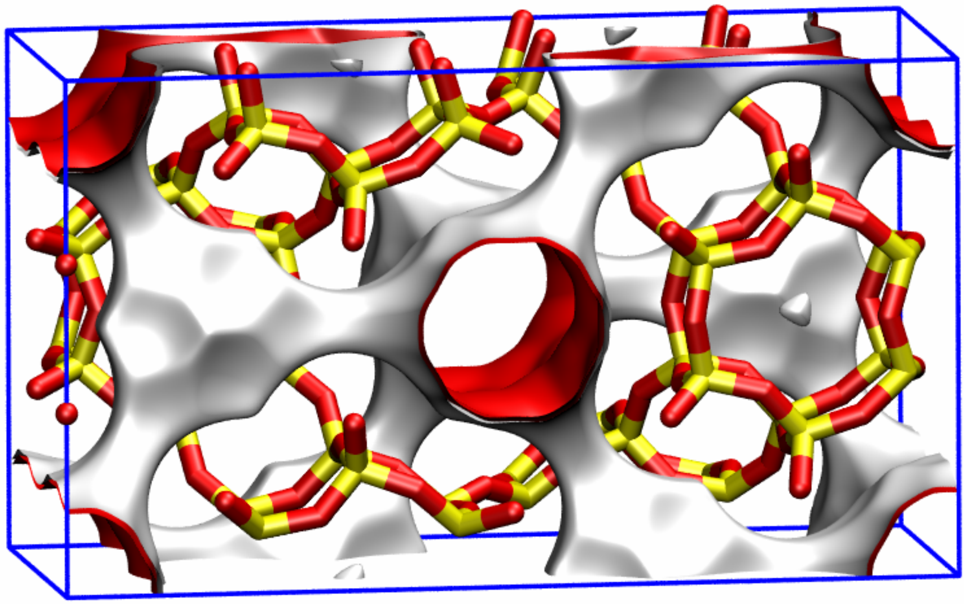

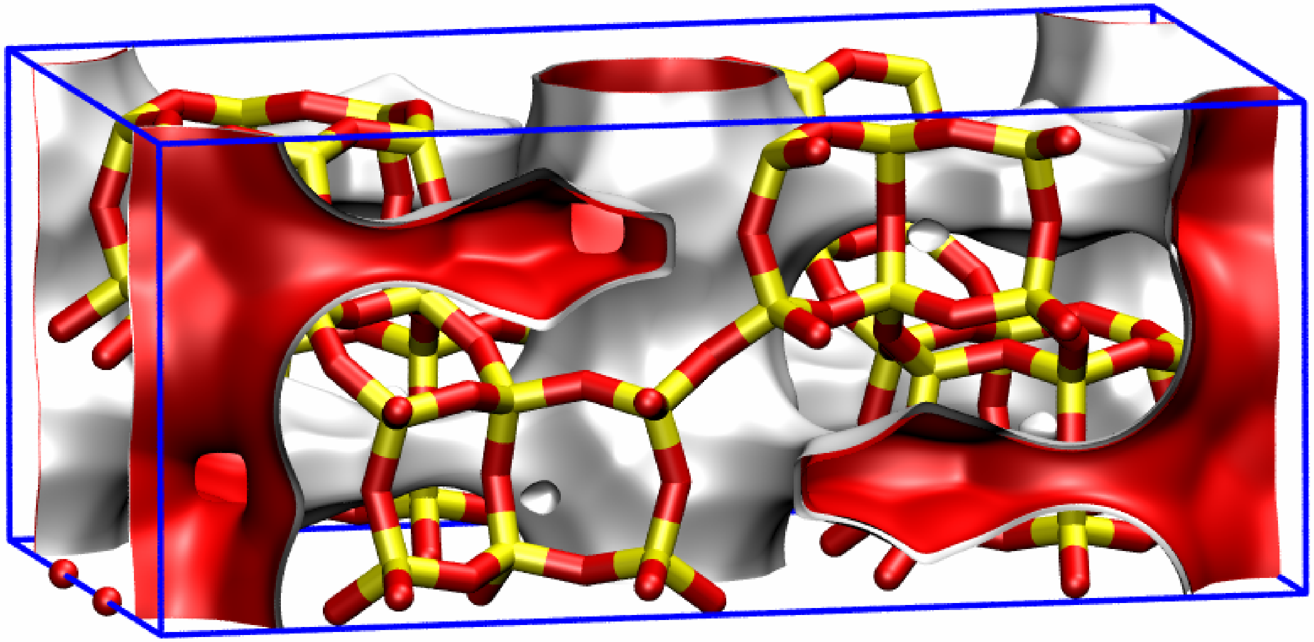

GME CBMC mixture simulations for CO_2 capture

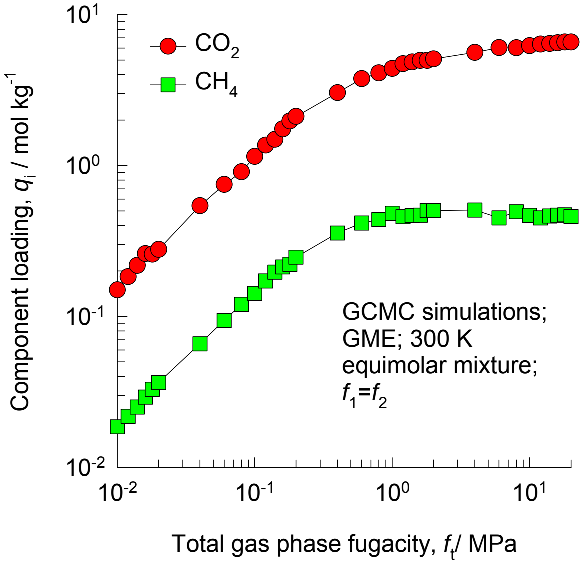

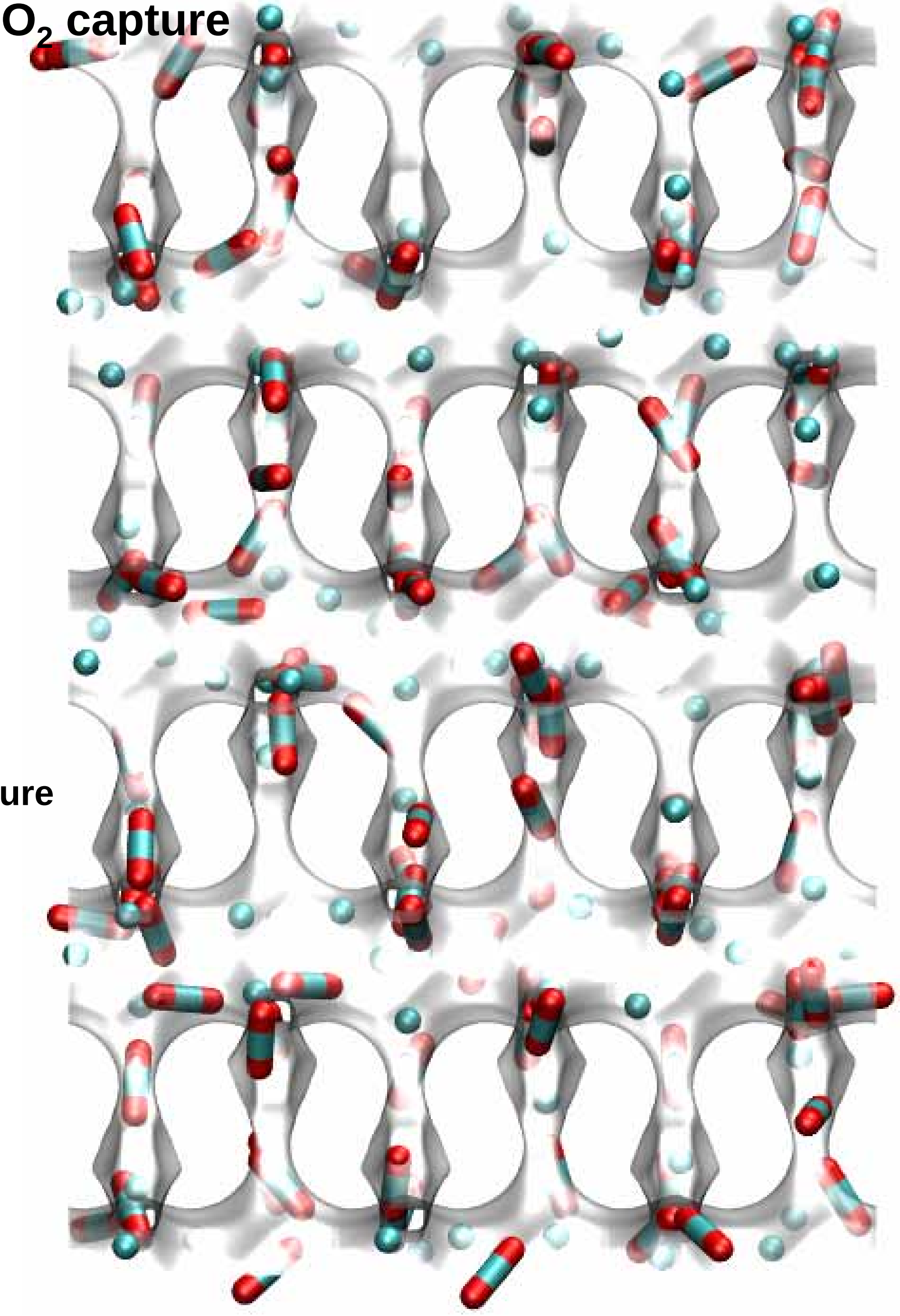

Snapshot of CO_2/CH_4 mixture

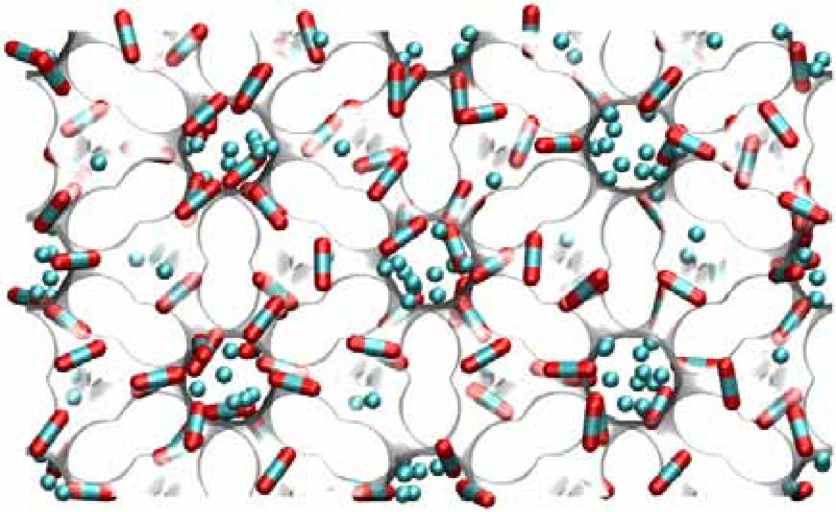

GME CBMC mixture simulations for CO_2 capture

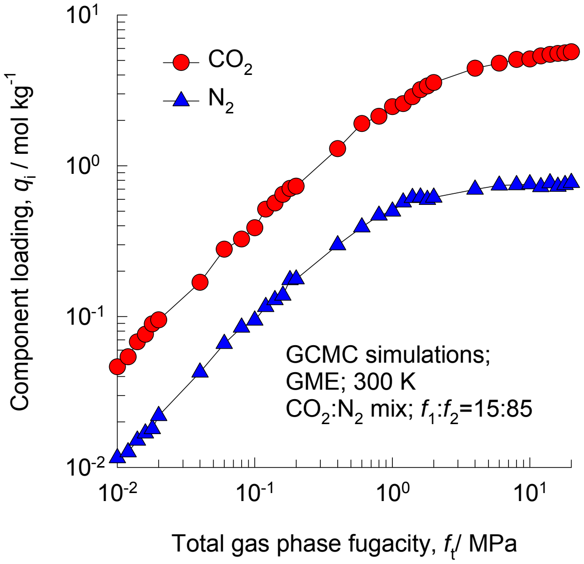

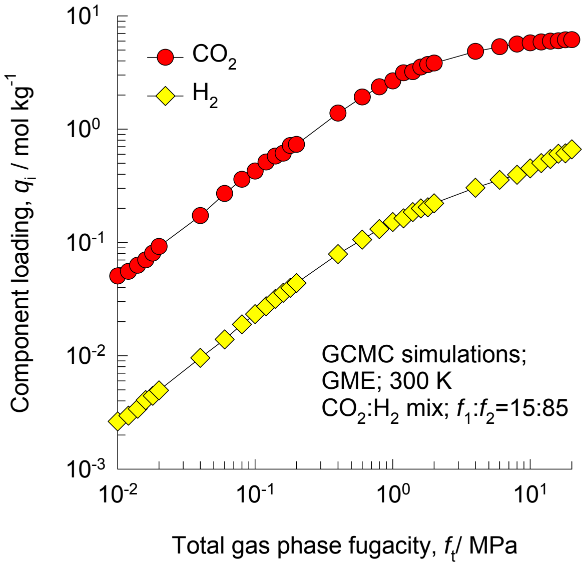

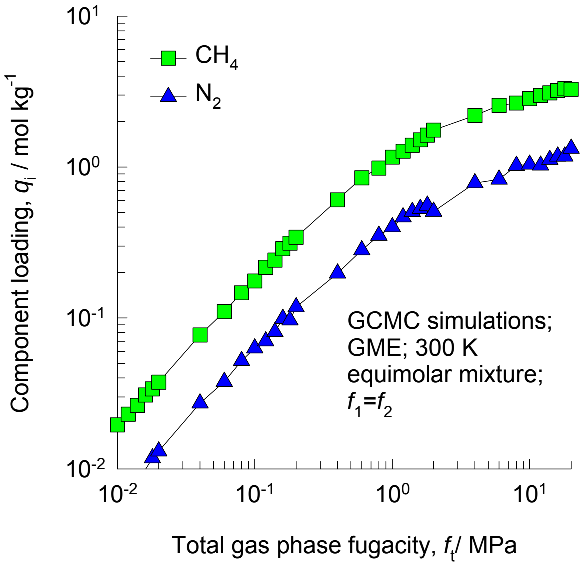

ISV pore landscape

To convert from molecules per unit cell to mol kg^{-1}, multiply by 0.260.
The pore volume is 0.278 cm^3/g.

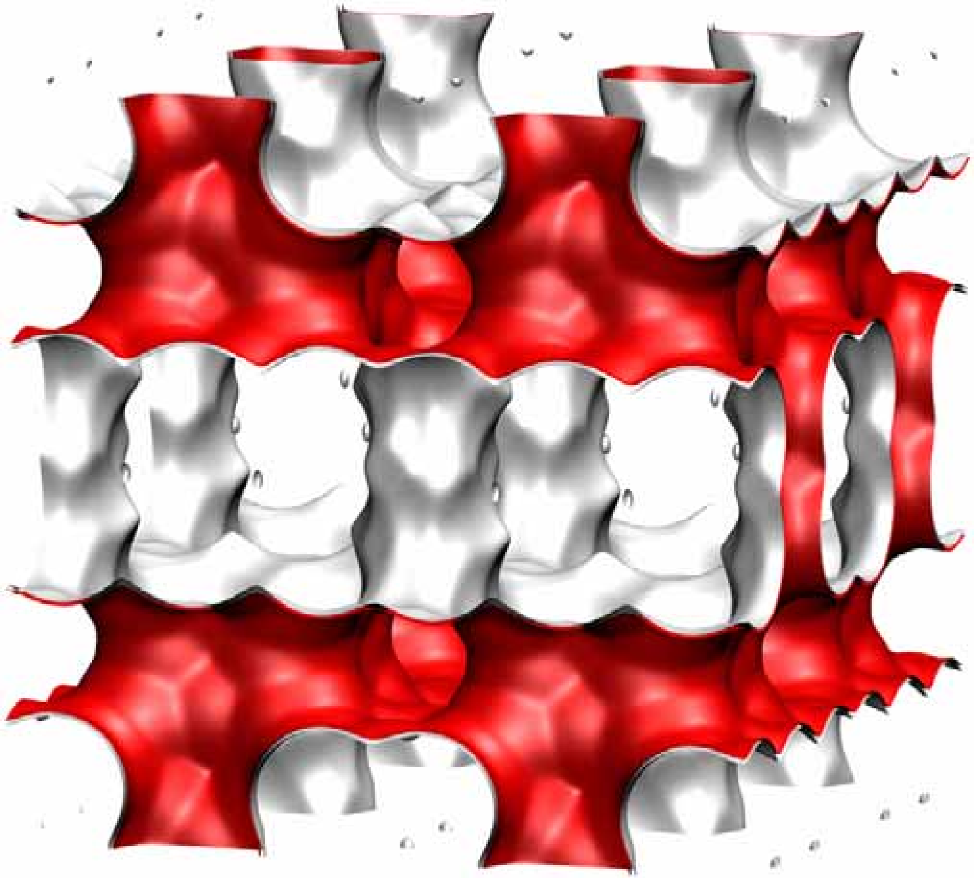

Snapshot of CO_2/CH_4 mixture

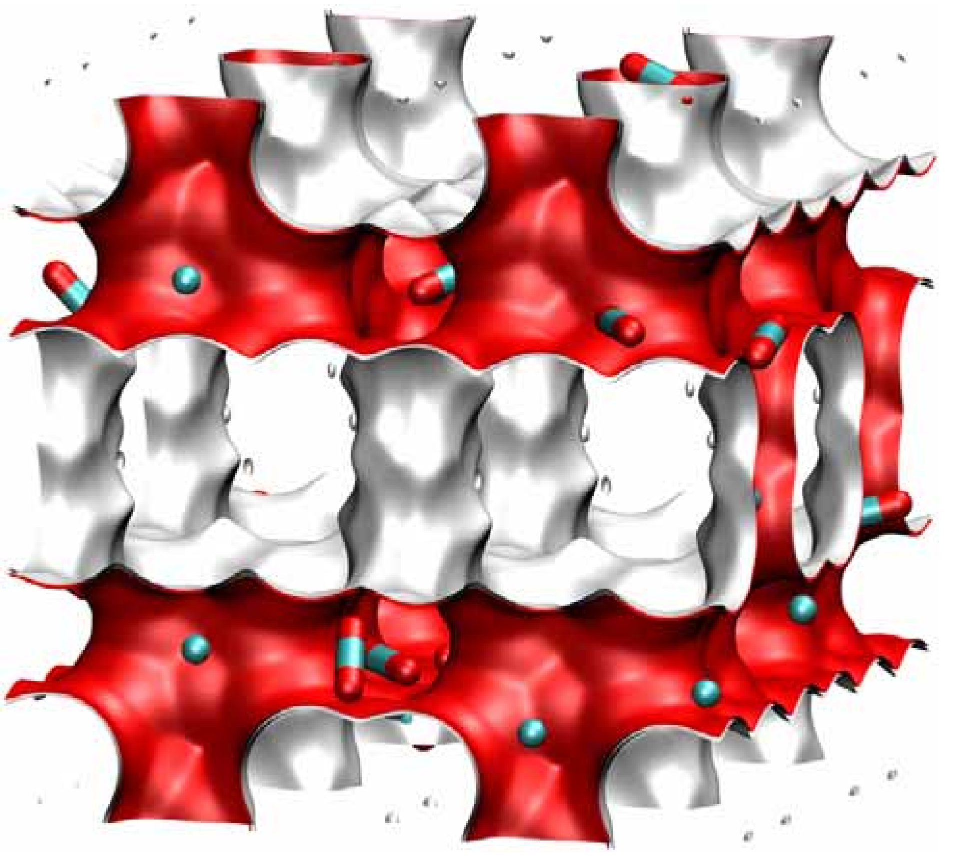

ISV CBMC mixture simulations for CO_2 capture

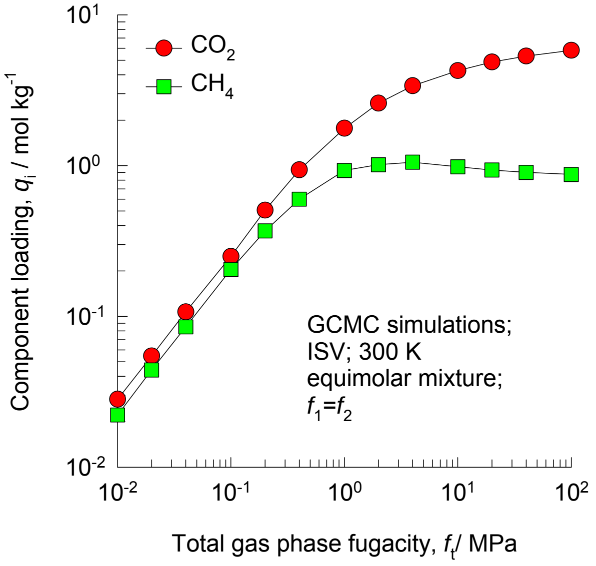

ITQ-29

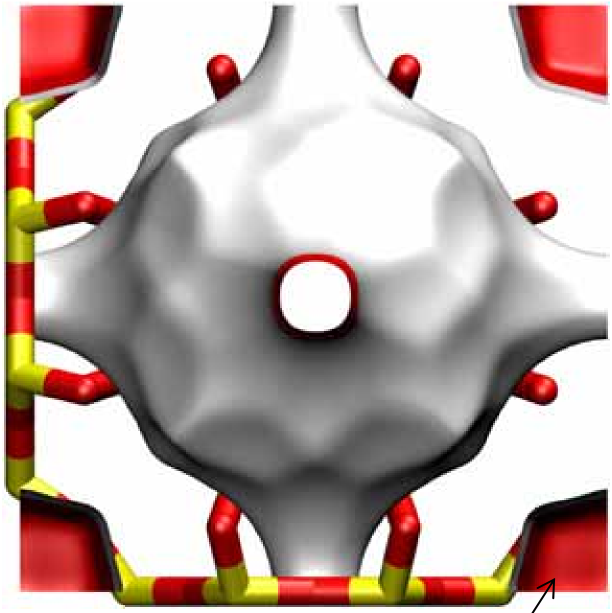

To convert from molecules per unit cell to mol kg^{-1}, multiply by 0.6935.
The pore volume is 0.283 cm^3/g.

The structural information for ITQ-29 is not available in the IZA atlas and is taken from Corma, Nature, 437 (2004) 287. The window size is slightly smaller than that of LTA Si.

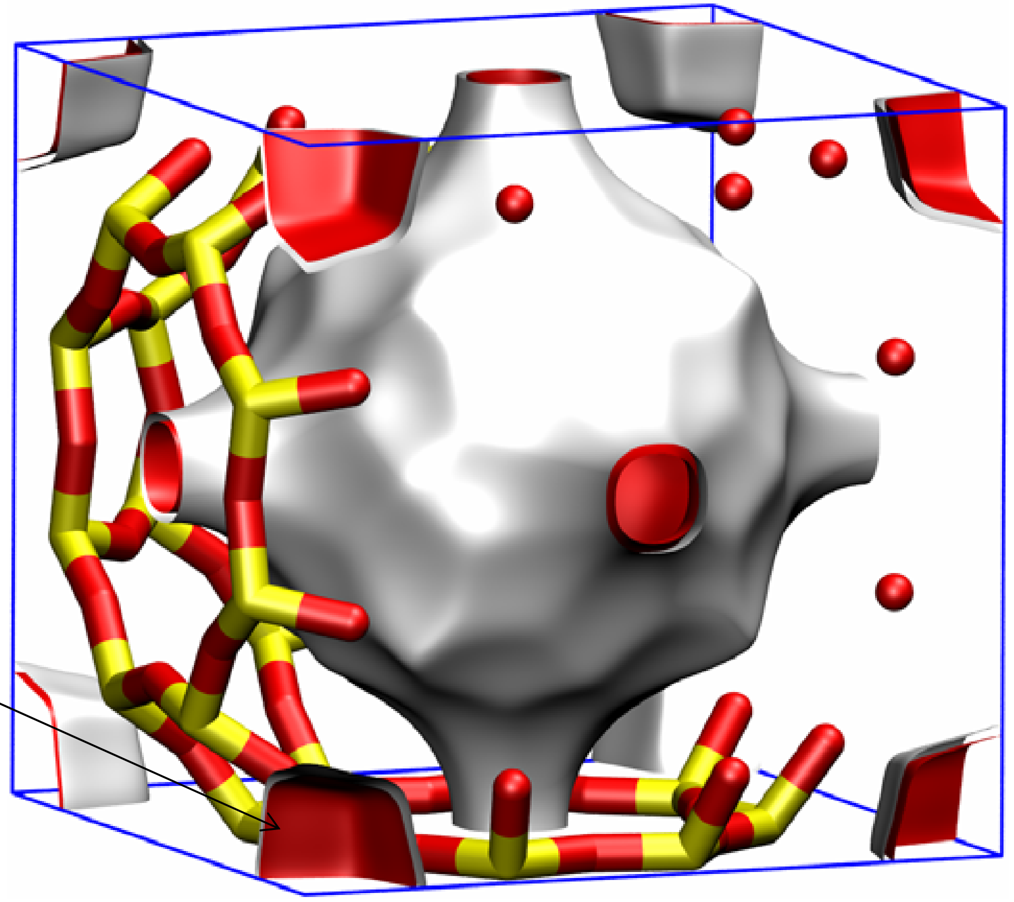

Inaccessible sodalite cages have been blocked in these simulations

ITQ-29 CBMC CO_2/CH_4 mixture simulations

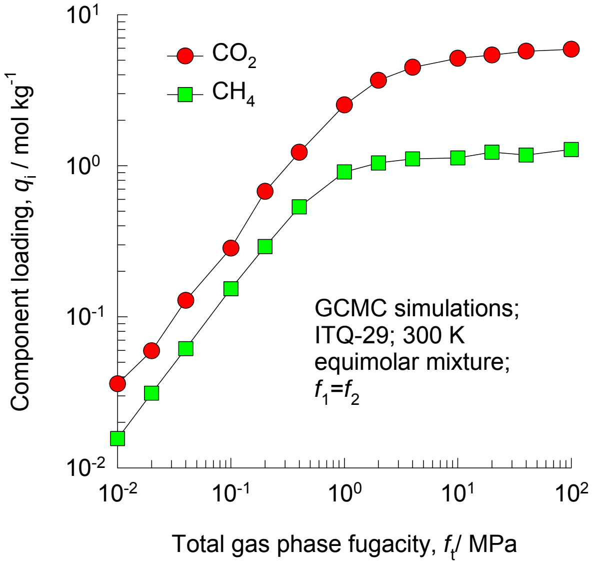

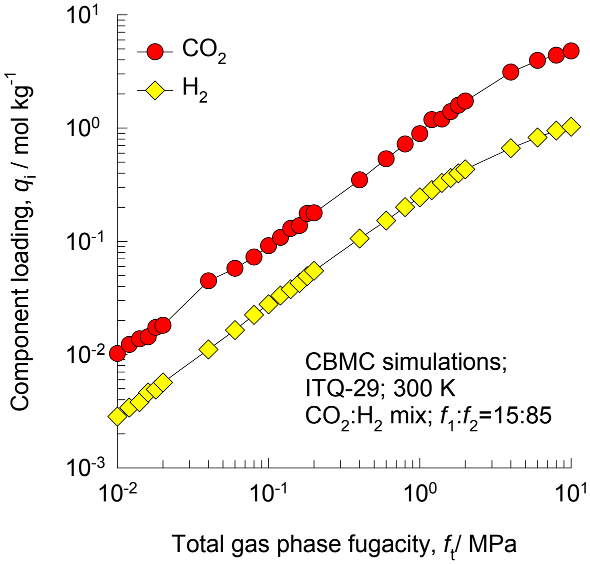

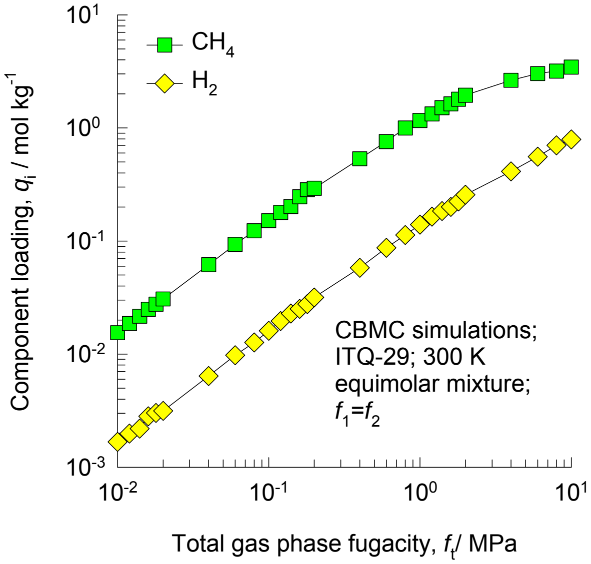

Snapshot of CO_2/CH_4 mixture

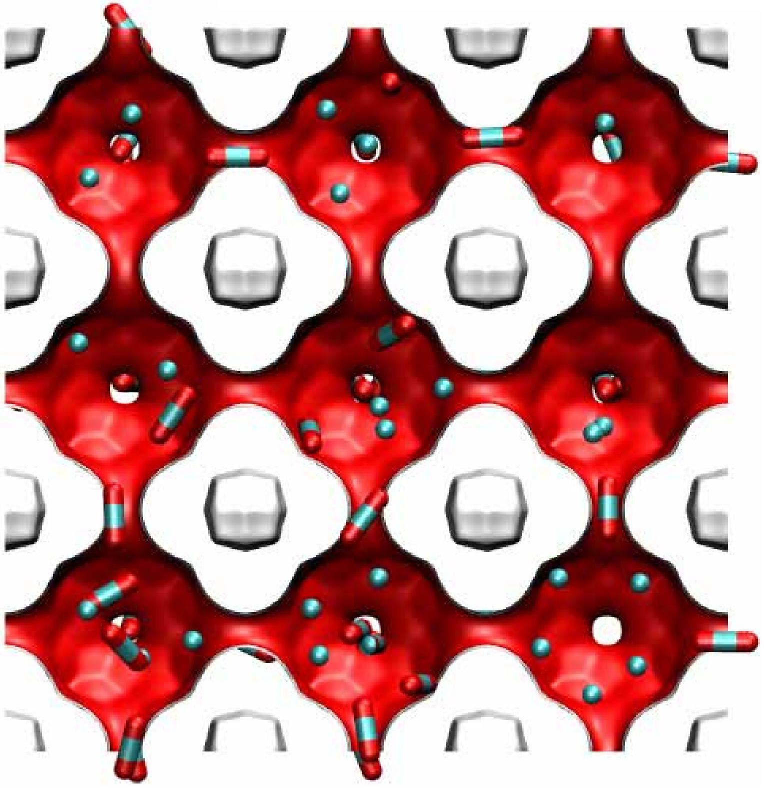

LTA-Si landscapes

To convert from molecules per unit cell to mol kg^{-1}, multiply by 0.08668
The pore volume is 0.310 cm^3/g.

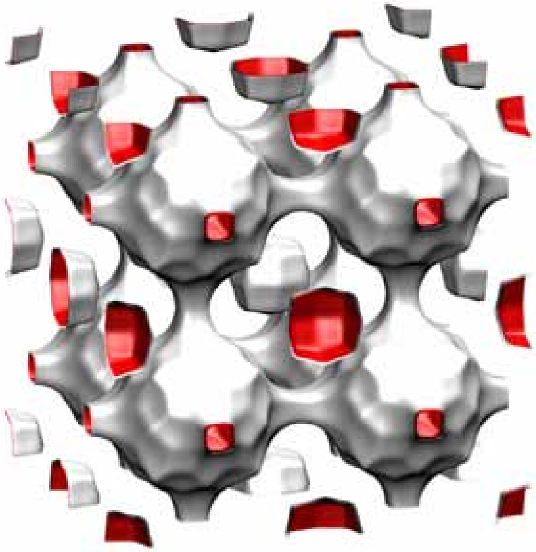

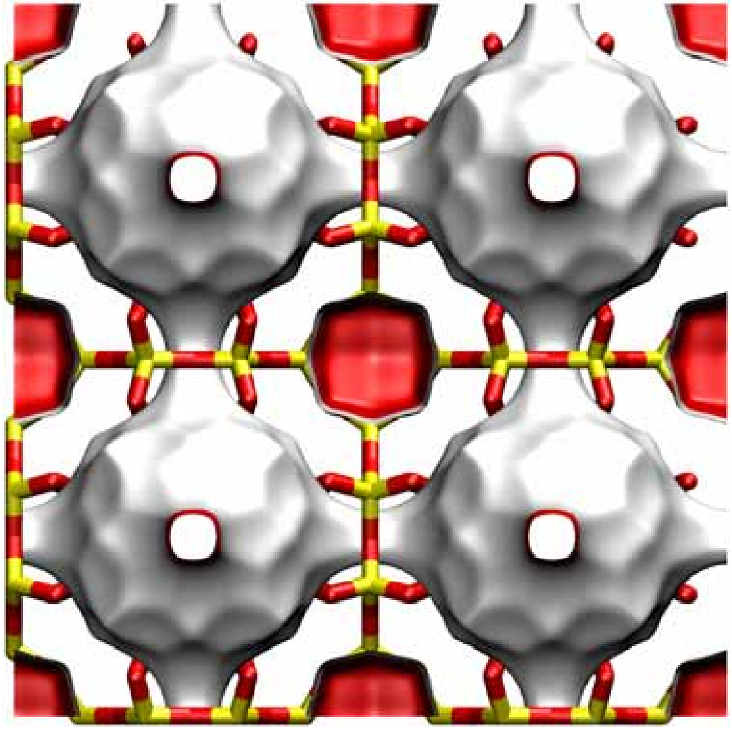

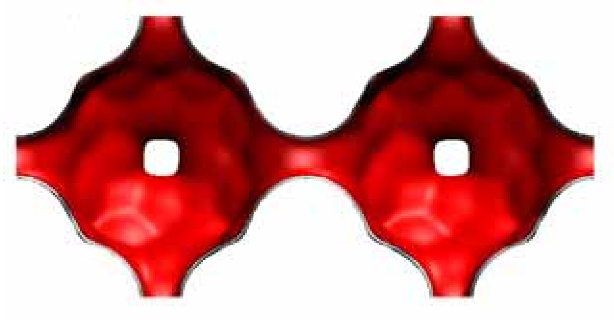

Snapshots
showing location
of CH_4 and CO_2

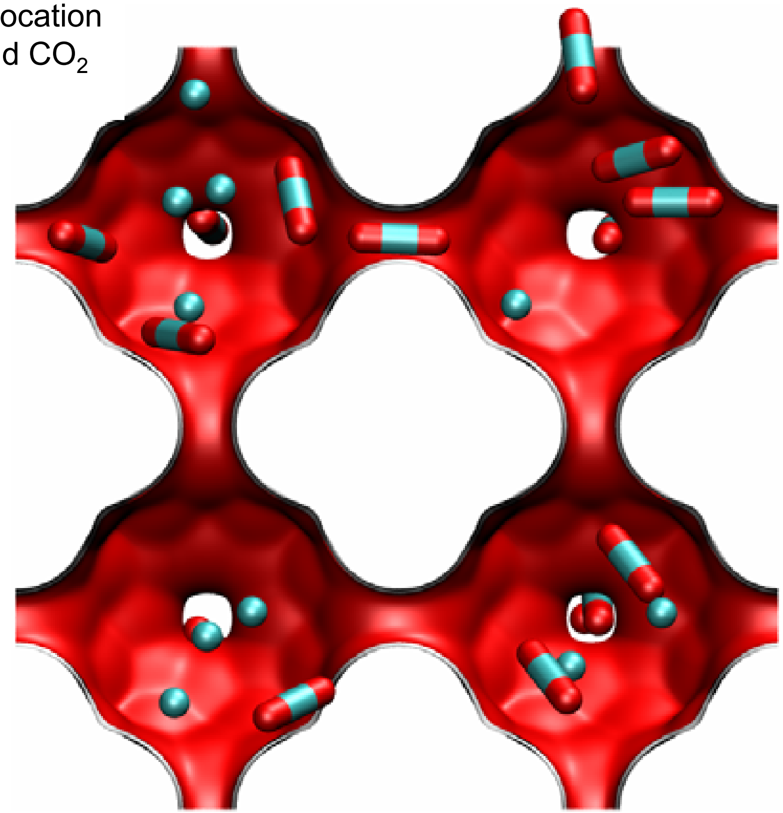

LTA-Si CBMC mixture simulations for CO_2 capture

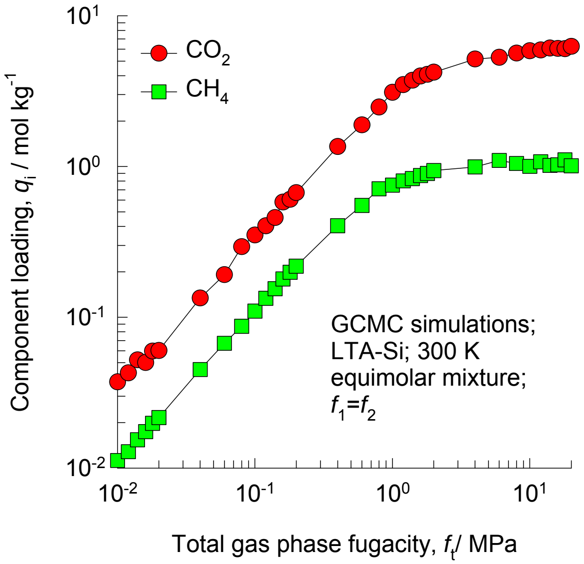

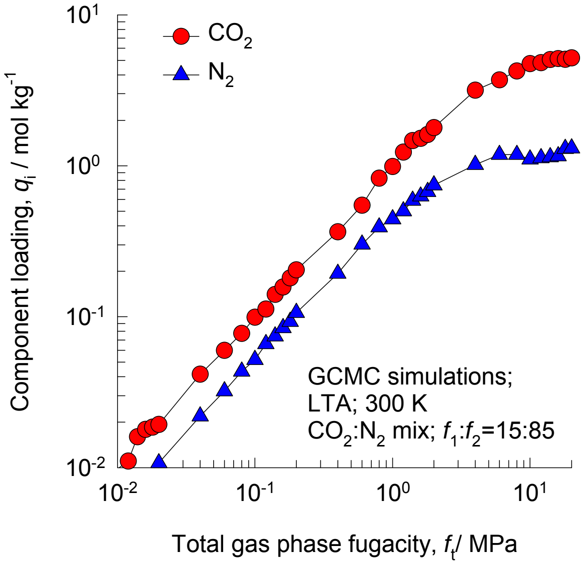

Inaccessible sodalite cages have been blocked in these simulations

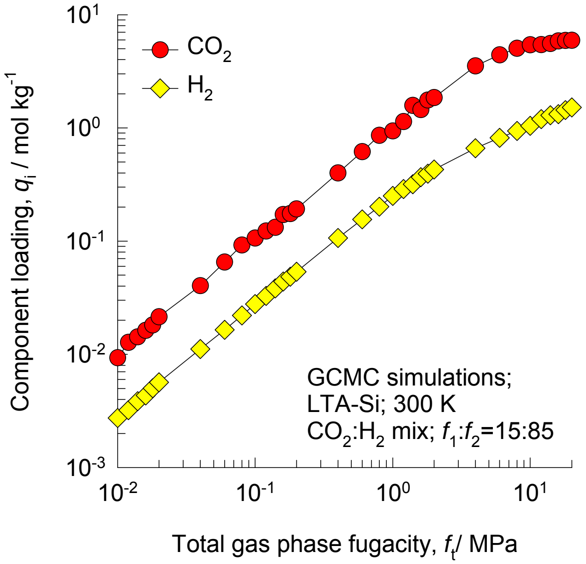

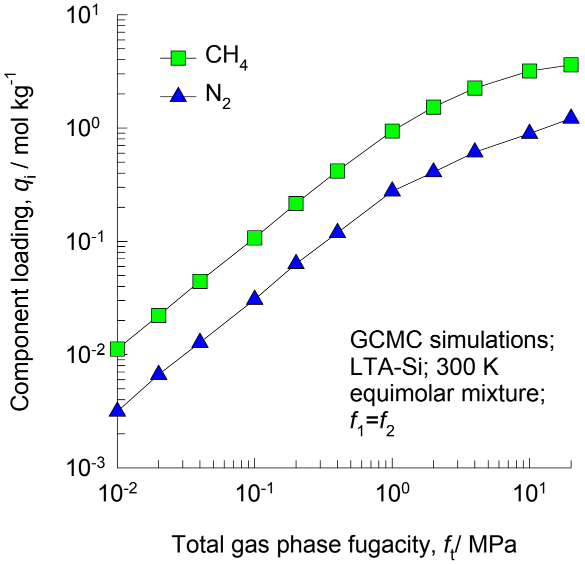

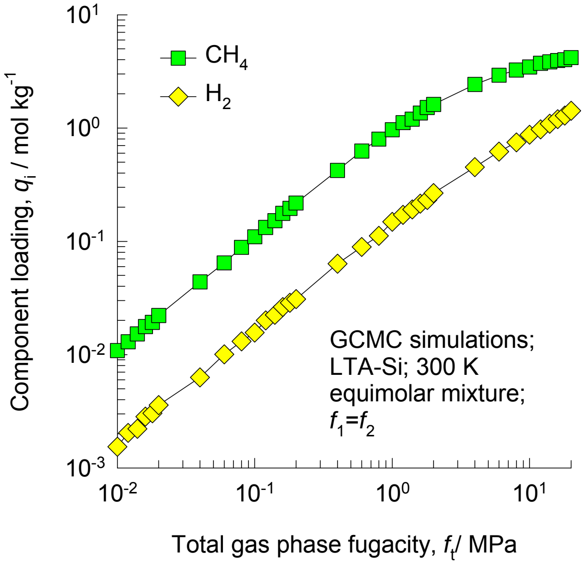

LTA-Si CBMC nC6/3MP/22DMB mixture simulations

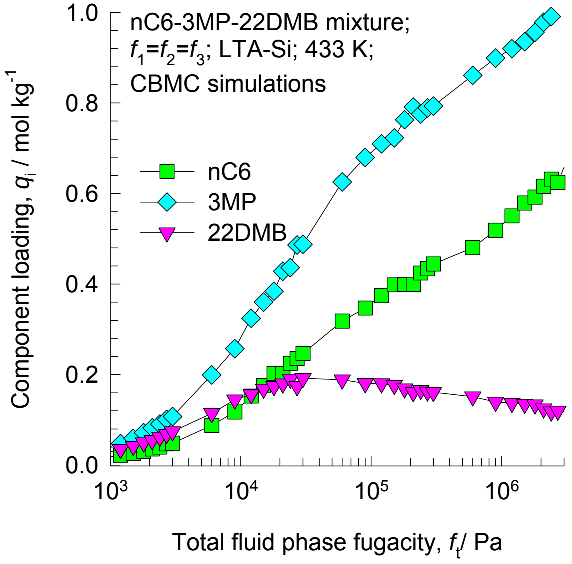

$$S_{ads} = \frac{\dfrac{q_{nC6}}{f_{nC6}} + \dfrac{q_{3MP}}{f_{3MP}}}{\dfrac{q_{22DMB}}{f_{22DMB}}}$$

Capacity is the total loading of nC6 + 3MP

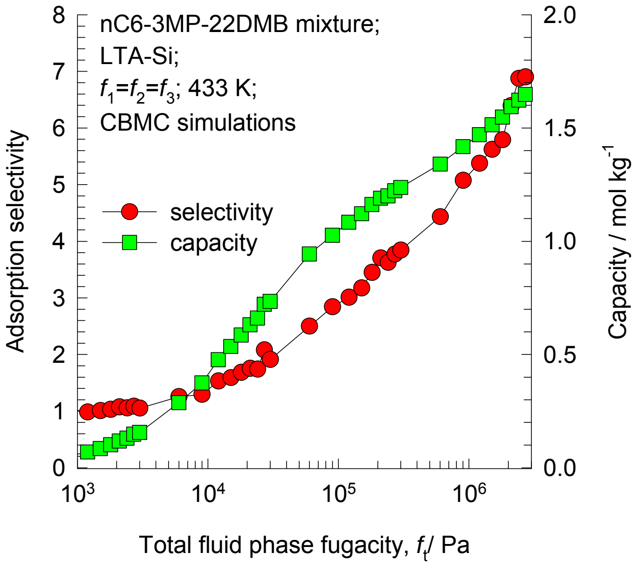

LTA-Si snapshot of hexane isomers

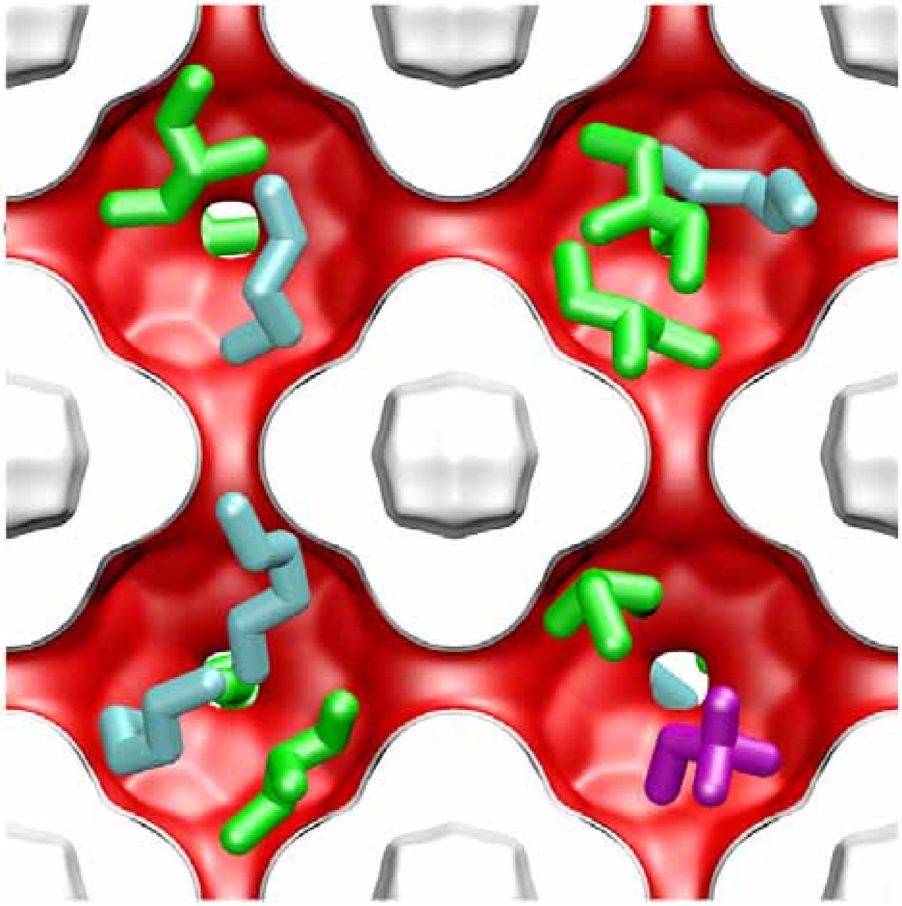

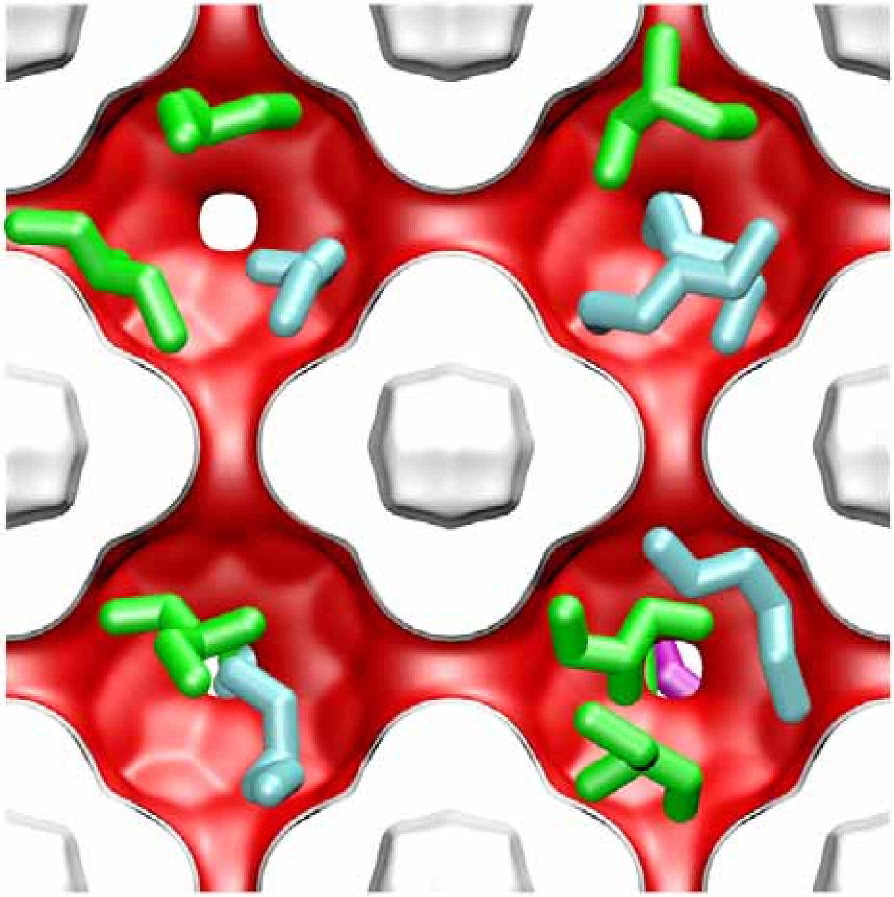

LTL pore landscapes

To convert from molecules per unit cell to mol kg^{-1}, multiply by 0.2311.
The pore volume is 0.170 cm^3/g.

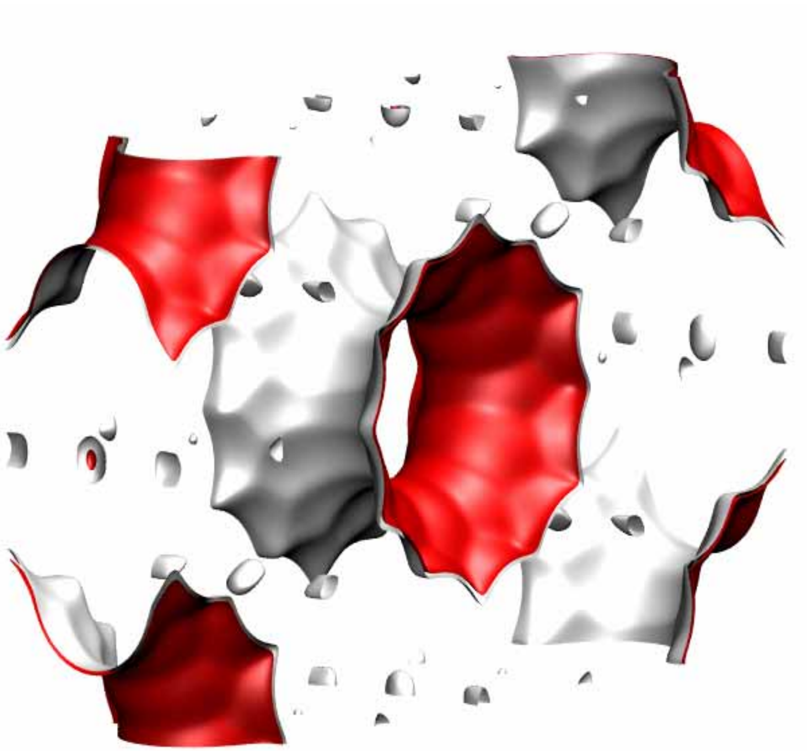

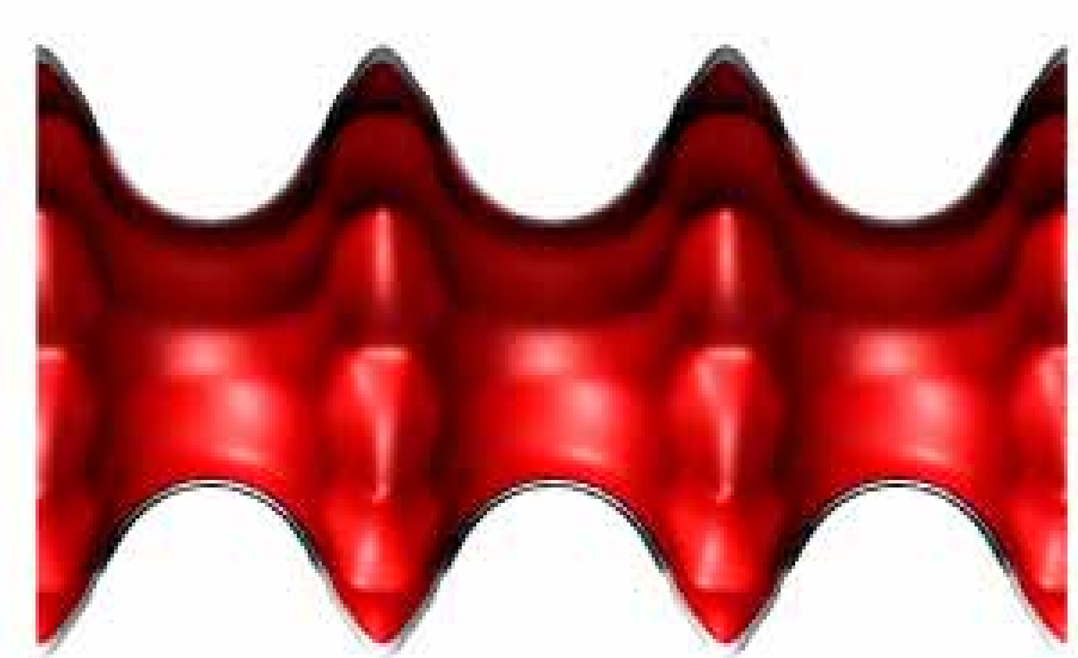

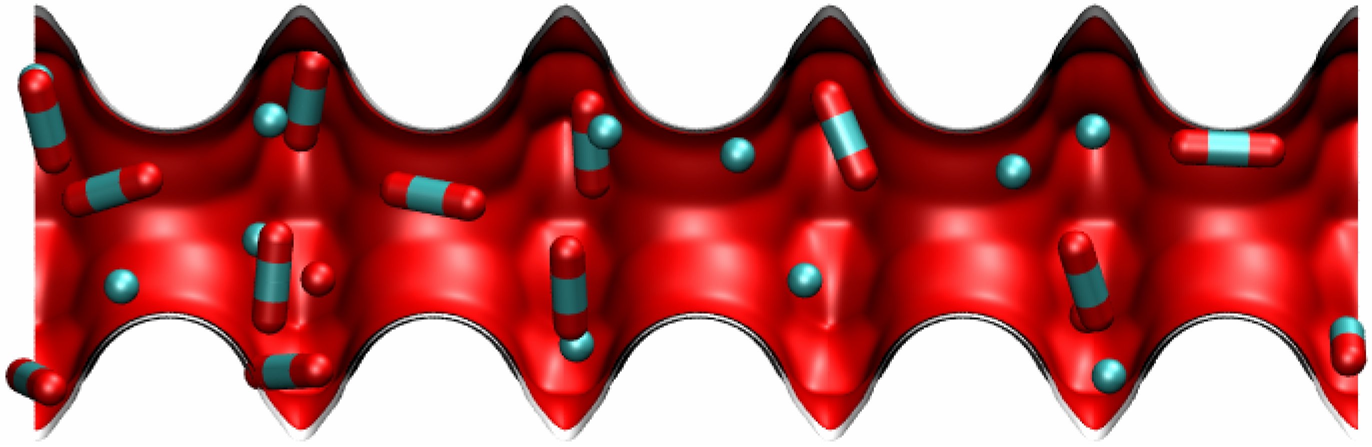

Snapshot of CO_2/CH_4 mixture

LTL CBMC mixture simulation results for CO_2 capture

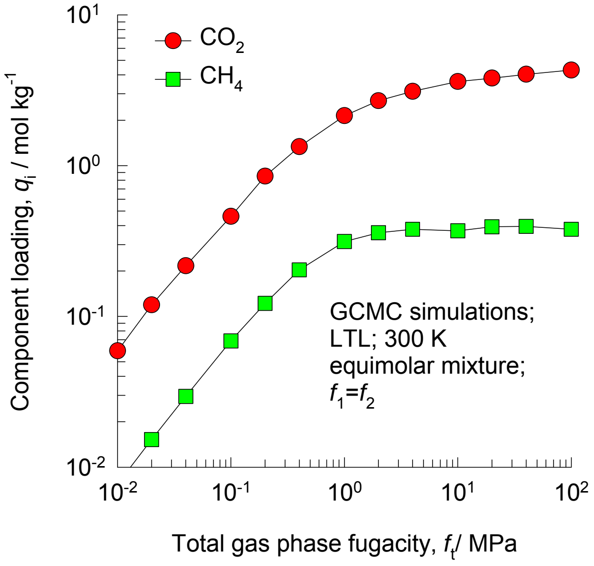

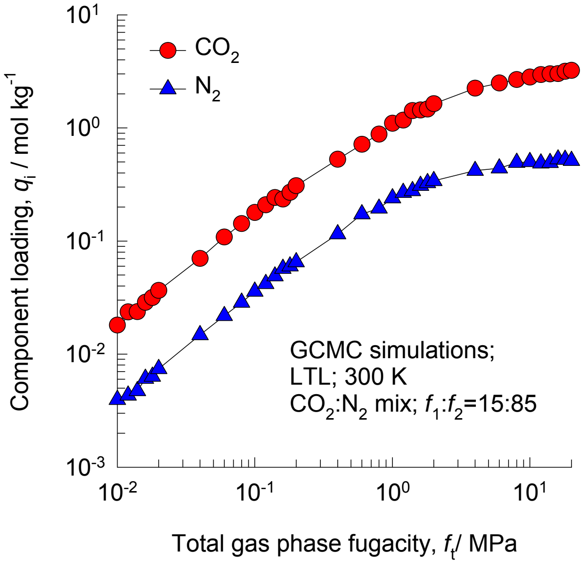

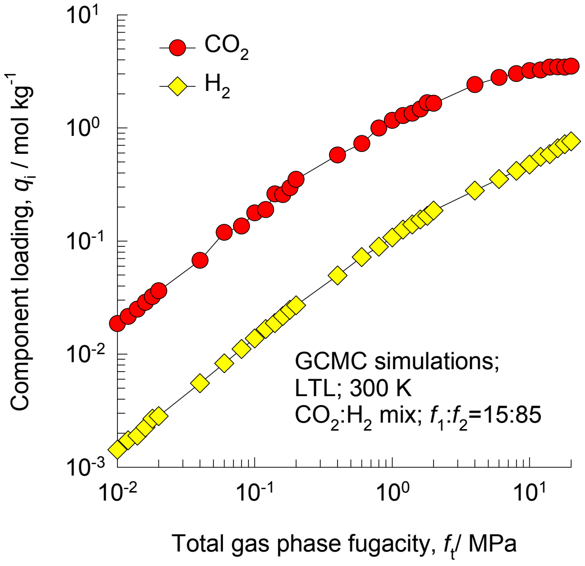

LTL CBMC nC6/3MP/22DMB mixture simulations

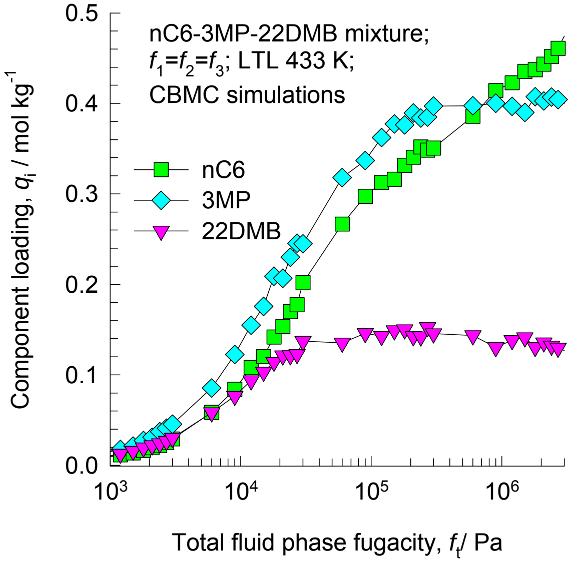

$$S_{ads} = \frac{\dfrac{q_{nC6}}{f_{nC6}} + \dfrac{q_{3MP}}{f_{3MP}}}{\dfrac{q_{22DMB}}{f_{22DMB}}}$$

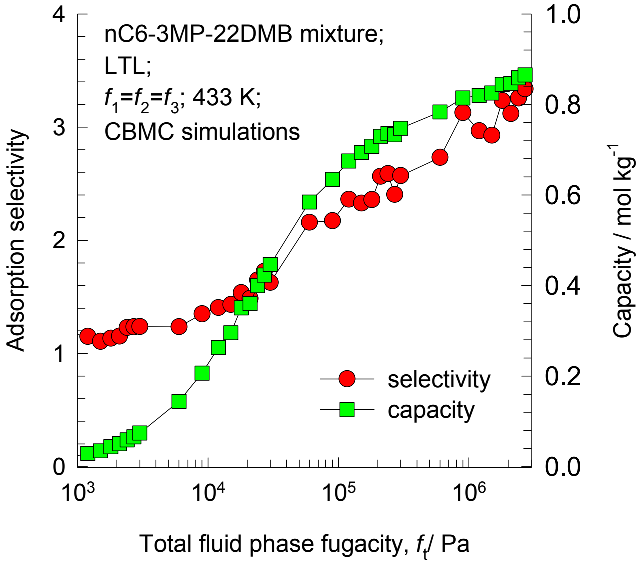

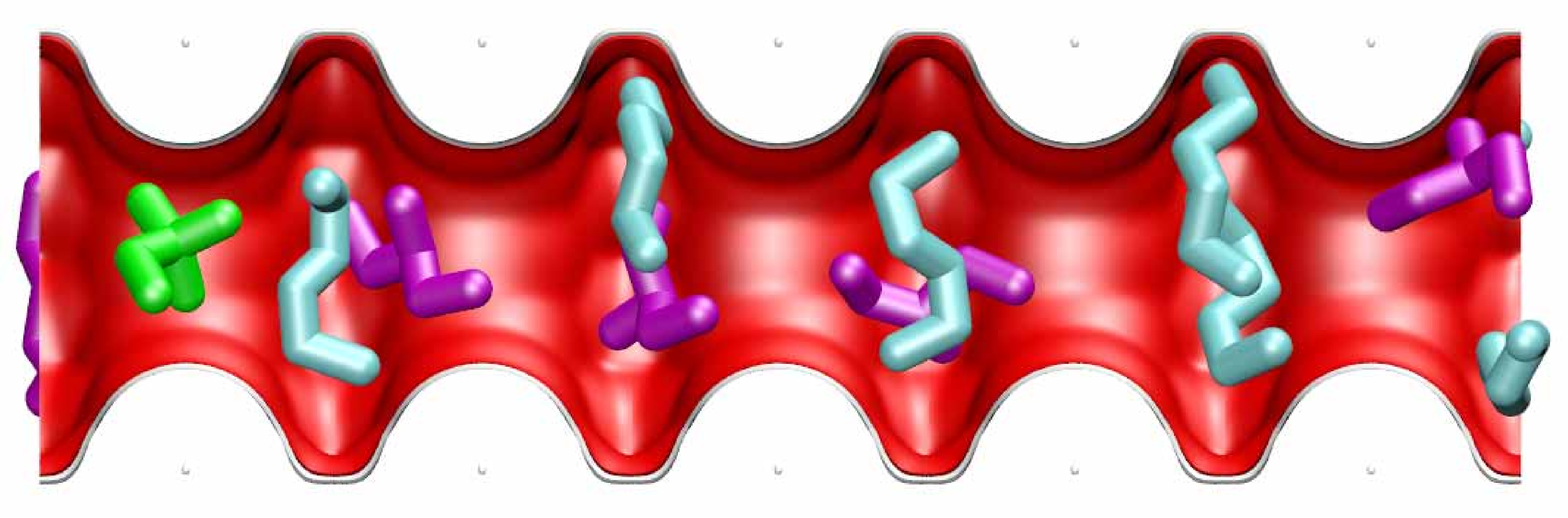

MFI pore landscape

10 ring channel
of MFI viewed along [100]

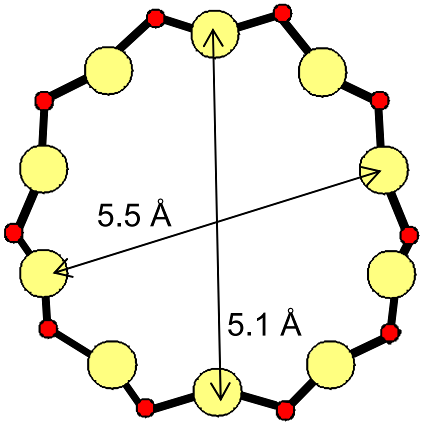

10 ring channel
of MFI viewed along [010]

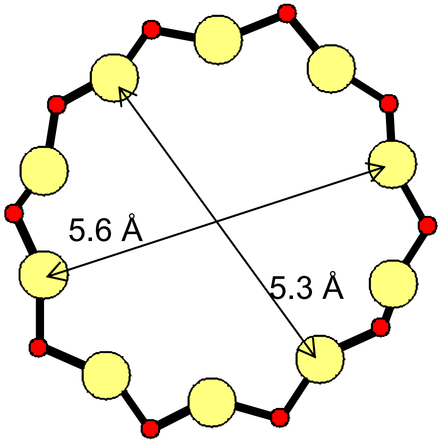

To convert from molecules per unit cell to mol kg^{-1}, multiply by 0.173366.
The pore volume is 0.165 cm^3/g.

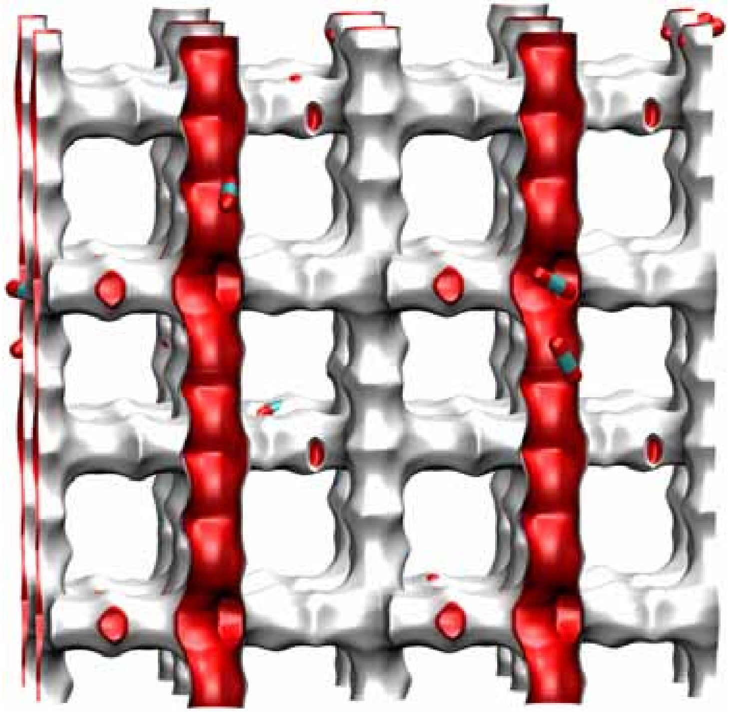

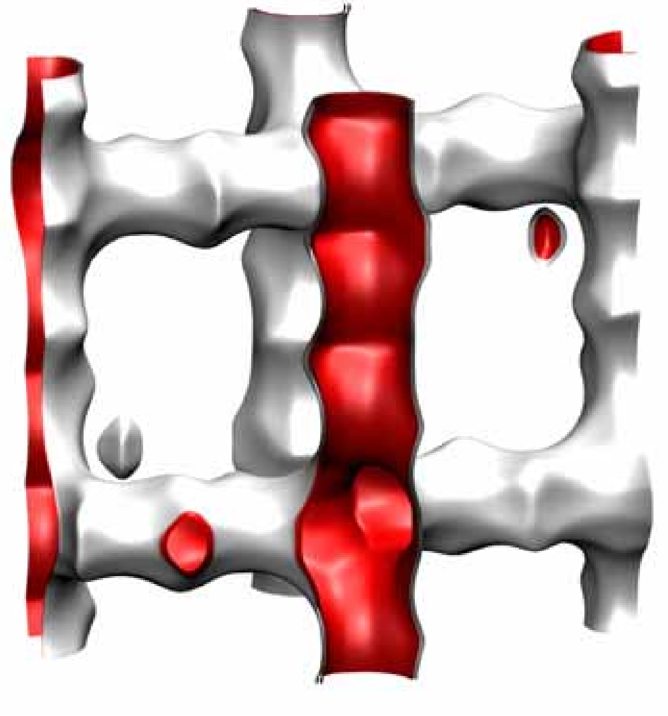

MFI CBMC mixture simulations for CO_2 capture

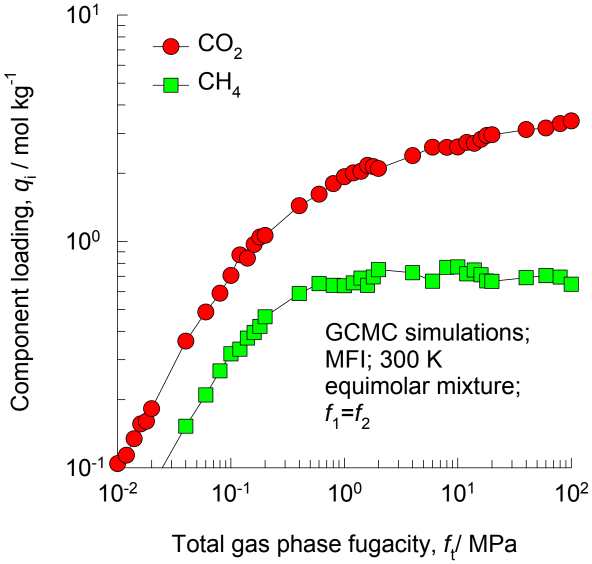

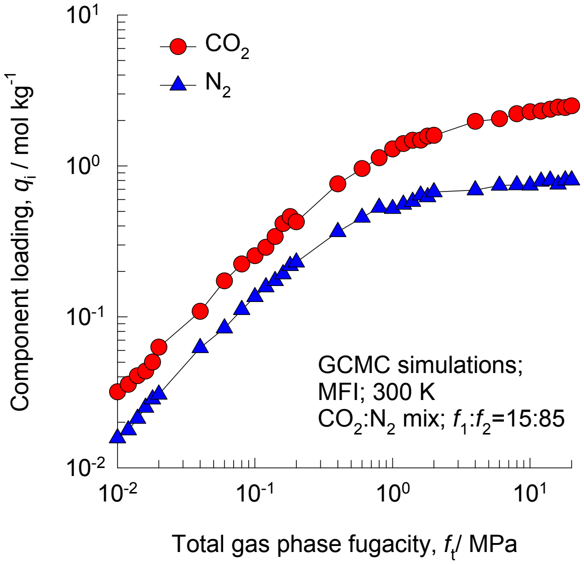

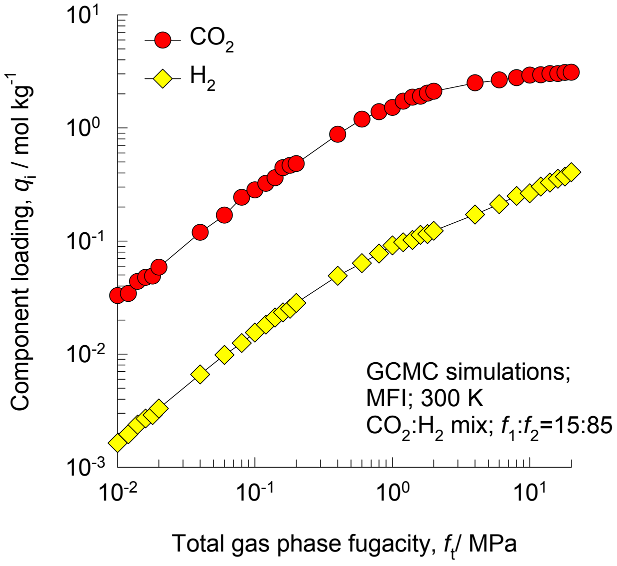

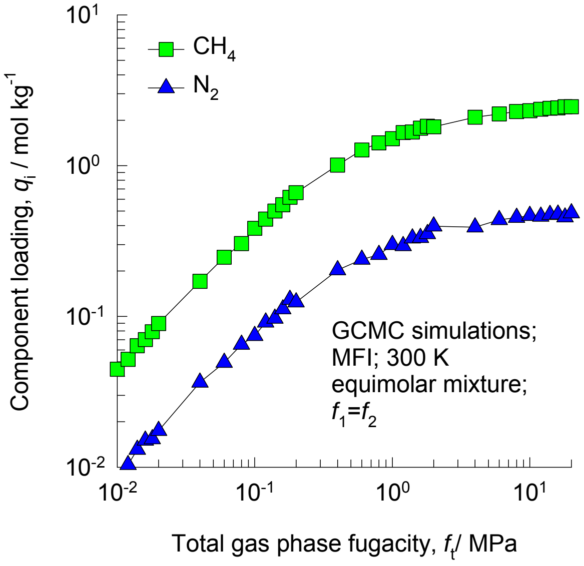

MFI CBMC pentanes mixture simulations

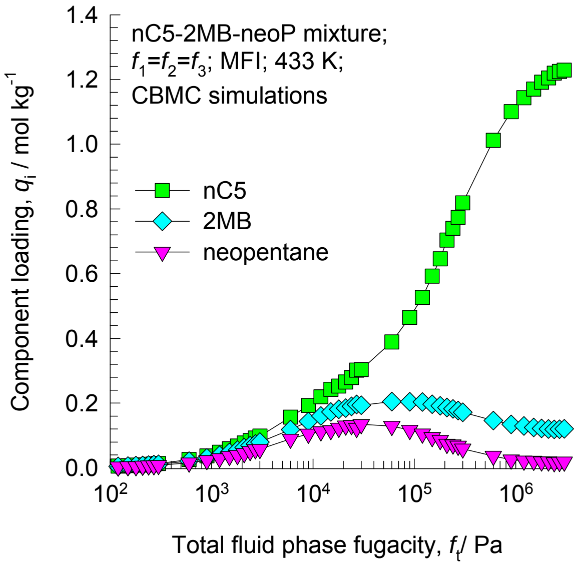

$$S_{ads} = \frac{\dfrac{q_{nC5}}{f_{nC5}} + \dfrac{q_{2MB}}{f_{2MB}}}{\dfrac{q_{neoP}}{f_{neoP}}}$$

Capacity is the total loading of nC5 + 2MB

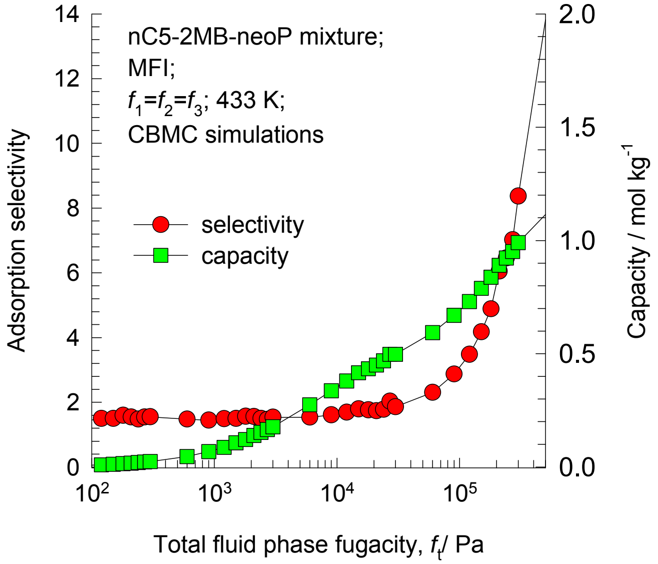

In order to understand the sharp decline in the loading for pressures exceeding 50 kPa, we plot below the component loadings versus the total loading in the mixture.

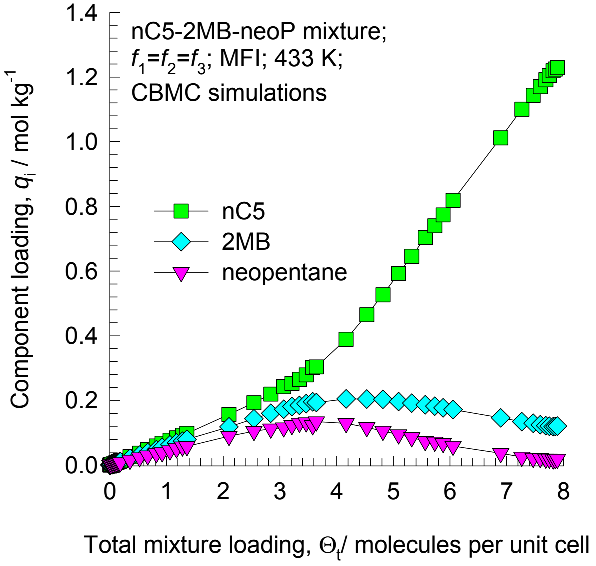

MFI CBMC nC6/3MP/22DMB mixture simulations

Capacity is the total loading of nC6 + 3MP

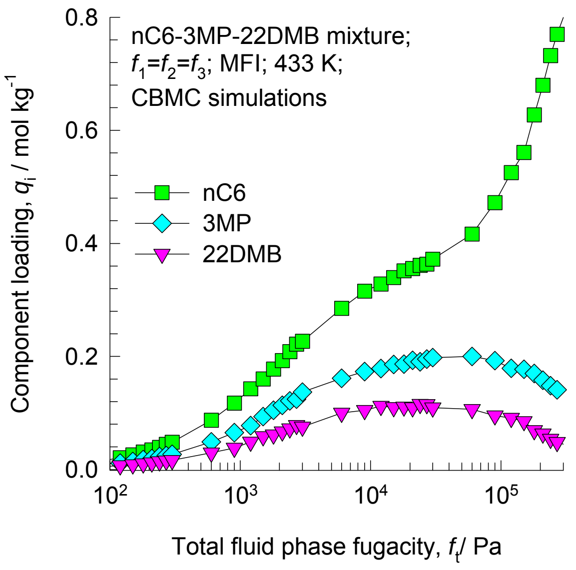

$$S_{ads} = \frac{\frac{q_{nC6}}{f_{nC6}} + \frac{q_{3MP}}{f_{3MP}}}{\frac{q_{22DMB}}{f_{22DMB}}}$$

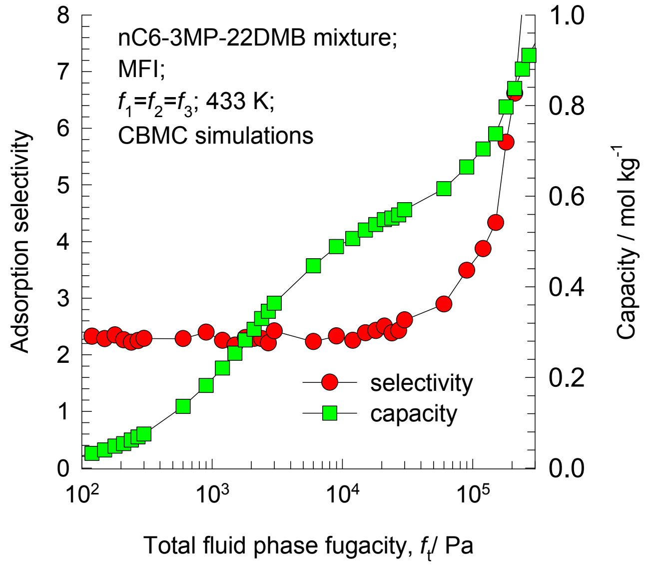

In order to understand the sharp decline in the loading for pressures exceeding 50 kPa, we plot below the component loadings versus the total loading in the mixture.

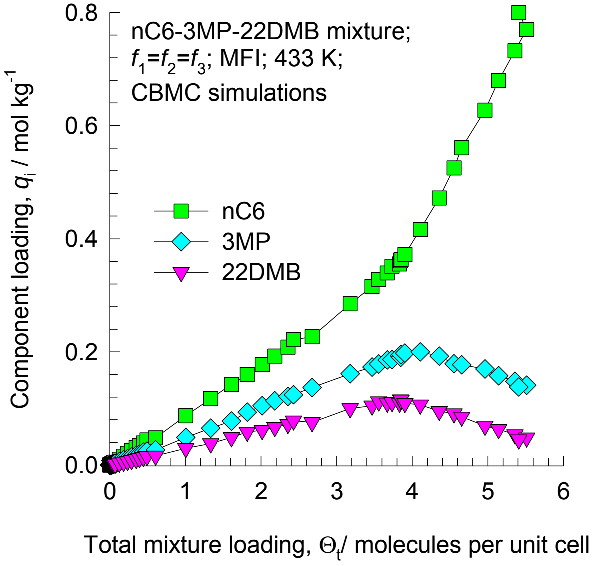

The linear molecule nC6 can locate along the straight and zig-zag channels.
The di-branched 22DMB can only locate at the intersections between the channels.
3MP prefers to locate also at the intersections.
There are 4 intersections per unit cell. The selectivity is heavily in favor of the linear molecules when the total loading exceeds 4 molecules per unit cell.

MFI snapshot of nC66/3MP/22DMB isomers

The linear molecule nC6 can locate along the straight and zig-zag channels.
The di-branched 22DMB can only locate at the intersections between the channels.
3MP prefers to locate also at the intersections.
There are 4 intersections per unit cell.

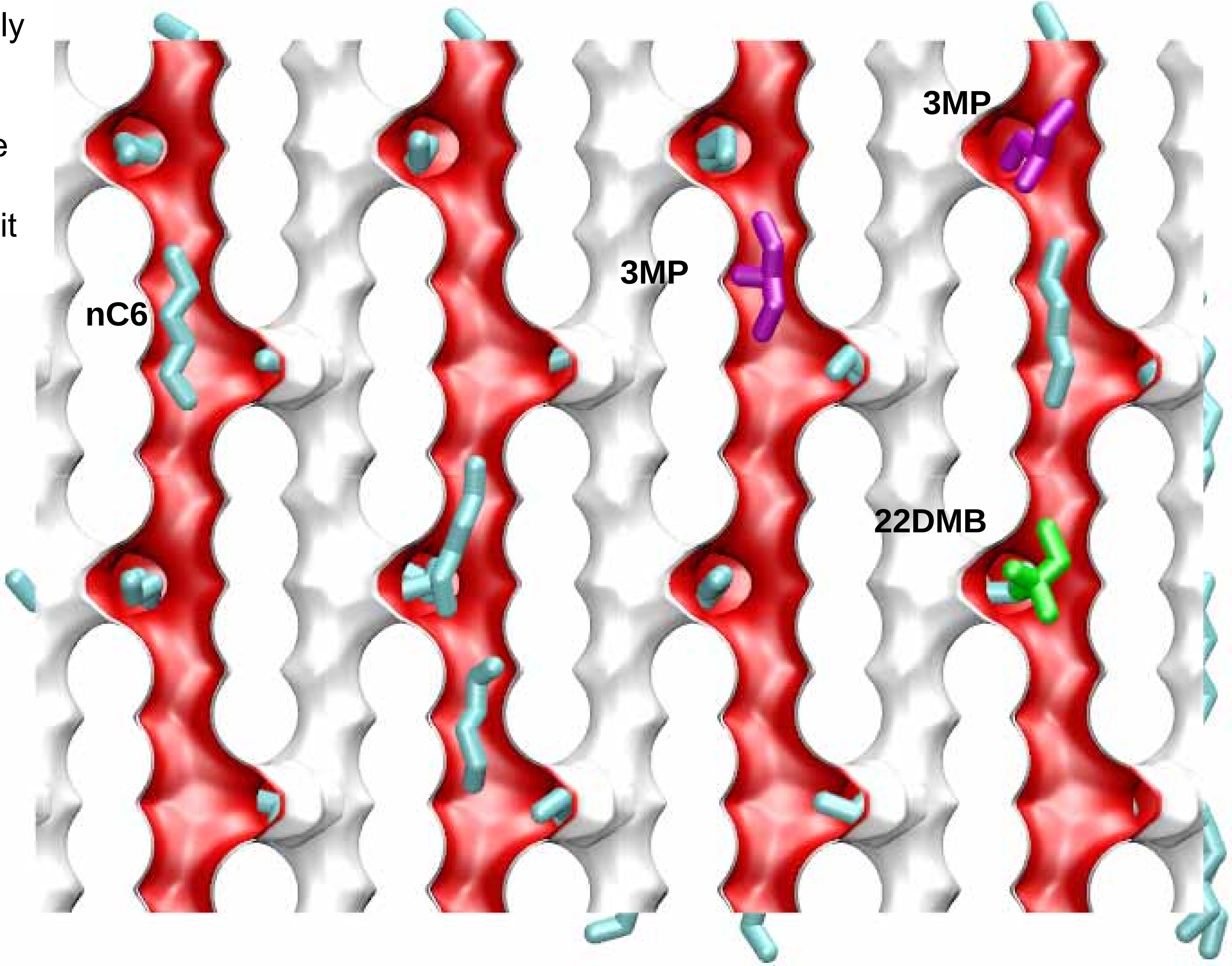

MFI CBMC nC6/2MP/3MP/22DMB/23DMB mixture simulations

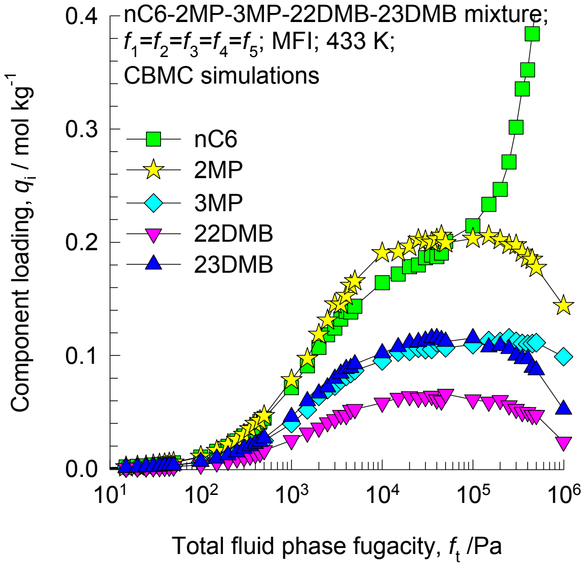

In order to understand the sharp decline in the loading for pressures exceeding 50 kPa, we plot below the relative component loadings versus the total loading in the mixture.

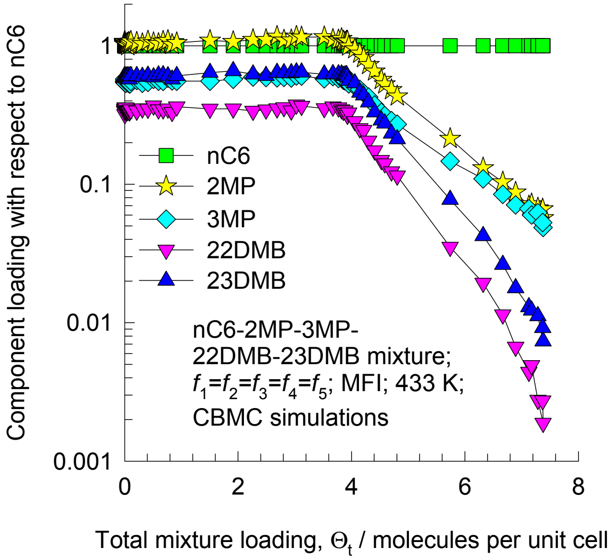

MFI CBMC nC6/2MP/3MP/22DMB/23DMB mixture simulations

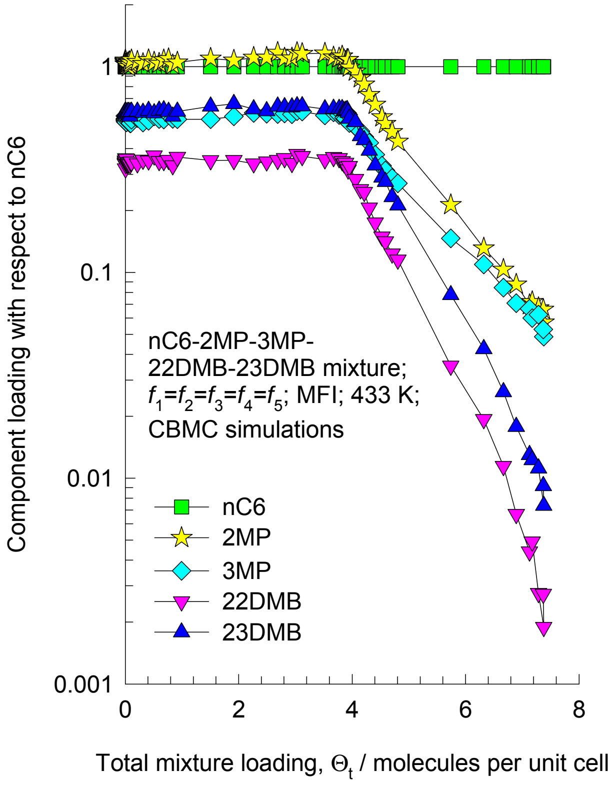

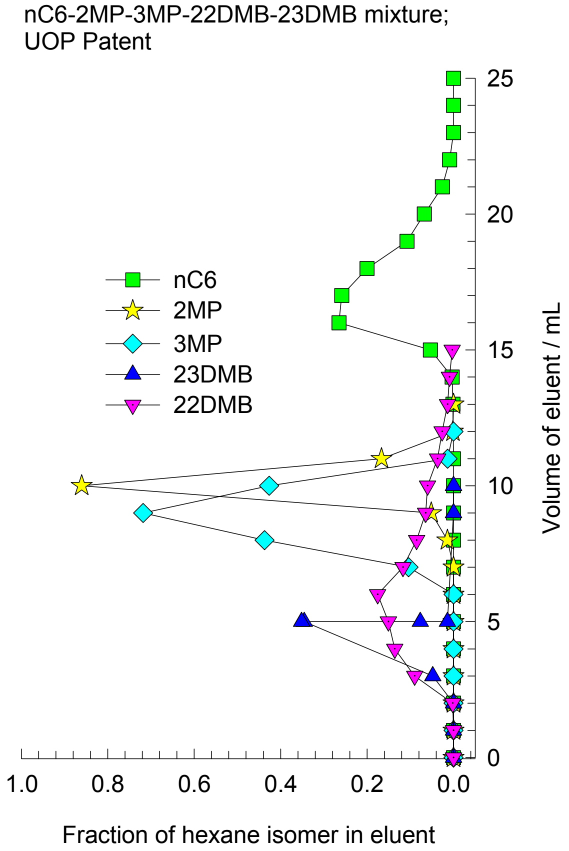

CBMC simulations give the same adsorption hierarchy as that in the elution curves presented in the UOP patents on alkanes isomer separation

H.W. Dandekar, G.A. Funk, R.D. Gillespie, H.A. Zinnen, C.P. McGonegal, M. Kojima, S.H. Hobbs, Process H.W. Dandekar, G.A. Funk, H.A. Zinnen, Process for separating and recovering multimethyl-branched alkanes, UOP Inc., USA., US 6069289, U.S., 2000.

Further discussions on this can be found in:

R. Krishna, B. Smit, S. Calero, Entropy effects during sorption of alkanes in zeolites, Chem. Soc. Rev. 31 (2002) 185-194.

The simulation data presented above were performed with the updated Dubbeldam force field.

MOR pore landscape

To convert from molecules per unit cell to mol kg^{-1}, multiply by 0.3467.
The pore volume is 0.166 cm^3/g.

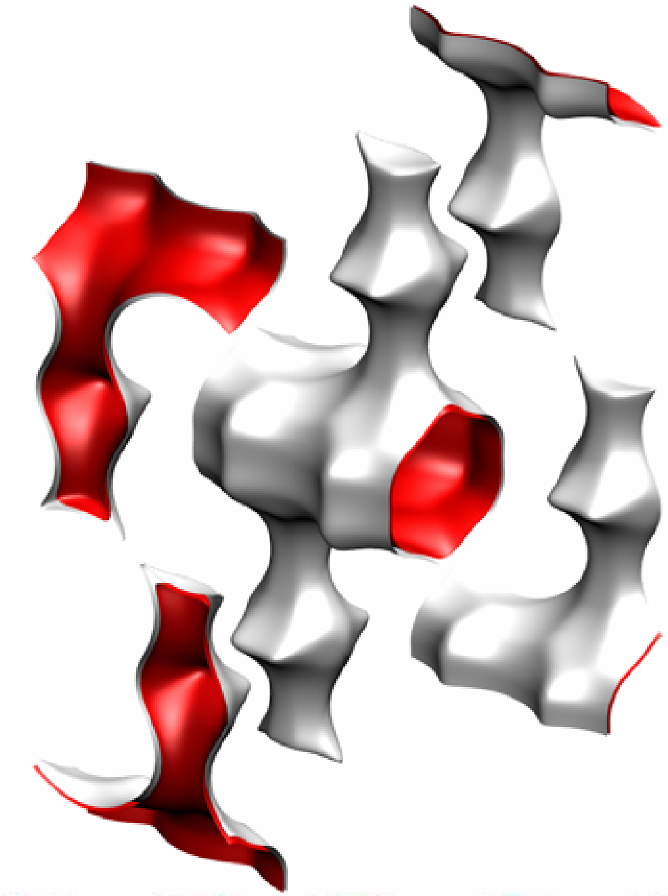

12-ring
main channels

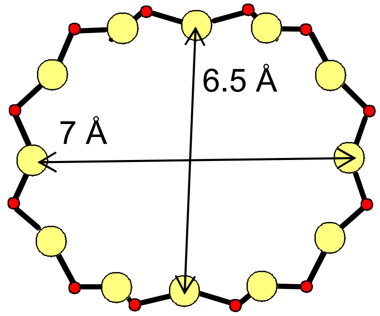

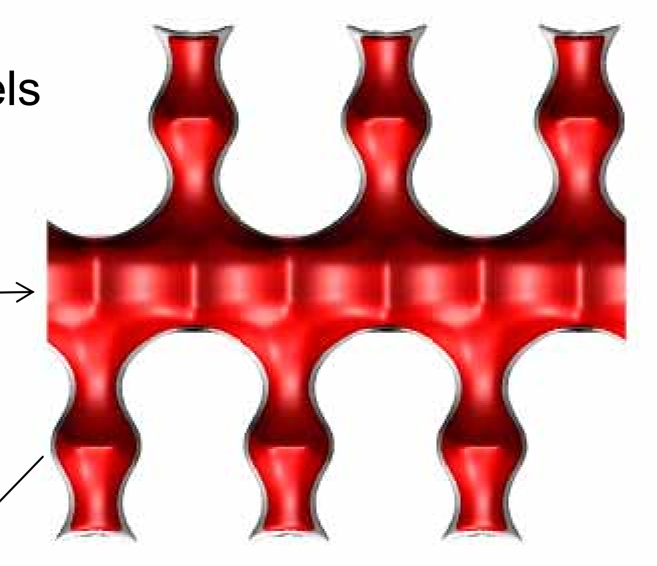

8-ring
side pockets

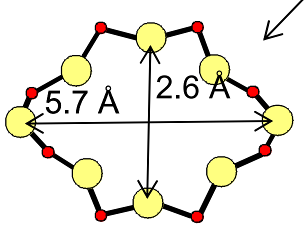

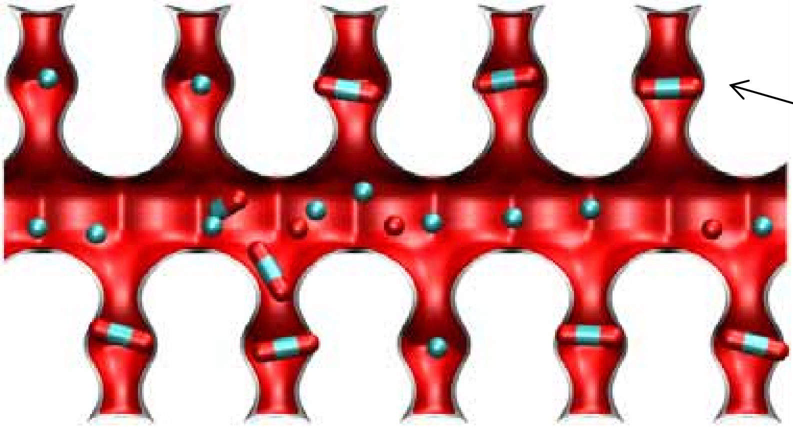

CO_2 preferentially locates in the side pockets and this is the reason for the high selectivity

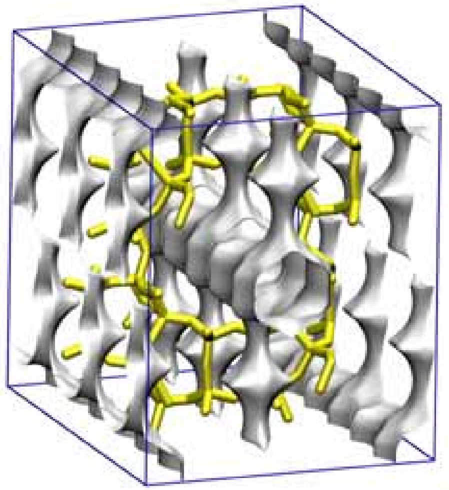

MOR CBMC mixture simulations for CO_2 capture

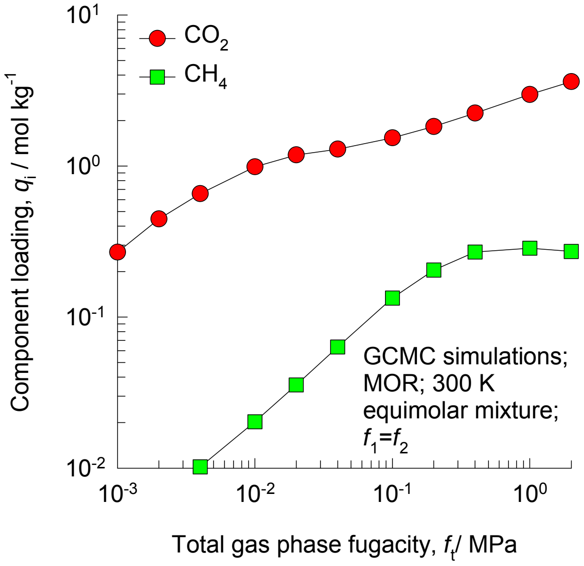

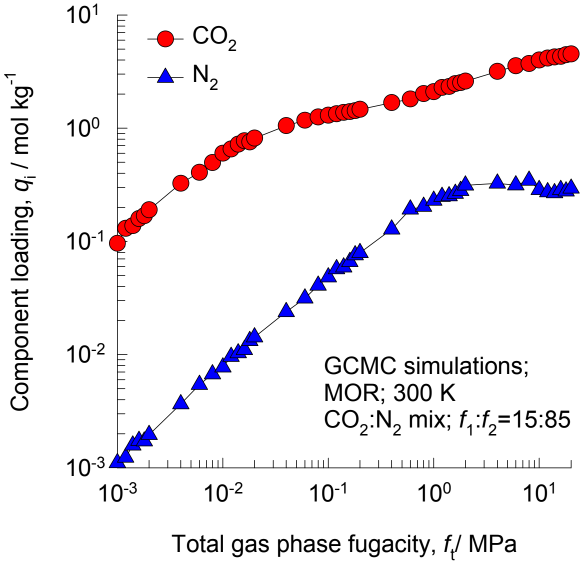

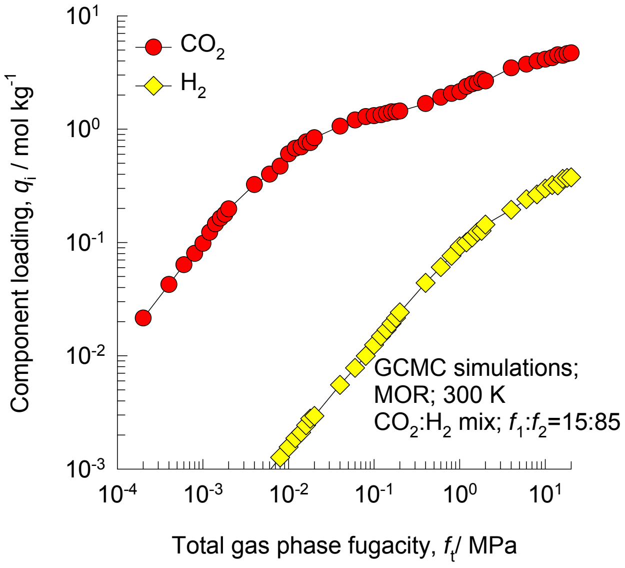

MOR CBMC nC6/3MP/22DMB mixture simulations

Capacity is the total loading of nC6 + 3MP

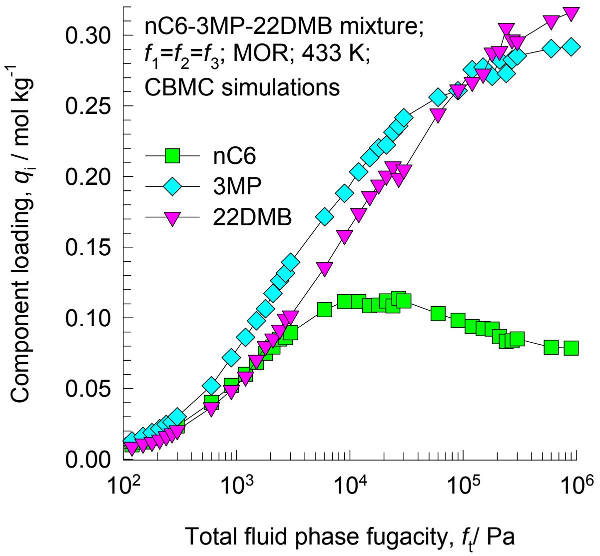

$$S_{ads} = \frac{\dfrac{q_{nC6}}{f_{nC6}} + \dfrac{q_{3MP}}{f_{3MP}}}{\dfrac{q_{22DMB}}{f_{22DMB}}}$$

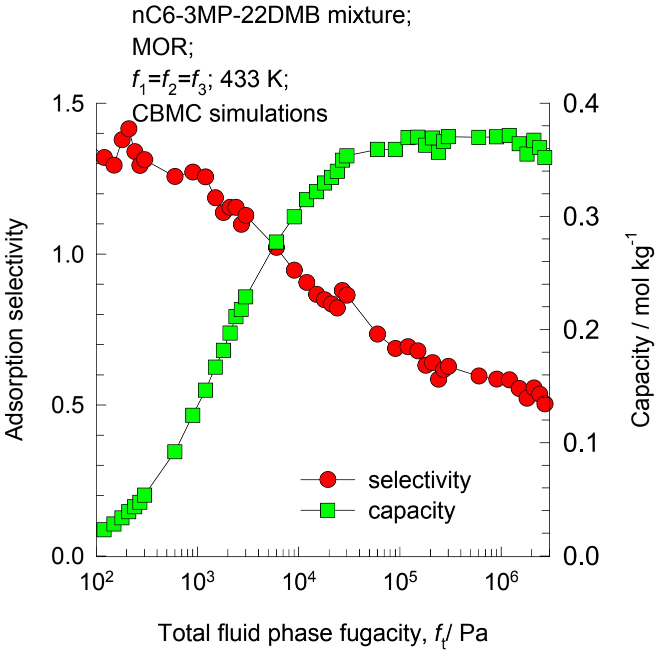

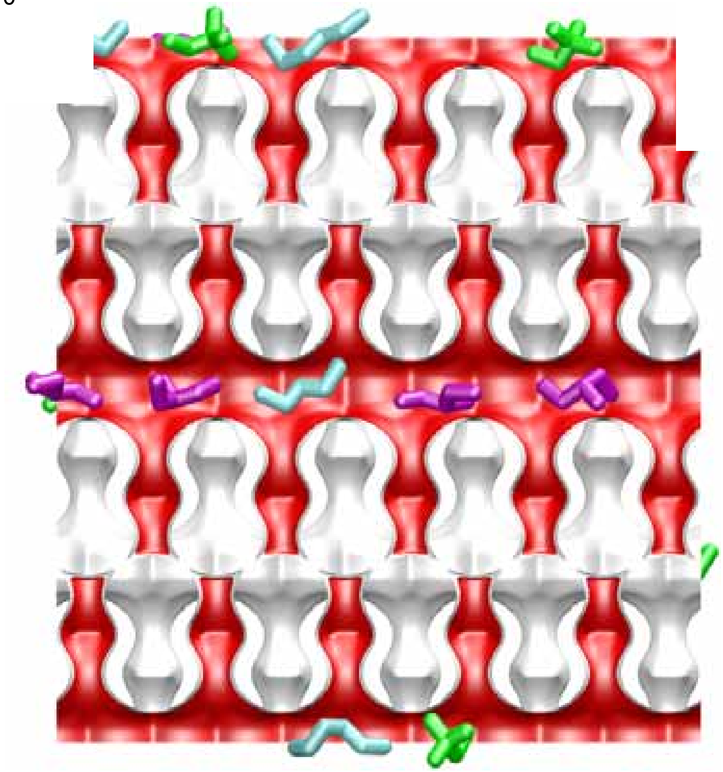

MTW pore landscape

MTW has 1D channel system:
12-ring channels of 5.6 x 6.0 Å

MTW has a 1D channel system

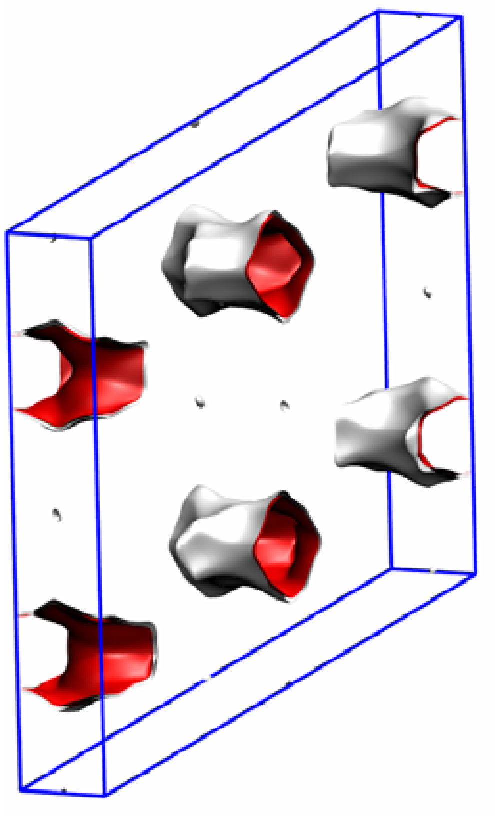

To convert from molecules per unit cell to mol kg-1, multiply by 0.2972.
The pore volume is 0.111 cm3/g.

Snapshot of CO_2/CH_4 mixture

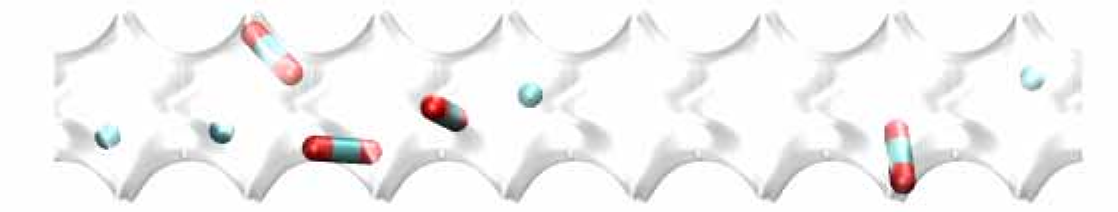

MTW CBMC mixture simulations for CO_2 capture

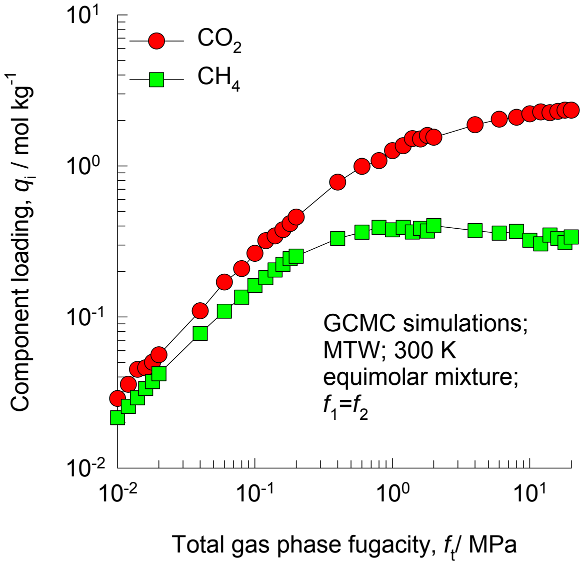

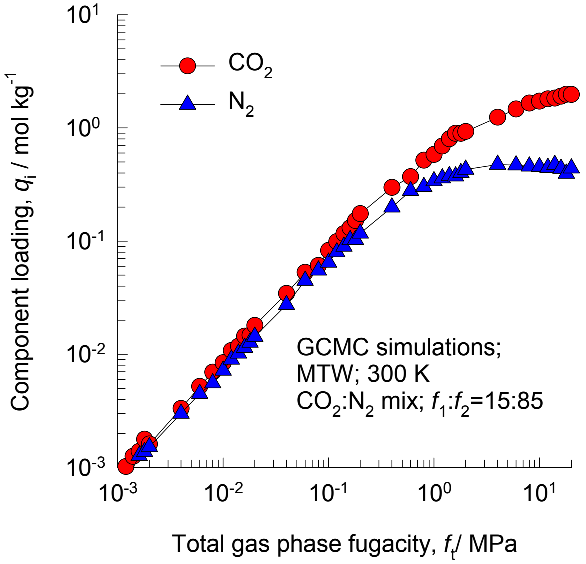

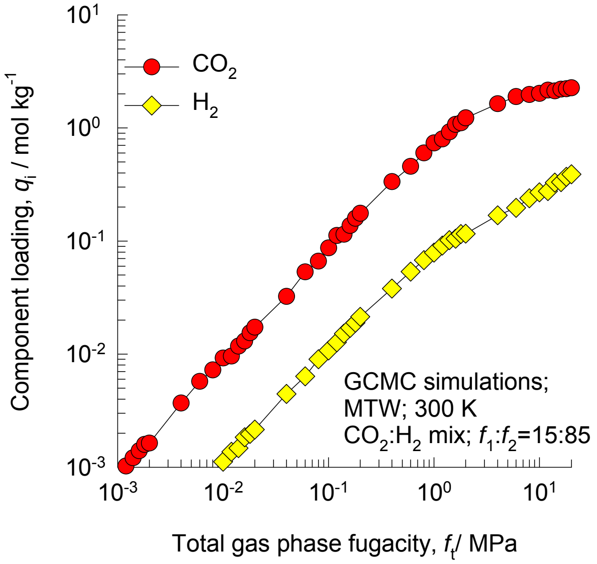

TON

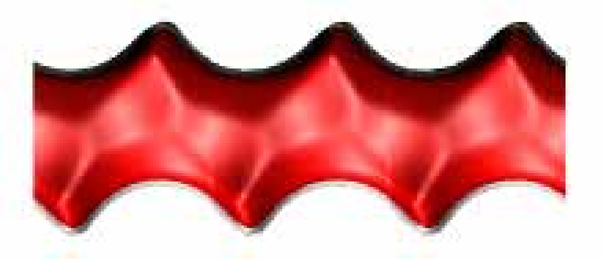

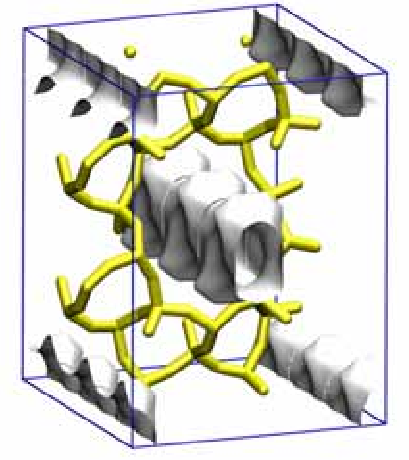

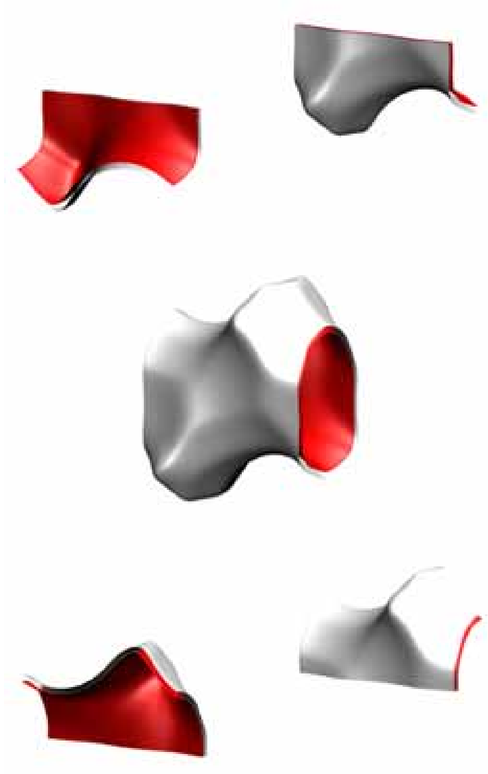

10-ring channel of TON

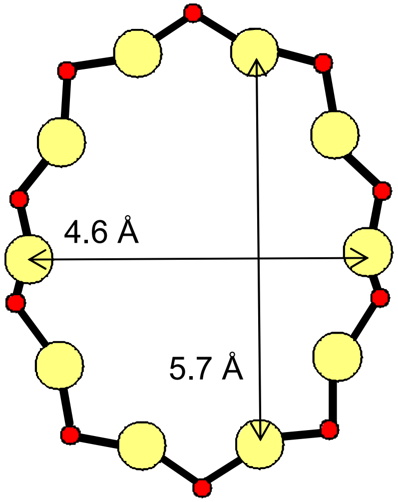

To convert from molecules per unit cell to mol kg^{-1}, multiply by 0.6934.
The pore volume is 0.097 cm^3/g.

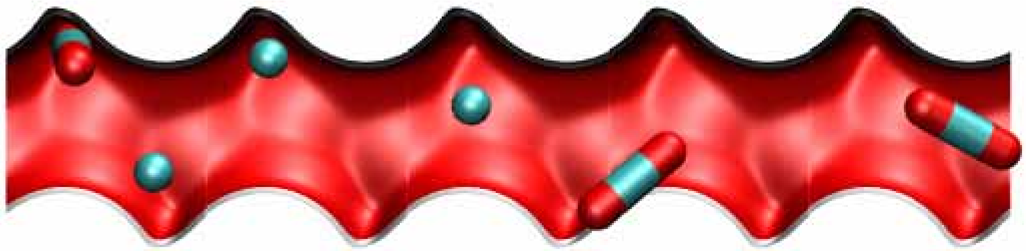

Snapshot of CO_2/CH_4 mixture

TON CBMC mixture simulations for CO_2 capture

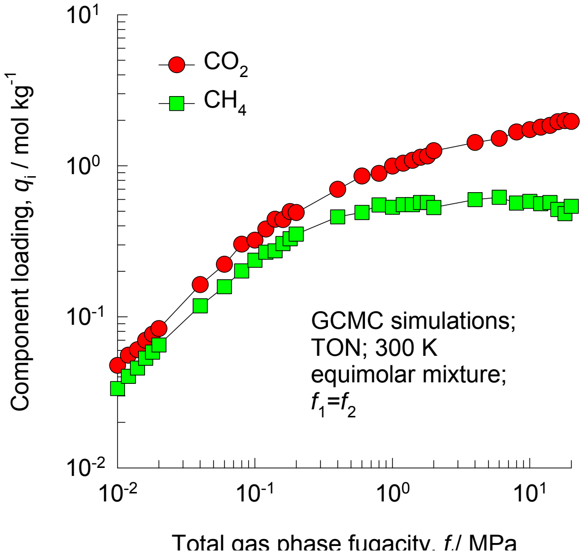

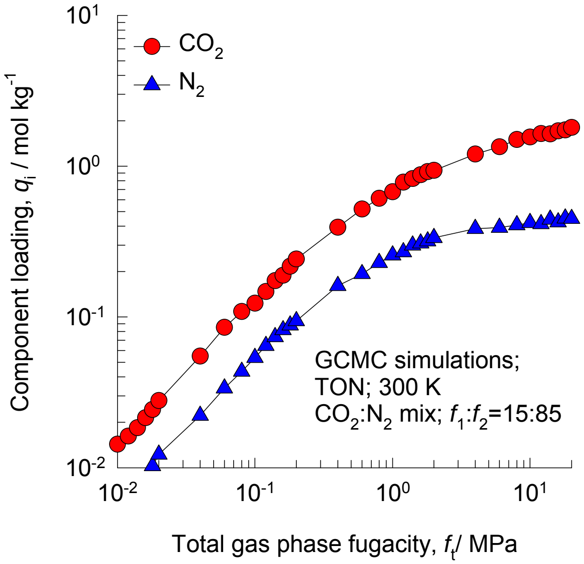

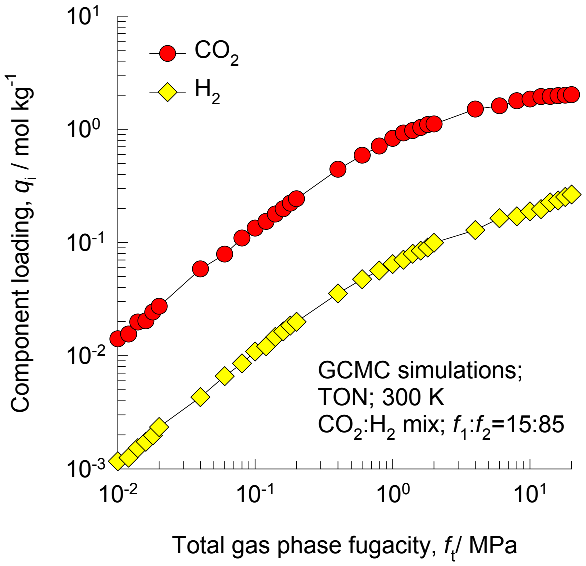

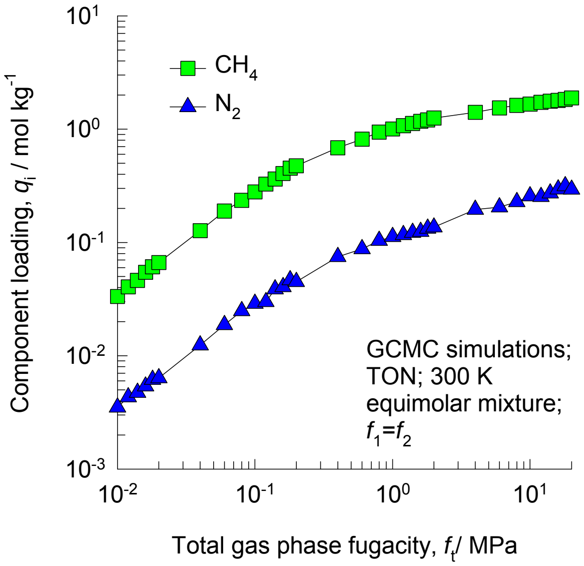

To convert from molecules per unit cell to mol kg^{-1}, multiply by 0.0433.
The pore volume is 0.344 cm^3/g.

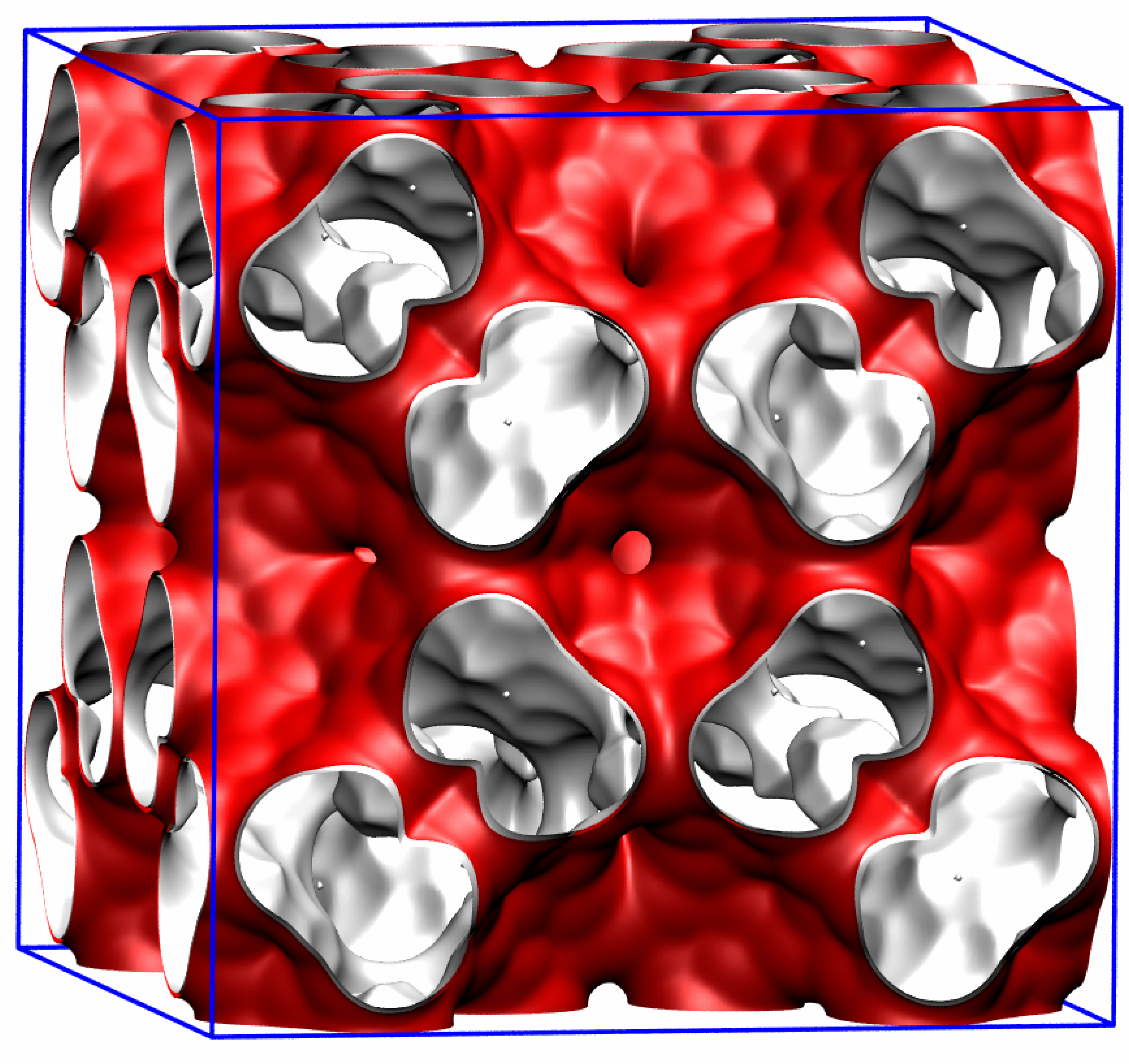

Unit cell of TSC

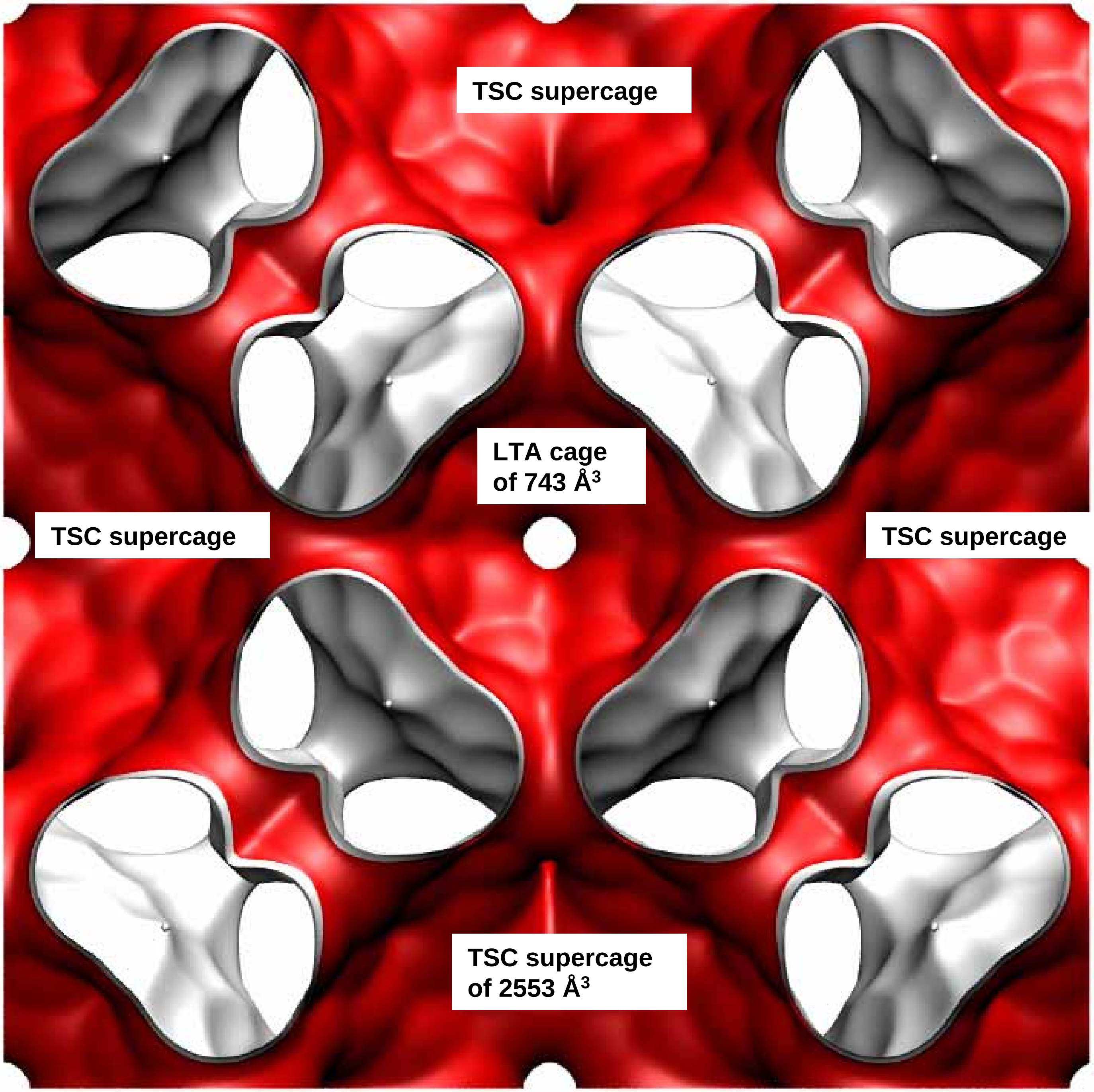

8-ring windows of two sizes:
4.2x4.2 Å along [100]
3.1x5.6 Å along [110]

Front plane of unit cell of TSC

TSC CBMC mixture simulations for CO_2 capture

Inaccessible
sodalite cages have been blocked in these simulations

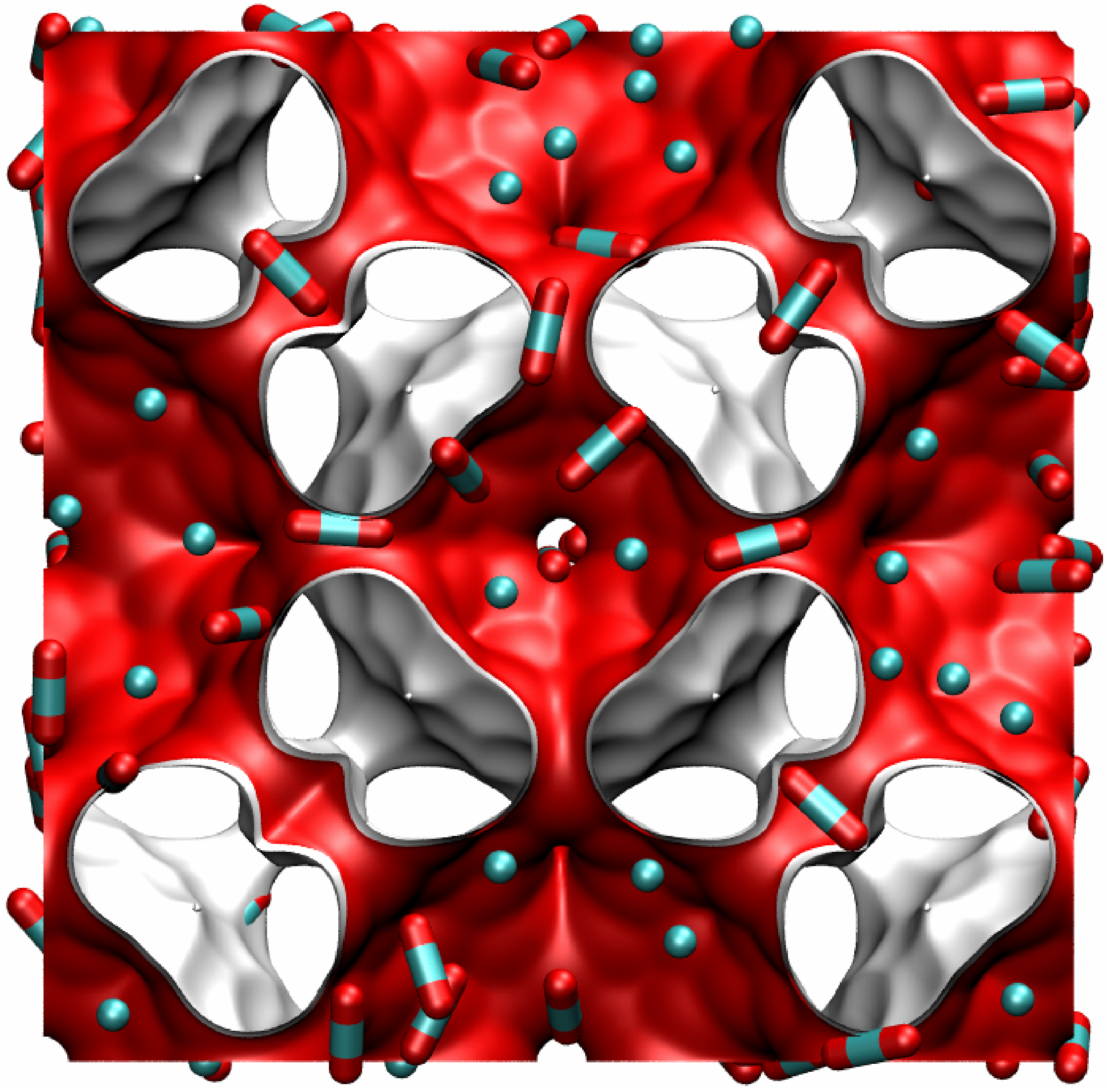

Snapshots showing location of CH_4 and CO_2

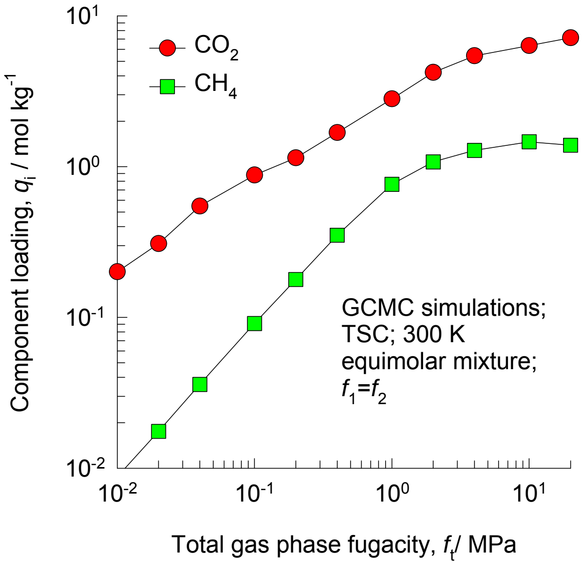

TSC CBMC mixture simulations for CO_2 capture

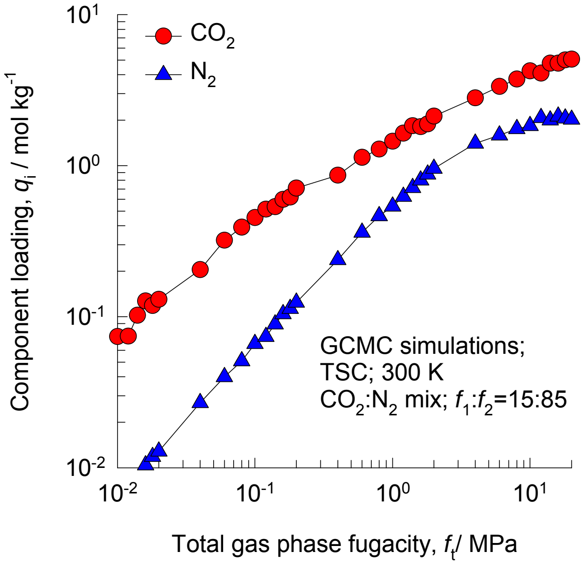

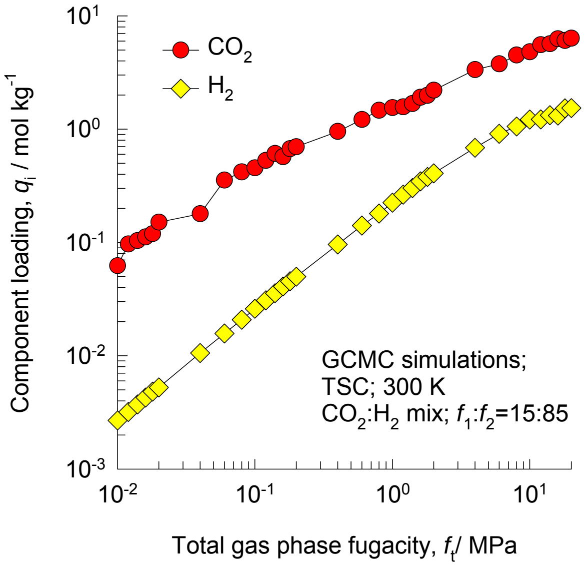

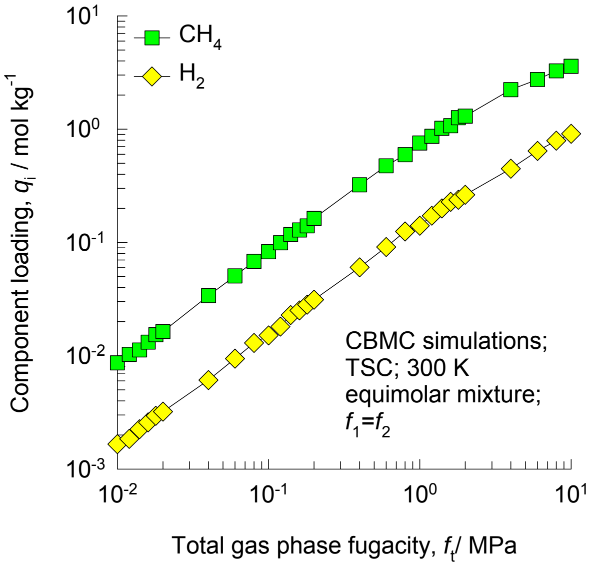

TSC CBMC nC6/3MP/22DMB mixture simulations

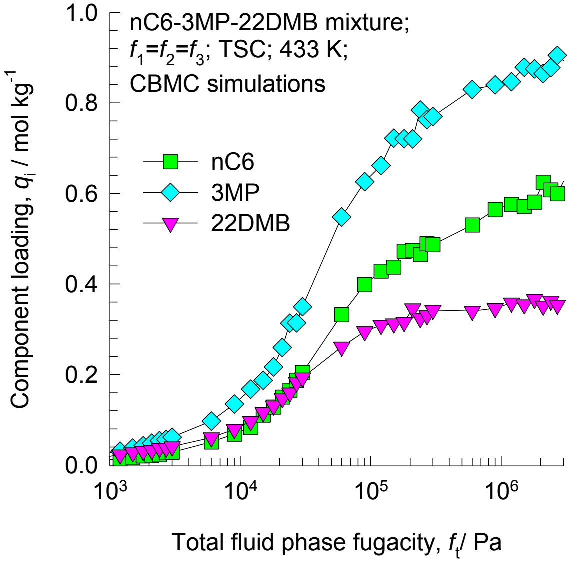

$$S_{ads} = \frac{\dfrac{q_{nC6}}{f_{nC6}} + \dfrac{q_{3MP}}{f_{3MP}}}{\dfrac{q_{22DMB}}{f_{22DMB}}}$$

Capacity is the total
loading of nC6 + 3MP

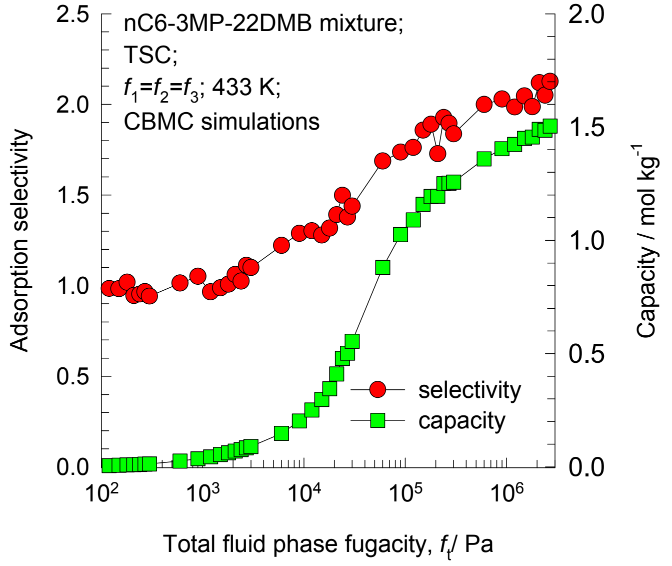

TSC snapshot of hexane isomers

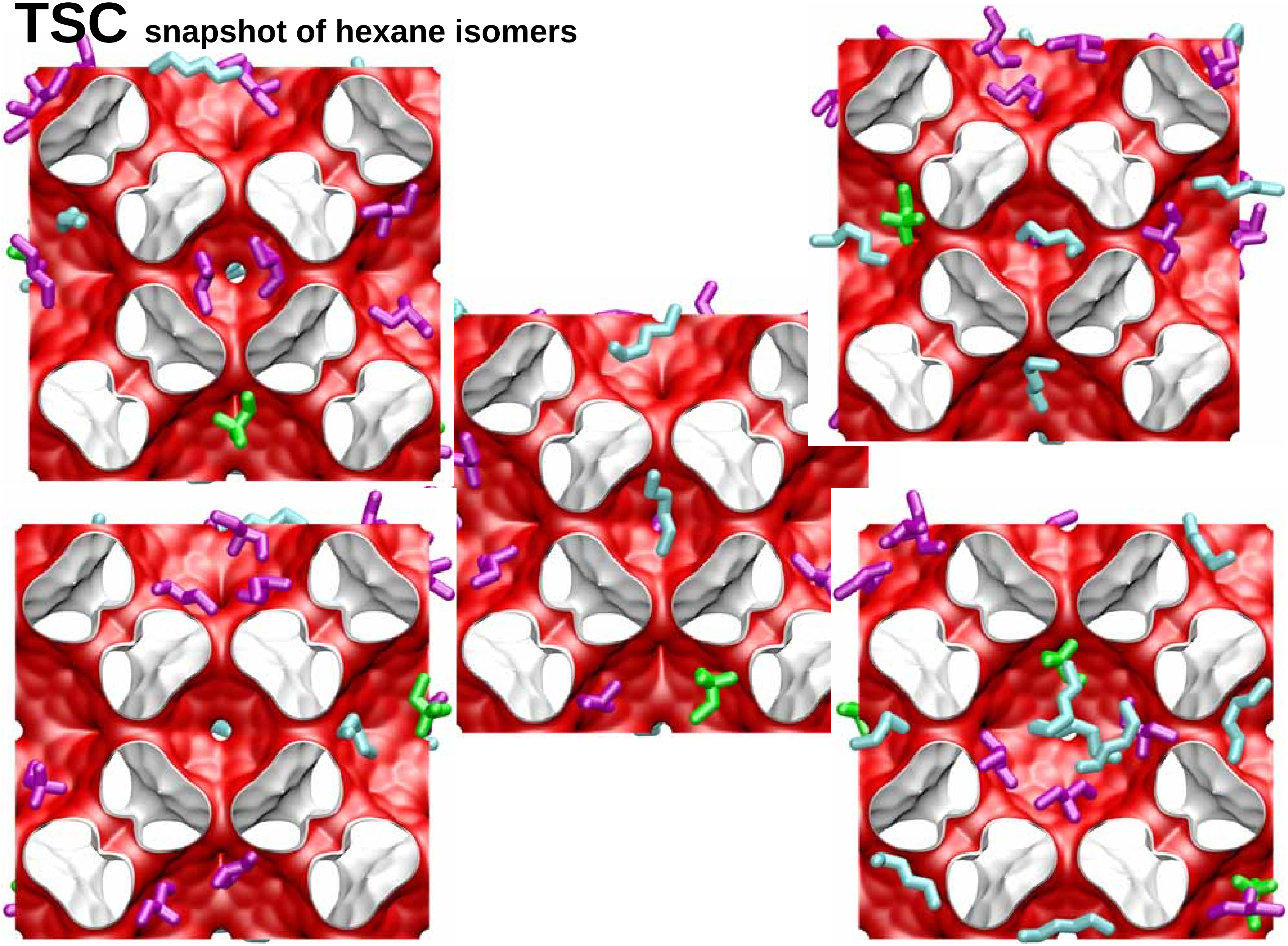

Additional all-silica zeolites that are not discussed in the manuscript

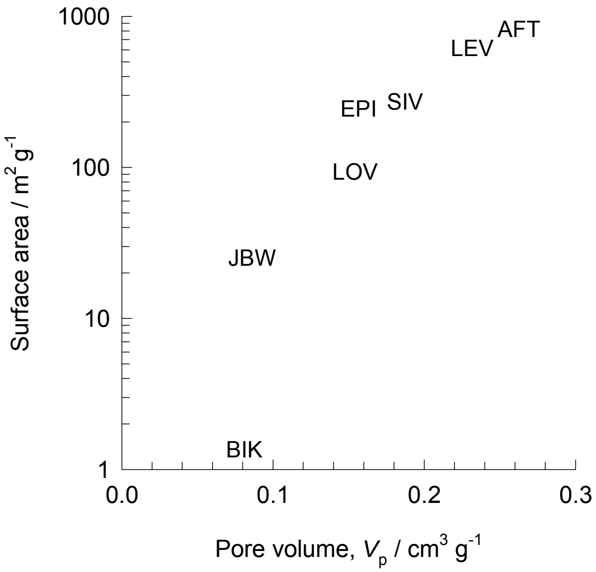

Seven zeolite structures, with structural information obtained from the IZA atlas were also screened for the adsorption selectivity. These are not discussed in the manuscript because even though their selectivity values for some of these zeolites are high, their capacities (delta loadings) are very low in all cases. There are also other issues with respect to accessibility of guest molecules. The highest selectivities are obtained with JBW and BIK that have extremely low surface areas.

AFT landscapes

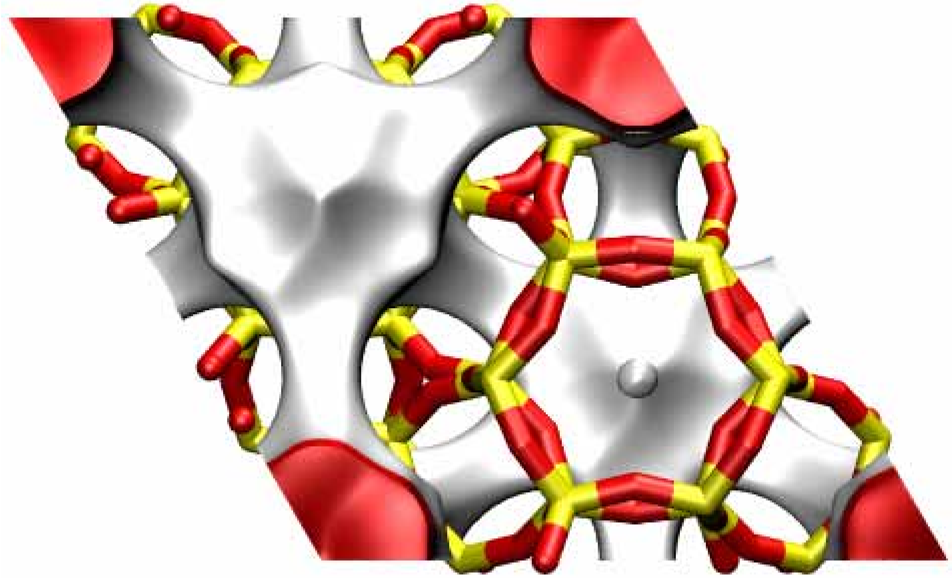

To convert from molecules per unit cell to mol kg^{-1}, multiply by 0.2311.
The pore volume is 0.2626 cm^3/g.

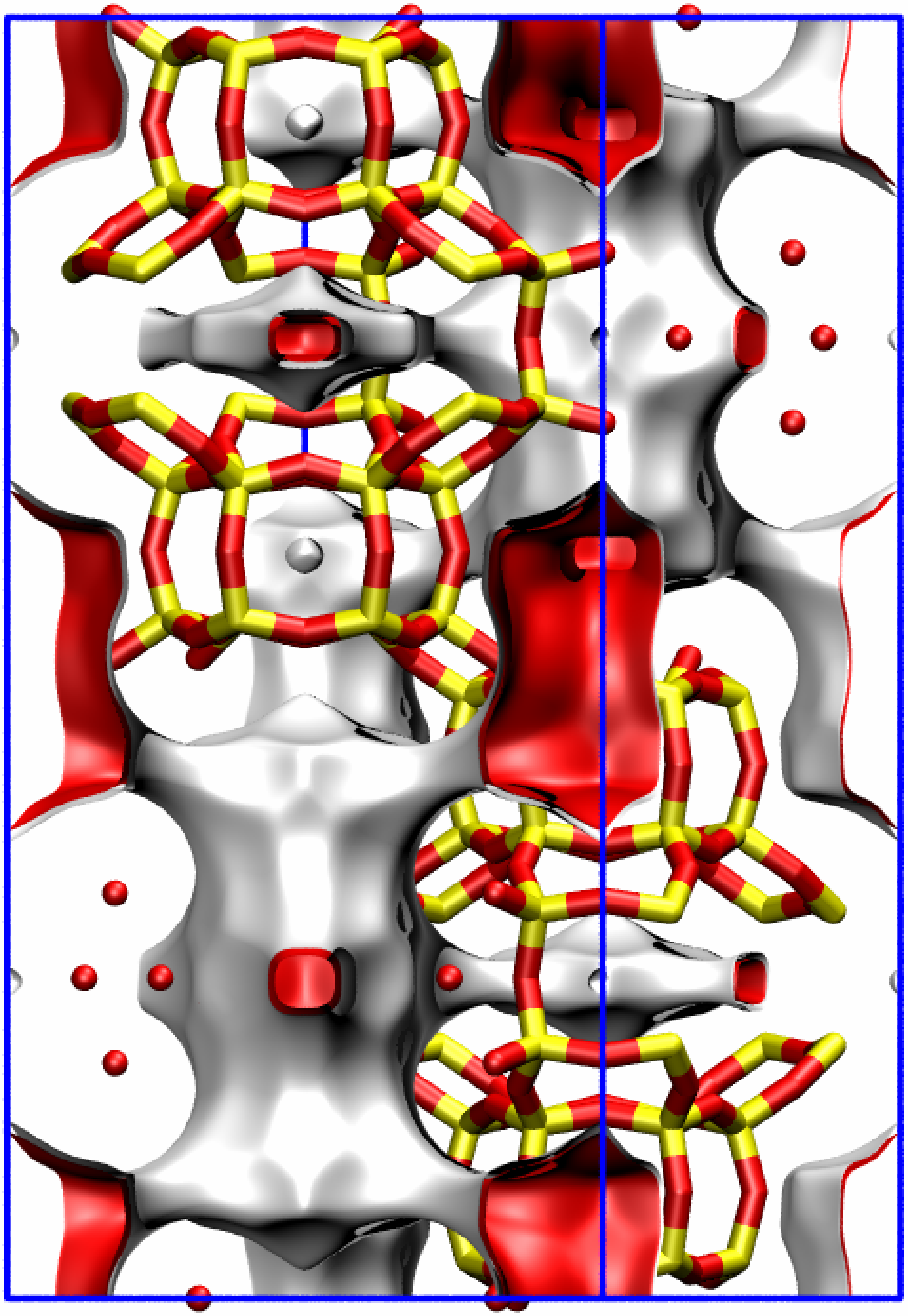

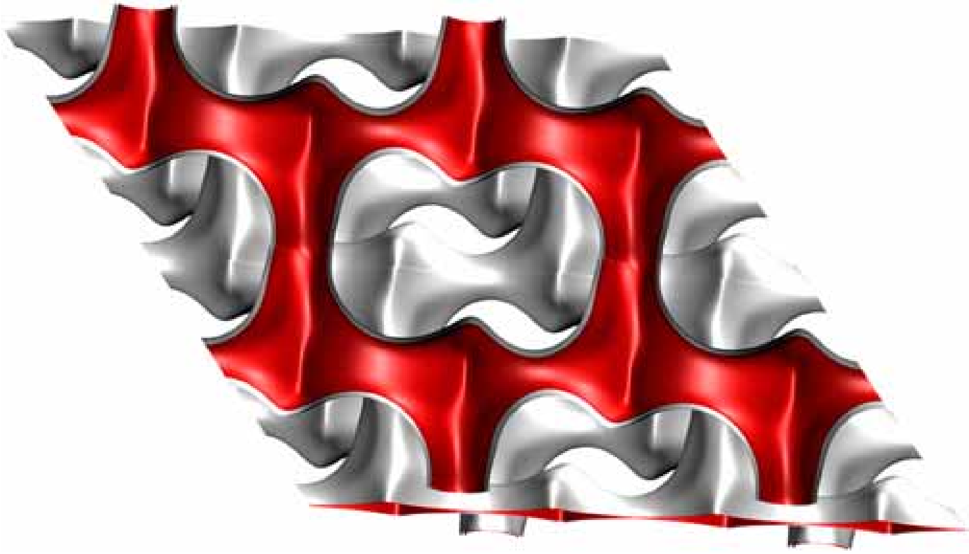

AFT CBMC mixture simulations for CO_2 capture

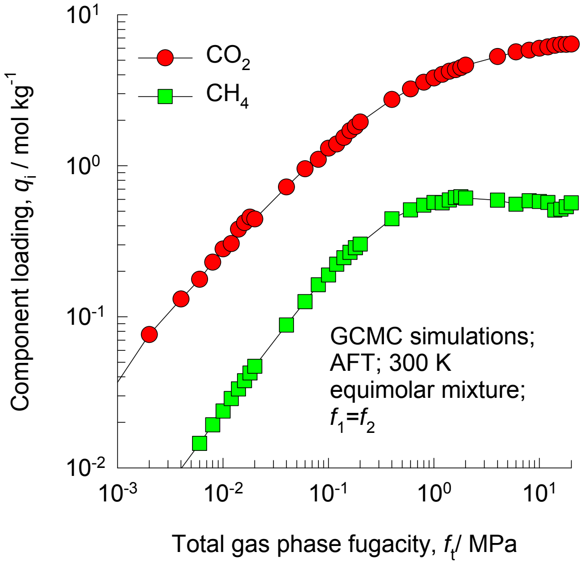

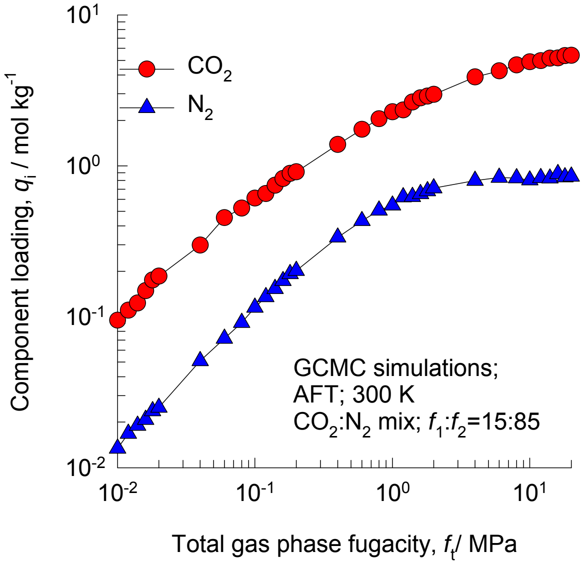

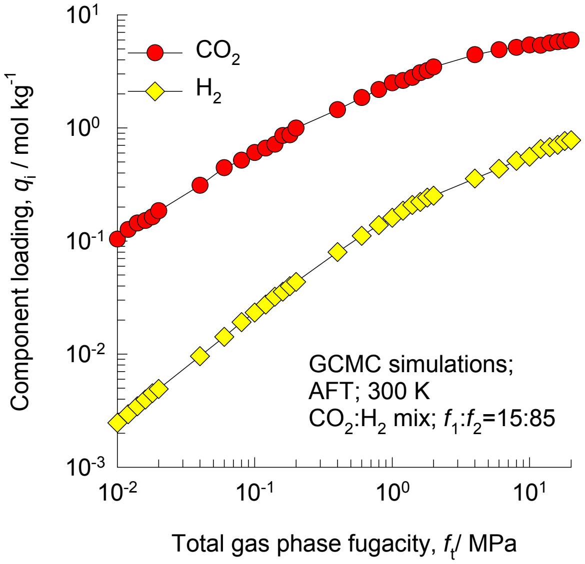

BIK landscapes

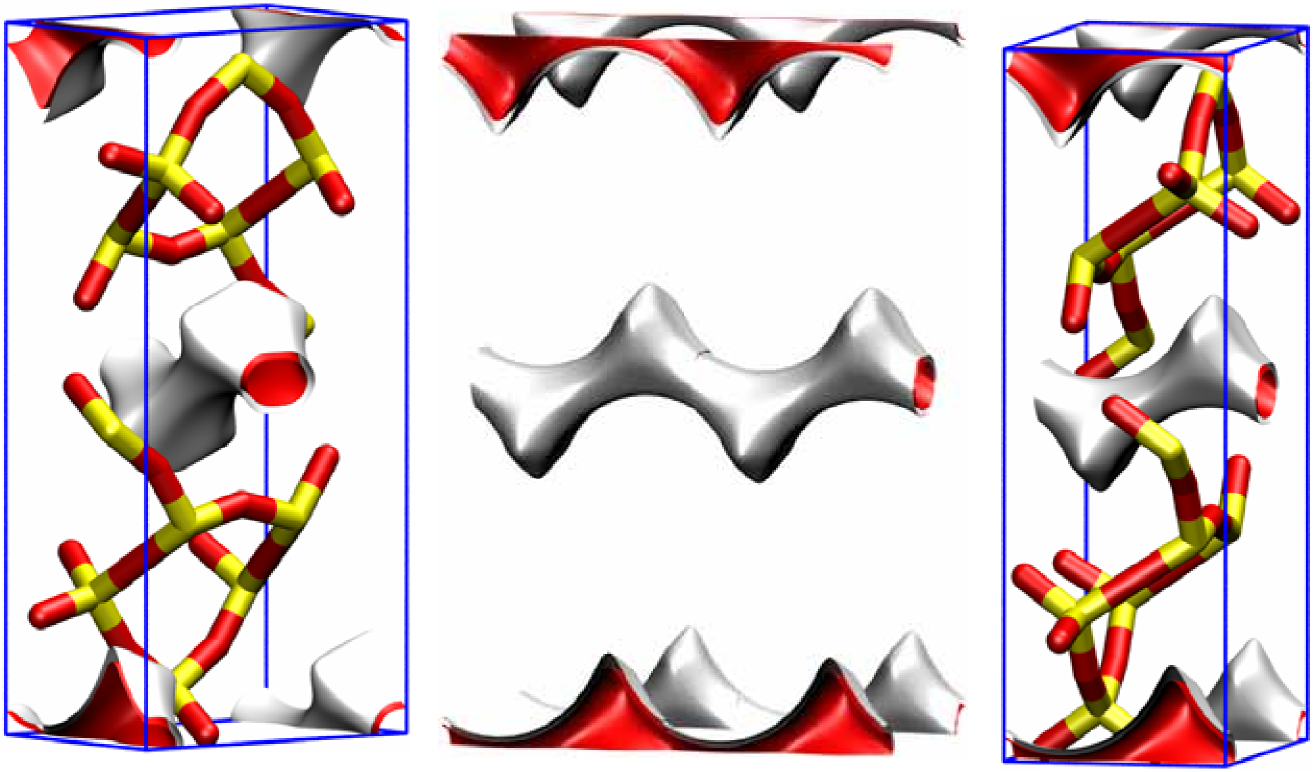

To convert from molecules per unit cell to mol kg^{-1}, multiply by 1.387.
The pore volume is 0.081 cm^3/g.

BIK snapshots

BIK has one-dimensional 8-ring channel structures of about 3.7 Å size. The channel topologies are such that CO_2 can nestle nicely in each channel segment. The curvature and size of the channels are energetically optimum for location of CO_2 molecules. CH_4 molecules are too severely constrained in the channel segments of BIK and can only occupy the more spacious vertex regions.

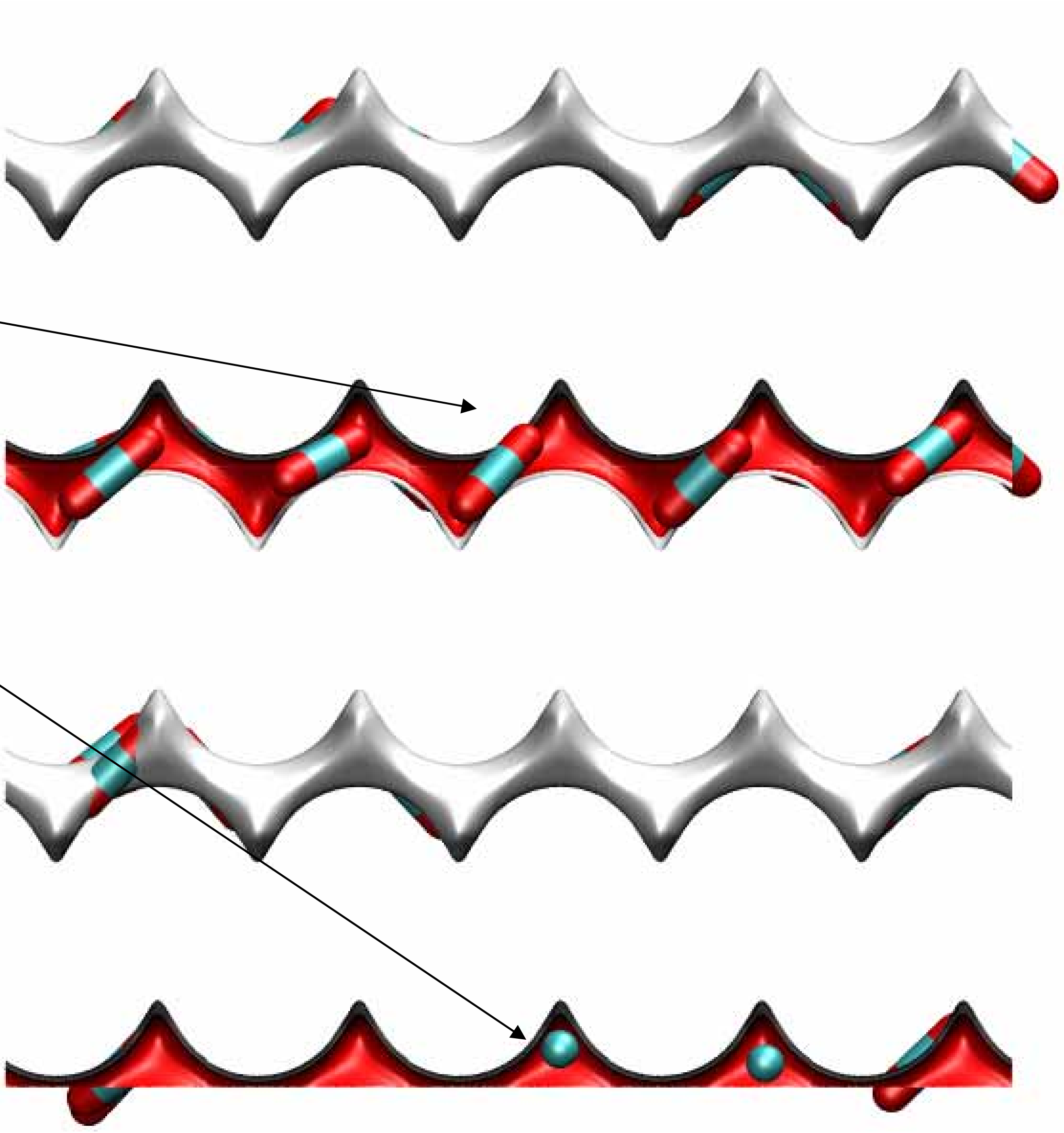

BIK CBMC mixture simulations for CO_2 capture

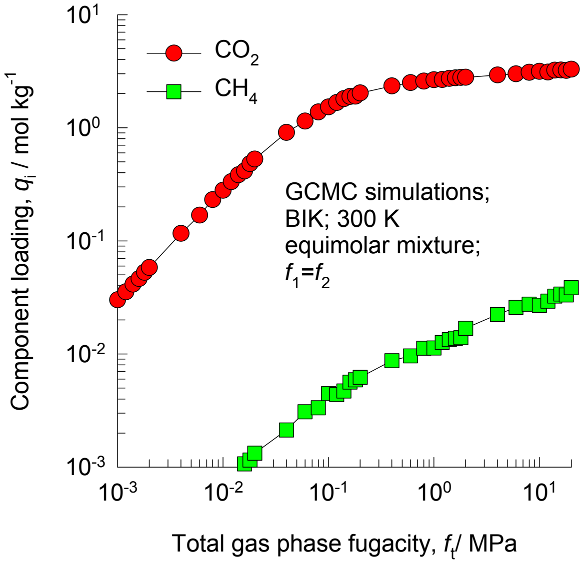

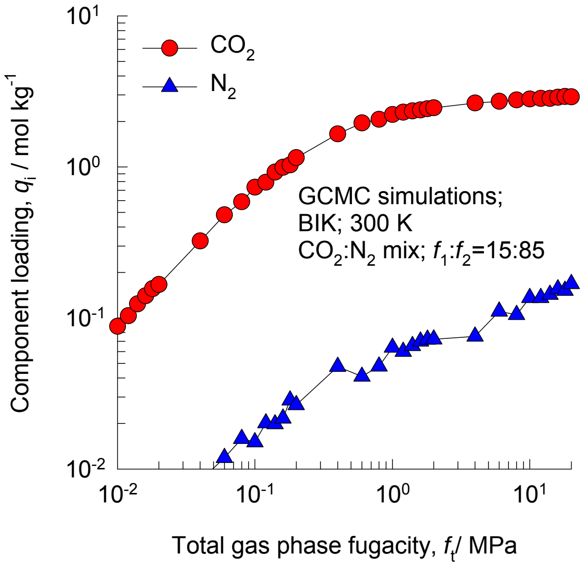

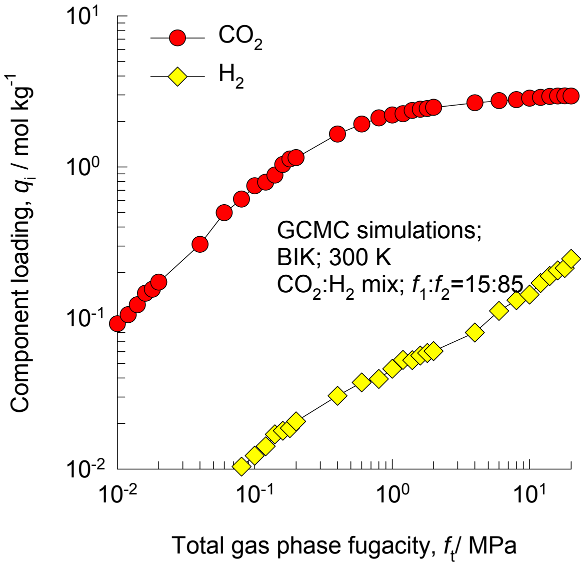

EPI landscapes

To convert from molecules per unit cell to mol kg^{-1}, multiply by 0.69346.
The pore volume is 0.156 cm^3/g.

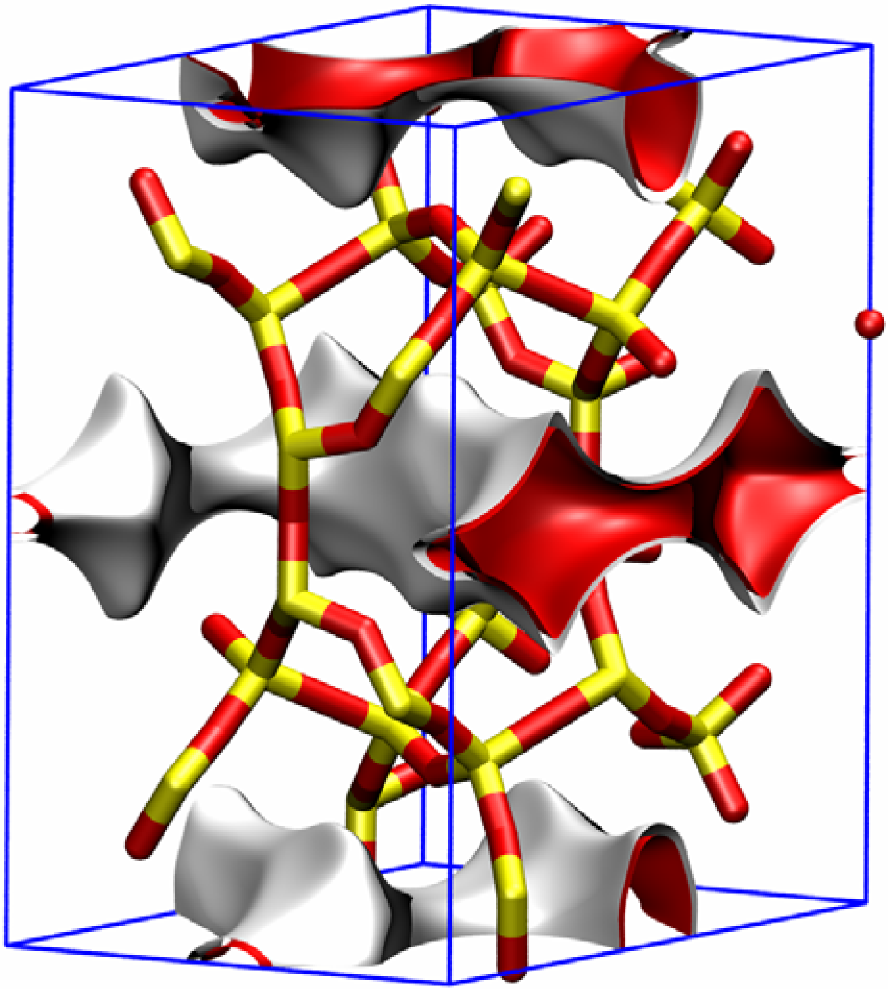

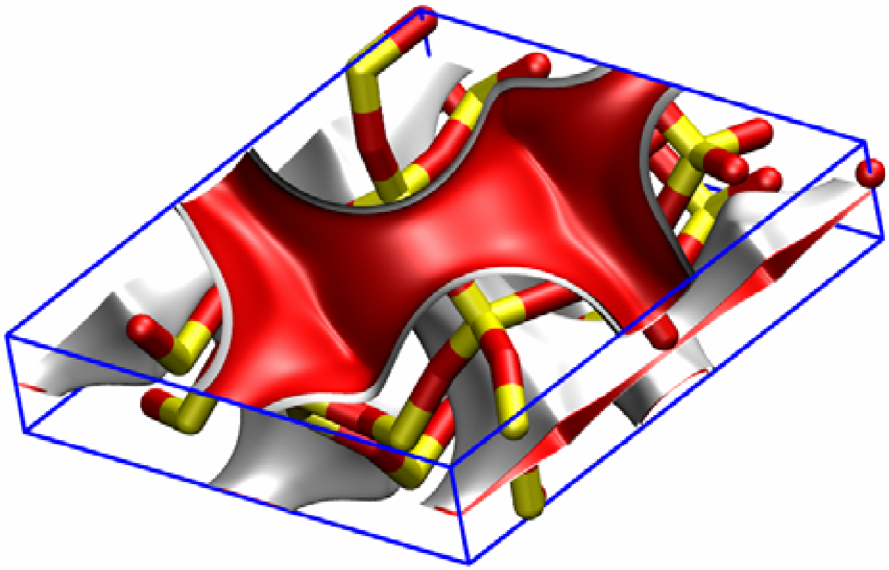

EPI CBMC mixture simulations for CO_2 capture

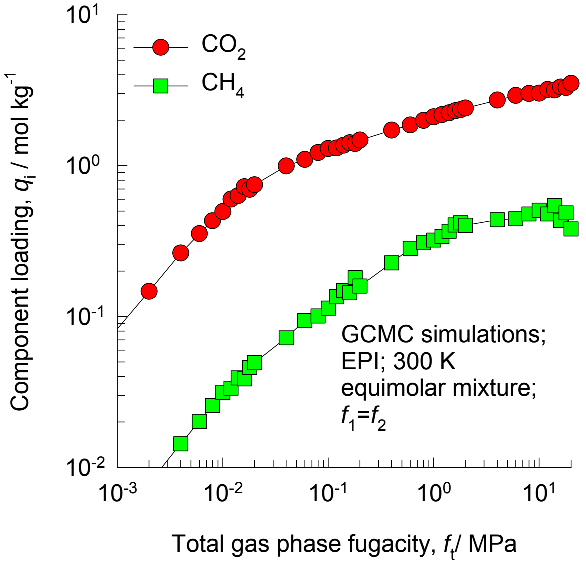

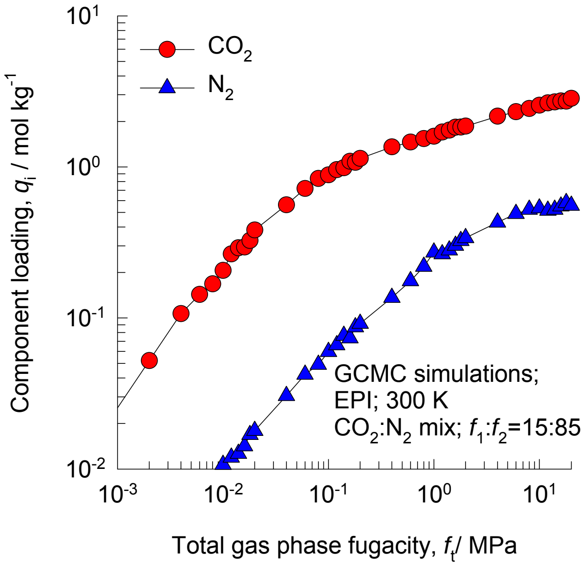

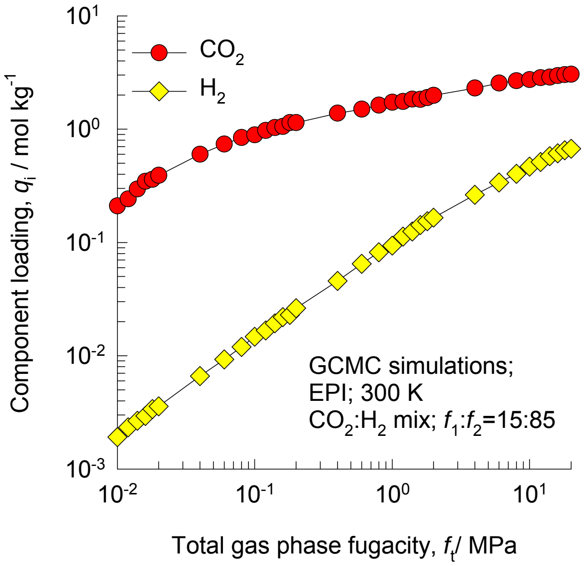

JBW landscapes

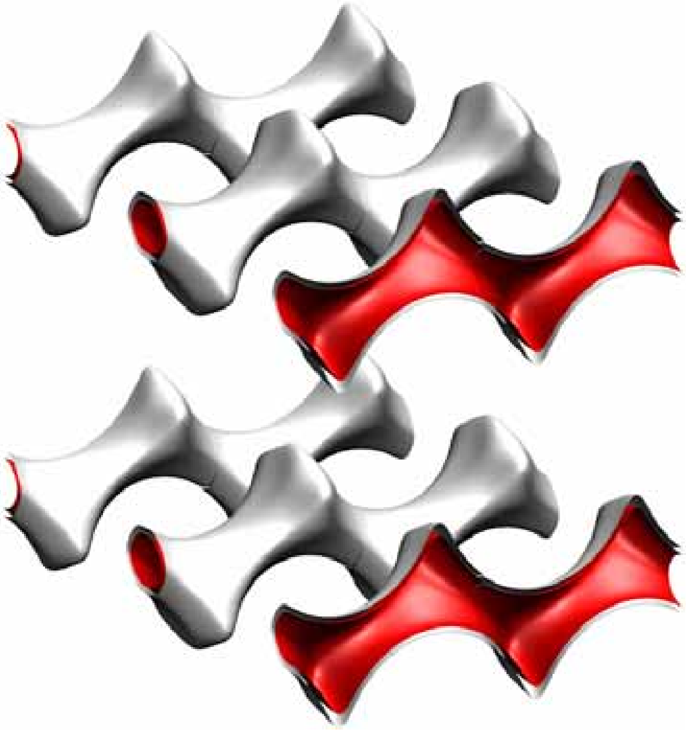

To convert from molecules per unit cell to mol kg^{-1}, multiply by 2.7738.
The pore volume is 0.086 cm^{3}/g.

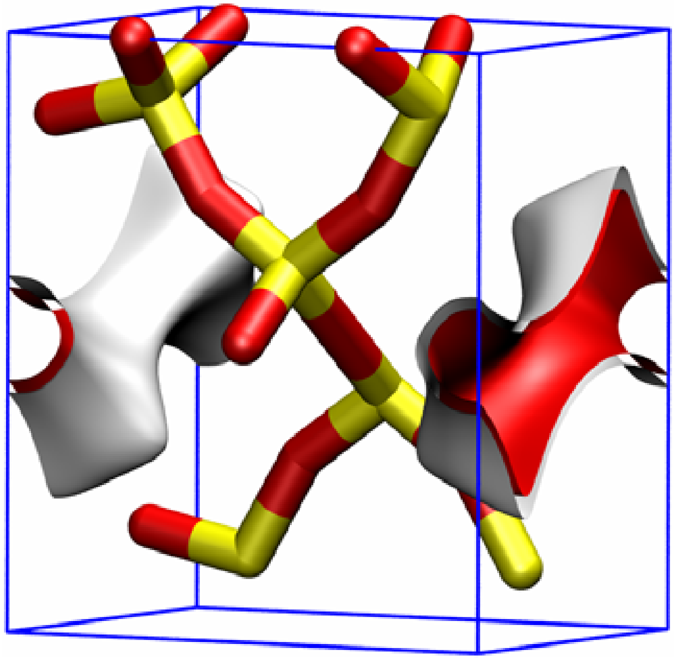

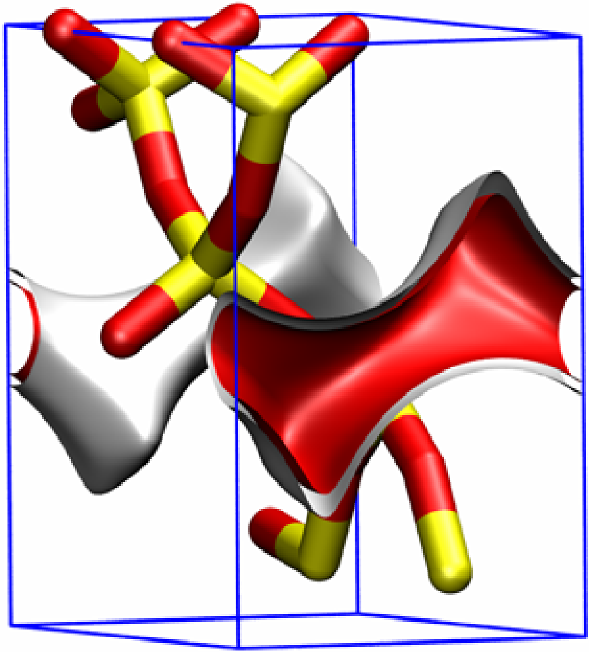

JBW snapshots

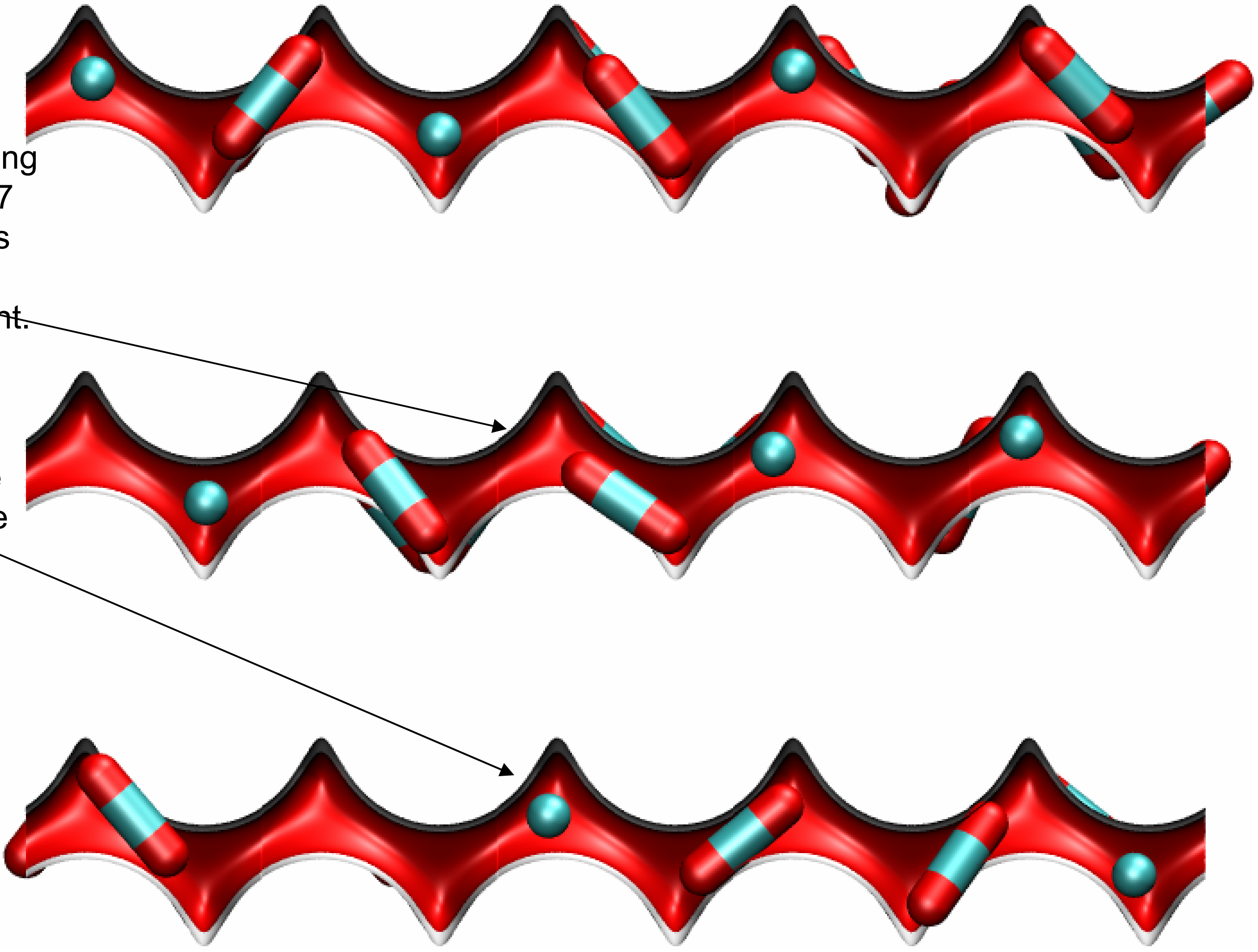

JBW has one-dimensional 8-ring channel structures of about 3.7 Å size. The channel topologies are such that CO_2 can nestle nicely in each channel segment. The curvature and size of the channels are energetically optimum for location of CO_2 molecules. CH_4 molecules are too severely constrained in the channel segments of BIK and can only occupy the more spacious vertex regions.

JBW CBMC mixture simulations for CO_2 capture

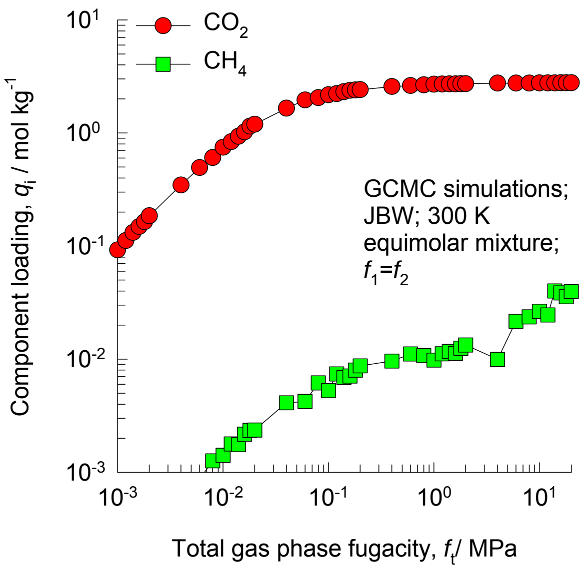

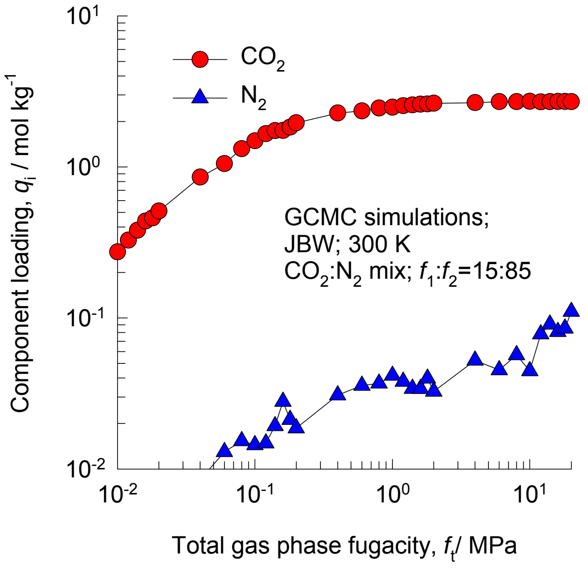

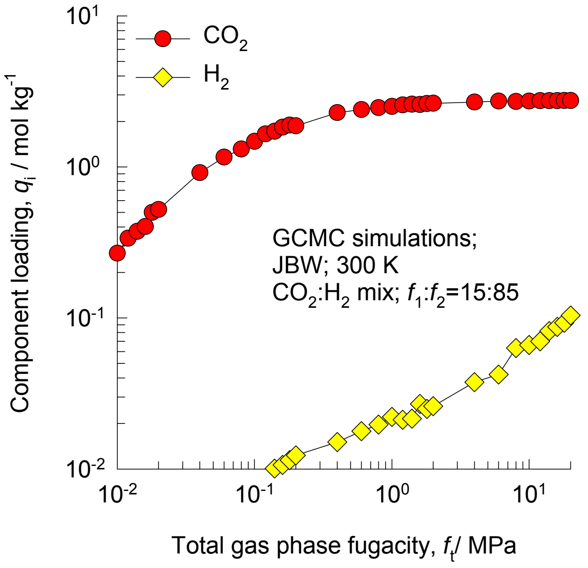

LEV landscapes

To convert from molecules per unit cell to mol kg^{-1}, multiply by 0.154.
The pore volume is 0.232 cm^3/g.

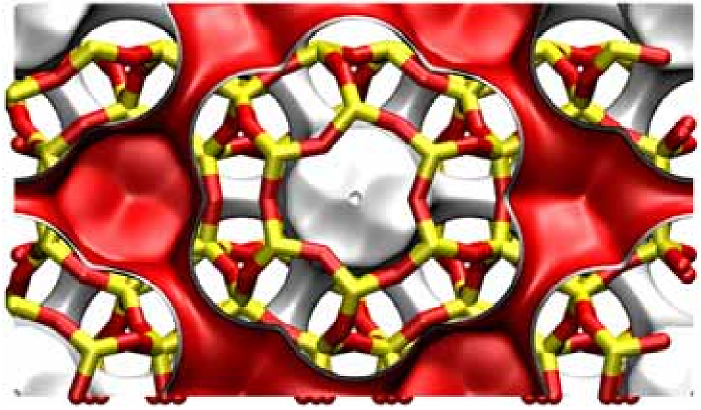

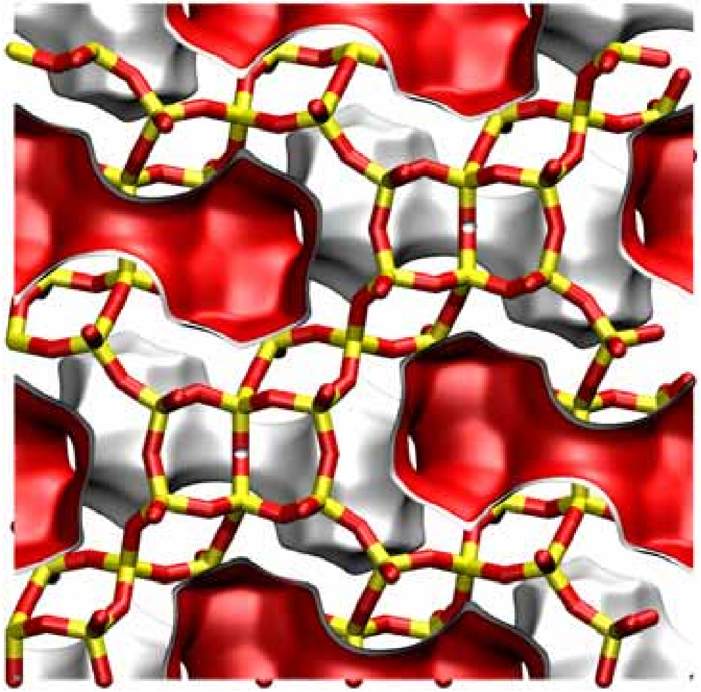

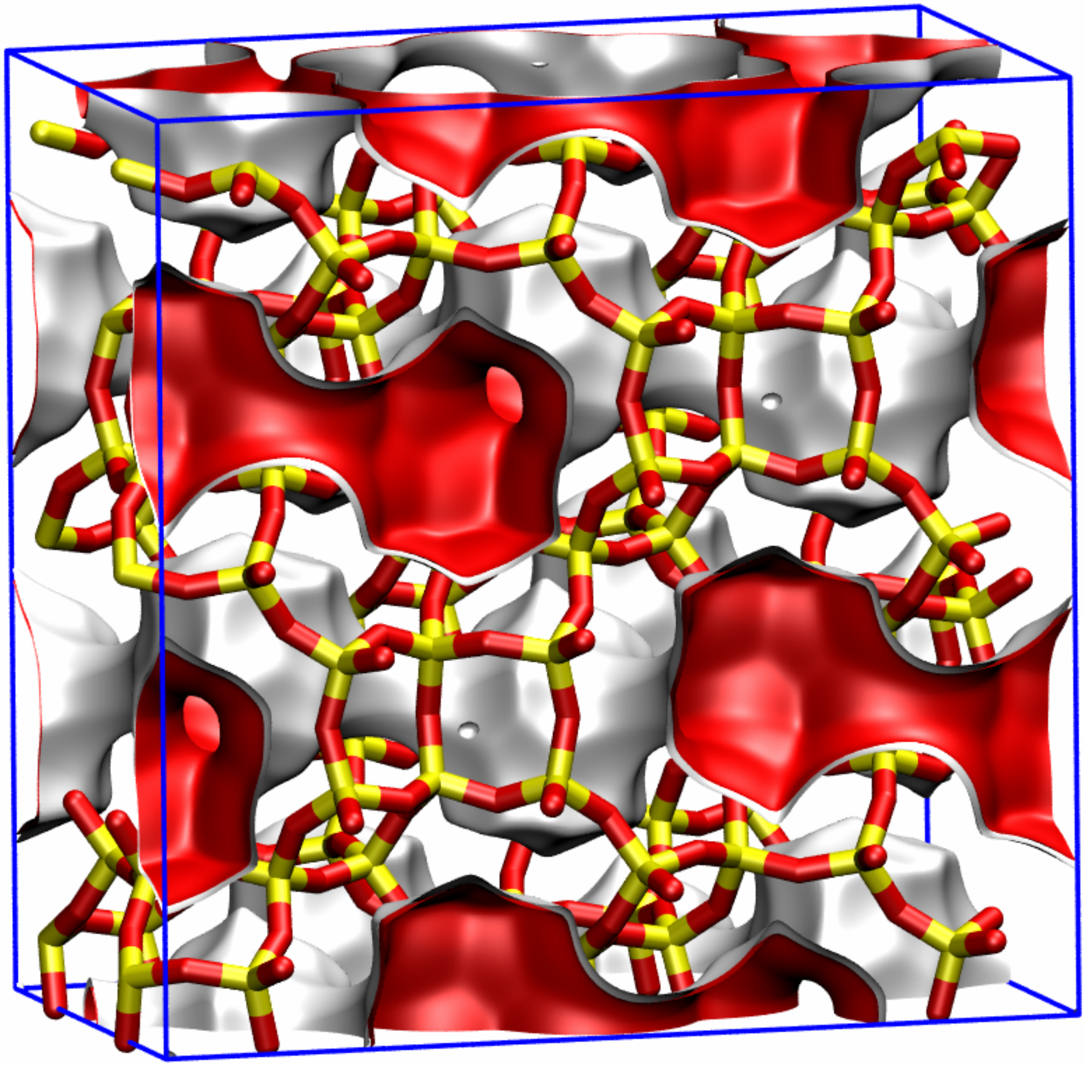

LEV CBMC mixture simulations for CO_2 capture

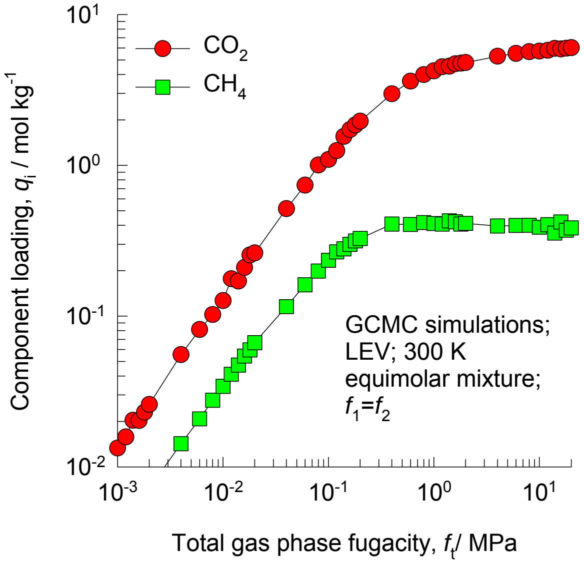

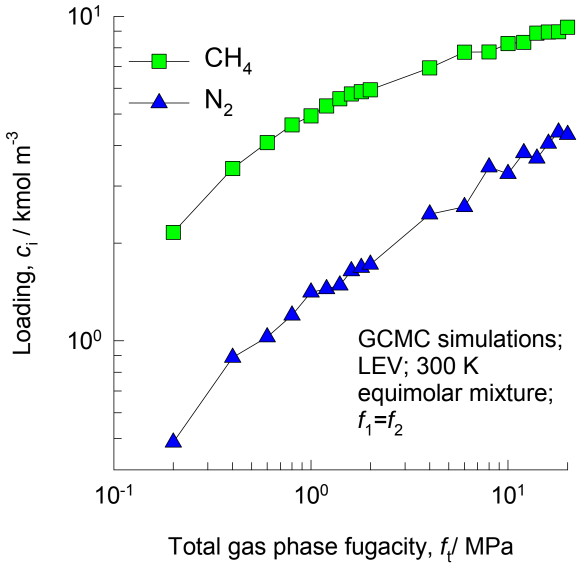

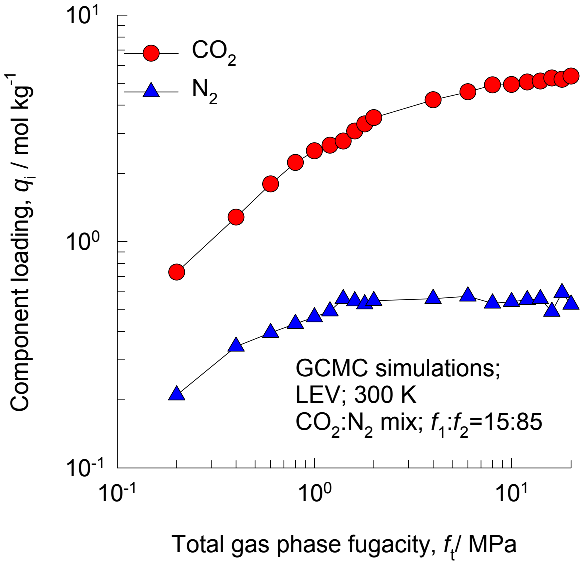

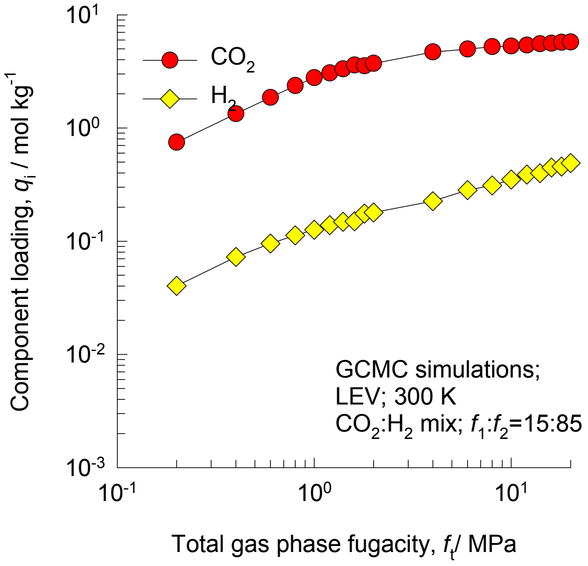

LOV landscapes

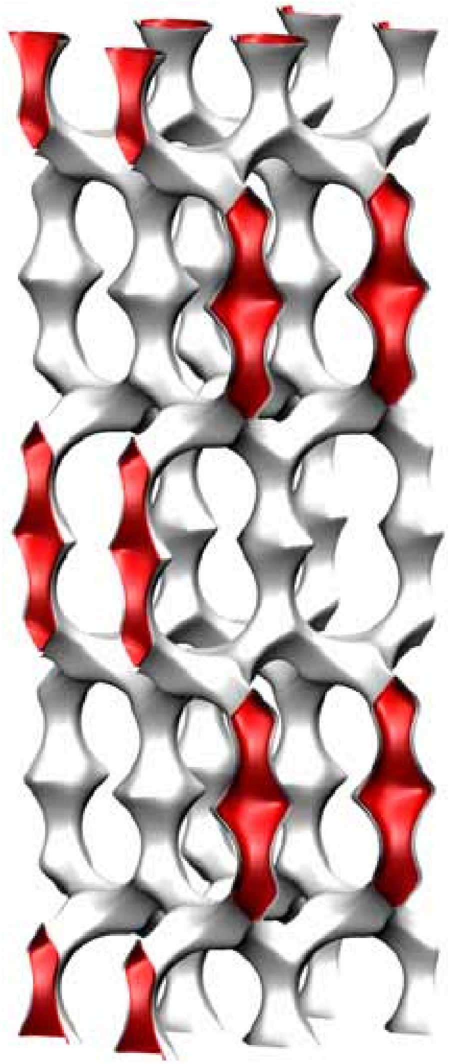

To convert from molecules per unit cell to mol kg^{-1}, multiply by 0.9246.
The pore volume is 0.154 cm^3/g.

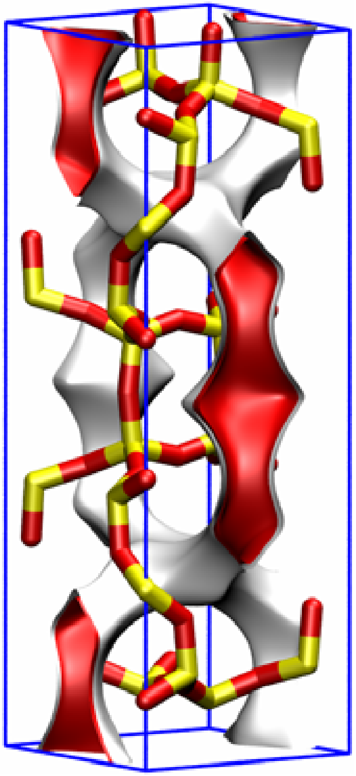

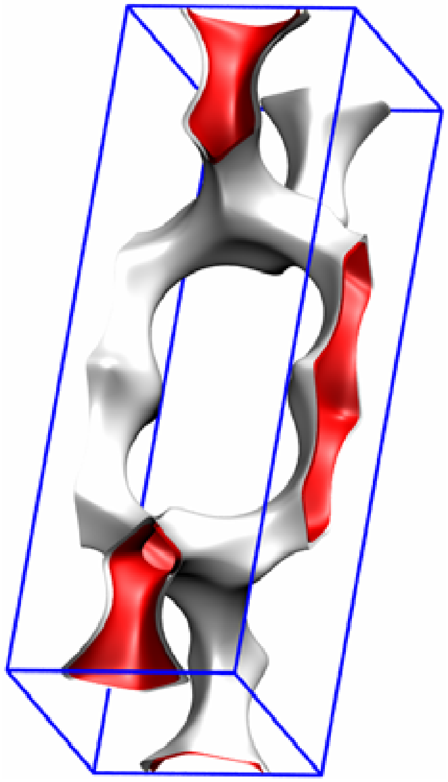

LOV snapshots

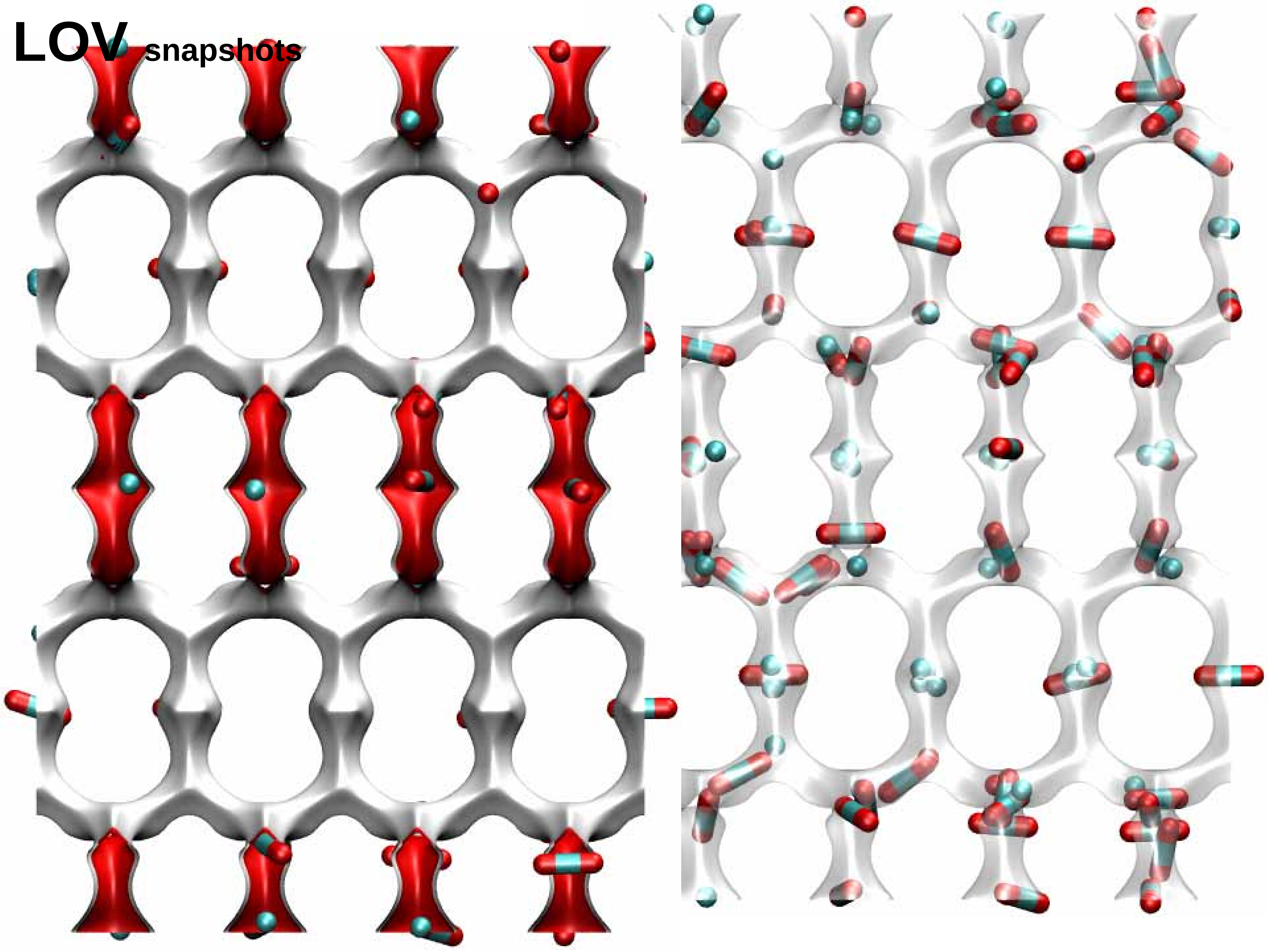

LOV CBMC mixture simulations for CO_2 capture

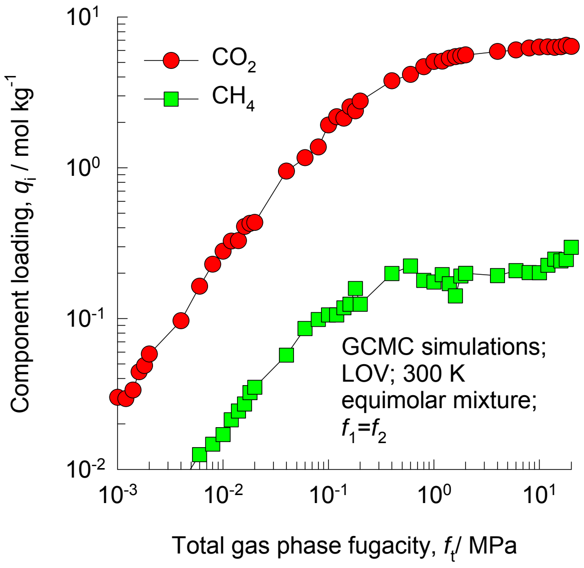

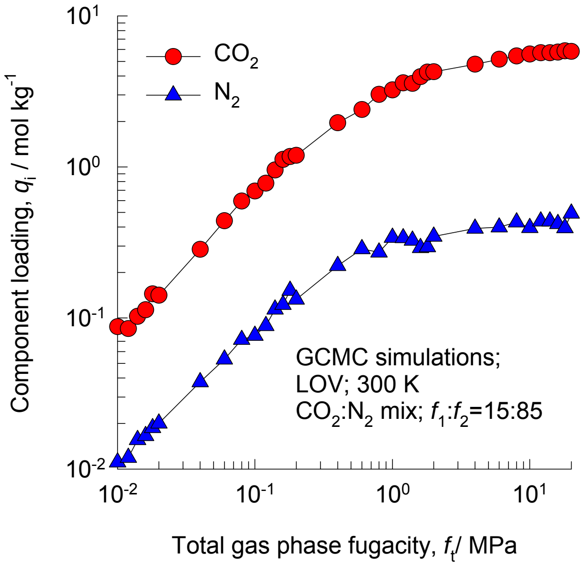

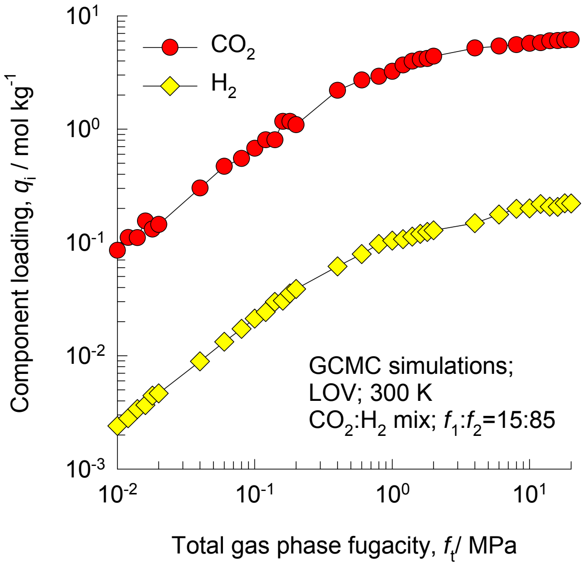

SIV landscapes

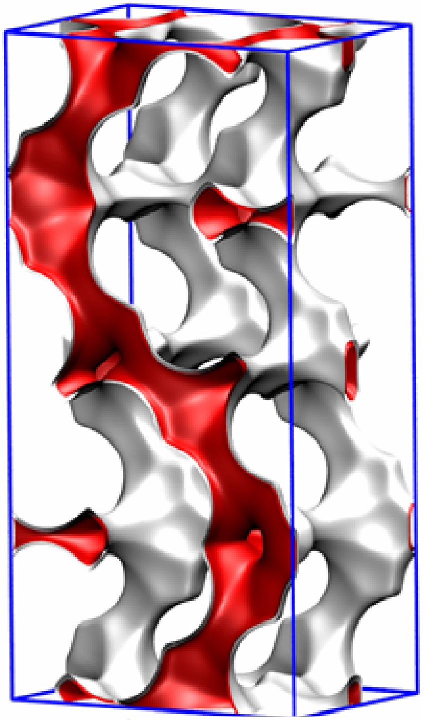

To convert from molecules per unit cell to mol kg^{-1}, multiply by 0.260.
The pore volume is 0.187 cm^3/g.

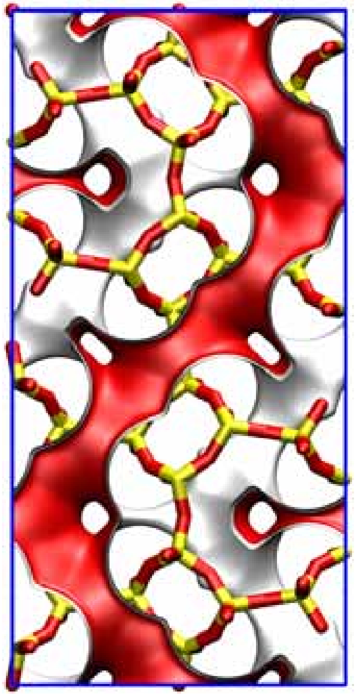

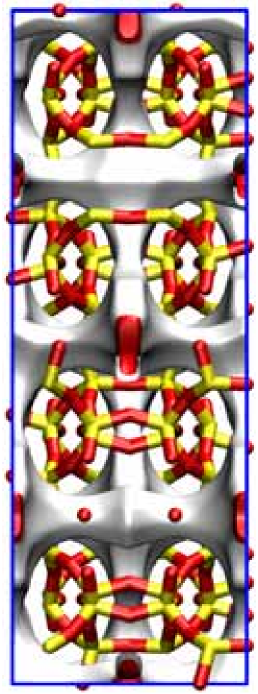

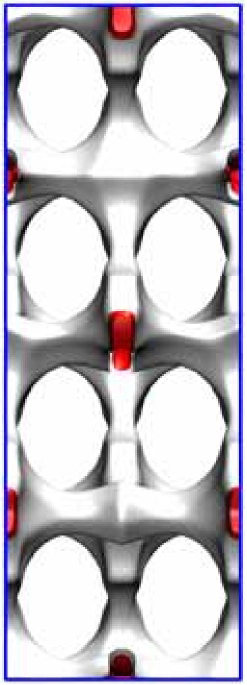

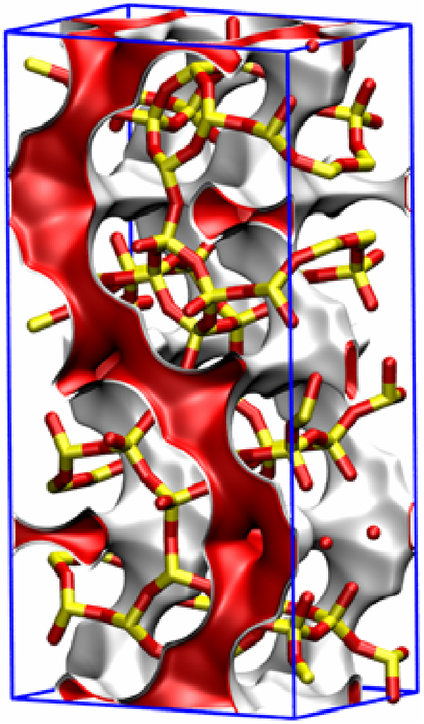

SIV snapshots

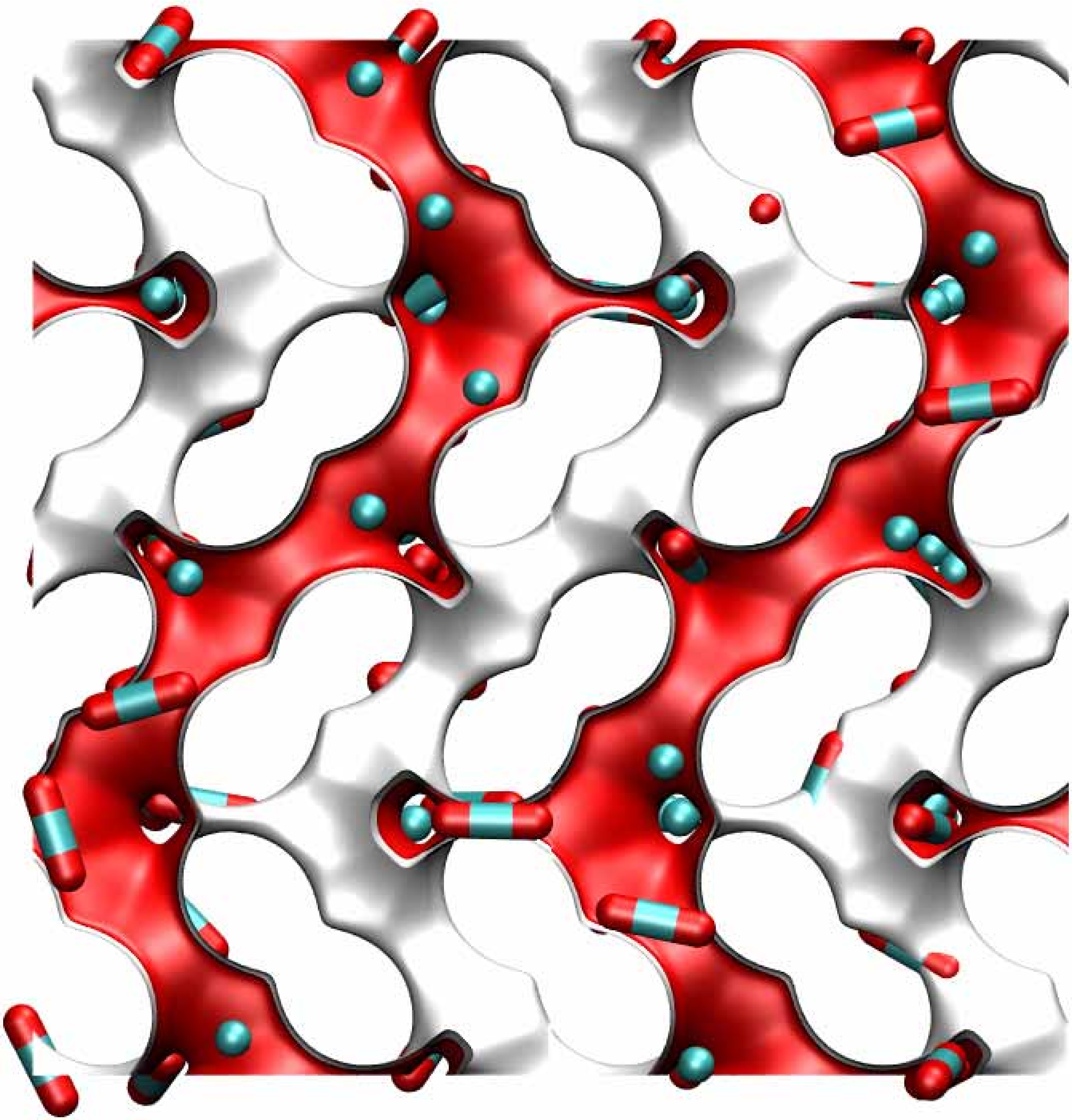

SIV CBMC mixture simulations for CO_2 capture

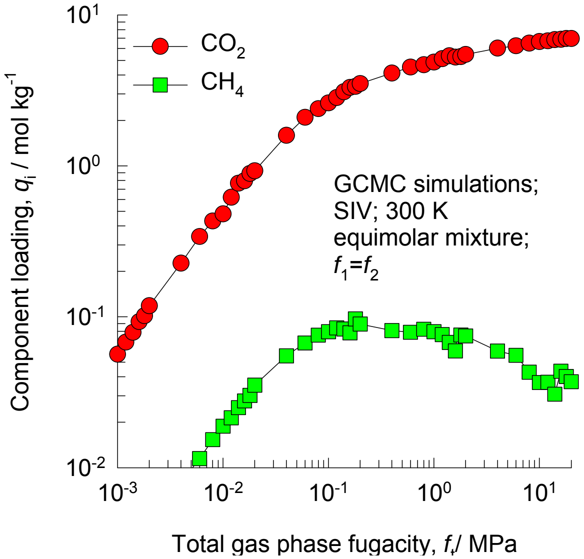

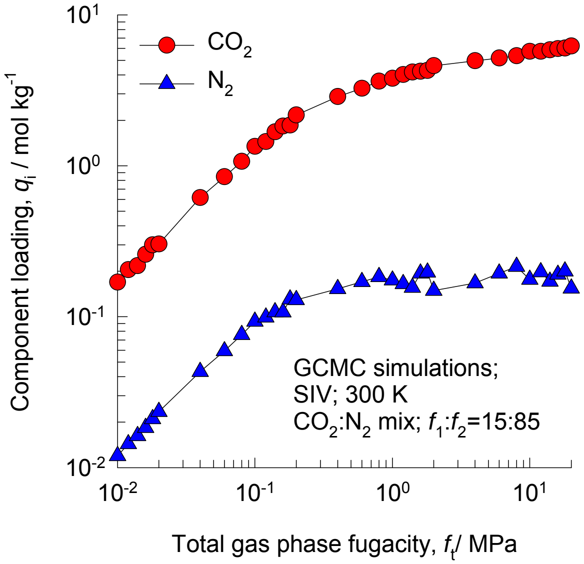

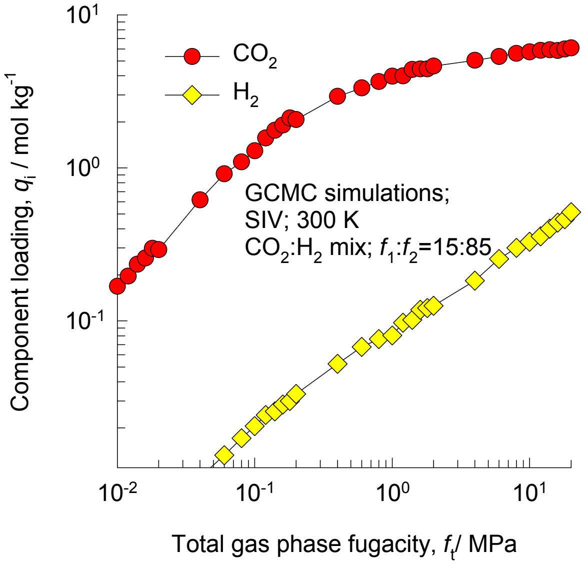

Comparison of selectivities for CO_2/CH_4 Separation with Additional all-silica zeolites

Comparison of S_{ads} for CO_2/CH_4

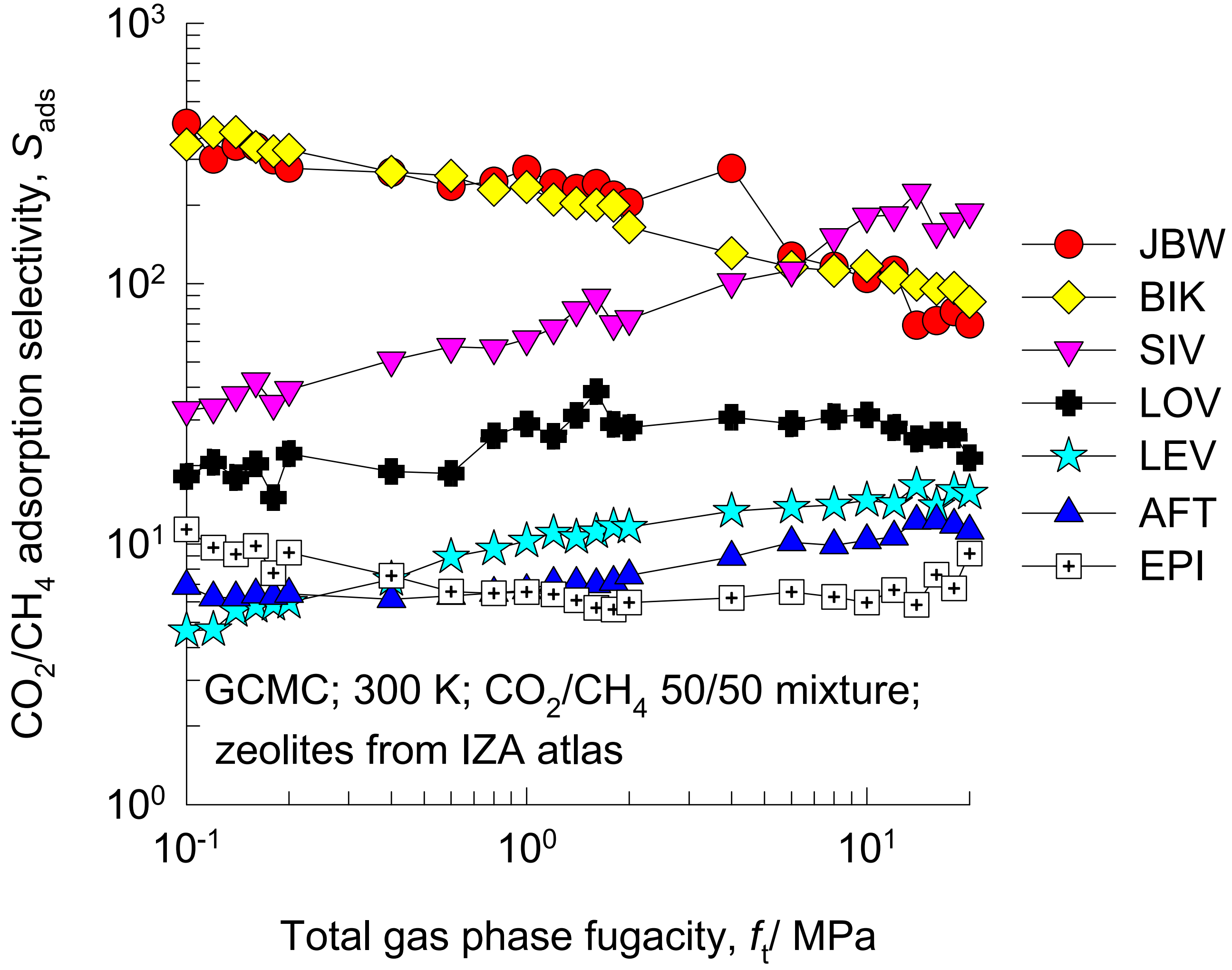

Selectivity vs capacity for CO_2/CH_4

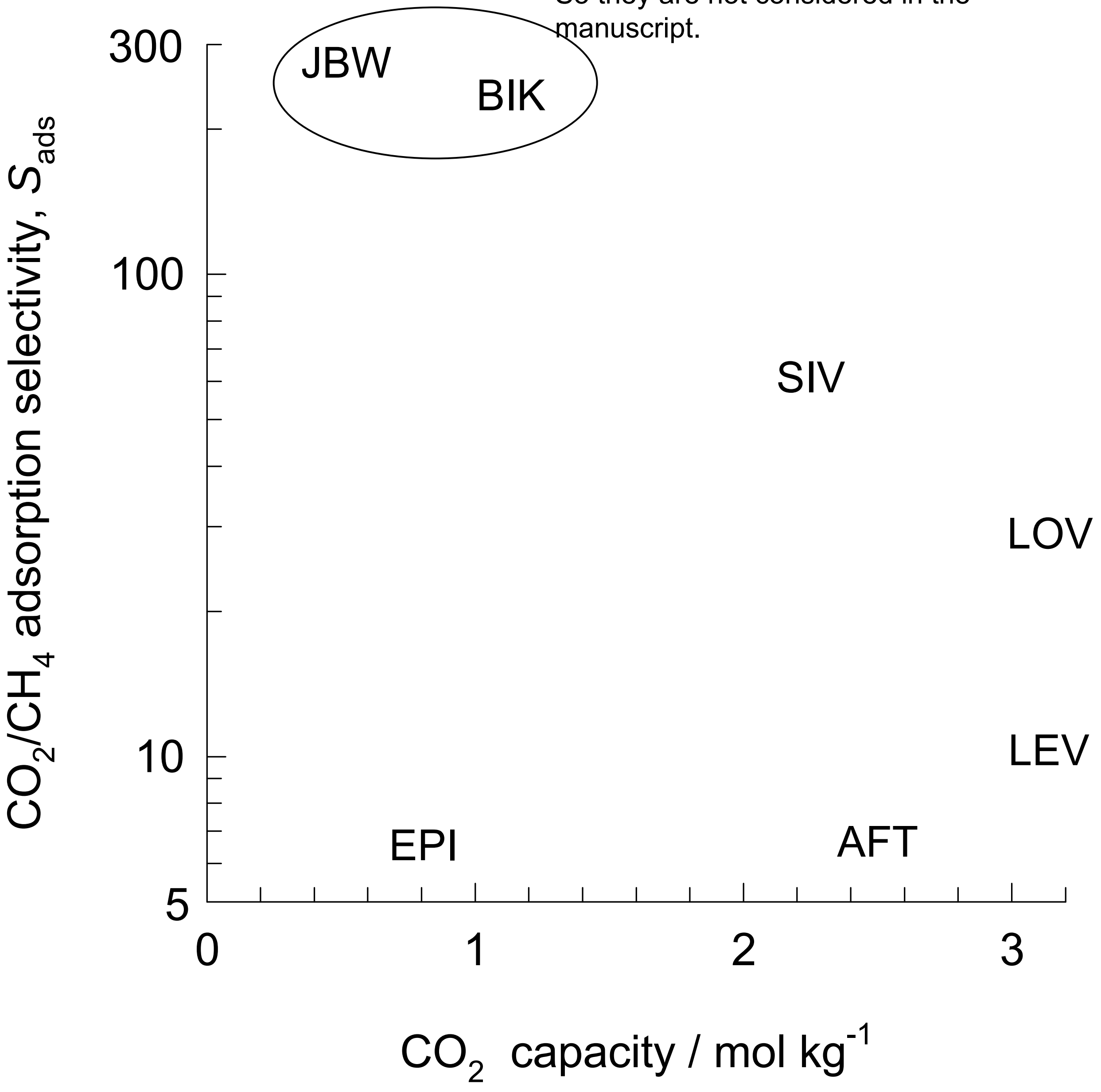

High selectivities, but poor capacities. So they are not considered in the manuscript.

300 K; CO_2/CH_4
Total gas phase fugacity, f_t = 1 MPa;
Mixture composition CO_2/CH_4 = 50/50

The CO_2 capacity is the difference in the component loading of CO_2 at a total pressure of 1 MPa and 0.1 MPa

All the 7 additional zeolites have low capacities

Comparison of selectivities for CO_2/N_2 separation with additional all-silica zeolites

Comparison of S_{ads} for CO_2/N_2

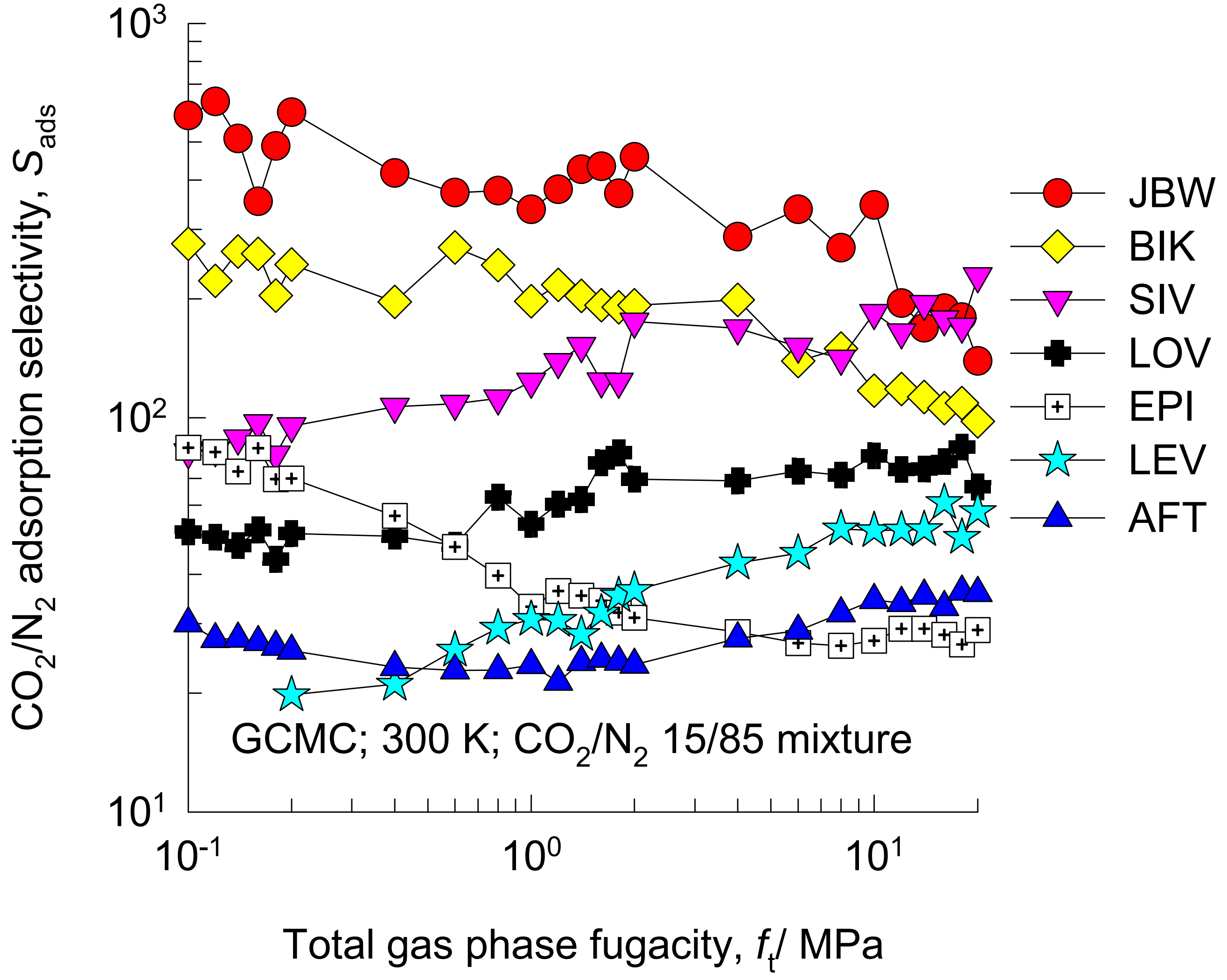

Selectivity vs capacity for CO_2/N_2

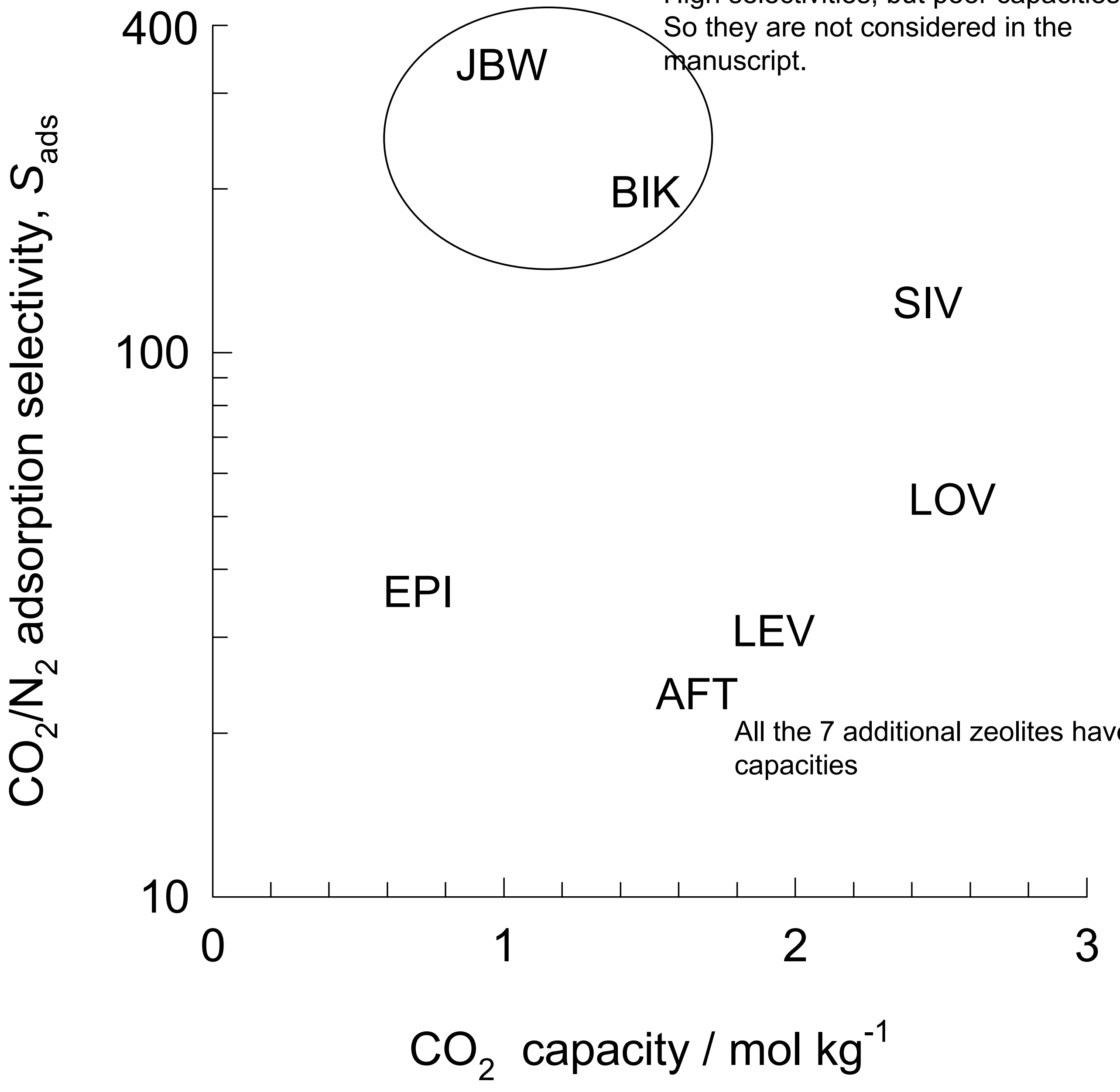

High selectivities, but poor capacities. So they are not considered in the manuscript.

All the 7 additional zeolites have low capacities

300 K; CO_2/N_2
Total gas phase fugacity, f_t = 1 MPa;
Mixture composition CO_2/N_2 = 15/85

The CO_2 capacity is the difference in the component loading of CO_2 at a total pressure of 1 MPa and 0.1 MPa

Comparison of selectivities for CO_2/H_2 separation with Additional all-silica zeolites

Comparison of S_{ads} for CO_2/H_2

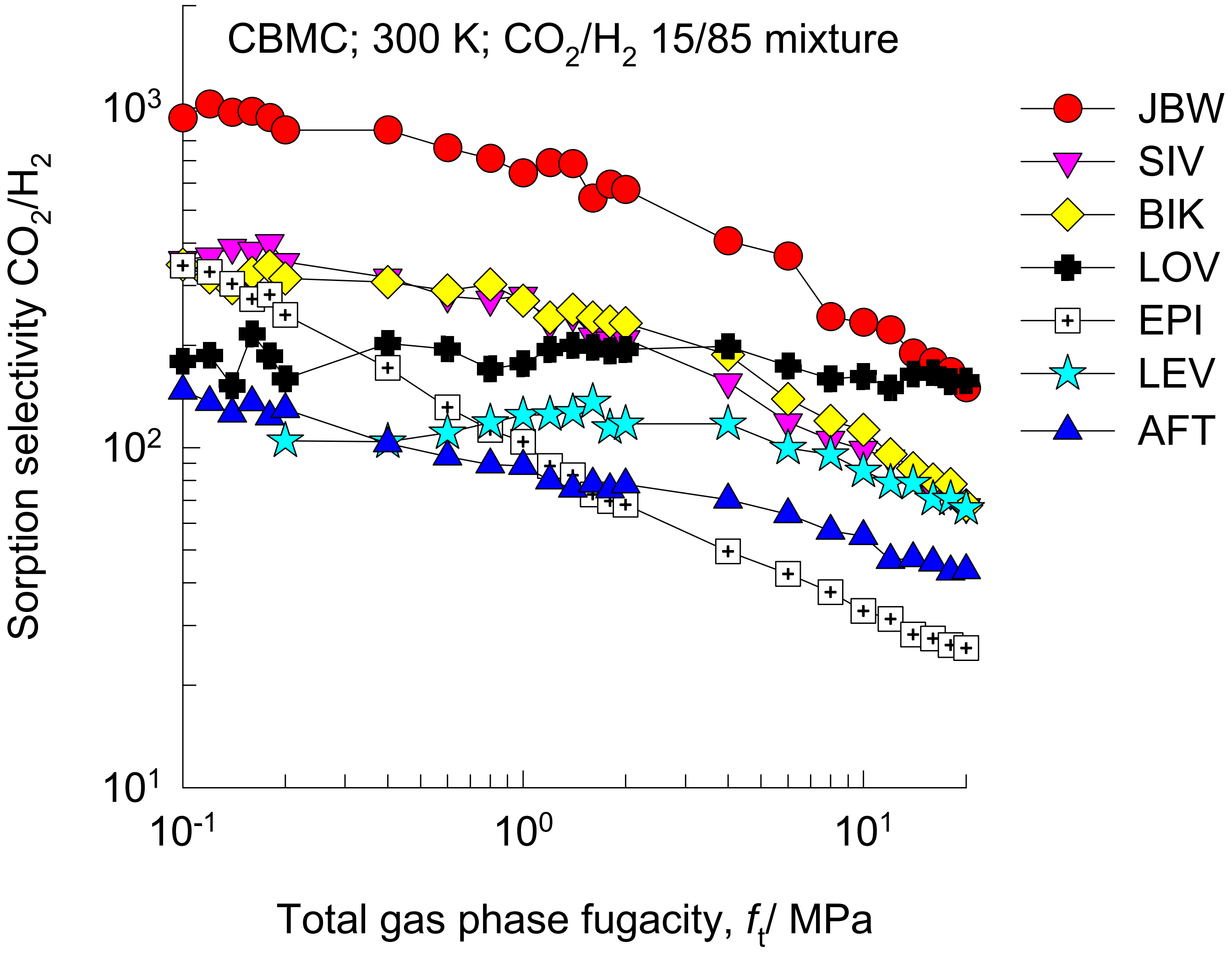

Selectivity vs capacity for CO_2/H_2

High selectivities, but poor capacities. So they are not considered in the manuscript.

300 K; CO_2/H_2
Total gas phase fugacity, f_t = 1 MPa;
Mixture composition CO_2/H_2 = 15/85

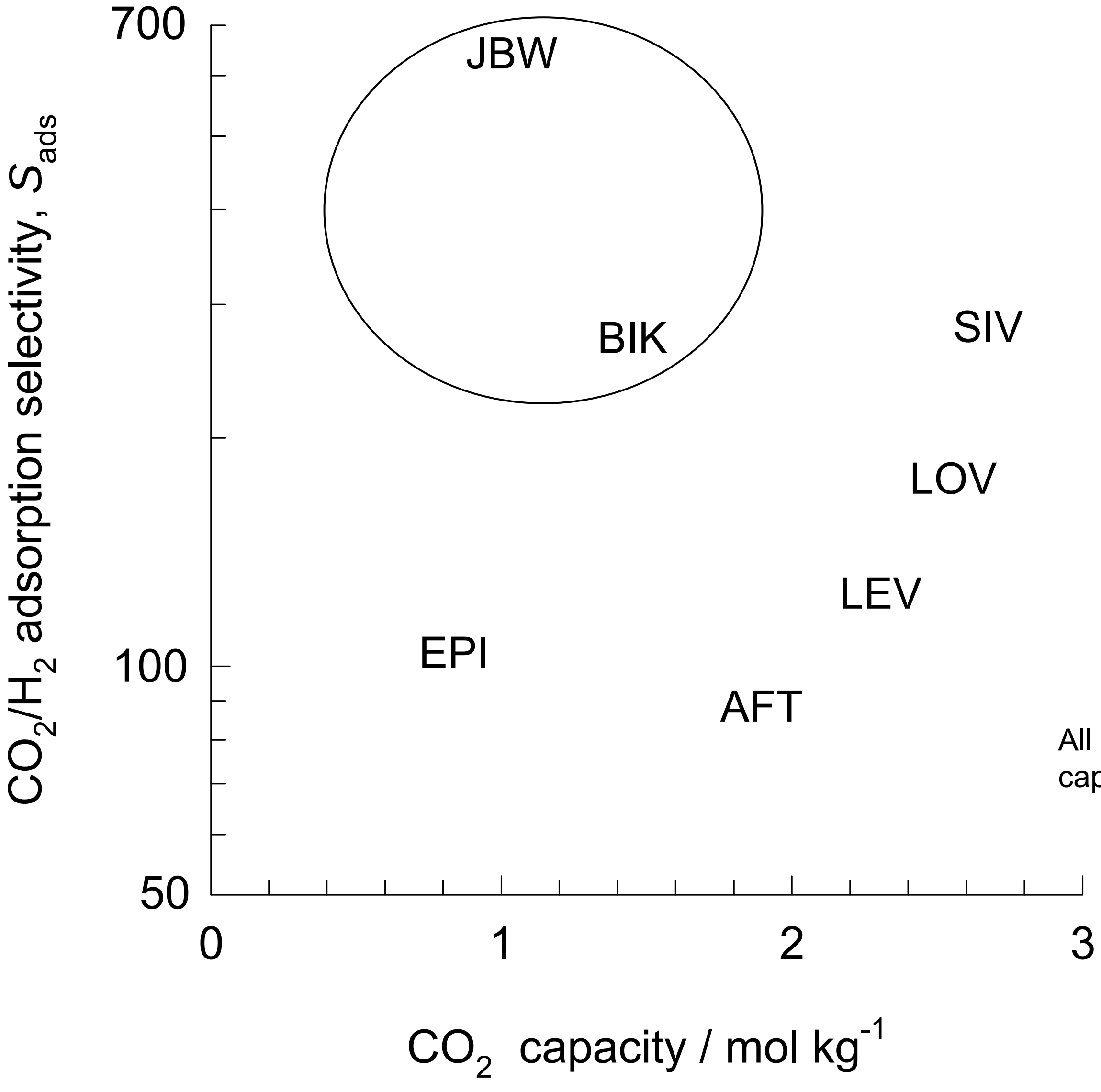

The CO_2 capacity is the difference in the component loading of CO_2 at a total pressure of 1 MPa and 0.1 MPa

All the 7 additional zeolites have low capacities

Zeolites with cations

NaY (138 Si, 54 Al, 54 Na+, Si/Al=2.55)

To convert from molecules per unit cell to mol kg^{-1}, multiply by 0.078628.
The pore volume is 0.303 cm^3/g.

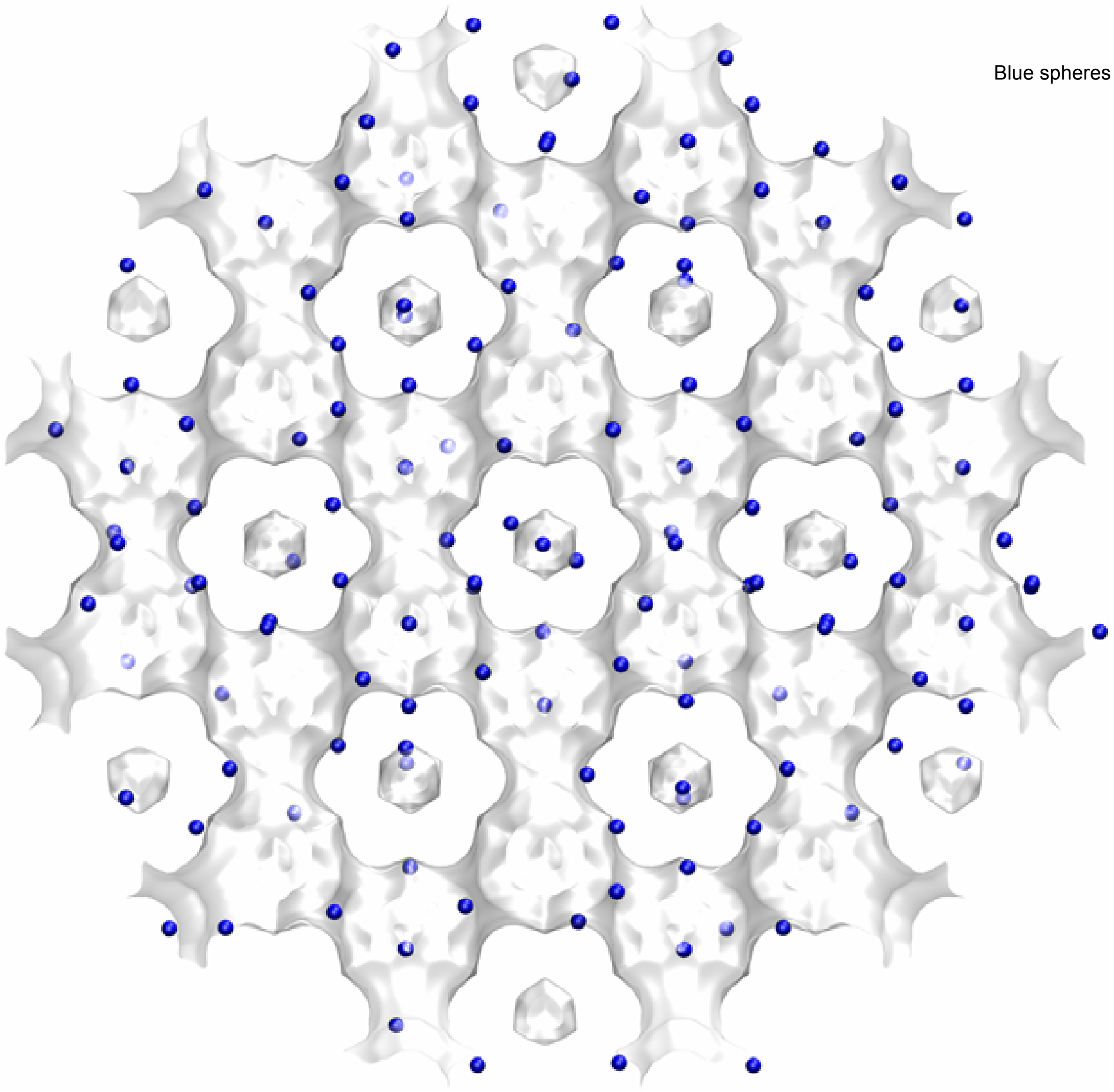

Blue spheres are catons

NaY CBMC mixture simulations for CO_2 capture

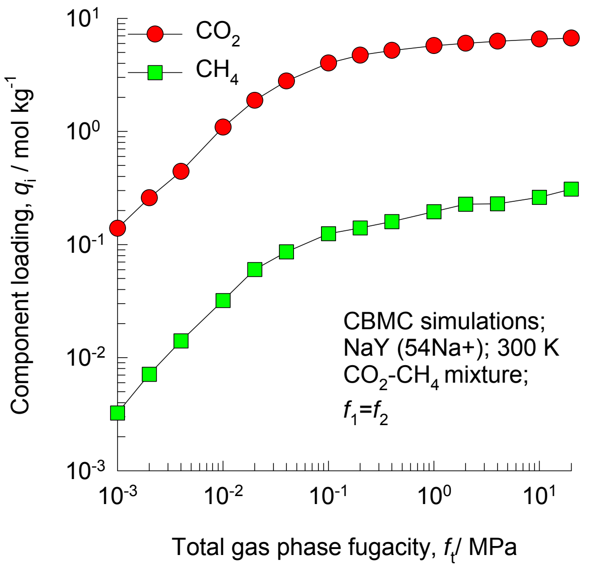

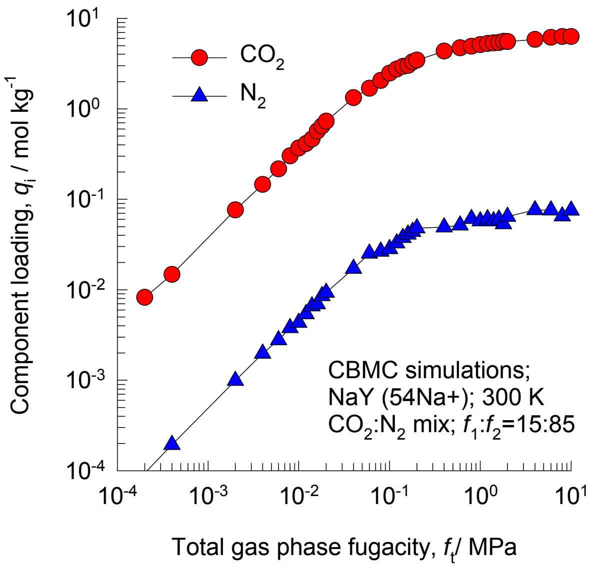

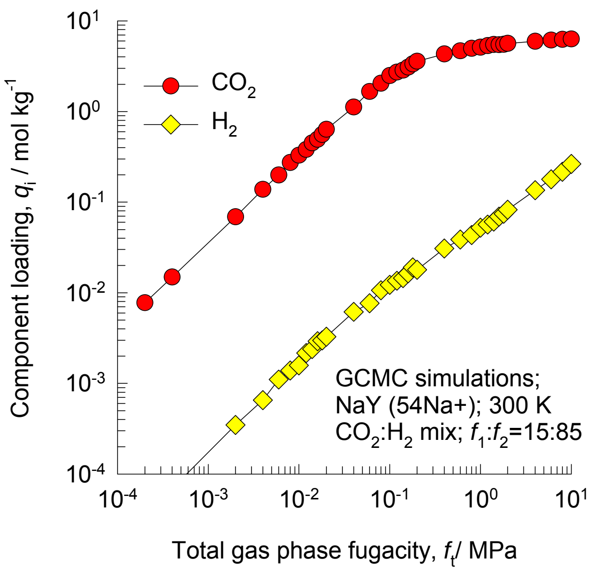

NaY CBMC nC6/3MP/22DMB mixture simulations

$$S_{ads} = \frac{\dfrac{q_{nC6}}{f_{nC6}} + \dfrac{q_{3MP}}{f_{3MP}}}{\dfrac{q_{22DMB}}{f_{22DMB}}}$$

Capacity is the total loading of nC6 + 3MP

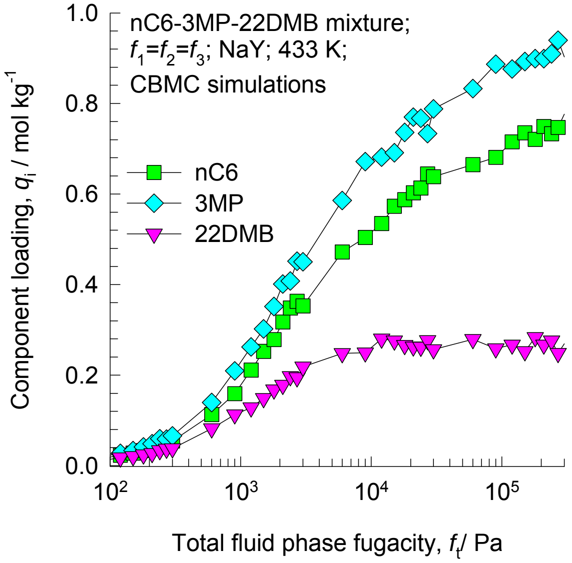

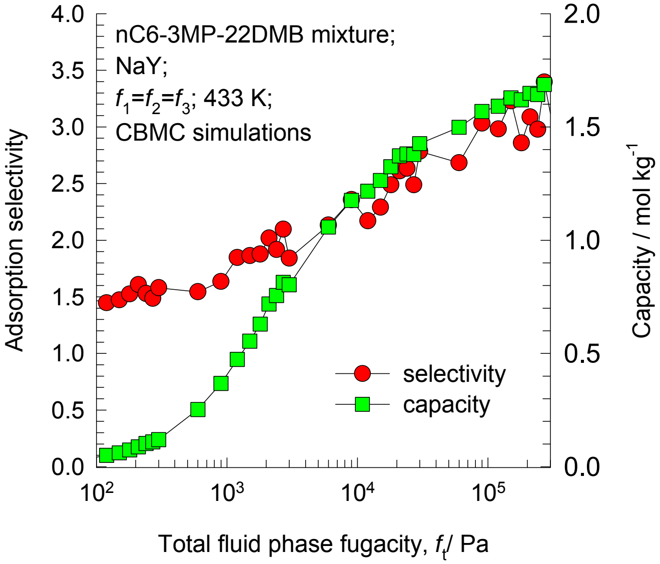

NaY snapshot of hexane isomers

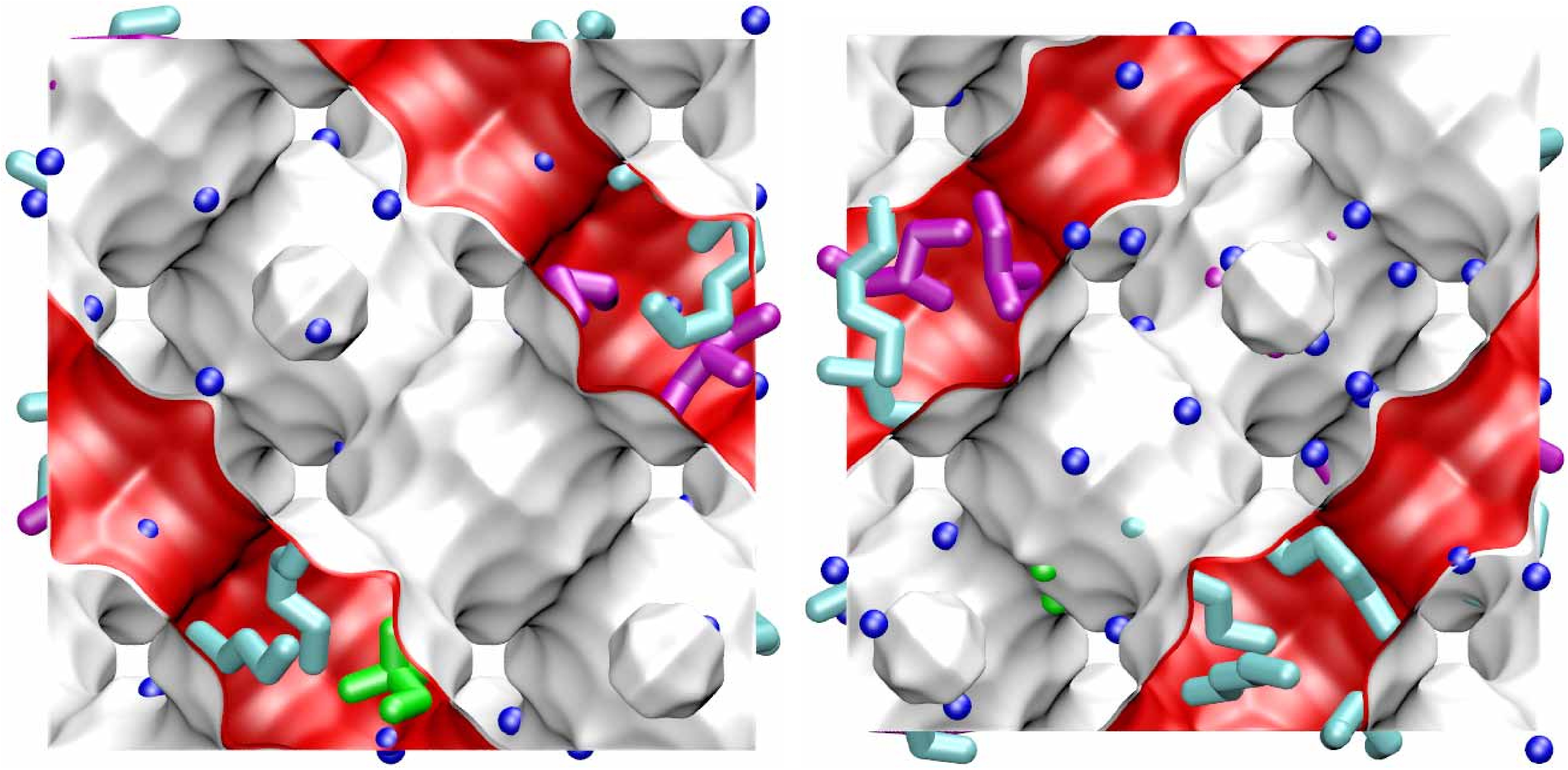

NaX (106 Si, 86 Al, 86 Na+, Si/Al=1.23)

To convert from molecules per unit cell to mol kg^{-1}, multiply by 0.0745.
The pore volume is 0.280 cm^3/g.

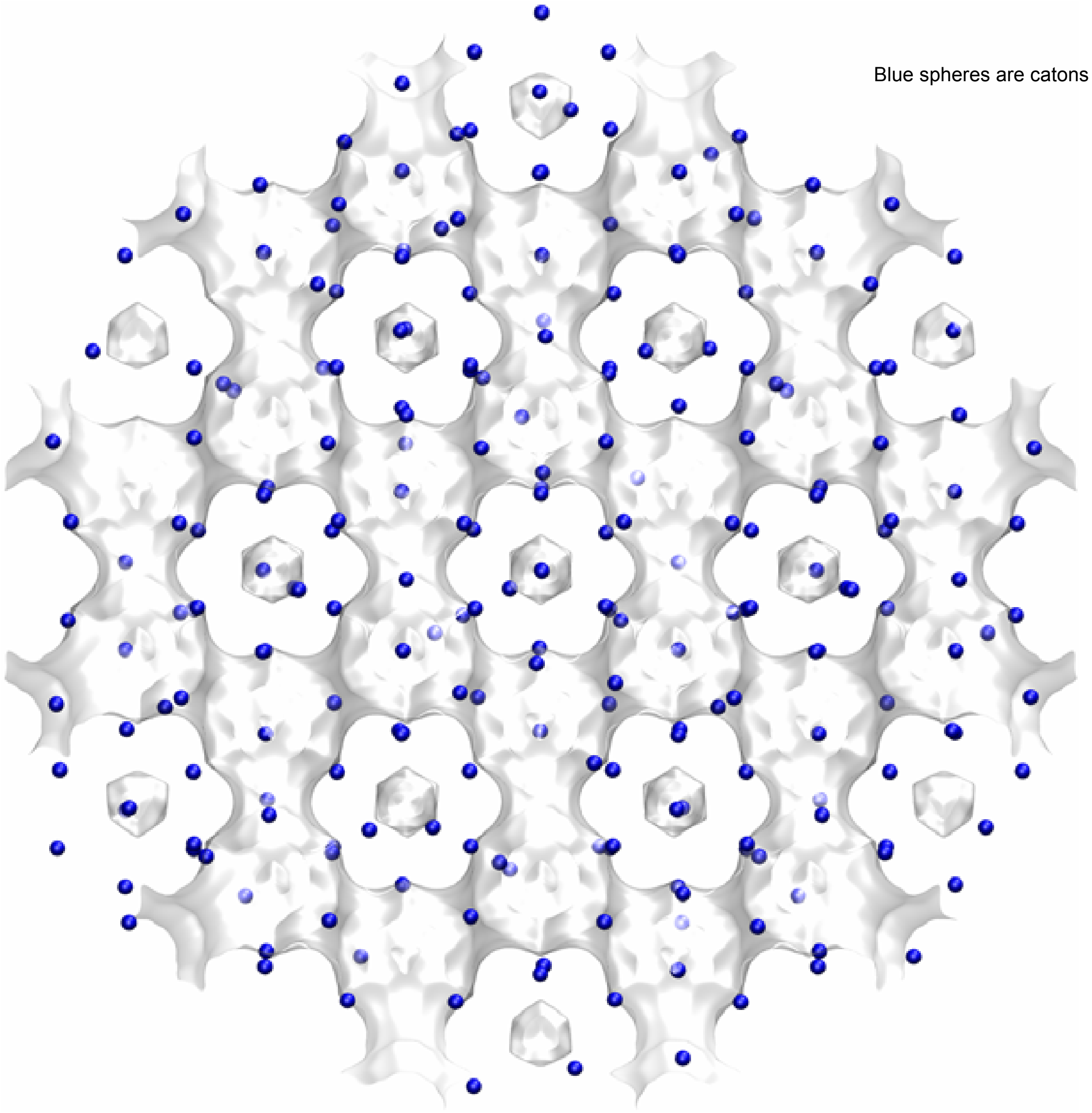

Blue spheres are catons

NaX CBMC mixture simulations for CO_2 capture

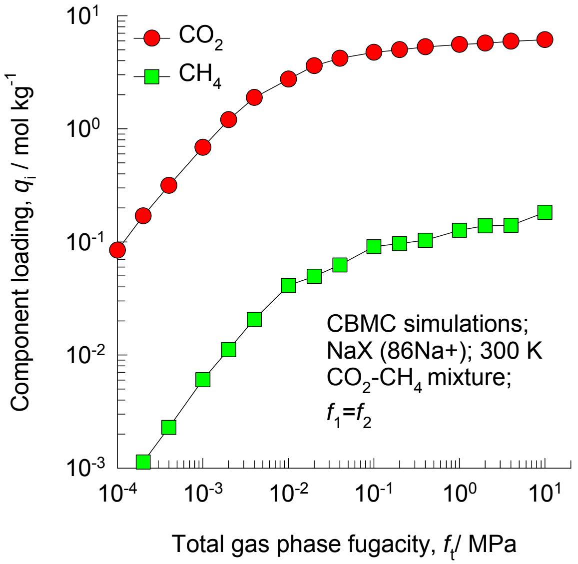

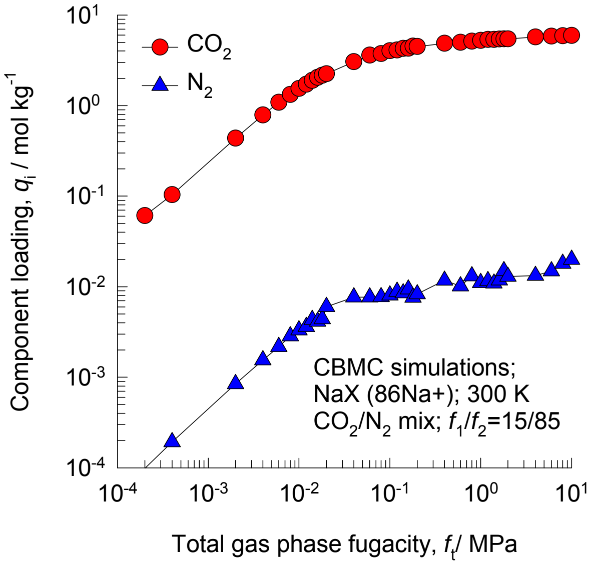

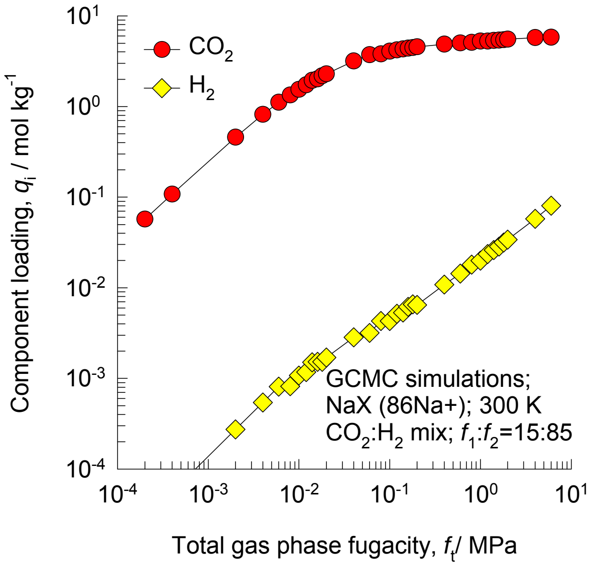

NaX CBMC nC6/3MP/22DMB mixture simulations

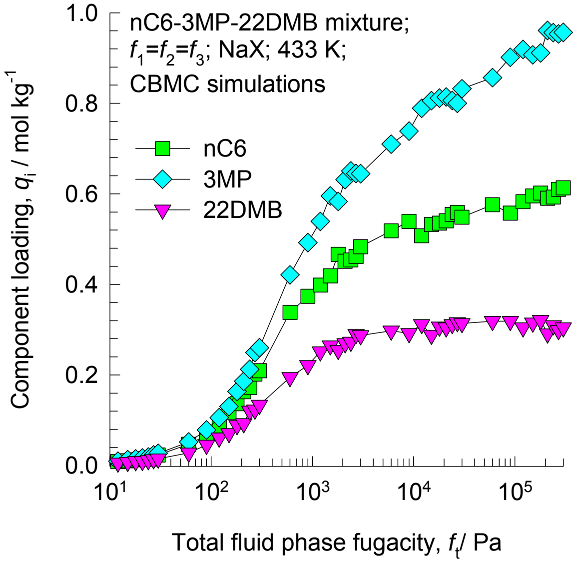

$$S_{ads} = \frac{\dfrac{q_{nC6}}{f_{nC6}} + \dfrac{q_{3MP}}{f_{3MP}}}{\dfrac{q_{22DMB}}{f_{22DMB}}}$$

Capacity is the total loading of nC6 + 3MP

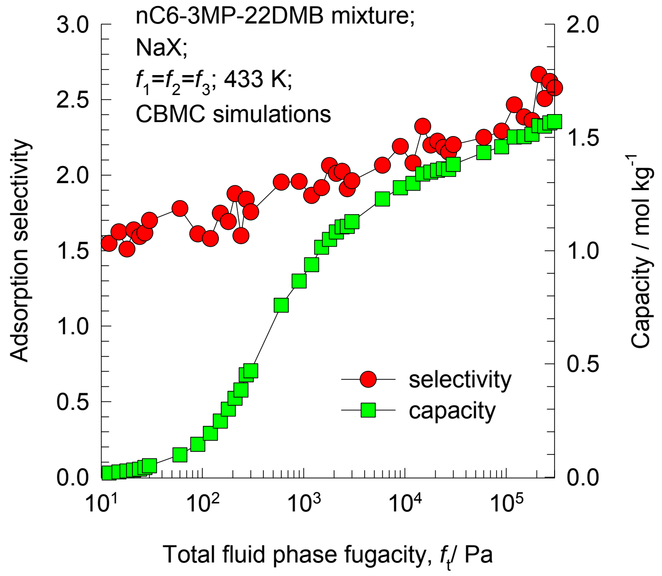

MOFs and ZIFs (in alphabetical order, but MOF-74 with Co, Mg, Ni, and Zn are kept together)

BeBTB pore landscapes

To convert from molecules per unit cell to mol kg^{-1}, multiply by 0.12179.
The pore volume is 1.908 cm^3/g.

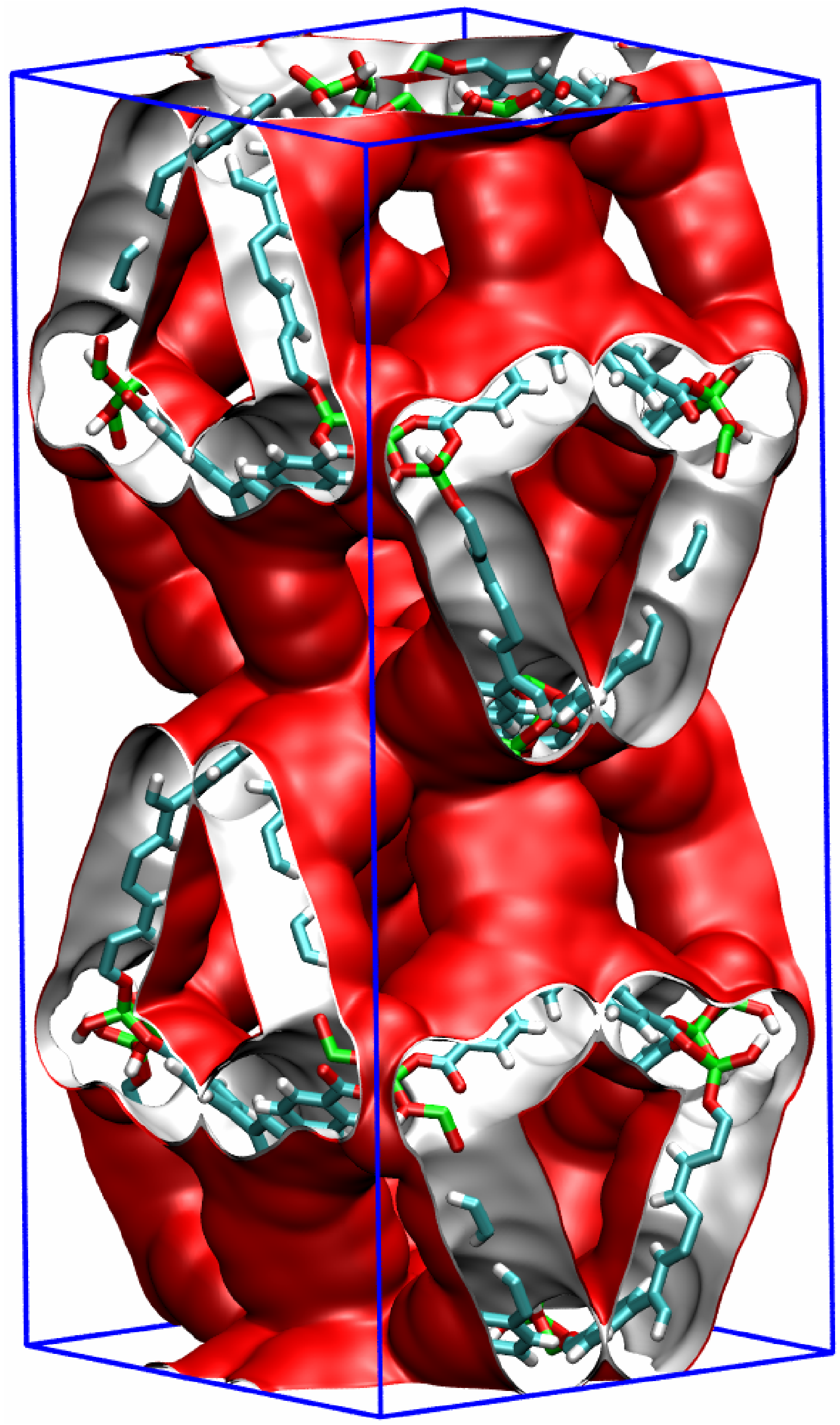

BeBTB CBMC mixture simulation results for CH_4/H_2 separation

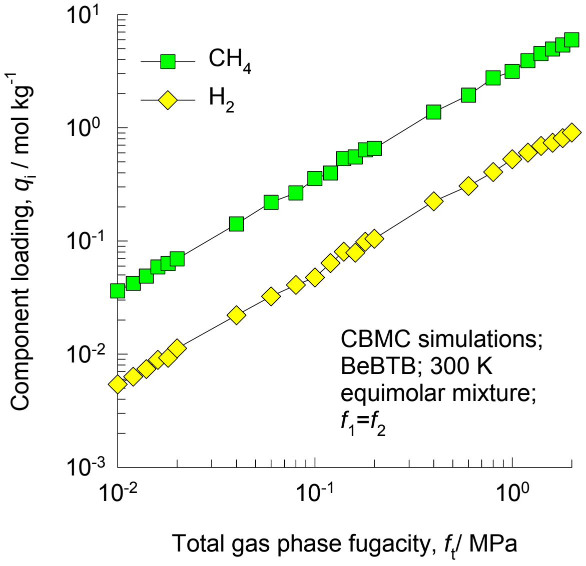

BeBTB CBMC pentanes mixture simulation results

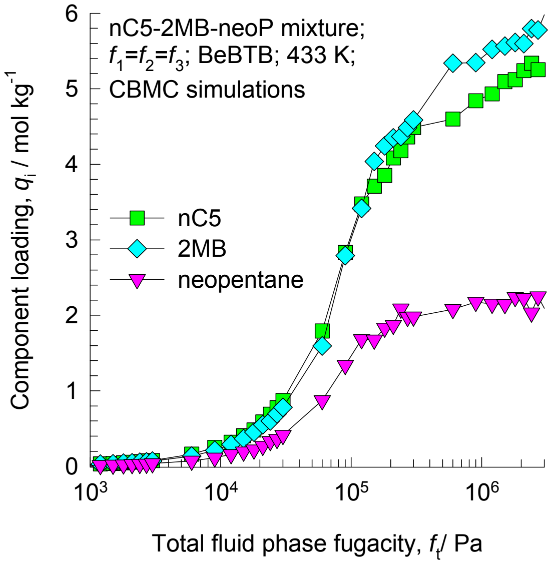

$$S_{ads} = \frac{\dfrac{q_{nC5}}{f_{nC5}} + \dfrac{q_{2MB}}{f_{2MB}}}{\dfrac{q_{neoP}}{f_{neoP}}}$$

Capacity is the total loading of nC5 + 2MB

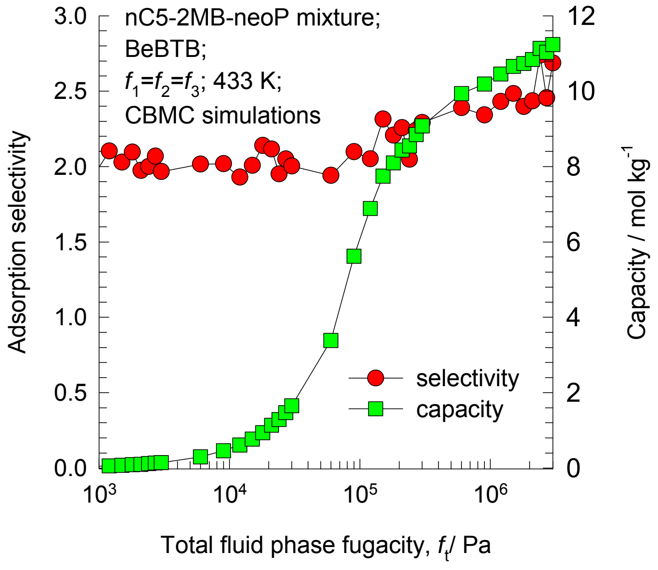

BeBTB CBMC nC6/3MP/22DMB mixture simulations

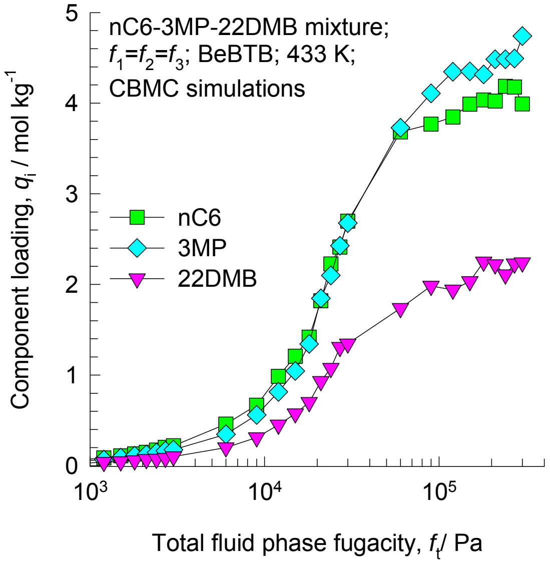

$$S_{ads} = \frac{\dfrac{q_{nC6}}{f_{nC6}} + \dfrac{q_{3MP}}{f_{3MP}}}{\dfrac{q_{22DMB}}{f_{22DMB}}}$$

Capacity is the total loading of nC6 + 3MP

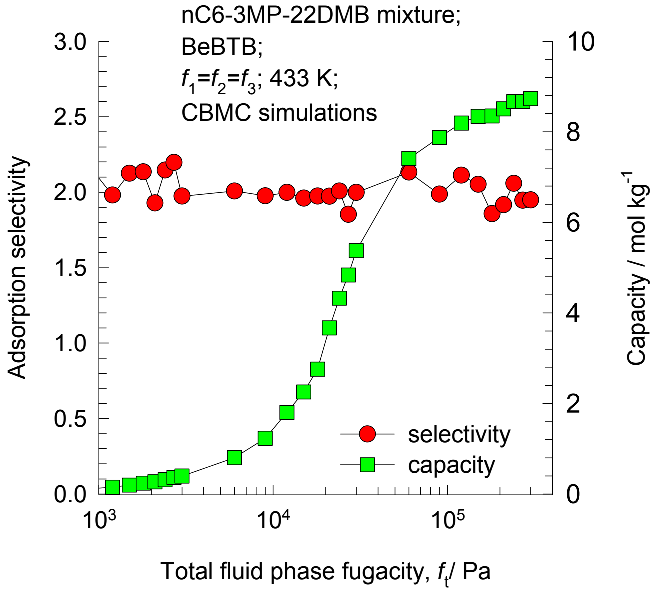

BeBTB CBMC nC6/2MP/3MP/22DMB/23DMB simulations

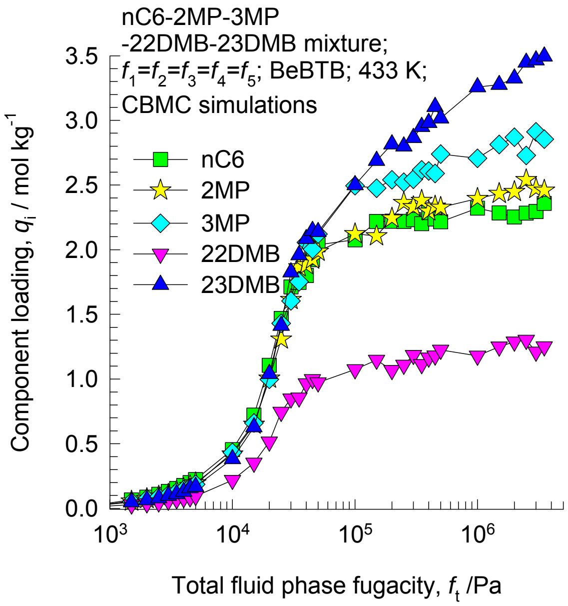

The 5-component mixture simulation shows that 22DMB can be separated from the rest of the mixture. But it is not possible to have clear separation of both the di-branched 22DMB and 23DMB from linear and mono-branched

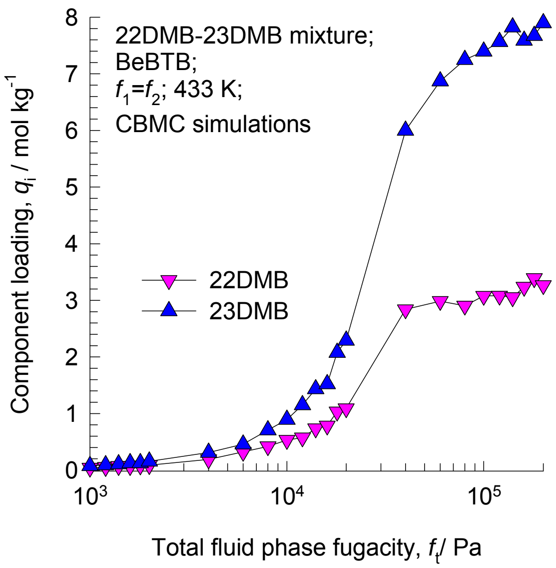

The 22DMB/23DMB binary mixture simulation demonstrates that the flatter 23DMB molecule has better interactions with the pore walls

BeBTB snapshot of nC66/3MP/22DMB hexane isomers

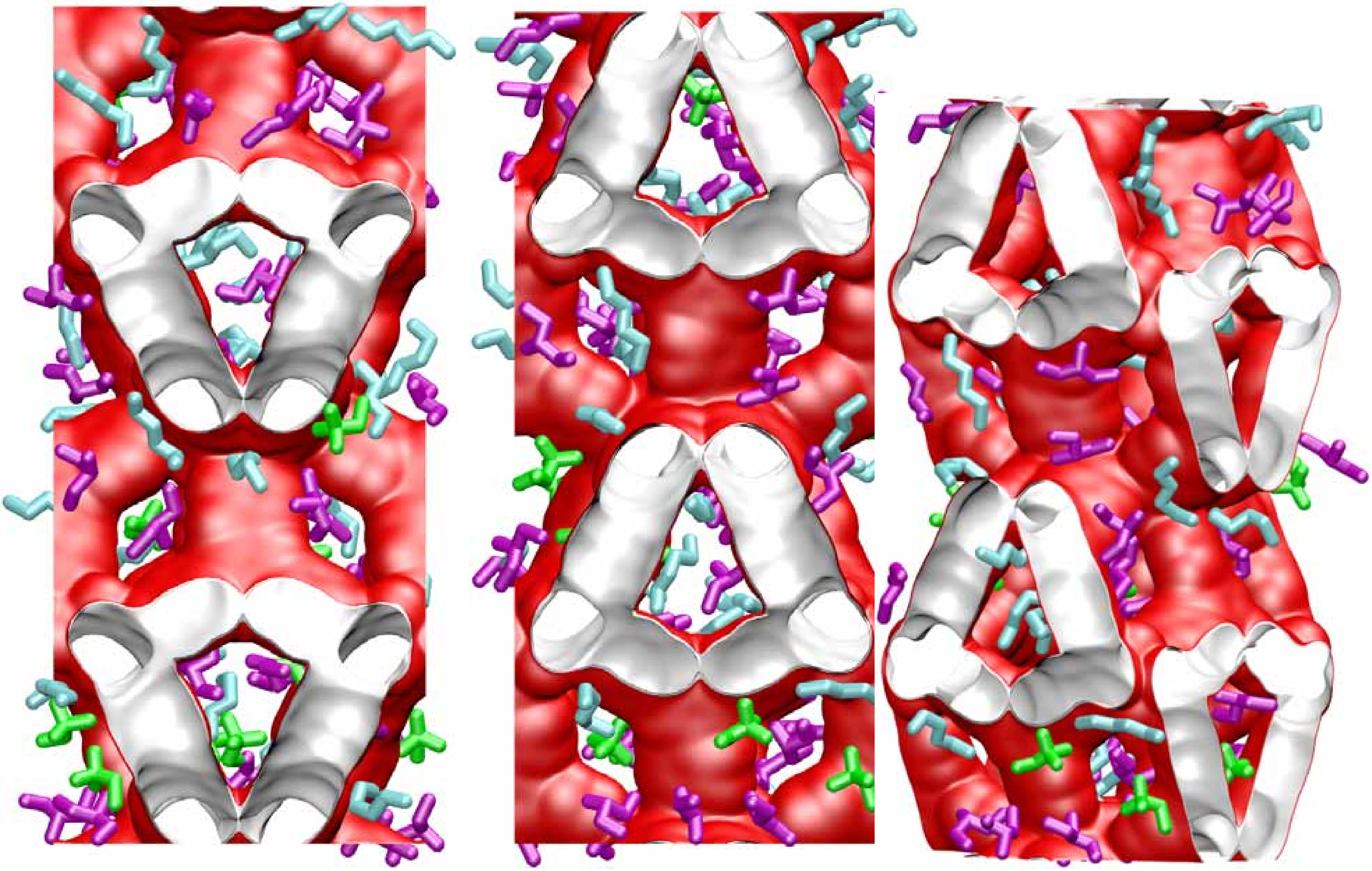

BeBTB snapshot of nC66/3MP/22DMB hexane isomers

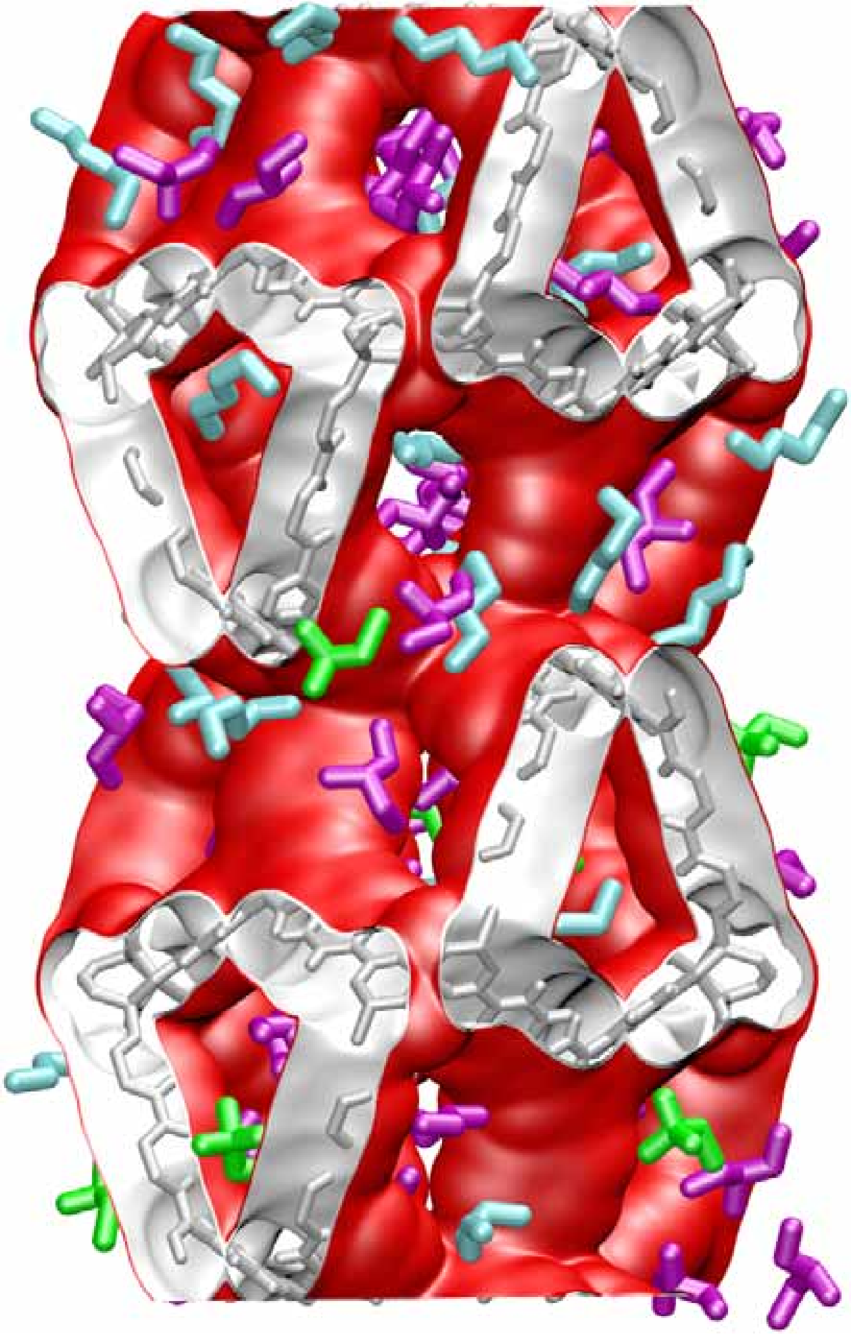

Co(BDP) pore landscapes

To convert from molecules per unit cell to mol kg^{-1}, multiply by 0.9362.
The pore volume is 0.927 cm^3/g.

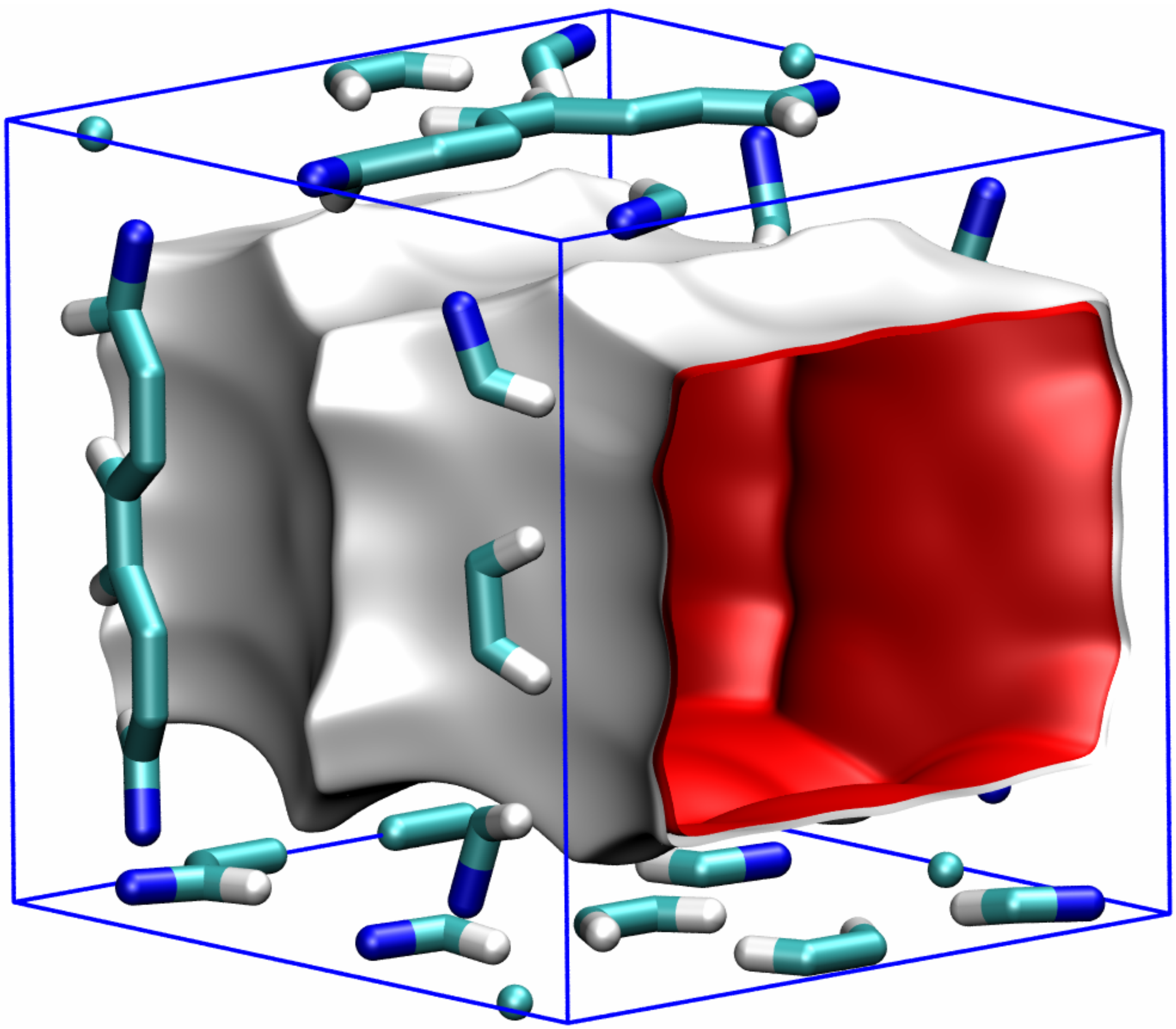

Co(BDP) CBMC mixture simulation results for CH_4/H_2 separation

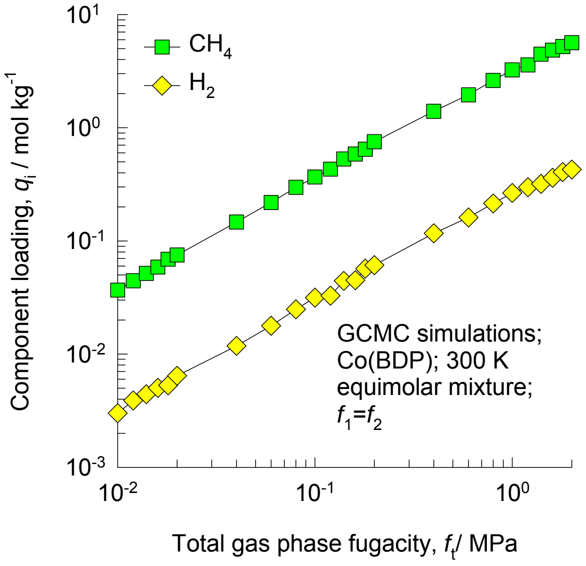

Co(BDP) CBMC pentanes mixture simulation results

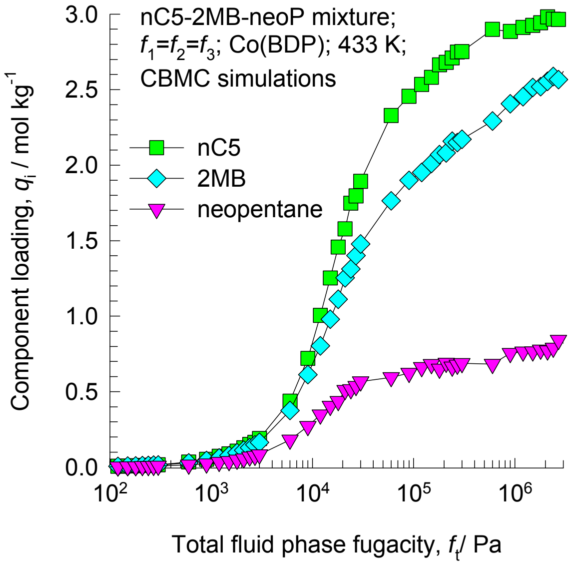

$$S_{ads} = \frac{\frac{q_{nC5}}{f_{nC5}} + \frac{q_{2MB}}{f_{2MB}}}{\frac{q_{neoP}}{f_{neoP}}}$$

Capacity is the total loading of nC5 + 2MB

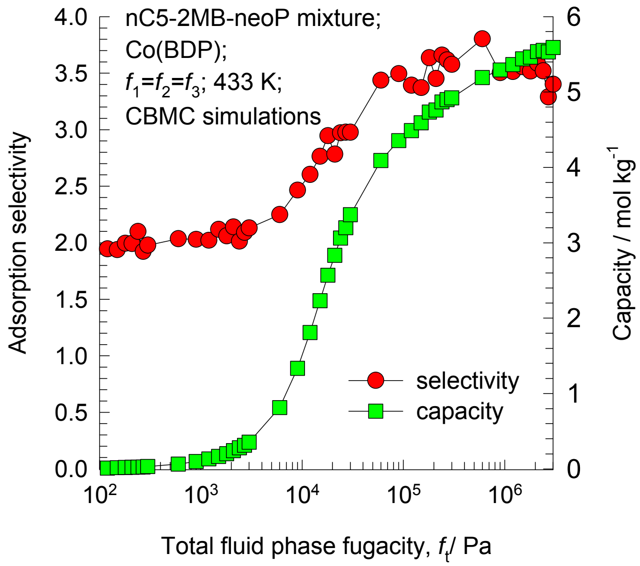

Snapshot of pure pentanes

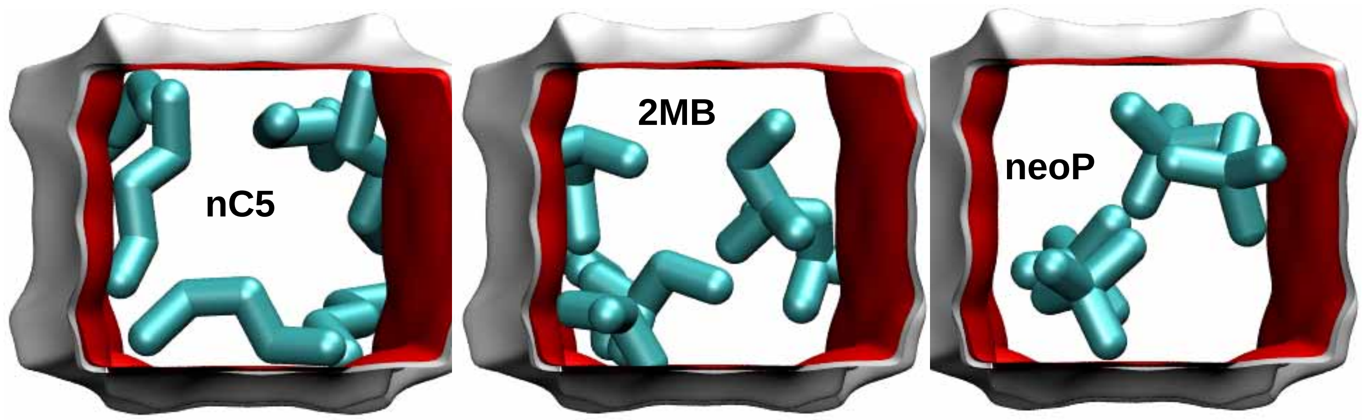

Co(BDP) CBMC nC6/3MP/22DMB mixture simulation results

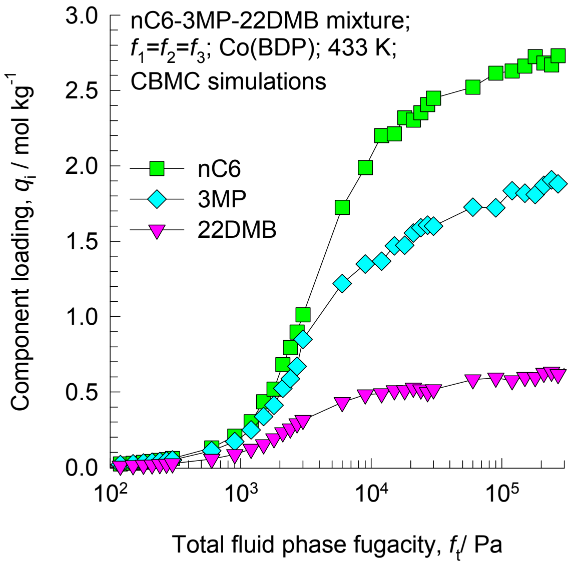

$$S_{ads} = \frac{\dfrac{q_{nC6}}{f_{nC6}} + \dfrac{q_{3MP}}{f_{3MP}}}{\dfrac{q_{22DMB}}{f_{22DMB}}}$$

Capacity is the total loading of nC6 + 3MP

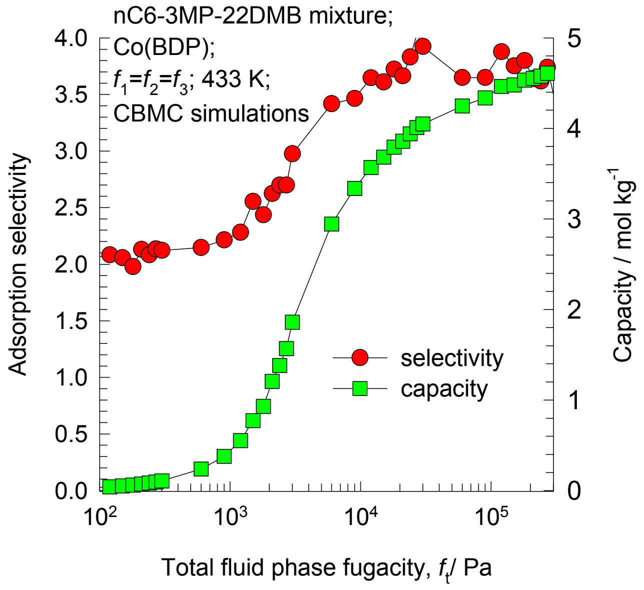

Snapshot of pure hexanes

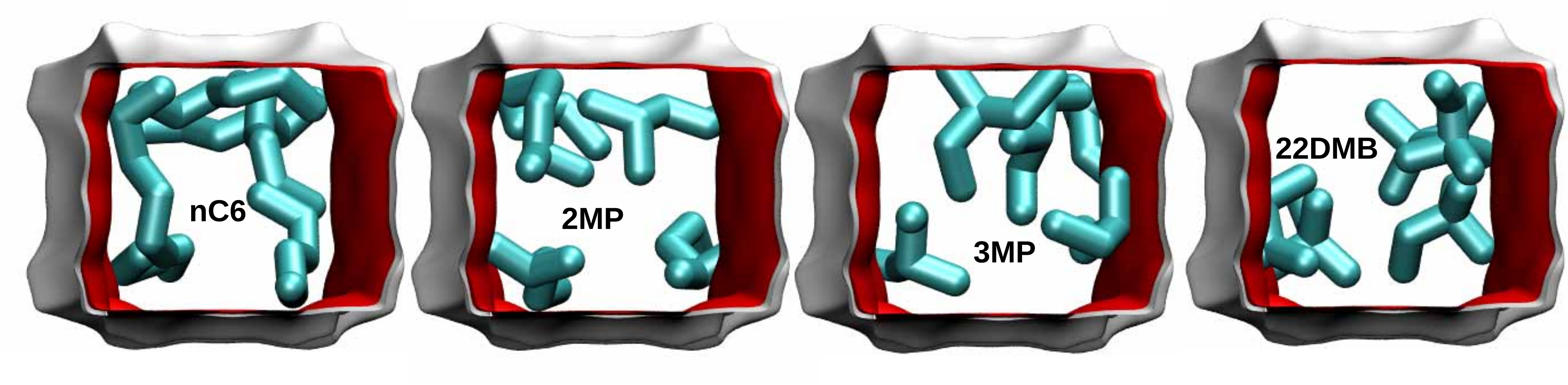

Co(BDP) CBMC nC6/2MP/3MP/22DMB/23DMB simulation results

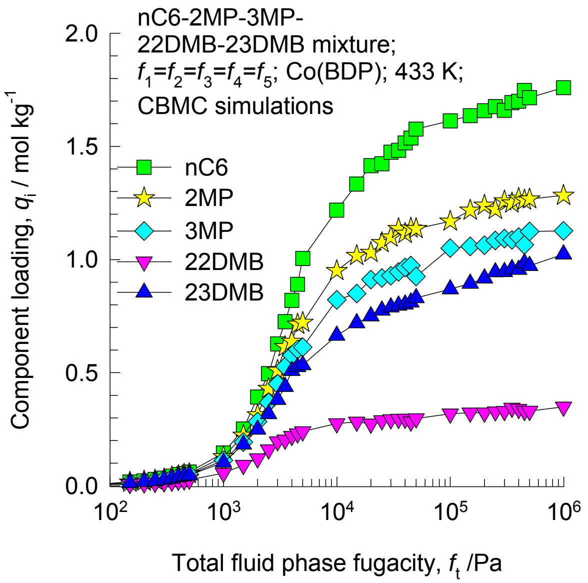

The 5-component mixture simulation shows that it is possible to have clear separation of both the di-branched 22DMB and 23DMB from linear and mono-branched

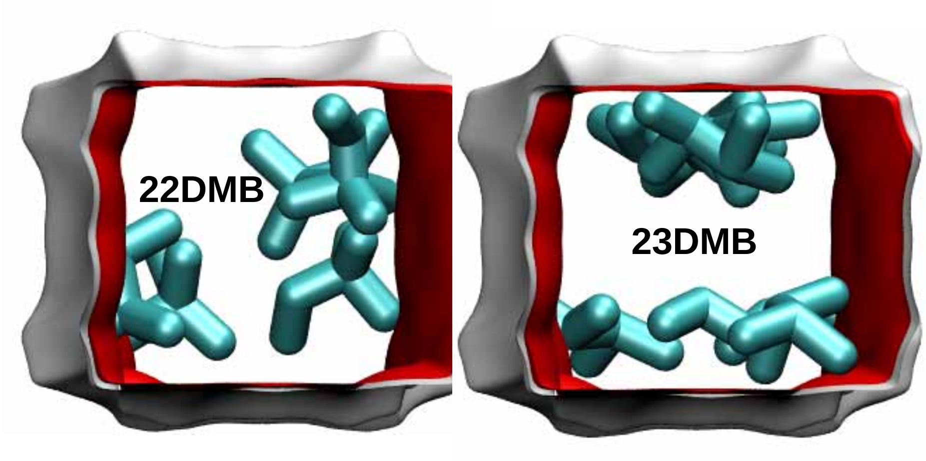

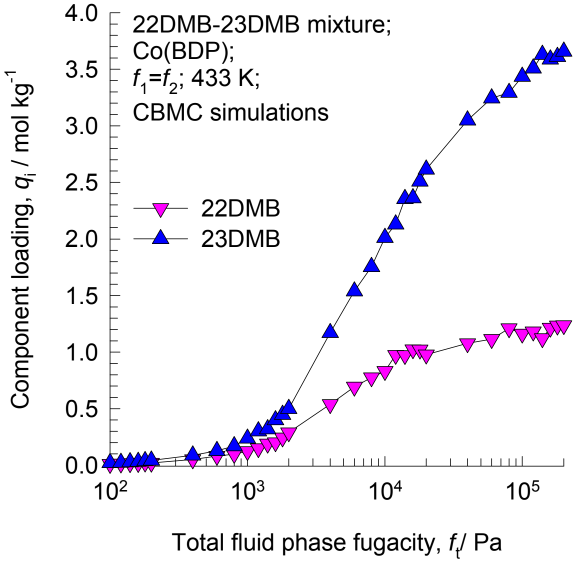

The 22DMB/23DMB binary mixture simulation demonstrates that the flatter 23DMB molecule has better interactions with the pore walls

Snapshot of CO_2/CH_4 mixture

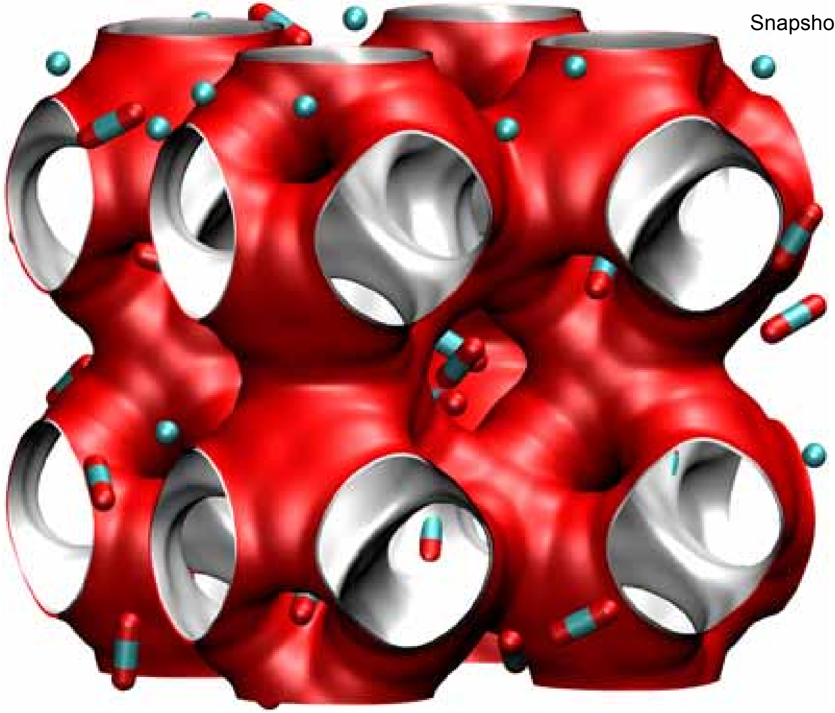

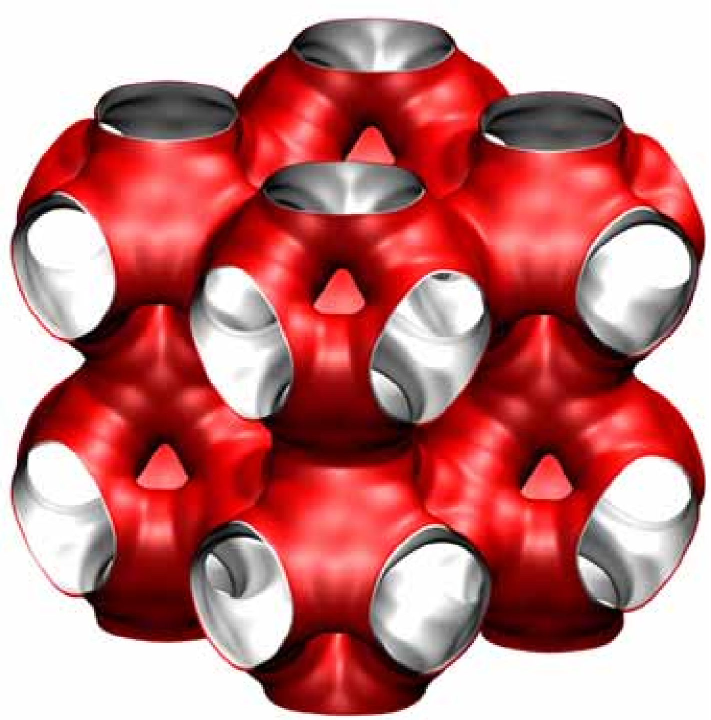

CuBTC

To convert from molecules per unit cell to mol kg^{-1}, multiply by 0.1034.
The pore volume is 0.848 cm^3/g.

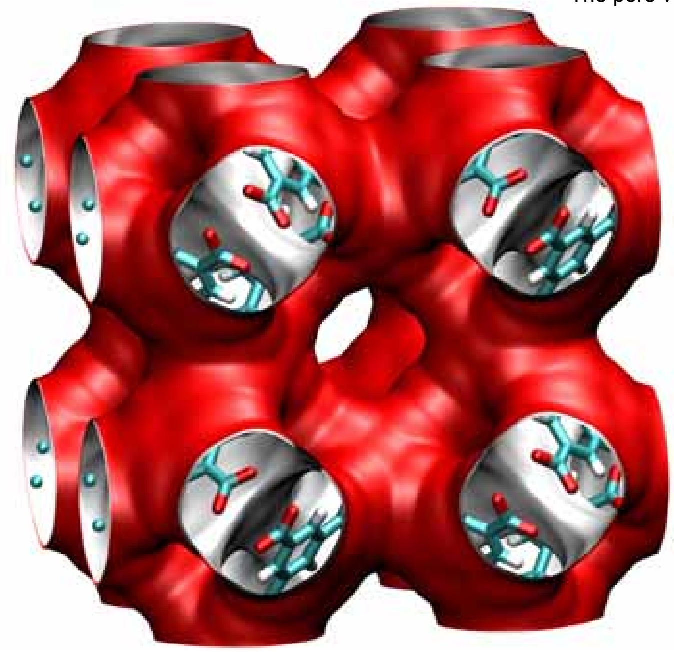

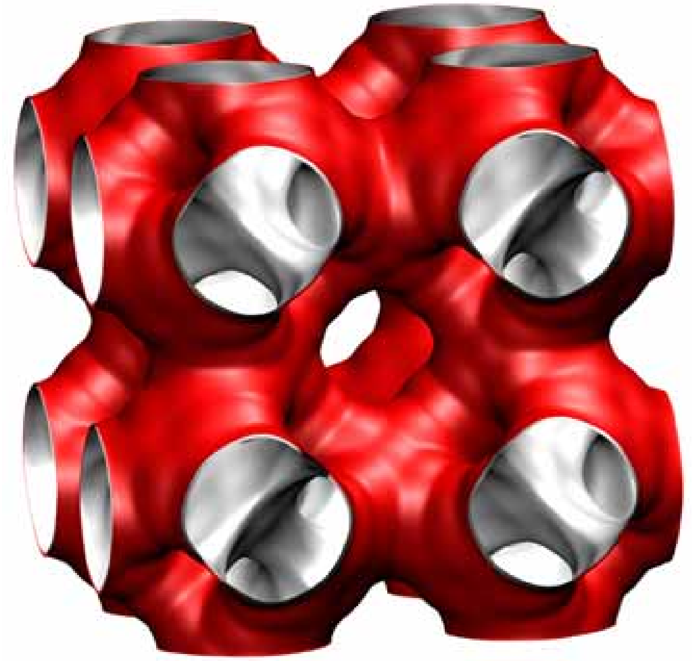

CuBTC pure component isotherms; experiments vs simulations

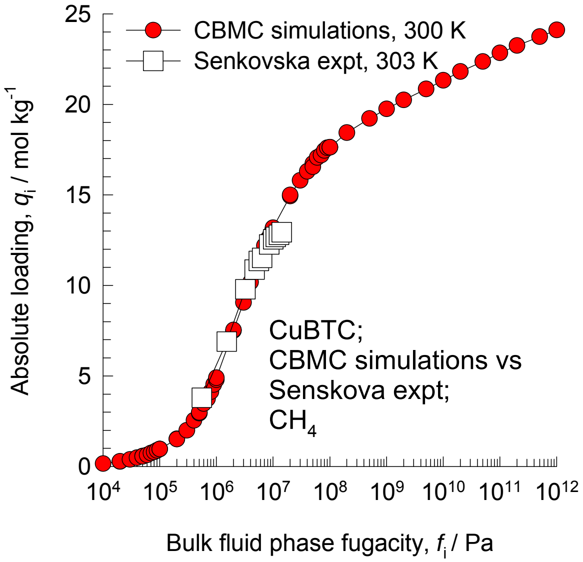

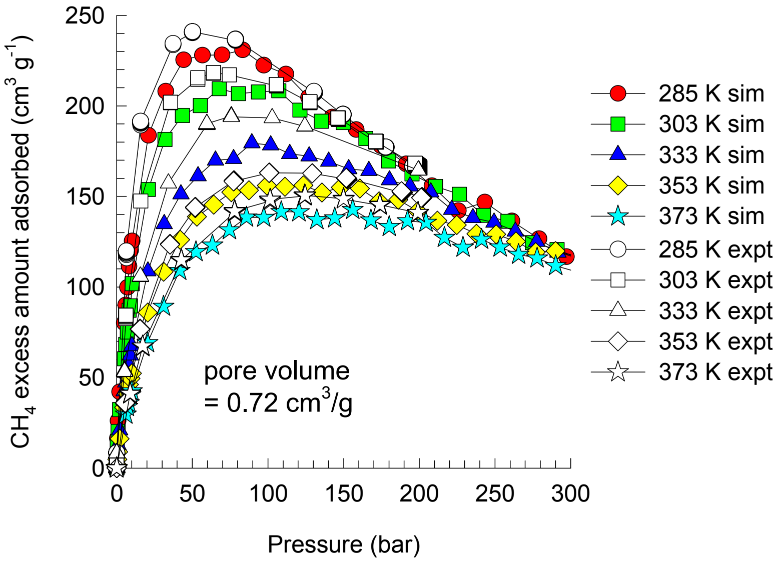

The experimental data are from:
I. Senkovska, S. Kaskel, High pressure methane adsorption in the metal-organic frameworks Cu3(btc)2, Zn2(bdc)2dabco, and Cr3F(H2O)2O(bdc)3, Microporous Mesoporous Mater. 112 (2008) 108-115.

The experimental data are from:
J. Getzschmann, I. Senkovska, D. Wallacher, M. Tovar, D. Fairen-Jimenez, T. Düren, J.M. van Baten, R. Krishna, S. Kaskel, Methane storage mechanism in the Metal-Organic Framework Cu3(btc)2: An in situ neutron diffraction study, Microporous Mesoporous Mater. 136 (2010) 50-58.

CuBTC CBMC mixture simulations for CO_2 capture

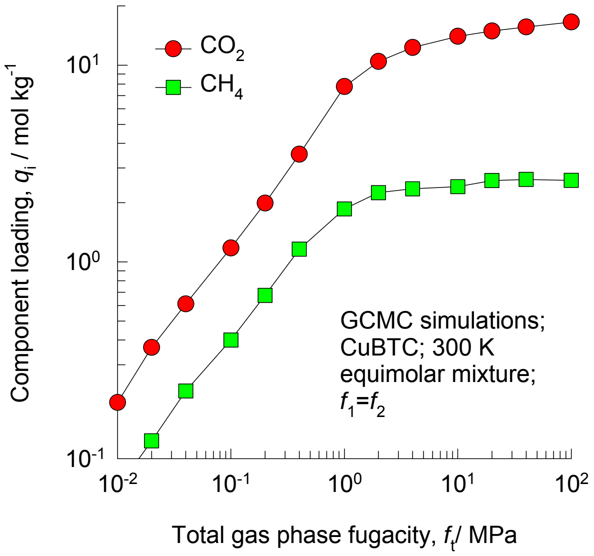

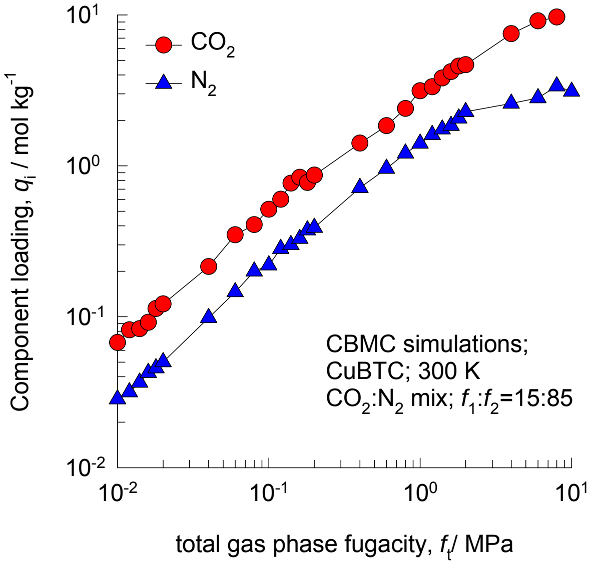

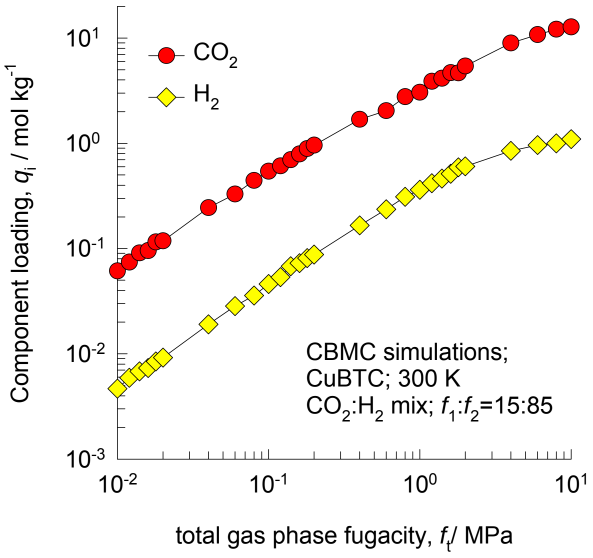

CuBTT pore landscapes

To convert from molecules per unit cell to mol kg^{-1}, multiply by 0.334.
The pore volume is 0.712 cm^3/g.

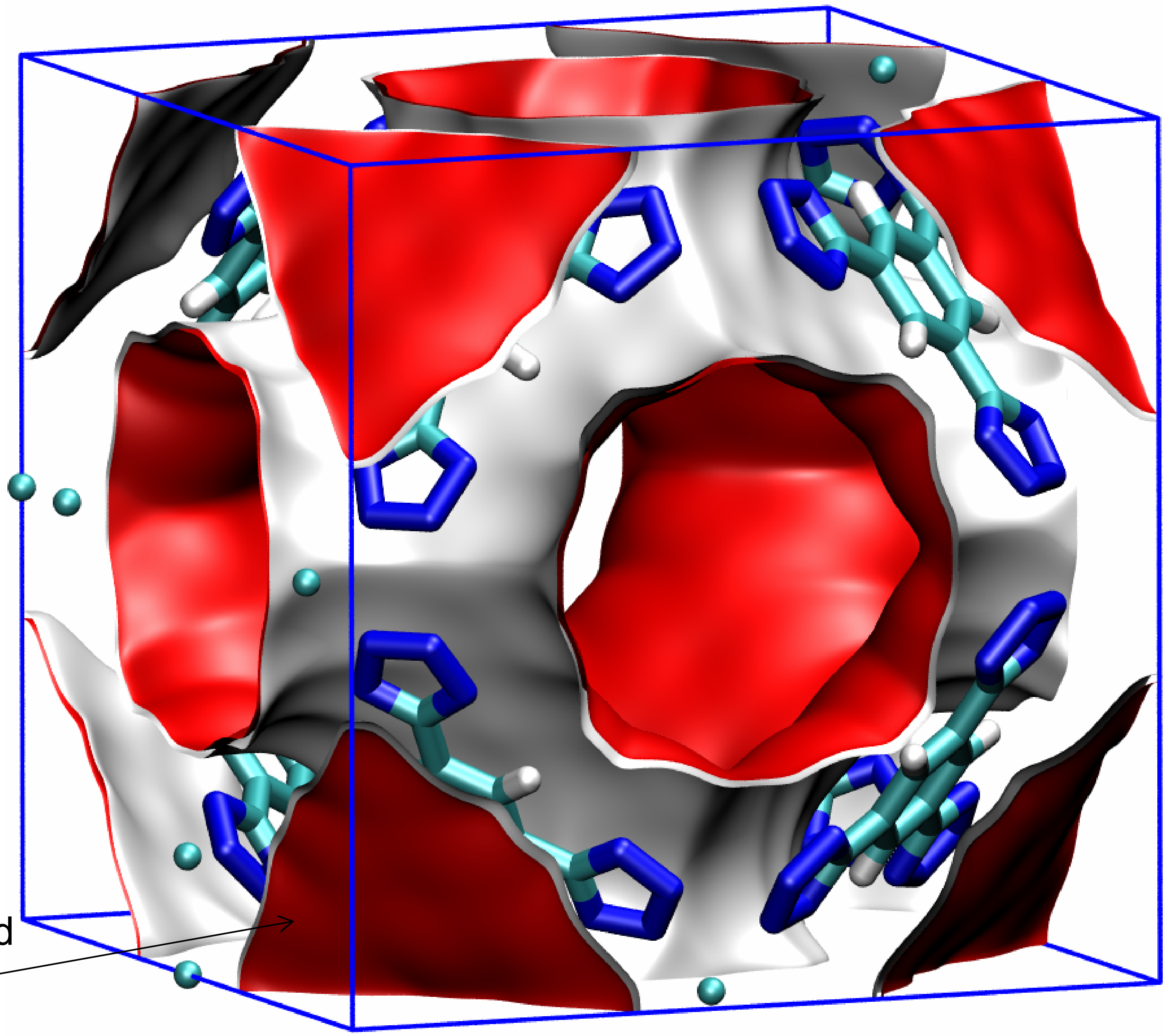

These inaccessible pockets were blocked in our simulations

CuBTT CBMC mixture simulation results for CH_4/H_2 separation

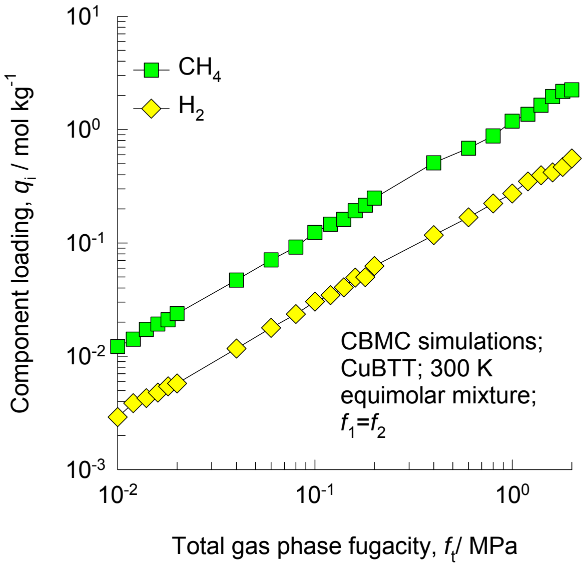

CuBTT CBMC pentanes mixture simulation results

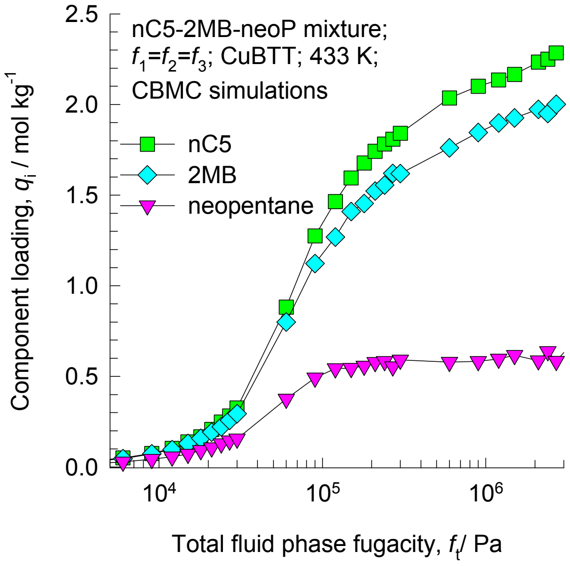

$$S_{ads} = \frac{\dfrac{q_{nC5}}{f_{nC5}} + \dfrac{q_{2MB}}{f_{2MB}}}{\dfrac{q_{neoP}}{f_{neoP}}}$$

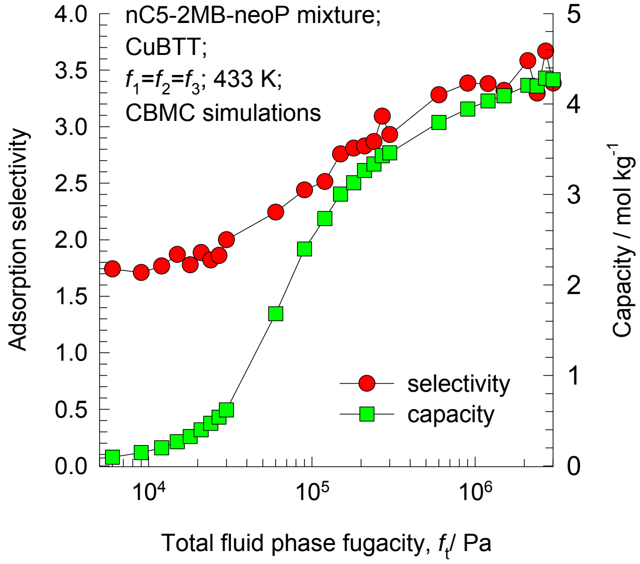

Capacity is the total
loading of nC5 + 2MB

CuBTT CBMC nC6/3MP/22DMB mixture simulation results

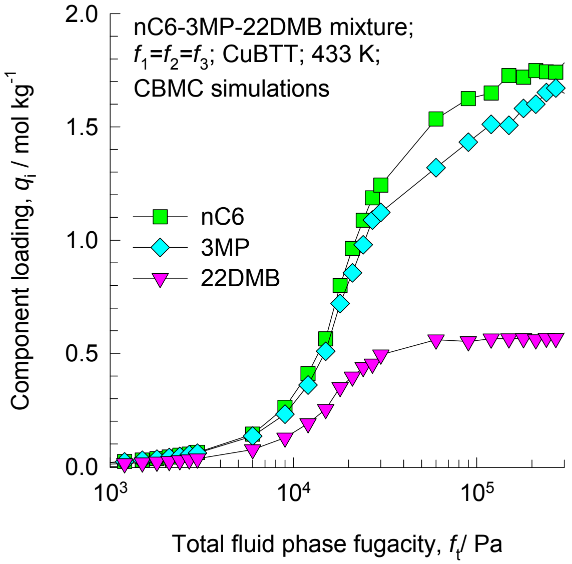

$$S_{ads} = \frac{\frac{q_{nC6}}{f_{nC6}} + \frac{q_{3MP}}{f_{3MP}}}{\frac{q_{22DMB}}{f_{22DMB}}}$$

Capacity is the total loading of nC6 + 3MP

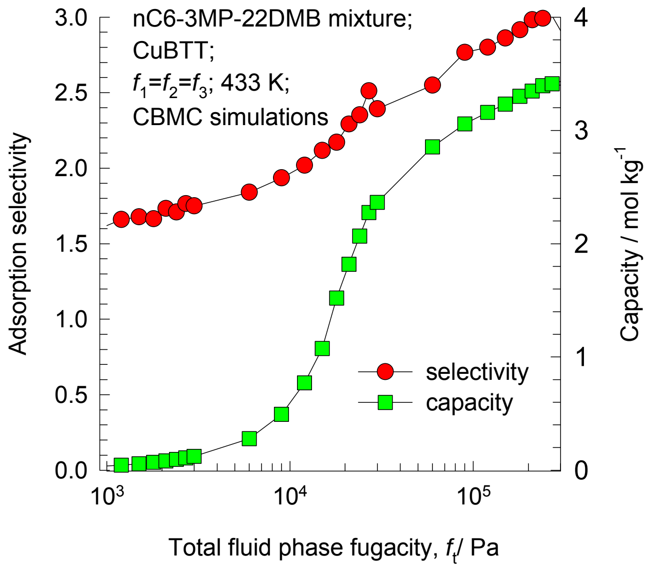

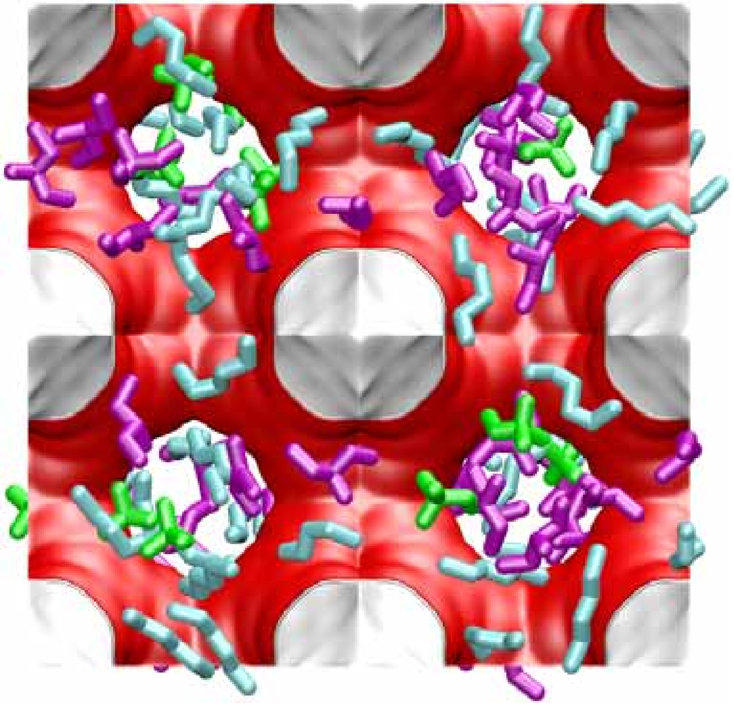

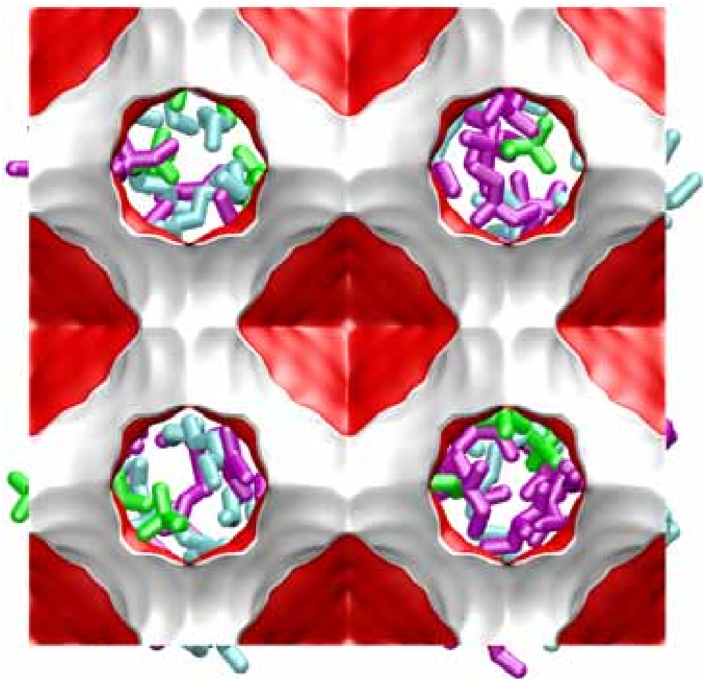

Snapshot of CO_2/CH_4 mixture

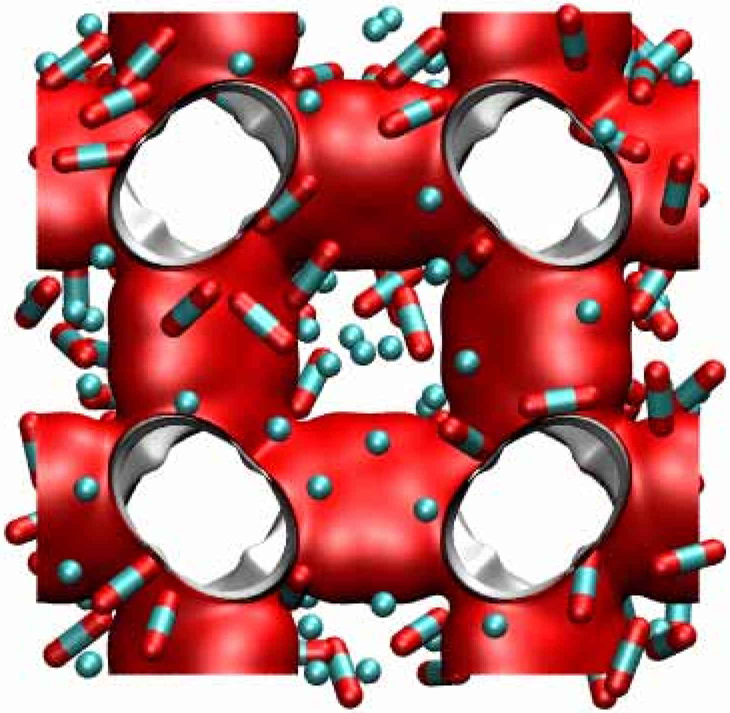

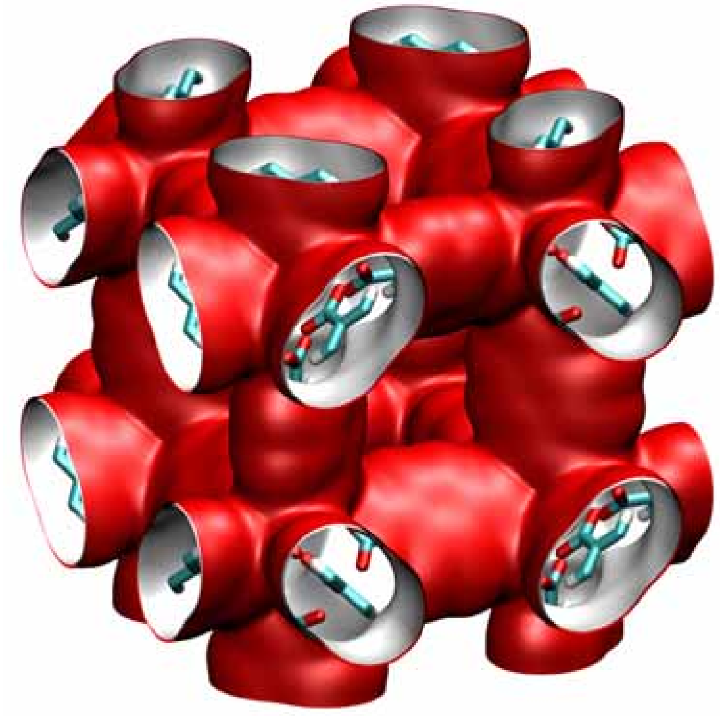

IRMOF-1

To convert from molecules per unit cell to mol kg^{-1}, multiply by 0.1624.
The pore volume is 1.369 cm^3/g.

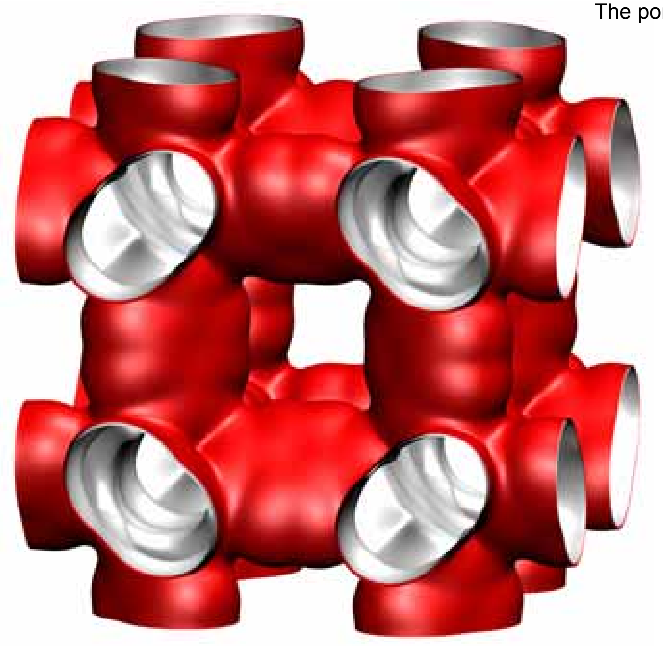

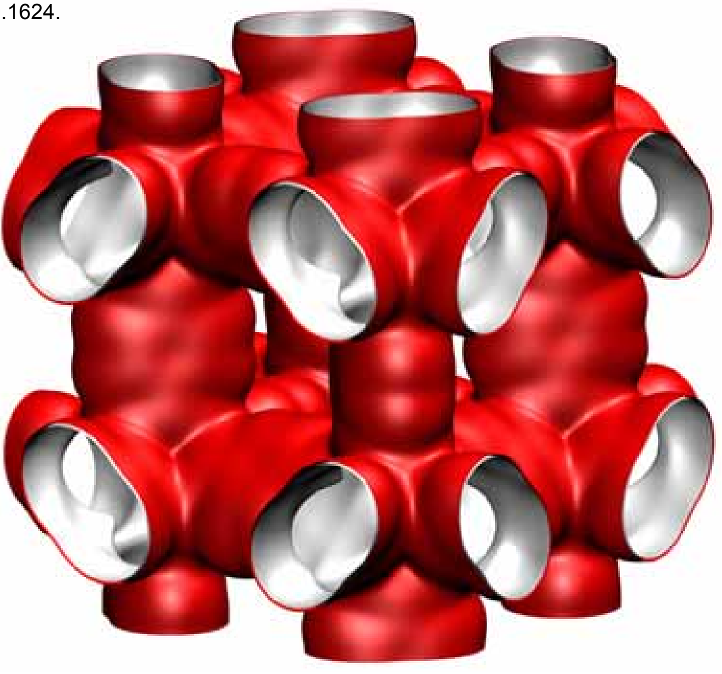

IRMOF-1 CBMC mixture simulations for CO_2 capture

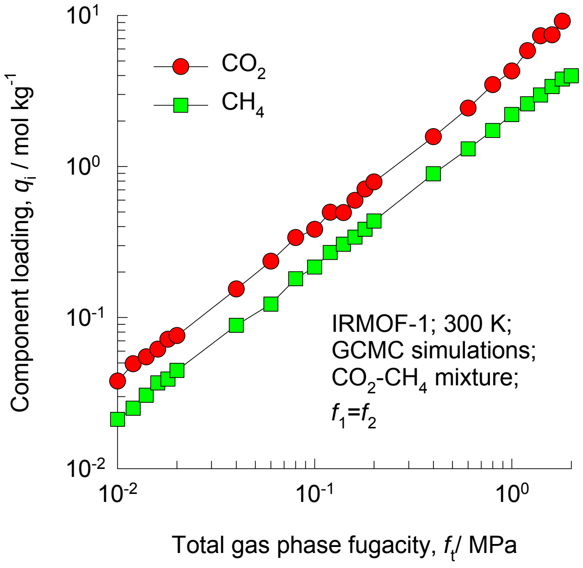

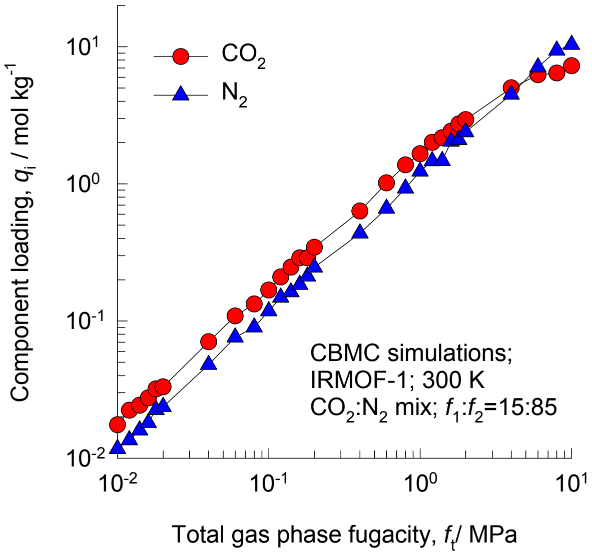

IRMOF-1 CBMC pentanes mixture simulations

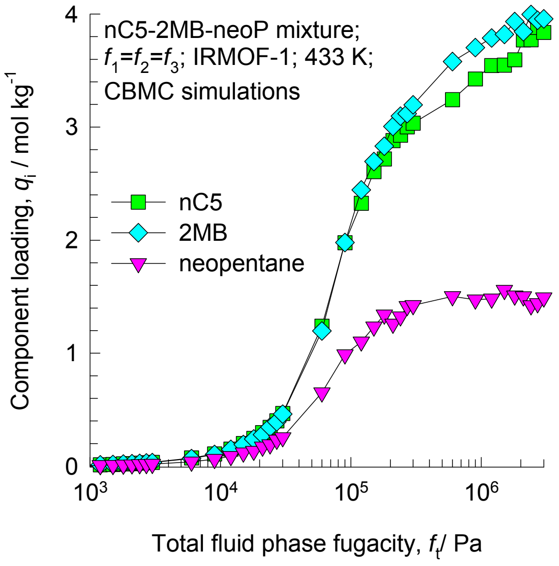

$$S_{ads} = \frac{\dfrac{q_{nC5}}{f_{nC5}} + \dfrac{q_{2MB}}{f_{2MB}}}{\dfrac{q_{neoP}}{f_{neoP}}}$$

Capacity is the total
loading of nC5 + 2MB

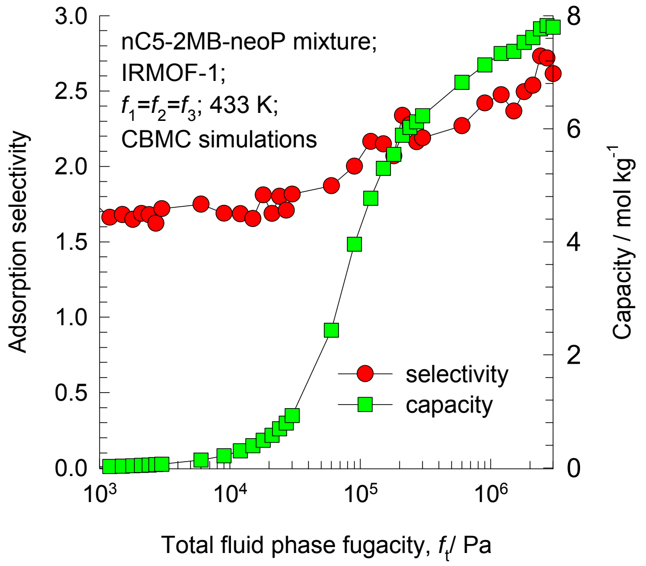

IRMOF-1 CBMC nC6/3MP/22DMB mixture simulations

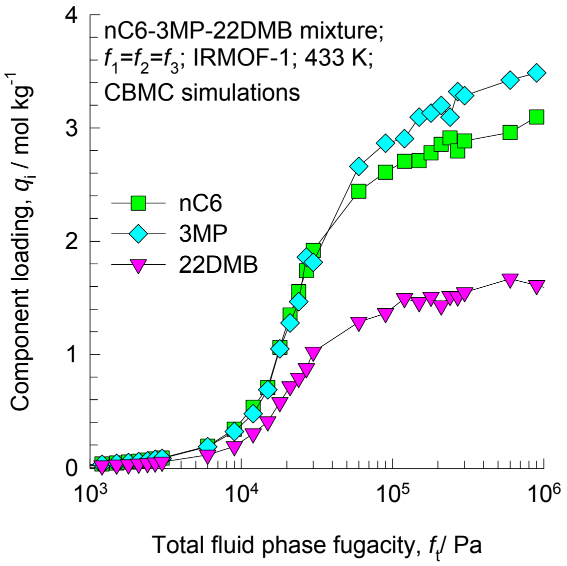

$$S_{ads} = \frac{\frac{q_{nC6}}{f_{nC6}} + \frac{q_{3MP}}{f_{3MP}}}{\frac{q_{22DMB}}{f_{22DMB}}}$$

Capacity is the total loading of nC6 + 3MP

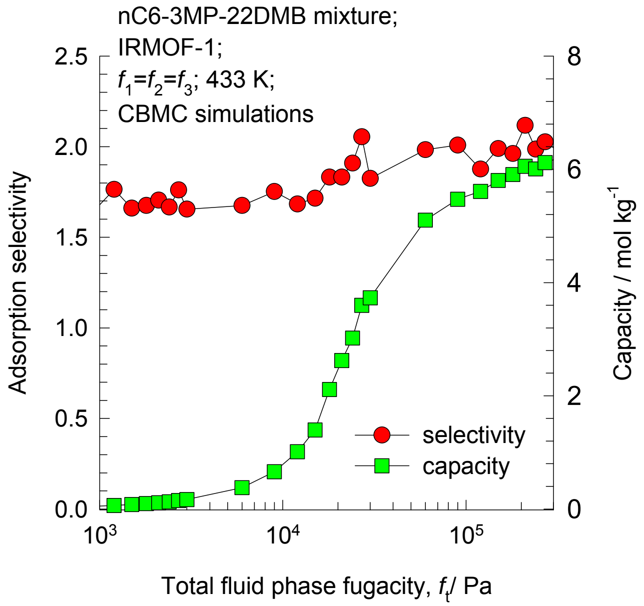

IRMOF-1 snapshot of nC66/3MP/22DMB mix

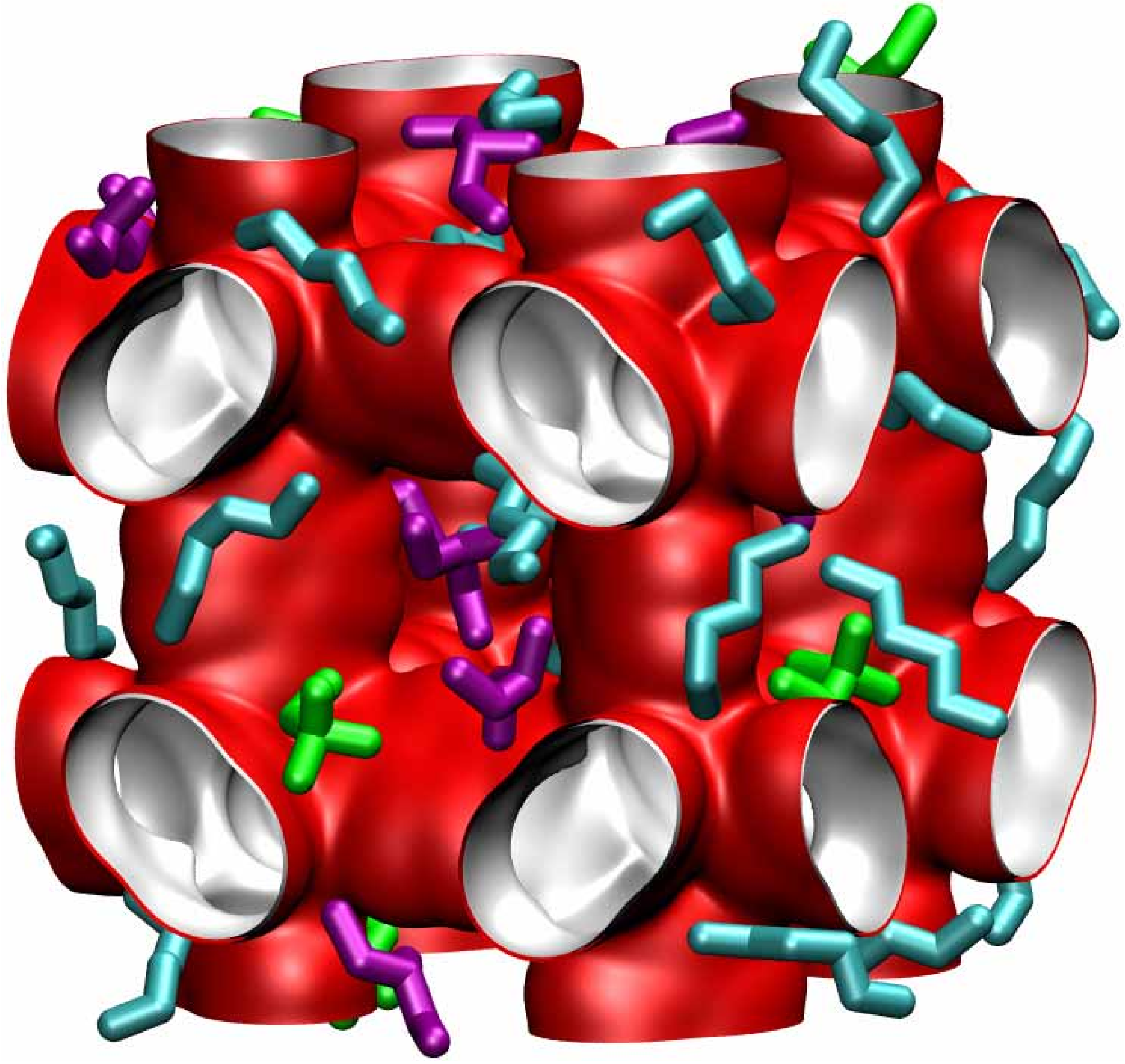

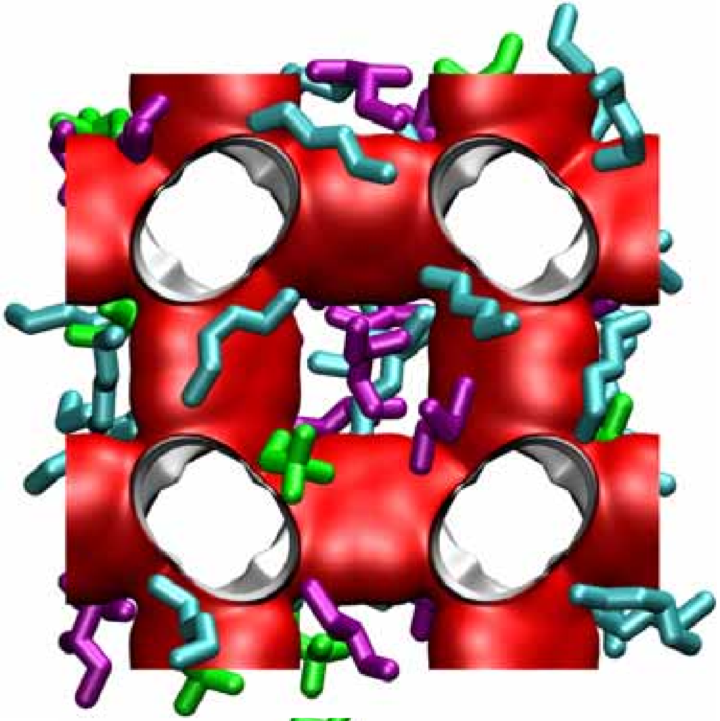

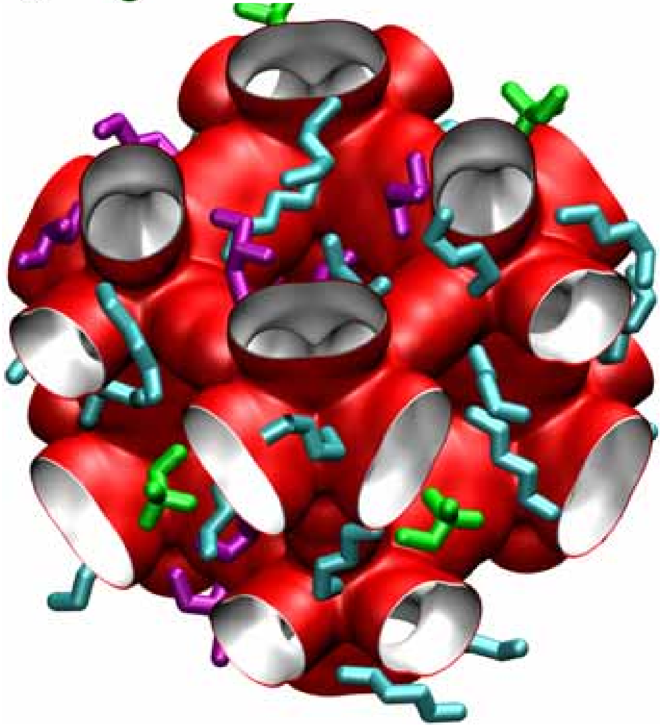

IRMOF-1 CBMC nC6/2MP/3MP/22DMB/23DMB simulations

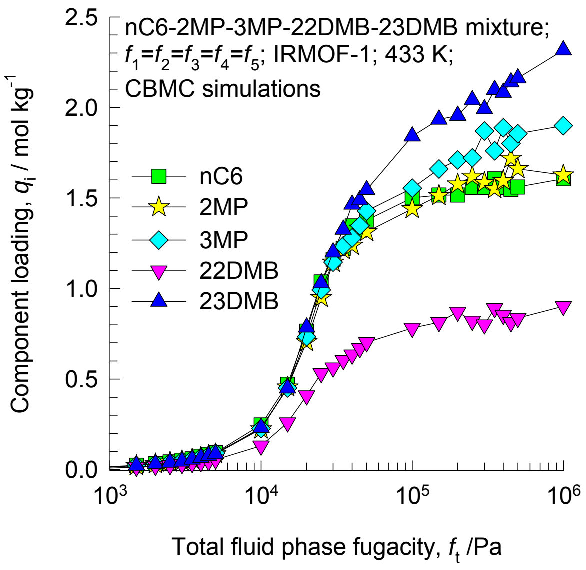

The 5-component mixture simulation shows that 22DMB can be separated from the rest of the mixture. But it is not possible to have clear separation of both the di-branched 22DMB and 23DMB from (linear + mono-branched)

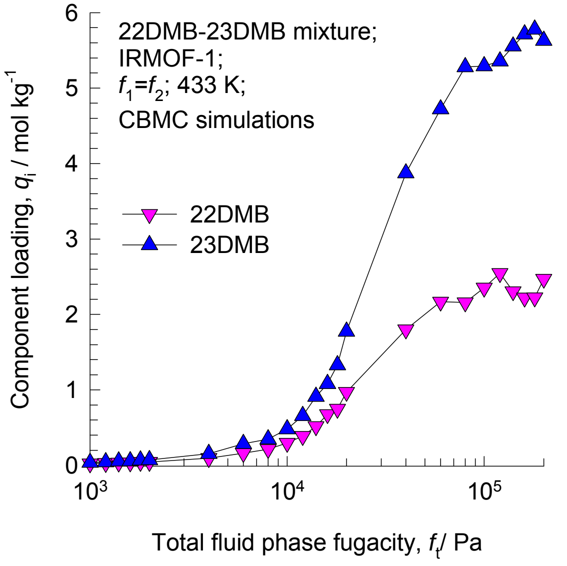

The 22DMB/23DMB binary mixture simulation demonstrates that the flatter 23DMB molecule has better interactions with the pore walls

MIL – 47 pore landscape

To convert from molecules per unit cell to mol kg^{-1}, multiply by 1.0824.
The pore volume is 0.606 cm^3/g.

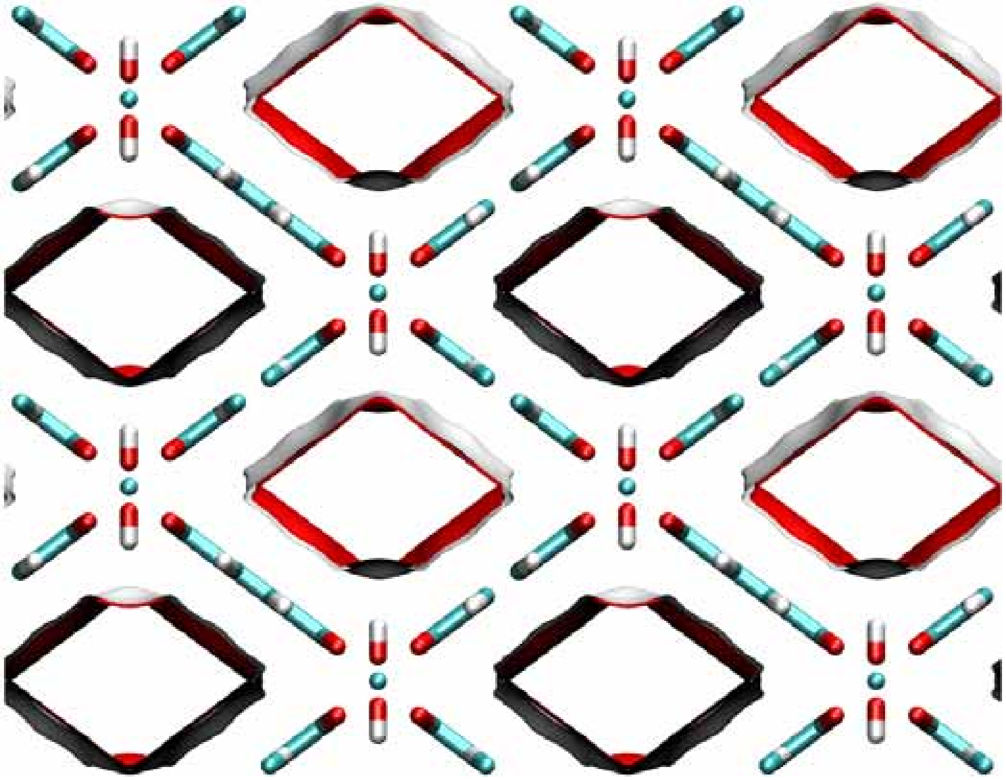

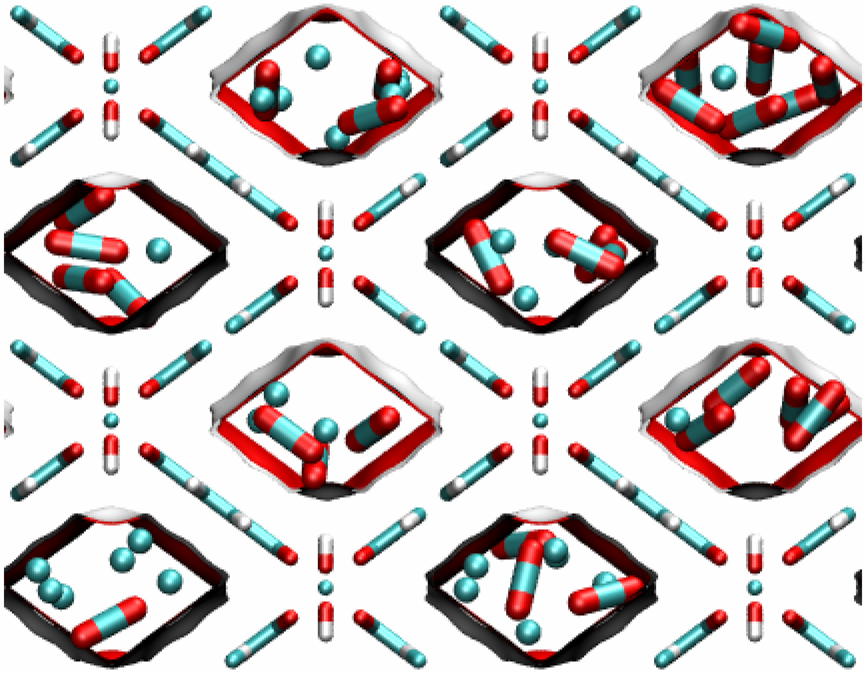

Snapshot of CO_2/CH_4 mixture

MIL-47 CBMC mixture simulations for CO_2 capture

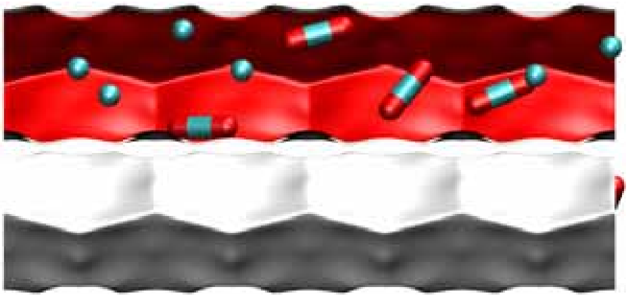

Snapshot of CO_2/CH_4 mixture

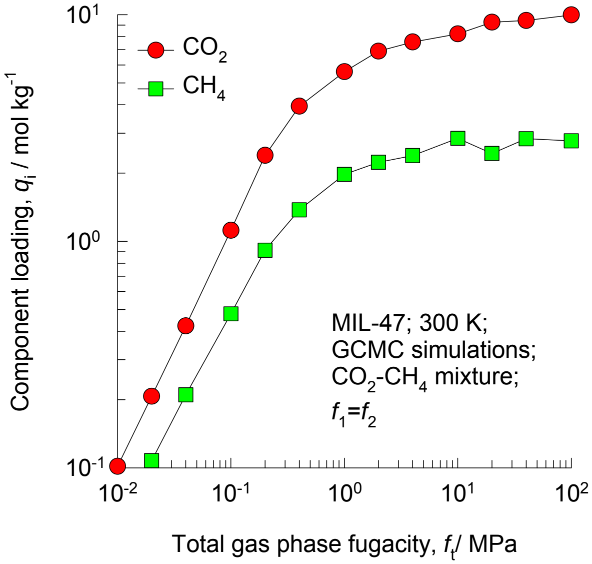

MIL – 53 (Cr) pore landscape

To convert from molecules per unit cell to mol kg^{-1}, multiply by 1.073.
The pore volume is 0.518 cm^3/g.

Simulation results presented are for –lp structure, i.e. large pore

Snapshot of CO_2/CH_4 mixture

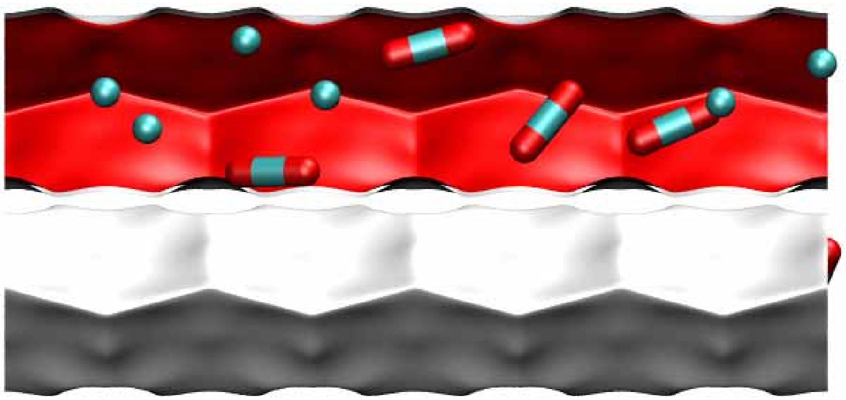

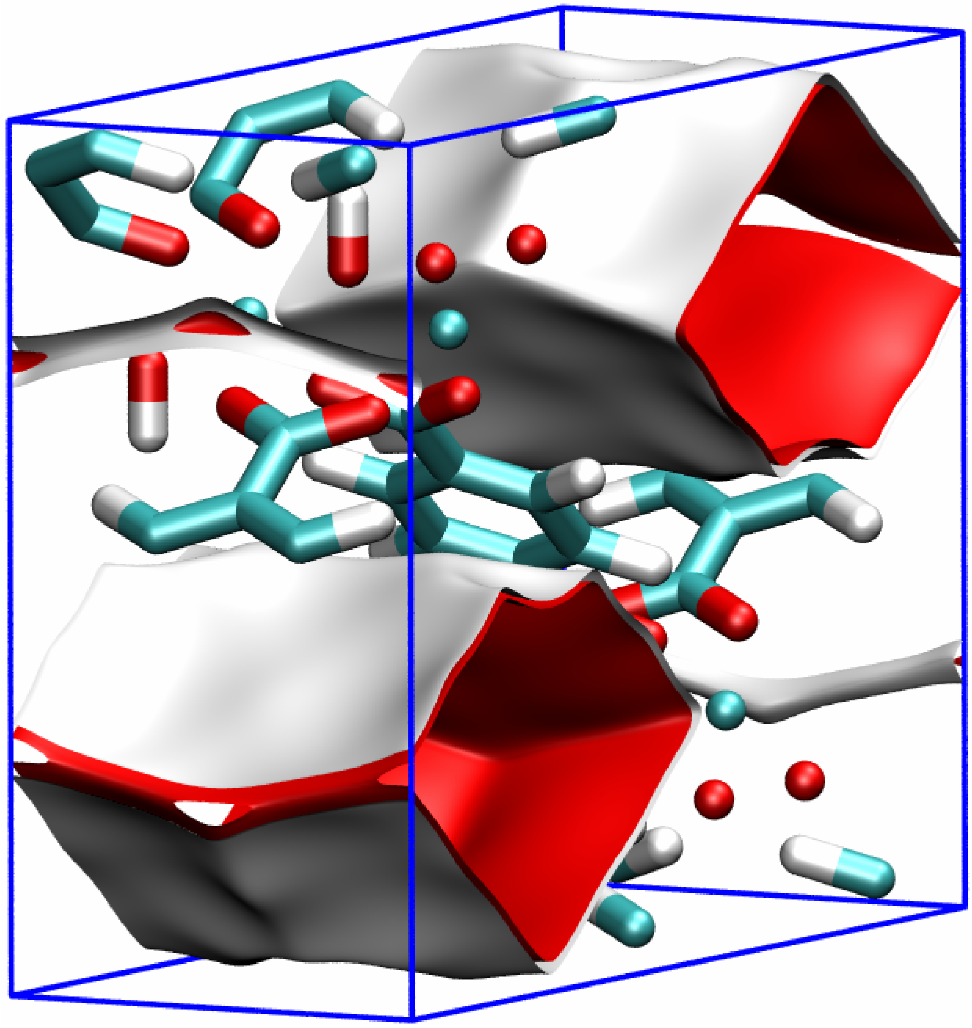

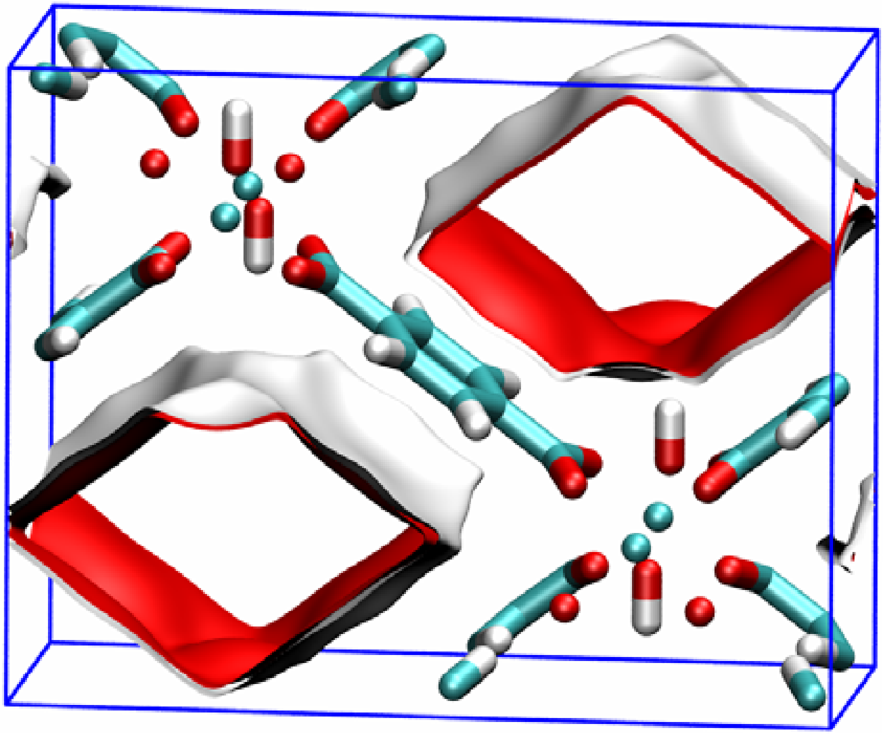

MIL-53(Cr)-lp CBMC mixture simulations for CO_2 capture

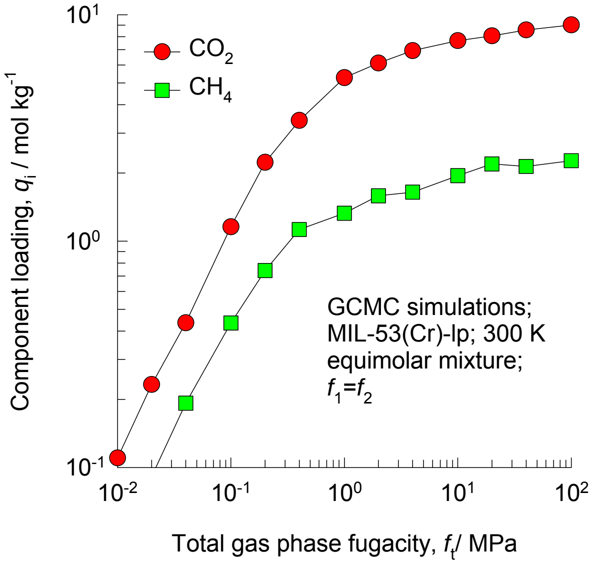

MIL-53(Cr)-lp CBMC hexanes mixture simulations

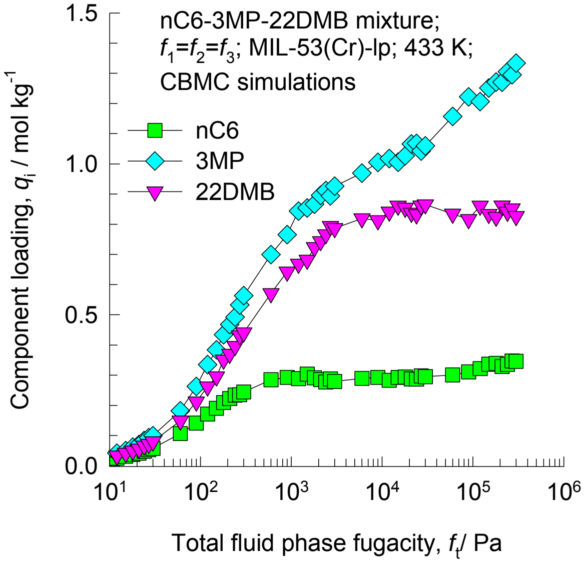

The 3-component mixture simulation shows that it is not possible to have separation of both the di-branched 22DMB from (linear + mono-branched)

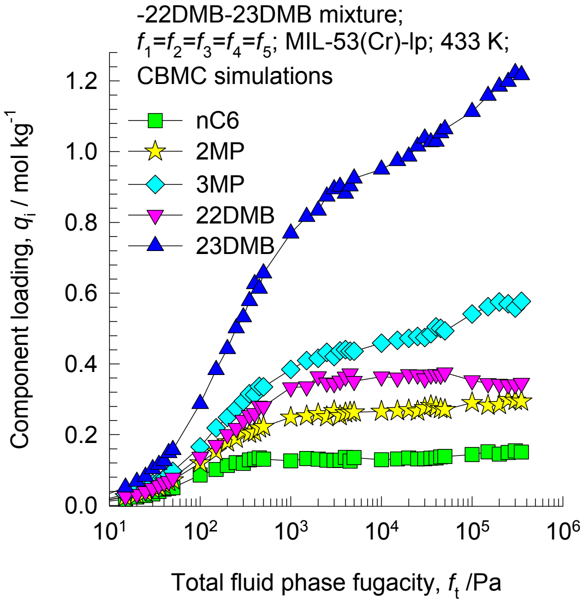

The 5-component mixture simulation shows that it is not possible to have separation of both the di-branched 22DMB and 23DMB from (linear + mono-branched)

The hierarchy of adsorption loadings of the C5 and C6 isomers suggests that molecular length entropy effects are in play. This is confirmed in the snapshots that follow

MIL-53(Cr)-lp C5 isomers snapshot

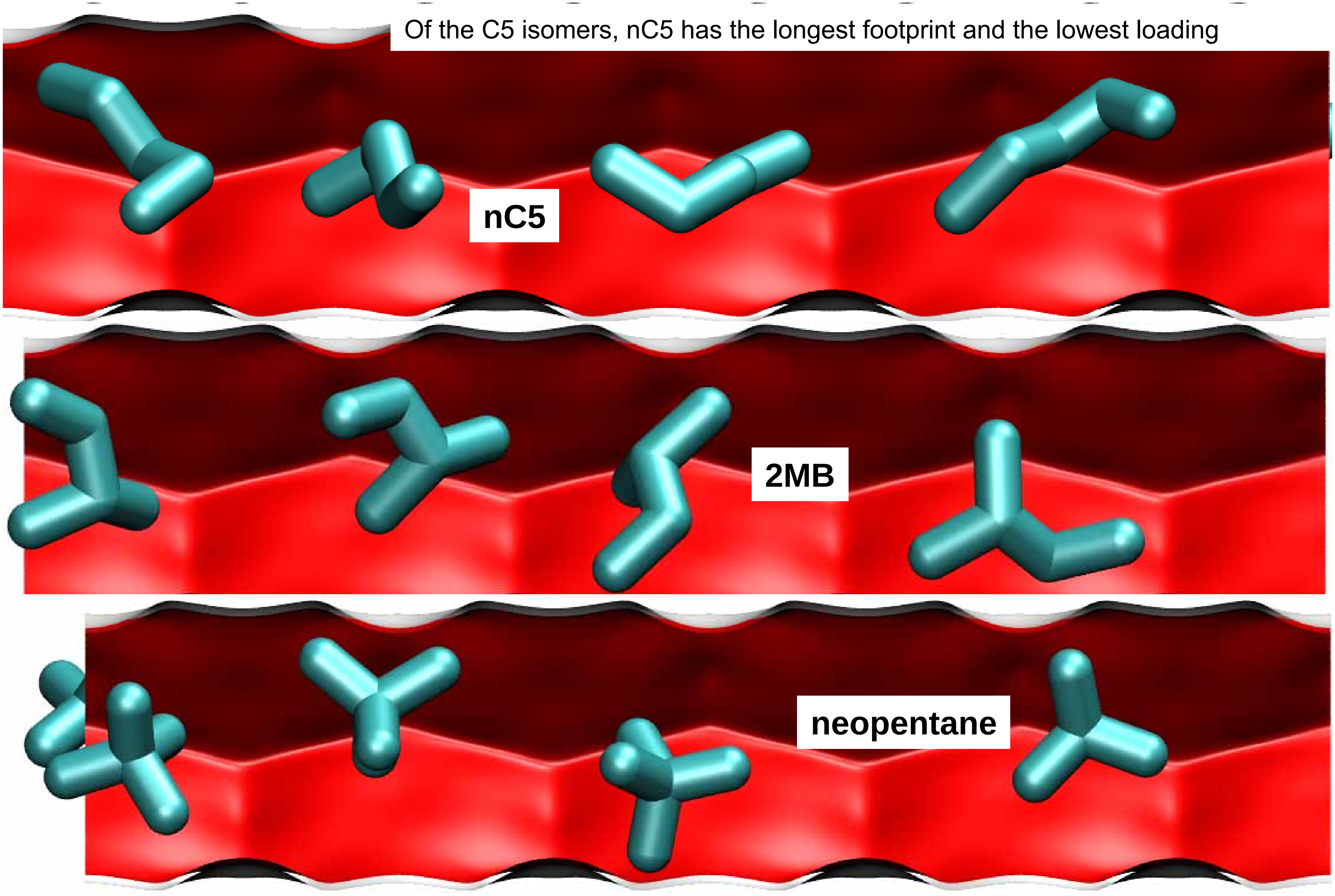

Of the C5 isomers, nC5 has the longest footprint and the lowest loading

MIL-53(Cr)-lp C6 isomers snapshot

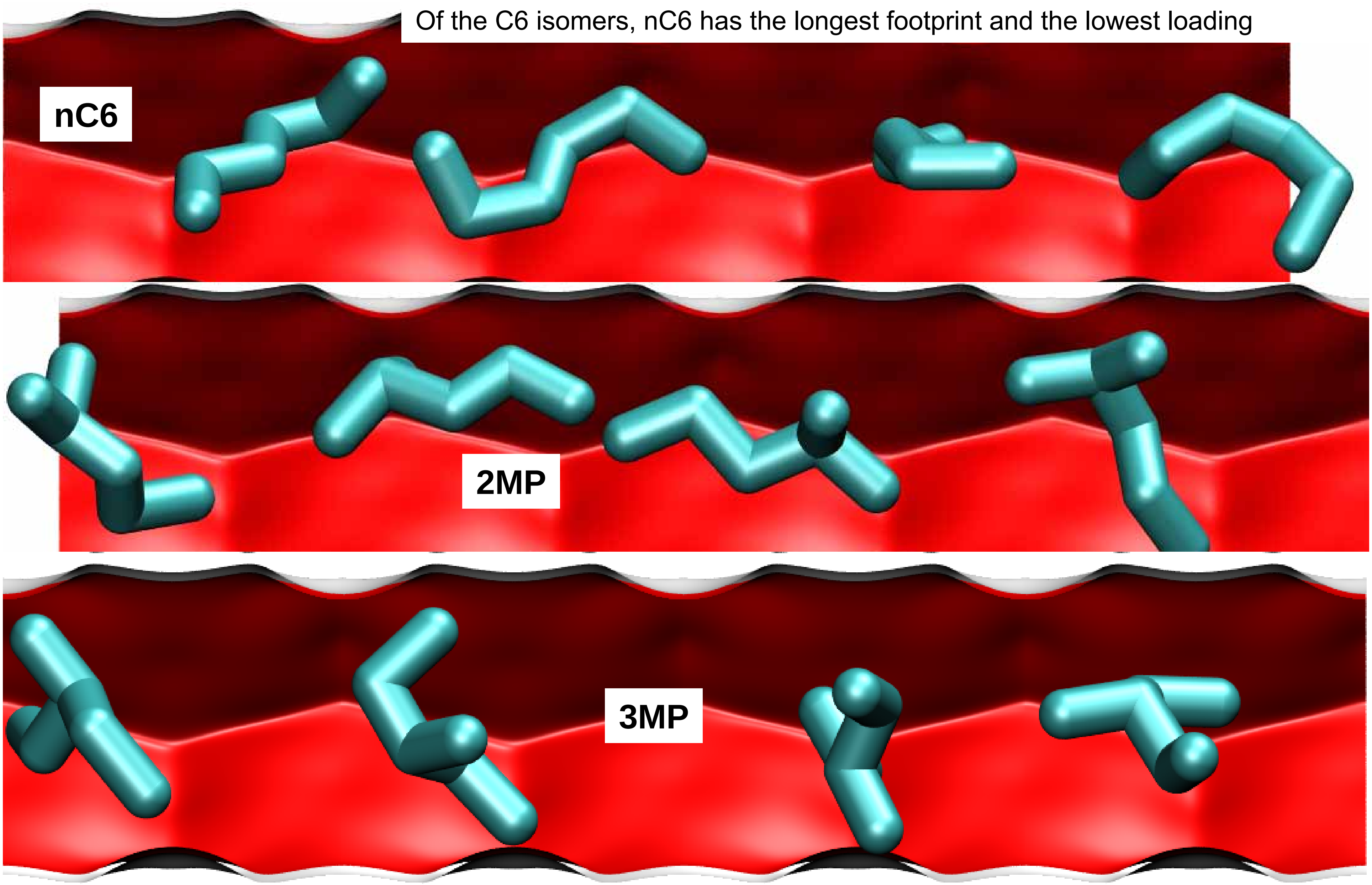

Of the C6 isomers, nC6 has the longest footprint and the lowest loading

MIL-53(Cr)-lp C6 isomers snapshot

Of the C6 isomers, 23DMB has the shortest footprint and the highest loading

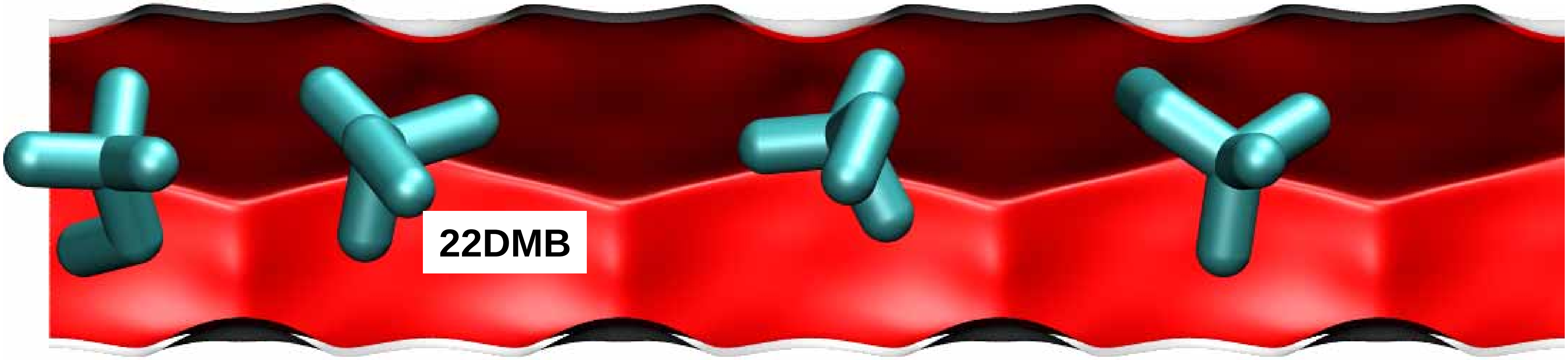

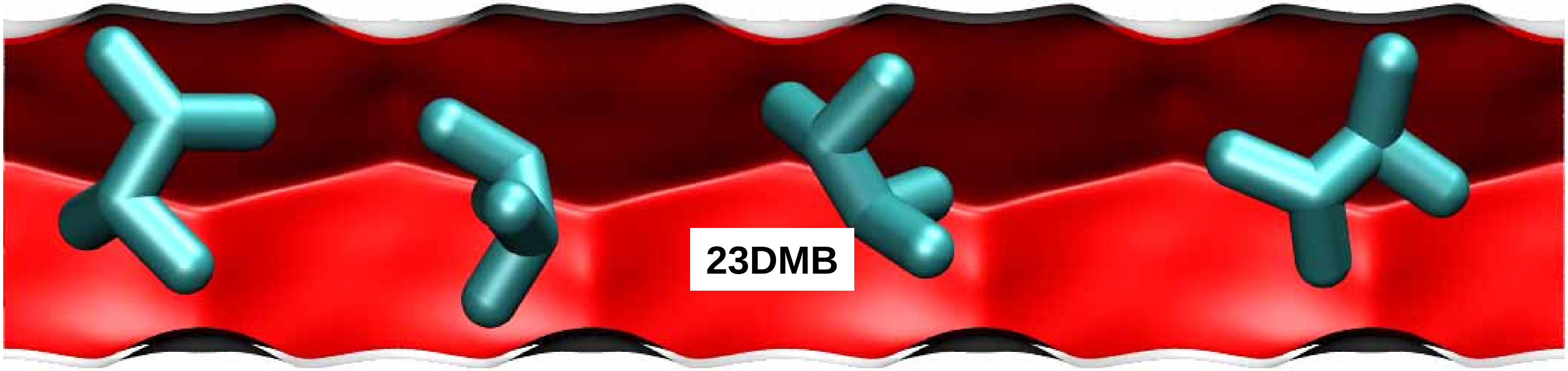

MgMOF-74 pore landscapes

To convert from molecules per unit cell to mol kg^{-1}, multiply by 0.458.
The pore volume is 0.782 cm^3/g.

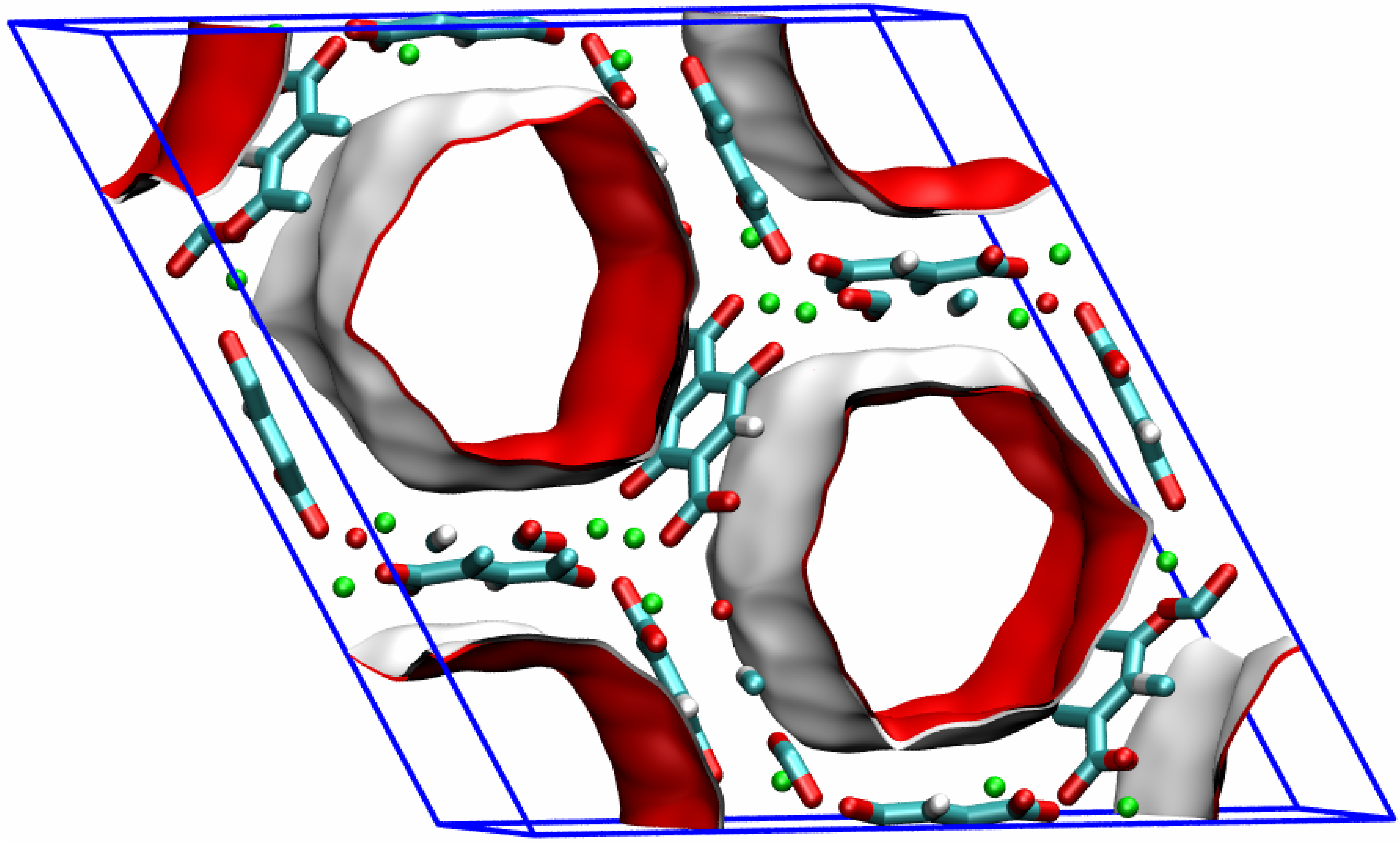

MgMOF-74 pure component isotherms; comparison with experiments

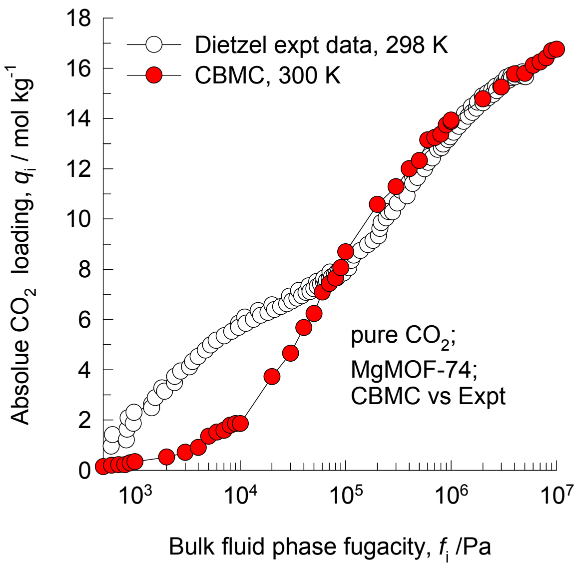

These simulation results are obtained using the force field information given in A.Ö. Yazaydın, R.Q. Snurr, T.H. Park, K. Koh, J. Liu, M.D. LeVan, A.I. Benin, P. Jakubczak, M. Lanuza, D.B. Galloway, J.J. Low, R.R. Willis, Screening of Metal-Organic Frameworks for Carbon Dioxide Capture from Flue Gas using a Combined Experimental and Modeling Approach, J. Am. Chem. Soc. 131 (2009) 18198-18199.

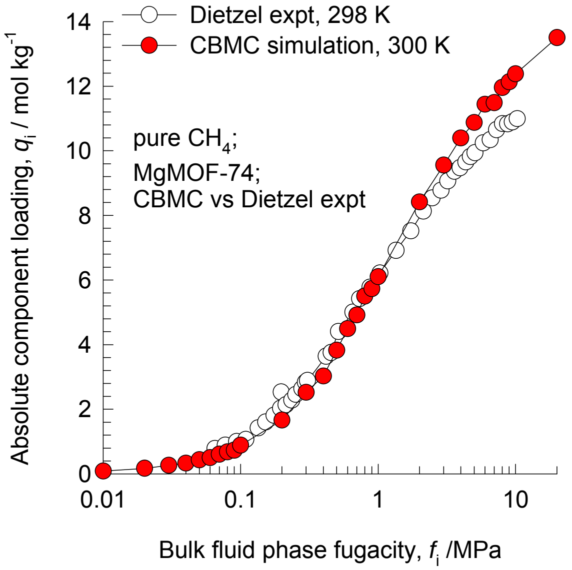

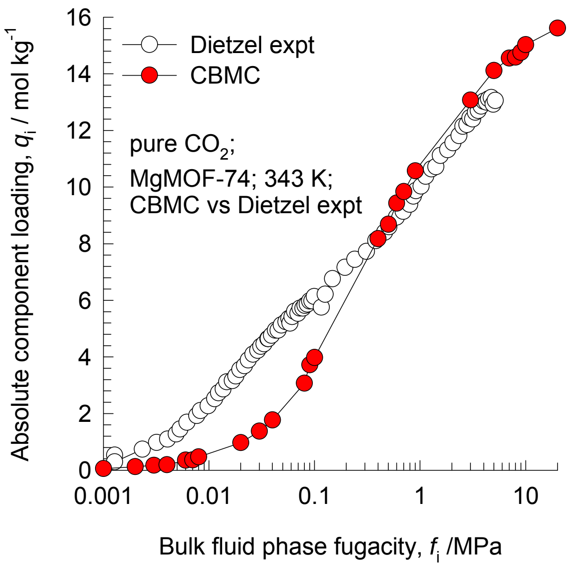

The experimental data is from P.D.C. Dietzel, V. Besikiotis, R. Blom, Application of metal–organic frameworks with coordinatively unsaturated metal sites in storage and separation of methane and carbon dioxide, J. Mater. Chem. 19 (2009) 7362-7370. The reported excess loadings have been converted to absolute loadings using the pore volume data, along with the Peng-Robinson equation of state.

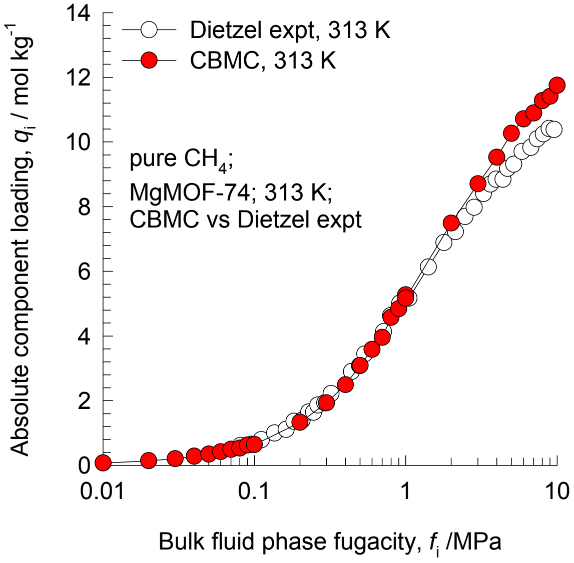

MgMOF-74 pure component isotherms; comparison with experiments

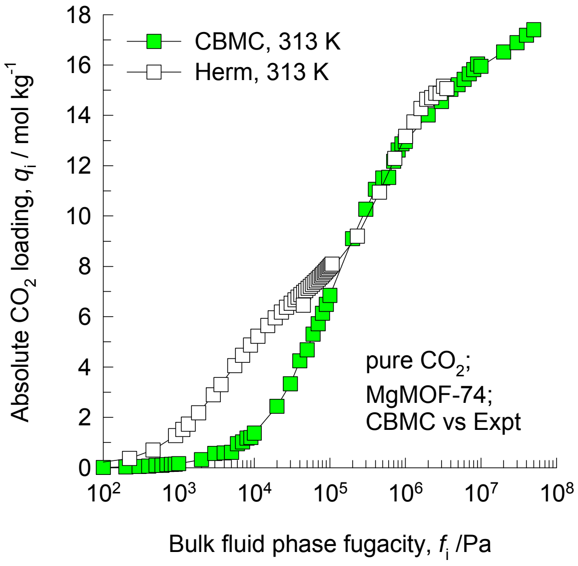

These simulation results are obtained using the force field information given in A.Ö. Yazaydın, R.Q. Snurr, T.H. Park, K. Koh, J. Liu, M.D. LeVan, A.I. Benin, P. Jakubczak, M. Lanuza, D.B. Galloway, J.J. Low, R.R. Willis, Screening of Metal-Organic Frameworks for Carbon Dioxide Capture from Flue Gas using a Combined Experimental and Modeling Approach, J. Am. Chem. Soc. 131 (2009) 18198-18199.

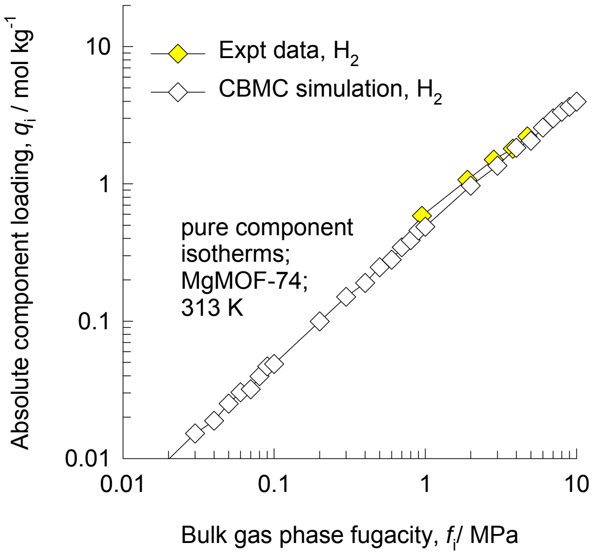

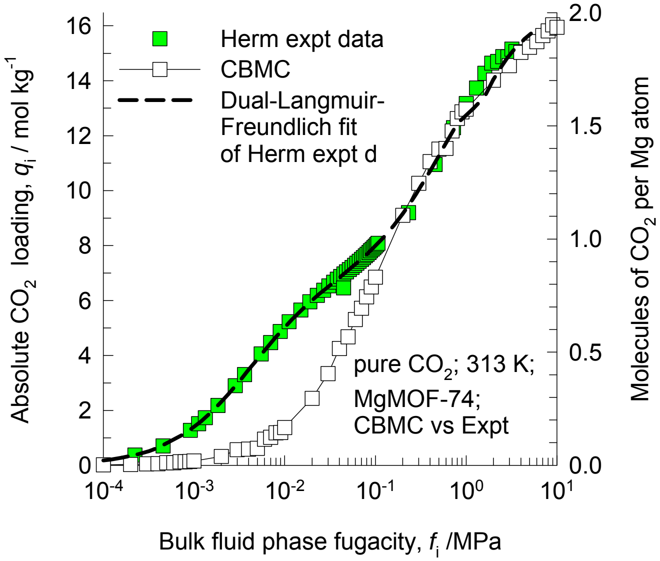

The experimental data for CO_2, and H_2 are from Z.R. Herm, J.A. Swisher, B. Smit, R. Krishna, J.R. Long, Metal-Organic Frameworks as Adsorbents for Hydrogen Purification and Pre-Combustion Carbon Dioxide Capture, J. Am. Chem. Soc. XXX (2011) XXX-XXX. (http://dx.doi.org/10.1021/ja111411q)

MgMOF-74 CBMC mixture simulation results for CO_2 capture

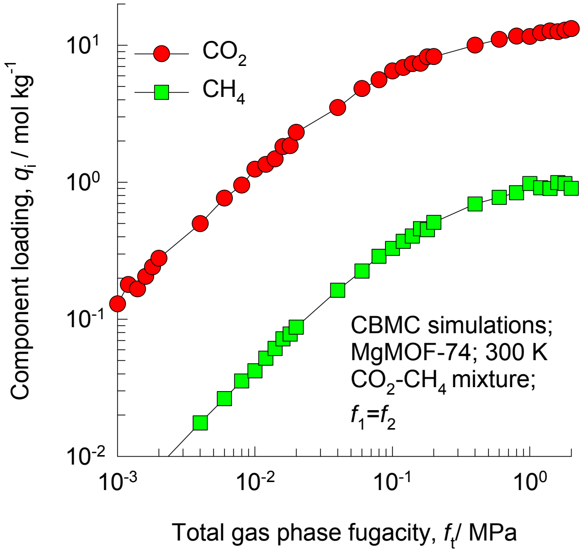

These simulation results are obtained using the force field information given in A.Ö. Yazaydın, R.Q. Snurr, T.H. Park, K. Koh, J. Liu, M.D. LeVan, A.I. Benin, P. Jakubczak, M. Lanuza, D.B. Galloway, J.J. Low, R.R. Willis, Screening of Metal-Organic Frameworks for Carbon Dioxide Capture from Flue Gas using a Combined Experimental and Modeling Approach, J. Am. Chem. Soc. 131 (2009) 18198-18199.

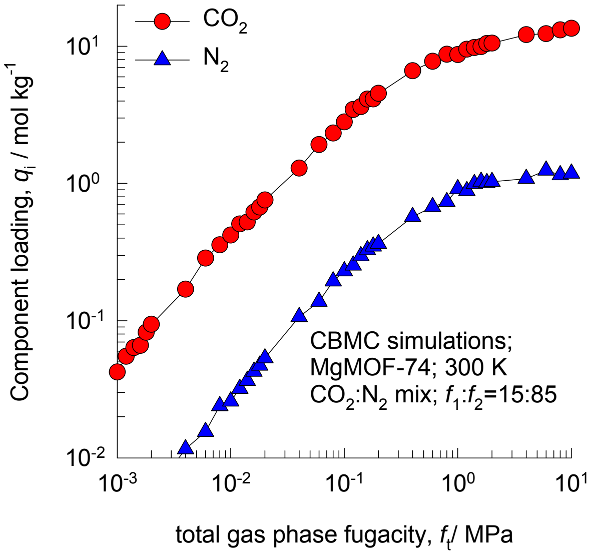

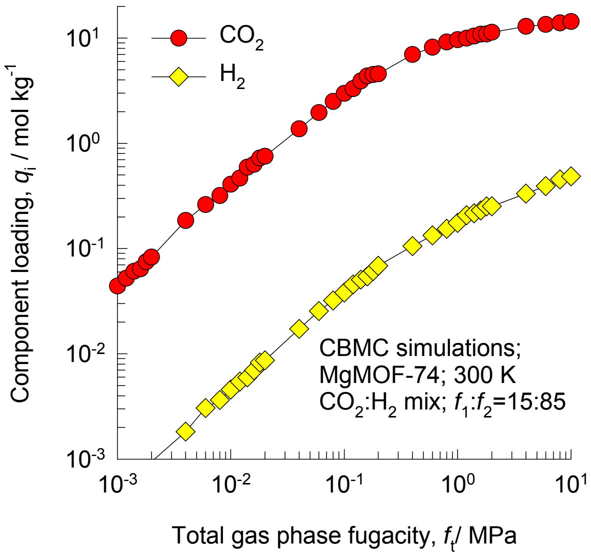

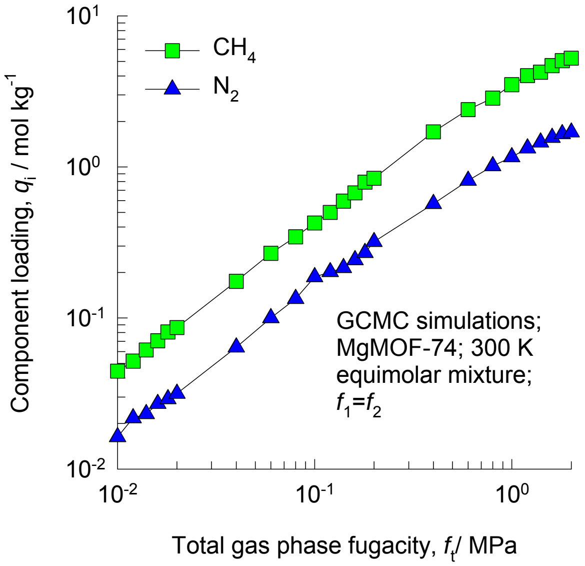

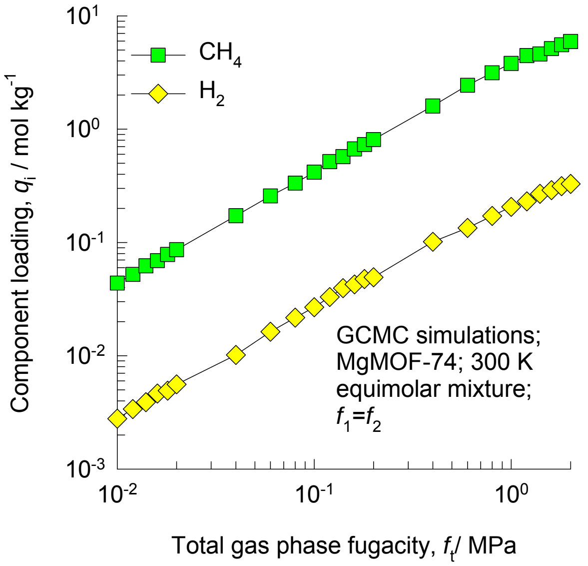

MgMOF-74 snapshot of CO_2 and CH_4 at a total fugacity of 1 MPa

Snapshots of CO_2 and CH_4 at a total gas phase fugacity of 1 MPa.

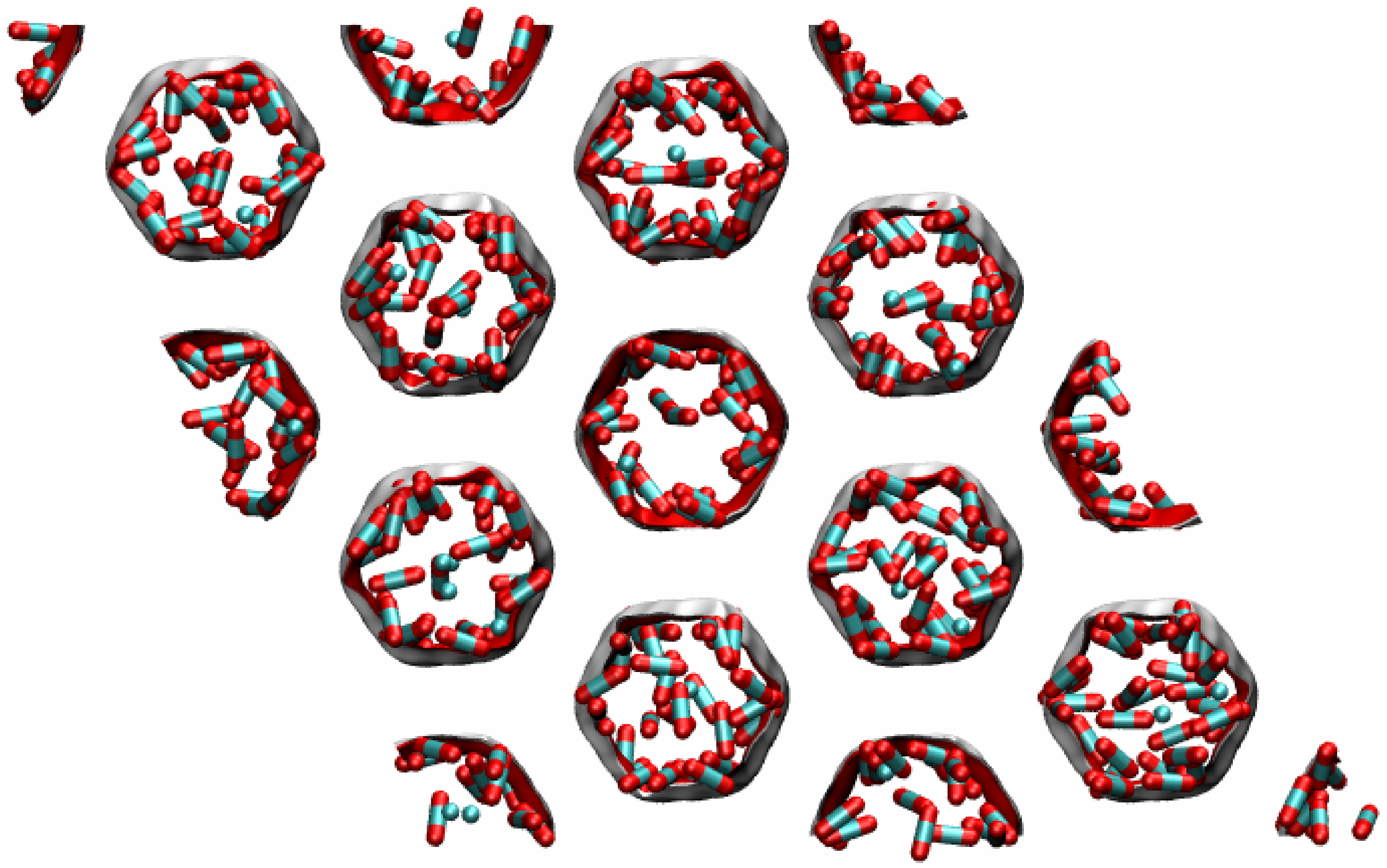

MgMOF-74 CBMC pentanes mixture simulation results

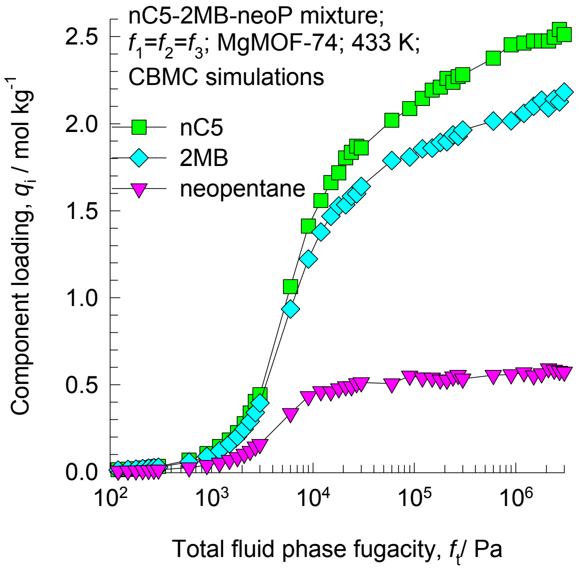

$$S_{ads} = \frac{\dfrac{q_{nC5}}{f_{nC5}} + \dfrac{q_{2MB}}{f_{2MB}}}{\dfrac{q_{neoP}}{f_{neoP}}}$$

Capacity is the total loading of nC5 + 2MB

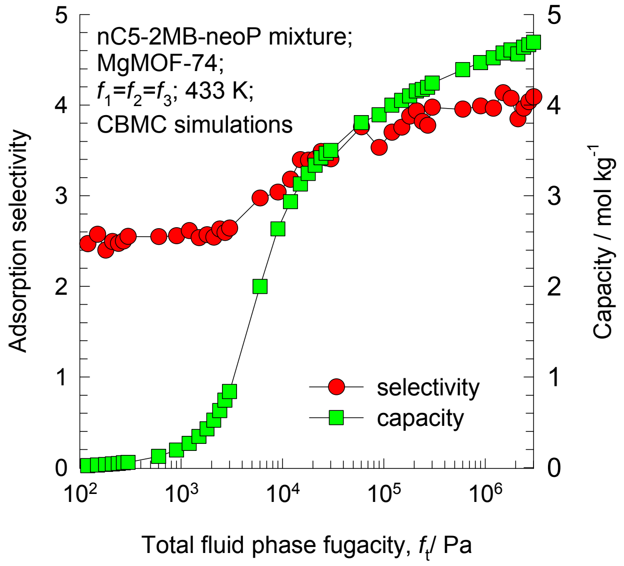

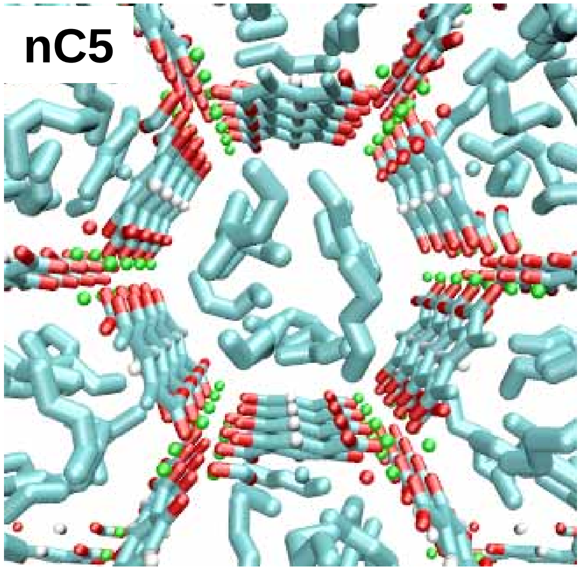

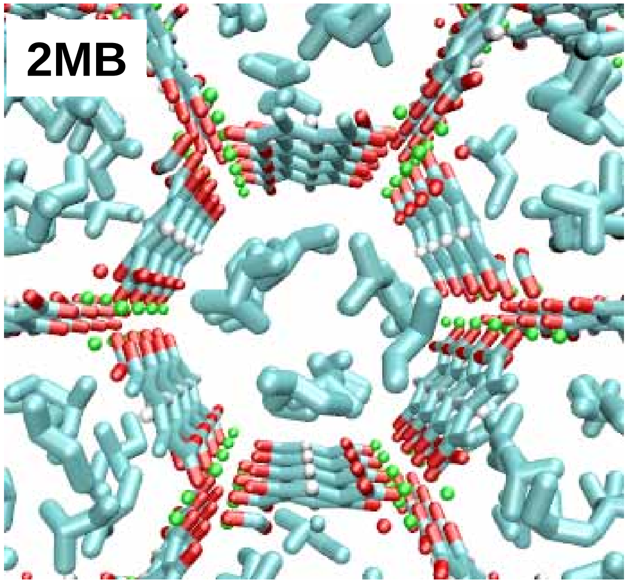

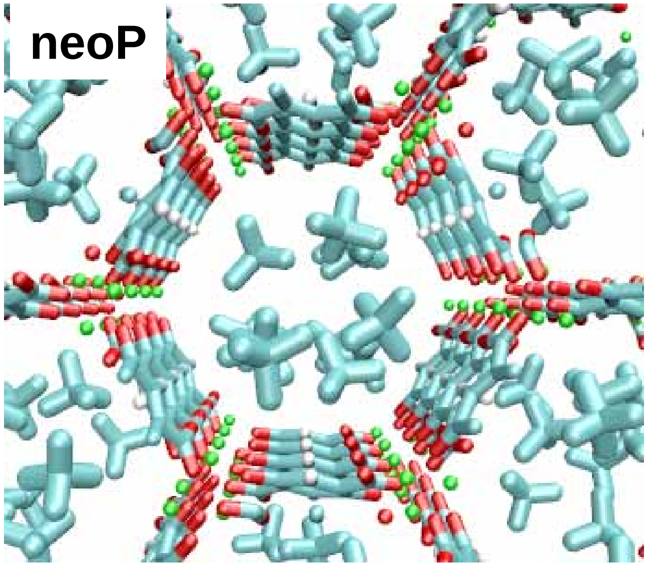

MgMOF-74 CBMC nC6/3MP/22DMB mixture simulations

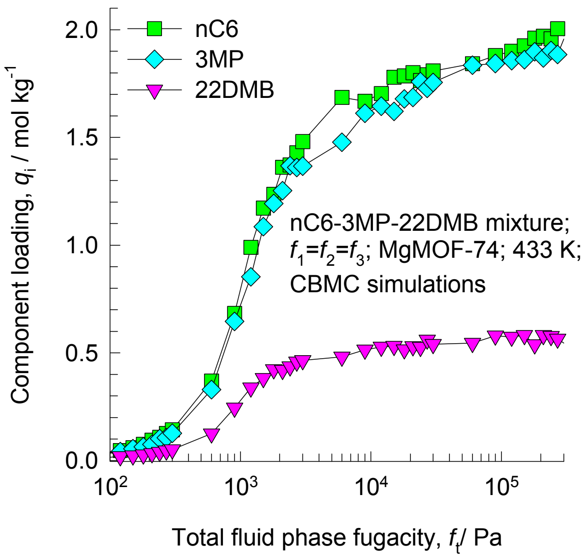

$$S_{ads} = \frac{\dfrac{q_{nC6}}{f_{nC6}} + \dfrac{q_{3MP}}{f_{3MP}}}{\dfrac{q_{22DMB}}{f_{22DMB}}}$$

Capacity is the total loading of nC6 + 3MP

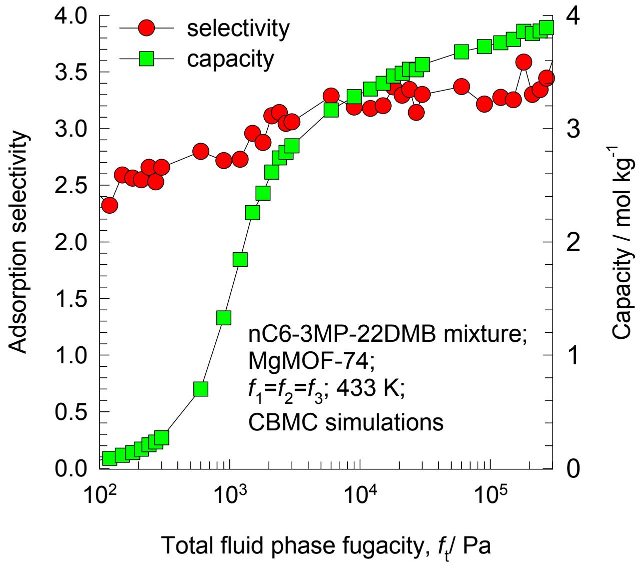

MgMOF-74 CBMC nC6/2MP/3MP/22DMB/23DMB simulations

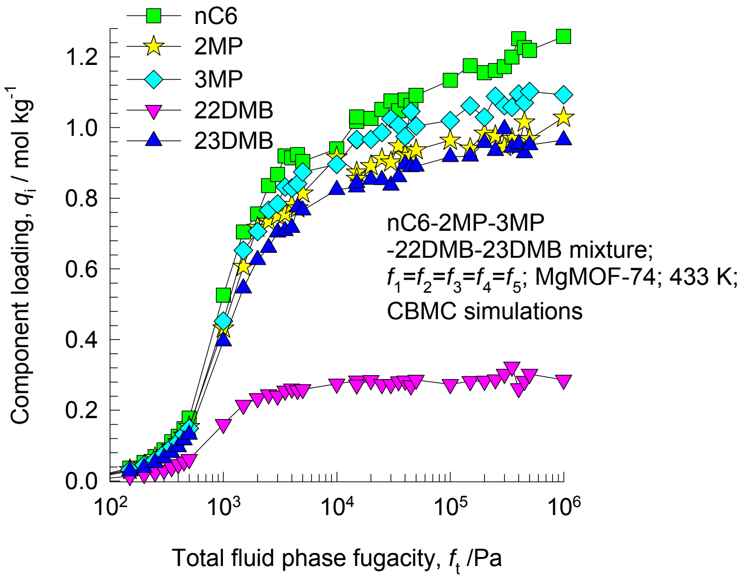

The 5-component mixture simulation shows that 22DMB can be separated from the rest of the mixture. But it is not possible to have clear separation of both the di-branched 22DMB and 23DMB from (linear + mono-branched)

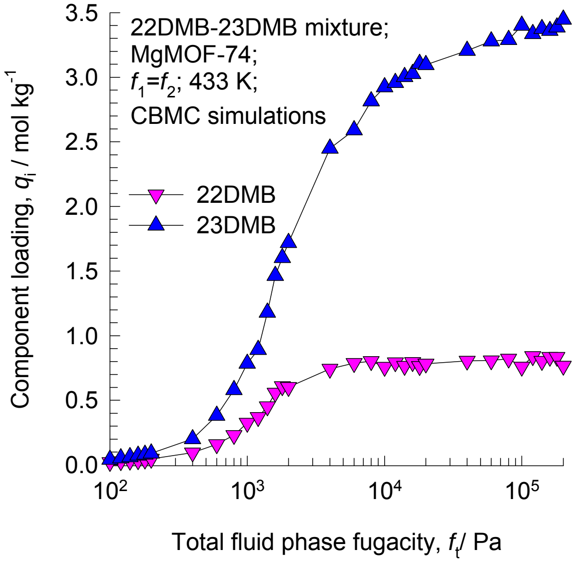

The 22DMB/23DMB binary mixture simulation demonstrates that the flatter 23DMB molecule has better interactions with the pore walls

MgMOF-74 snapshot of pure hexanes

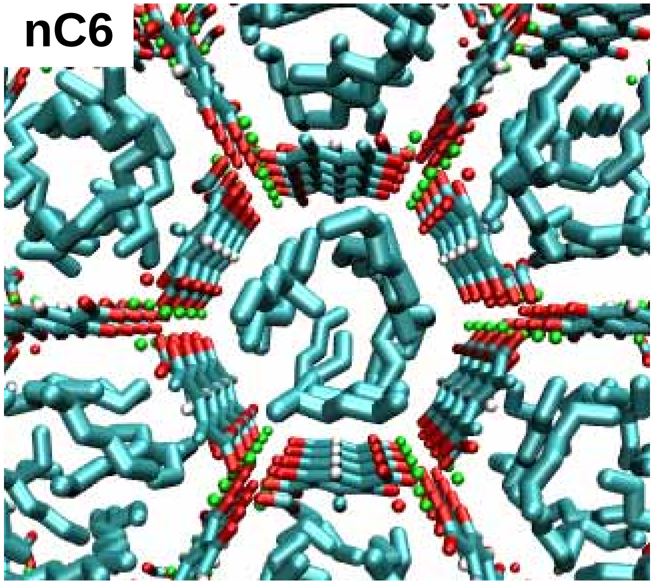

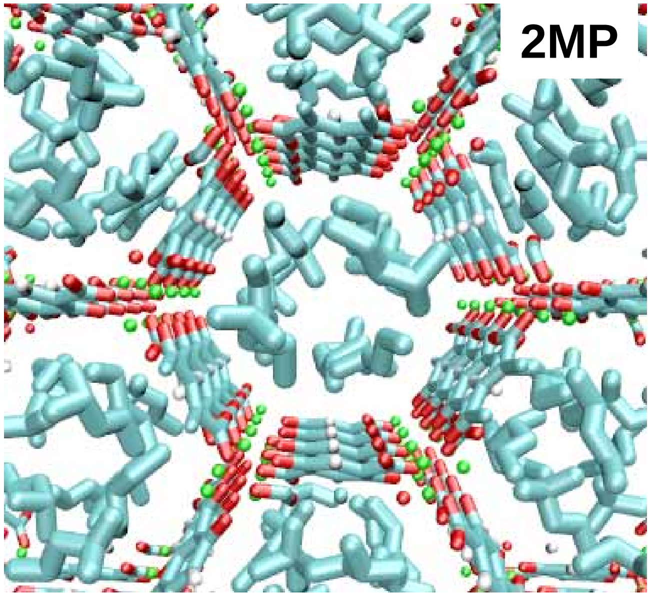

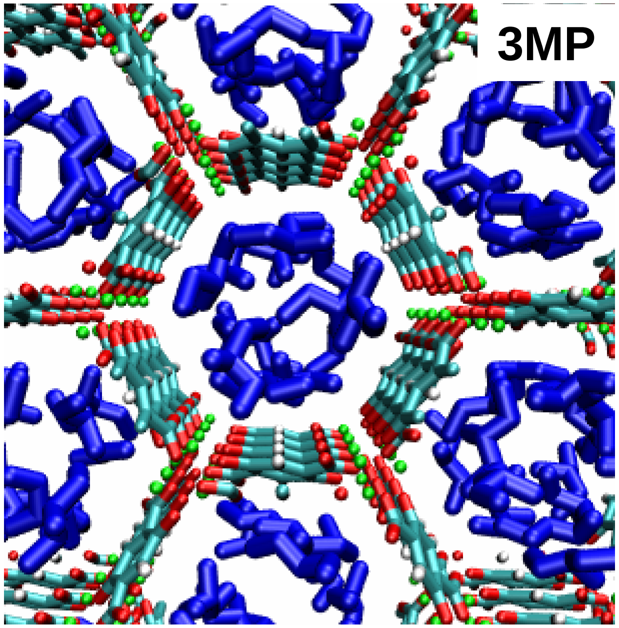

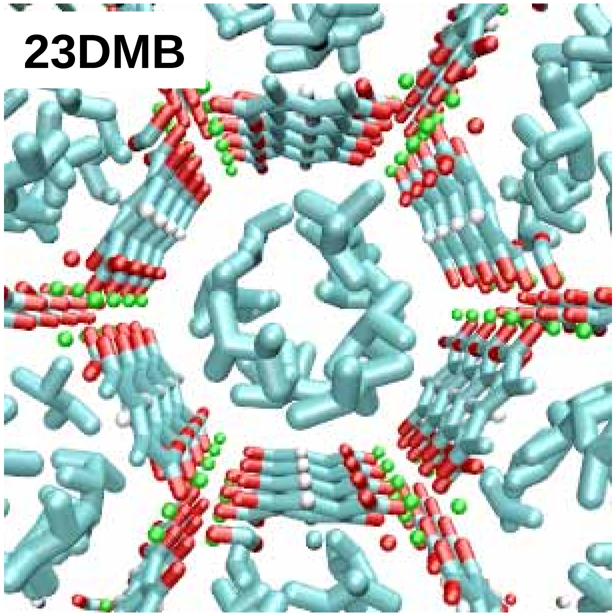

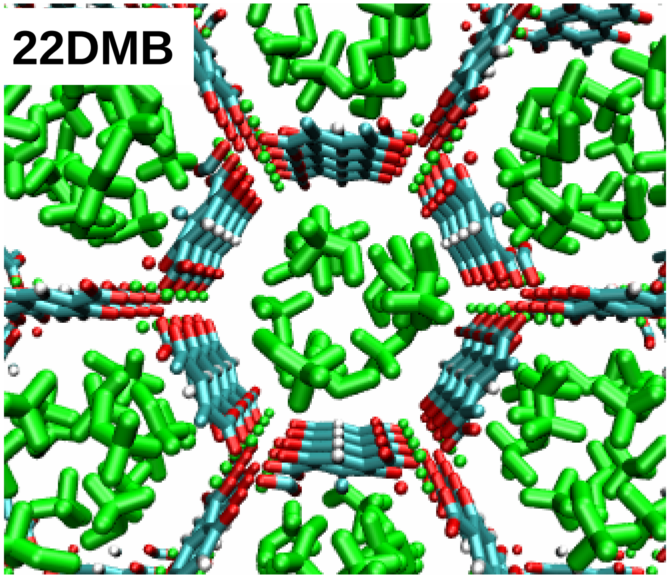

ZnMOF-74 pore landscapes

To convert from molecules per unit cell to mol kg^{-1}, multiply by 0.342.
The pore volume is 0.582 cm^{3}/g.

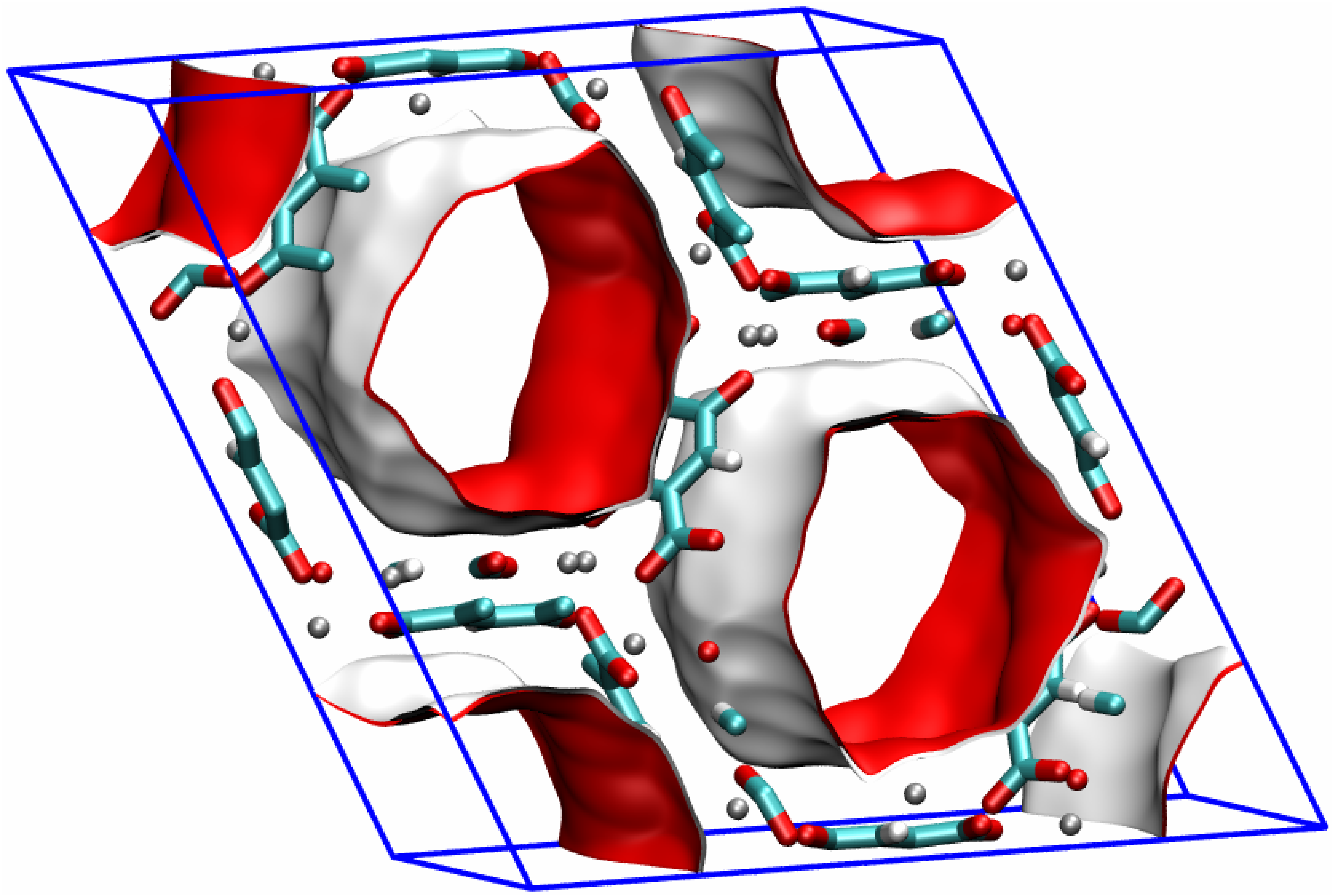

ZnMOF-74 snapshots

Snapshots of CO_2 and CH_4 at a total gas phase fugacity of 1 MPa.

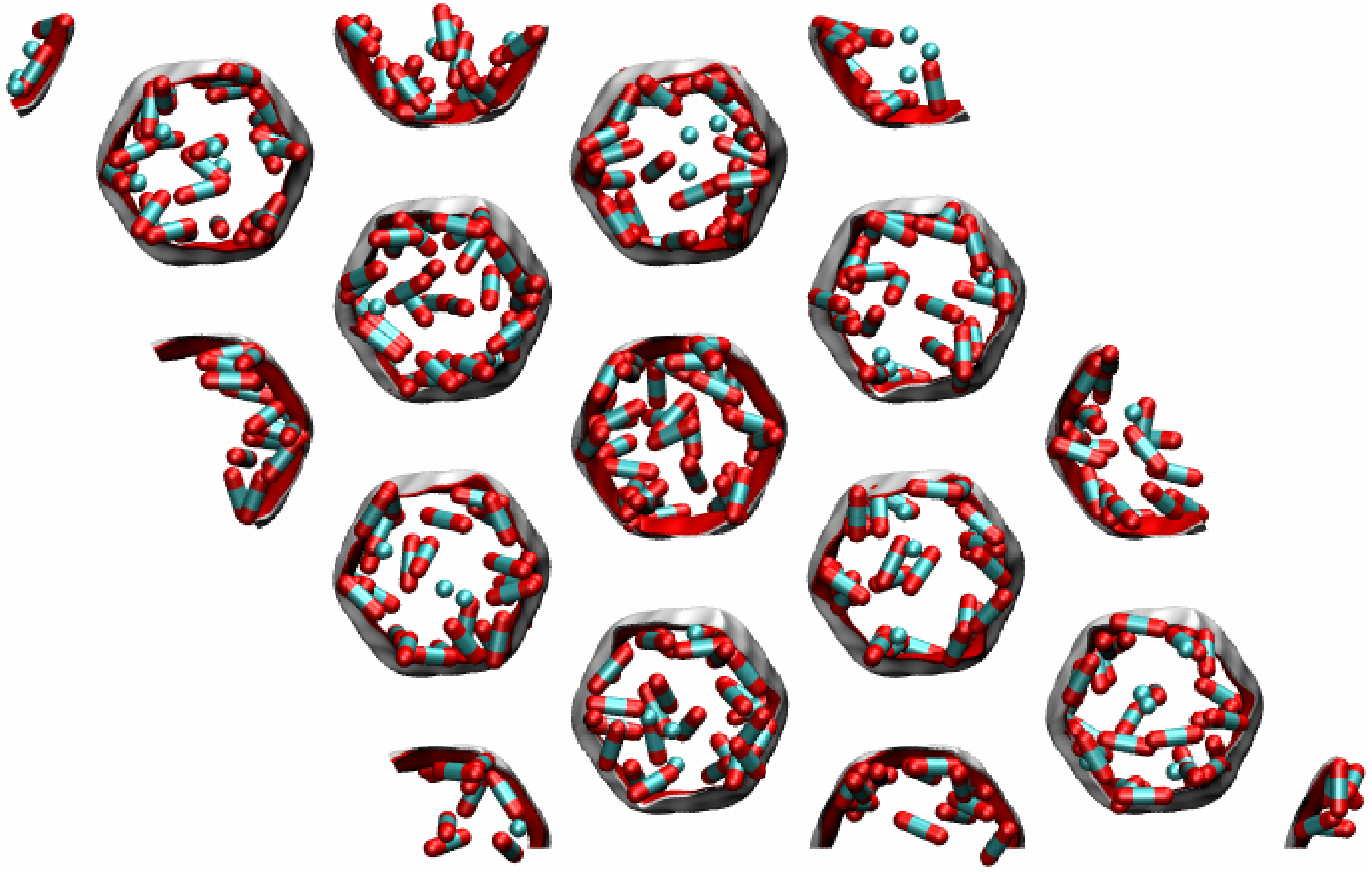

ZnMOF-74 CBMC mixture simulation results for CO_2 capture

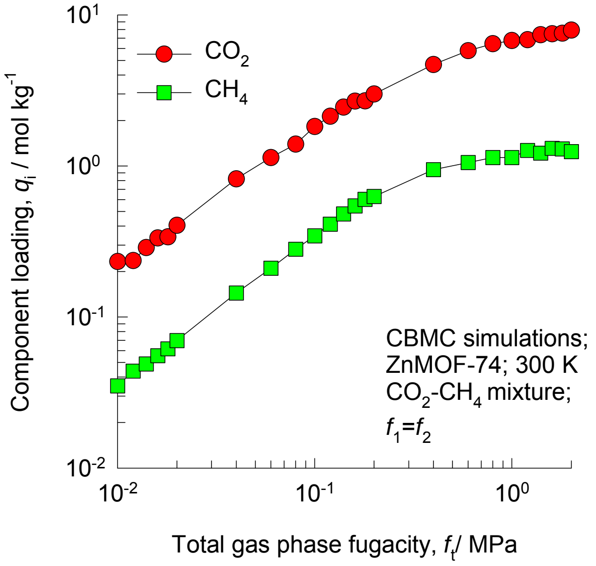

These simulation results are obtained using the force field information given in A.Ö. Yazaydın, R.Q. Snurr, T.H. Park, K. Koh, J. Liu, M.D. LeVan, A.I. Benin, P. Jakubczak, M. Lanuza, D.B. Galloway, J.J. Low, R.R. Willis, Screening of Metal-Organic Frameworks for Carbon Dioxide Capture from Flue Gas using a Combined Experimental and Modeling Approach, J. Am. Chem. Soc. 131 (2009) 18198-18199.

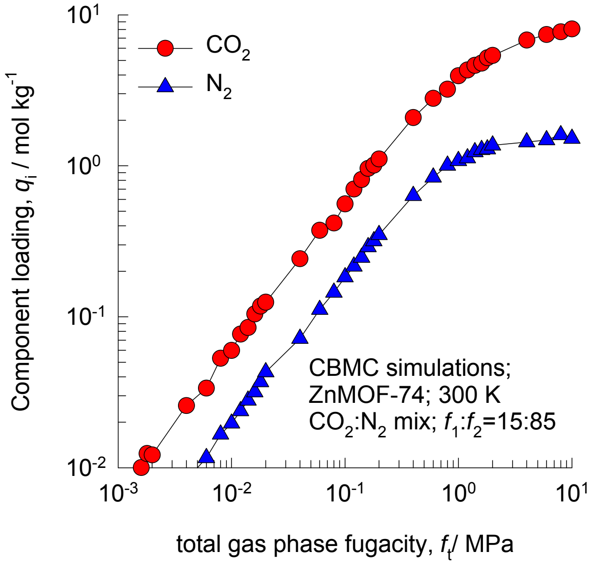

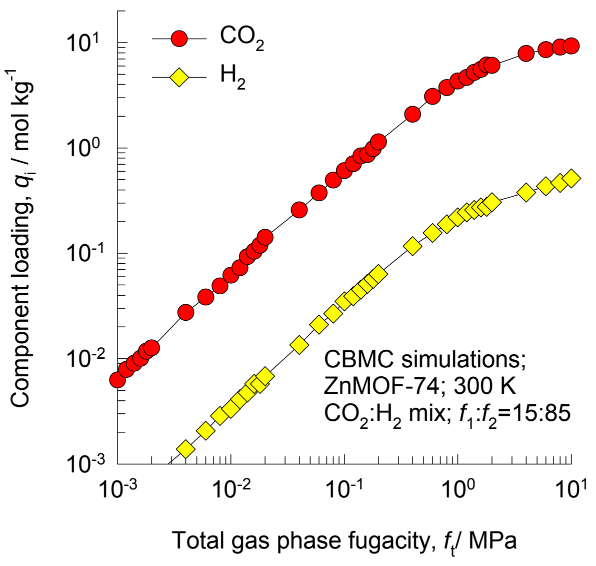

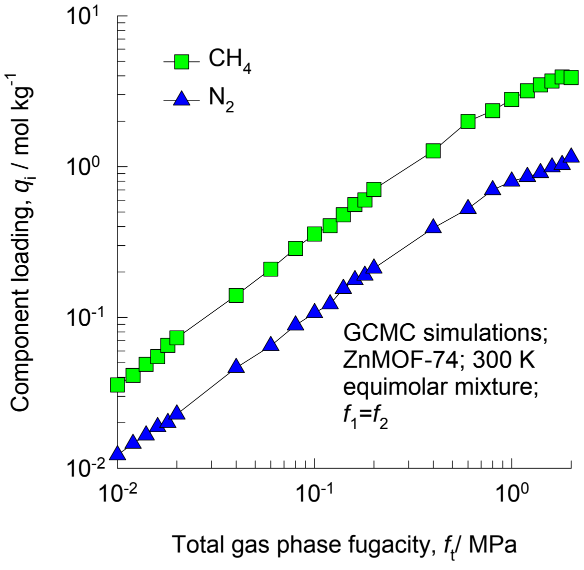

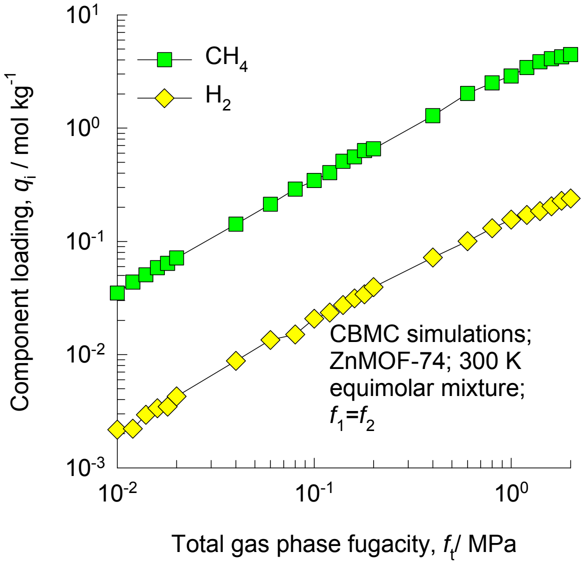

ZnMOF-74 CBMC pentanes mixture simulation results

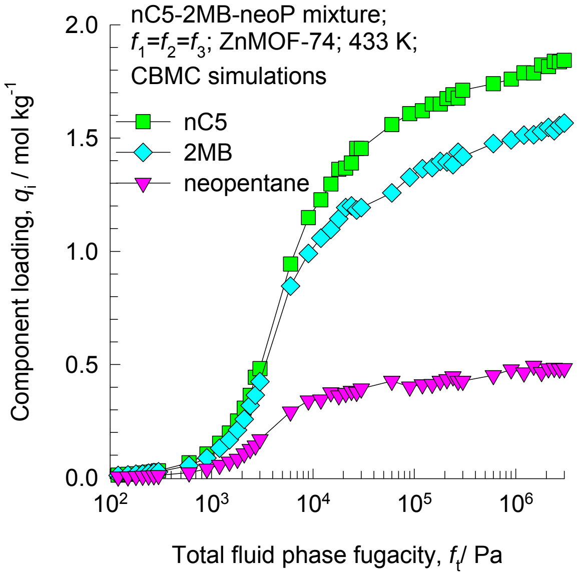

$$S_{ads} = \frac{\dfrac{q_{nC5}}{f_{nC5}} + \dfrac{q_{2MB}}{f_{2MB}}}{\dfrac{q_{neoP}}{f_{neoP}}}$$

Capacity is the total
loading of nC5 + 2MB

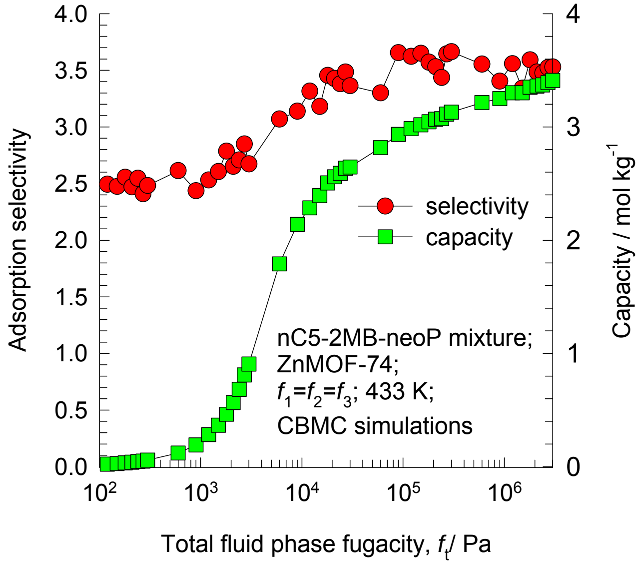

ZnMOF-74 CBMC nC6/3MP/22DMB mixture simulations

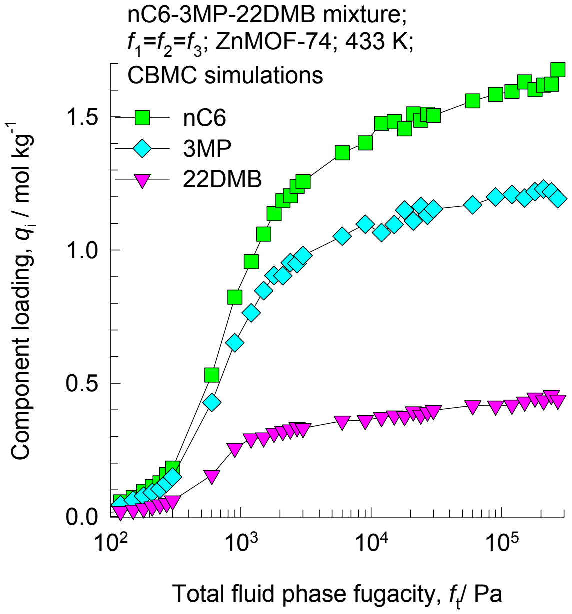

$$S_{ads} = \frac{\dfrac{q_{nC6}}{f_{nC6}} + \dfrac{q_{3MP}}{f_{3MP}}}{\dfrac{q_{22DMB}}{f_{22DMB}}}$$

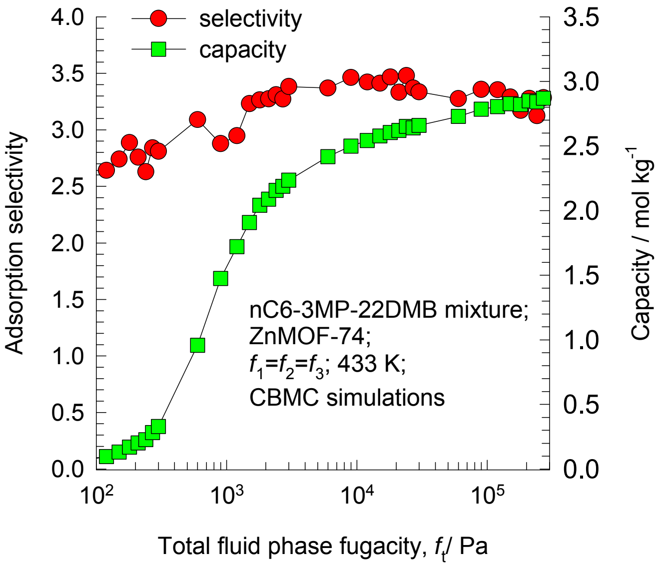

Capacity is the total
loading of nC6 + 3MP

ZnMOF-74 CBMC nC6/2MP/3MP/22DMB/23DMB simulations

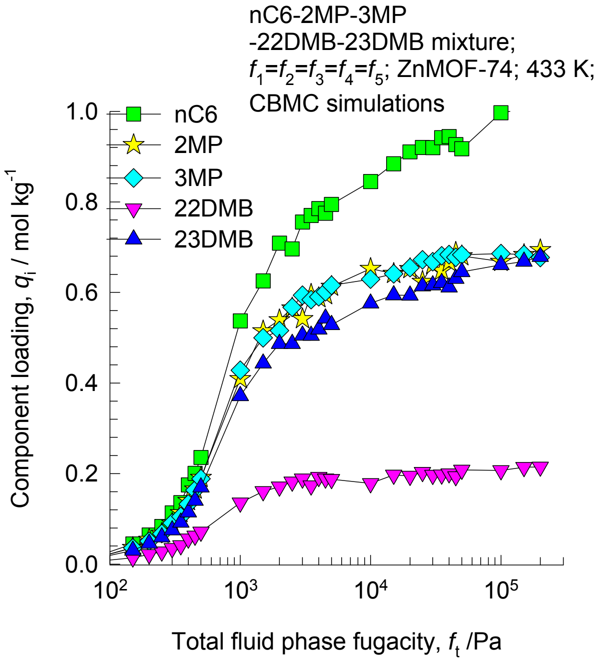

The 5-component mixture simulation shows that 22DMB can be separated from the rest of the mixture. But it is not possible to have clear separation of both the di-branched 22DMB and 23DMB from (linear + mono-branched)

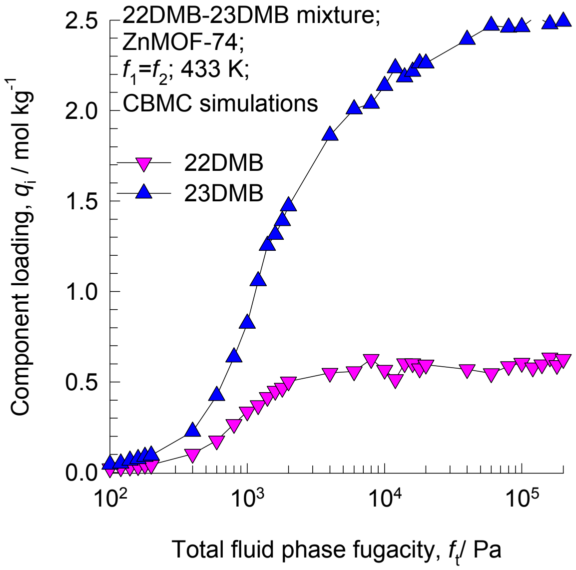

The 22DMB/23DMB binary mixture simulation demonstrates that the flatter 23DMB molecule has better interactions with the pore walls

ZnMOF-74 snapshot of pure hexanes

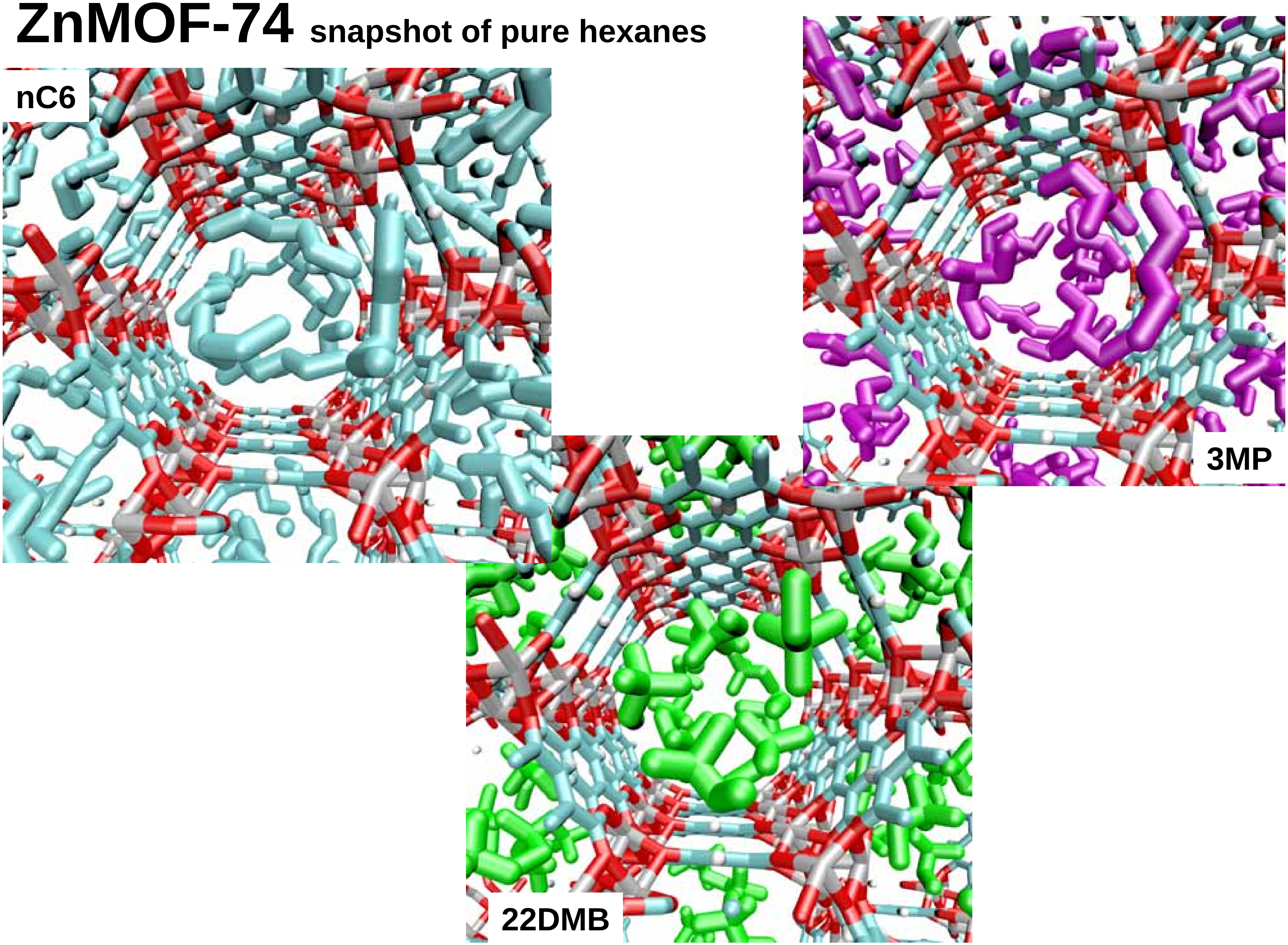

CoMOF-74 pore landscapes

To convert from molecules per unit cell to mol kg^{-1}, multiply by 0.356264

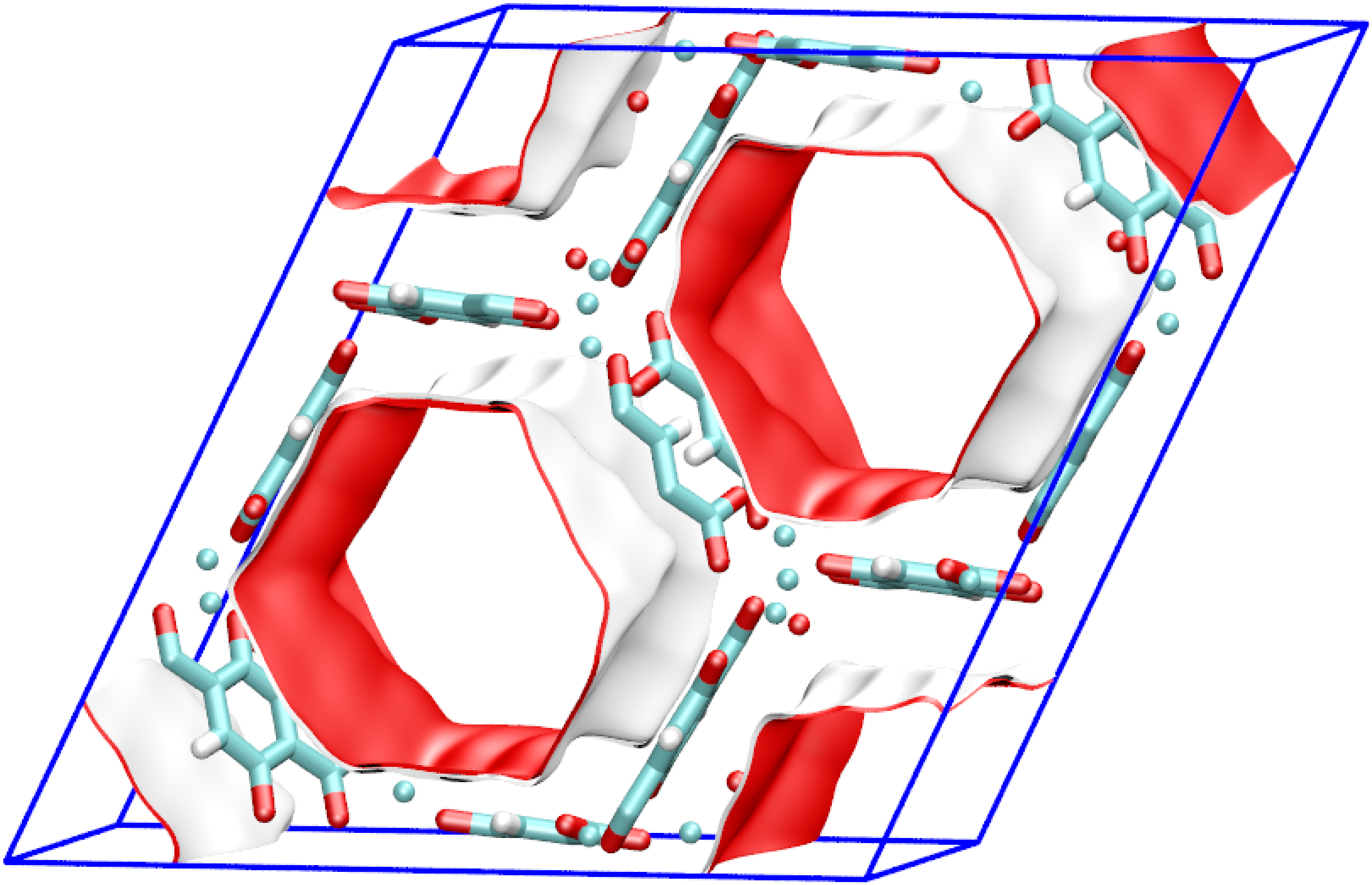

CoMOF-74 CBMC mixture simulation results for CH_4/H_2 separation

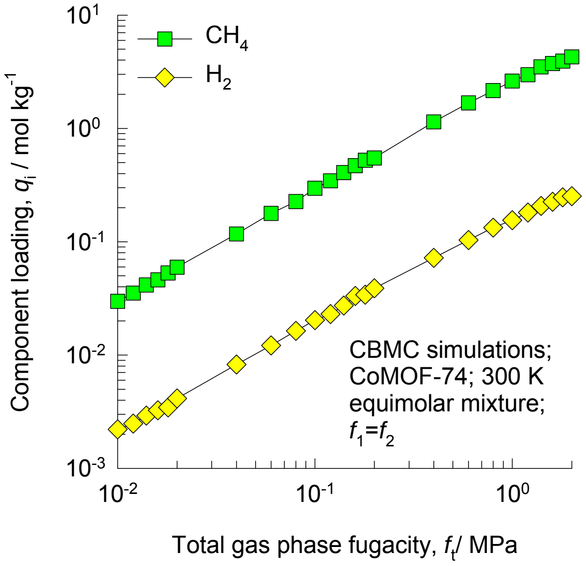

These simulation results are obtained using the force field information given in A.Ö. Yazaydın, R.Q. Snurr, T.H. Park, K. Koh, J. Liu, M.D. LeVan, A.I. Benin, P. Jakubczak, M. Lanuza, D.B. Galloway, J.J. Low, R.R. Willis, Screening of Metal-Organic Frameworks for Carbon Dioxide Capture from Flue Gas using a Combined Experimental and Modeling Approach, J. Am. Chem. Soc. 131 (2009) 18198-18199.

NiMOF-74 pore landscapes

To convert from molecules per unit cell to mol kg^{-1}, multiply by 0.356813

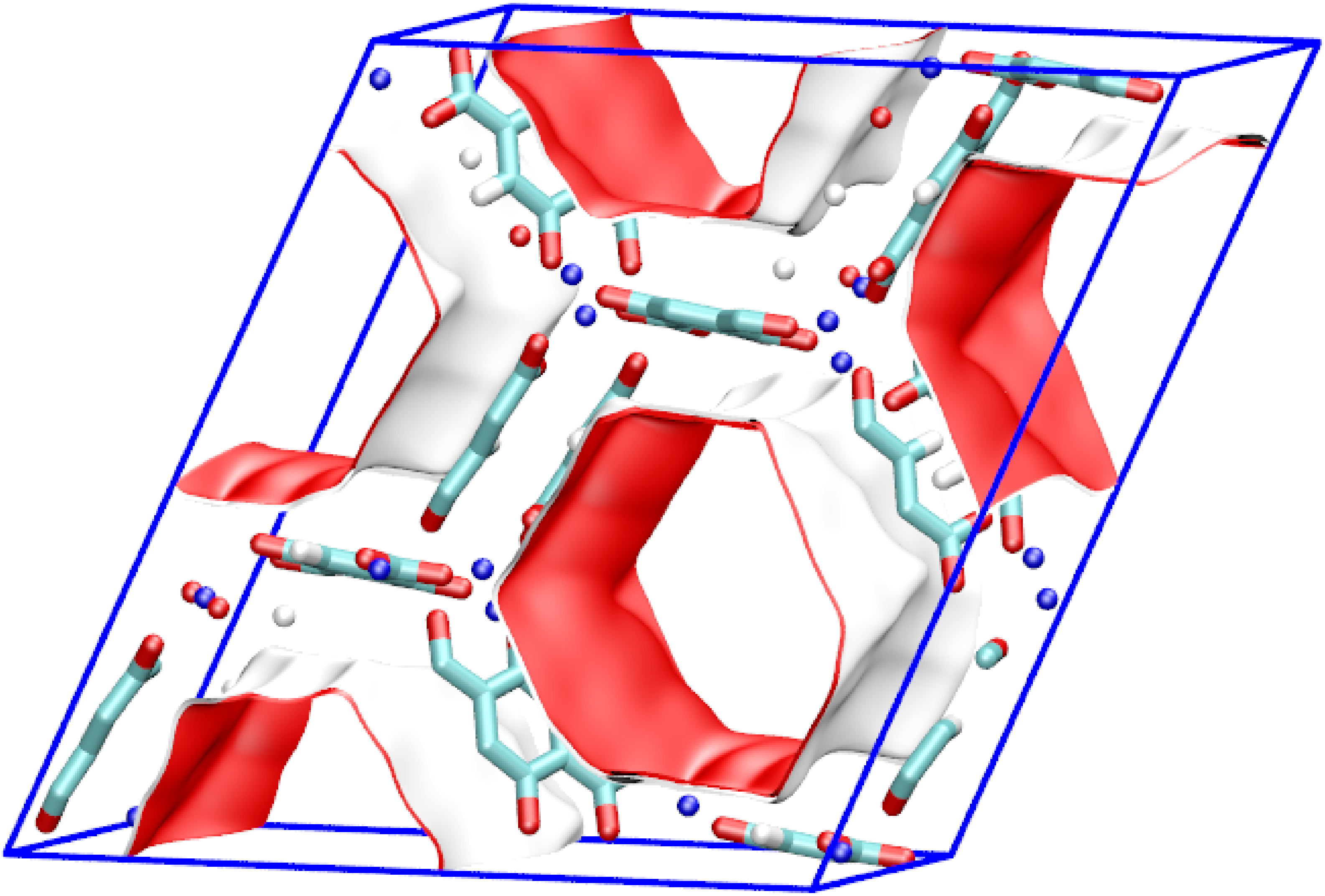

NiMOF-74 CBMC mixture simulation results for CH_4/H_2 separation

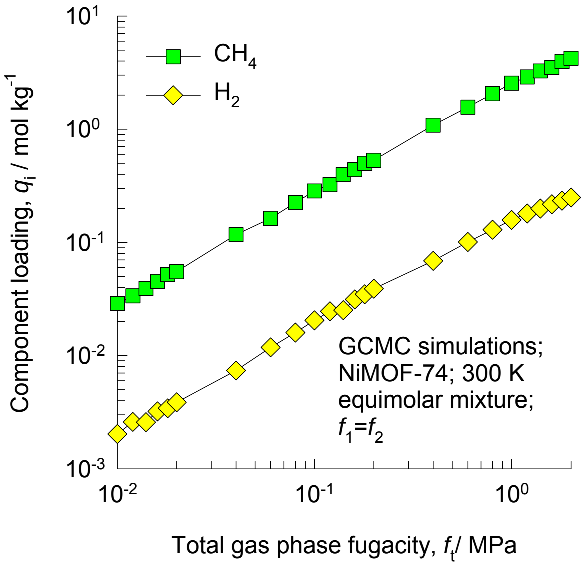

These simulation results are obtained using the force field information given in A.Ö. Yazaydın, R.Q. Snurr, T.H. Park, K. Koh, J. Liu, M.D. LeVan, A.I. Benin, P. Jakubczak, M. Lanuza, D.B. Galloway, J.J. Low, R.R. Willis, Screening of Metal-Organic Frameworks for Carbon Dioxide Capture from Flue Gas using a Combined Experimental and Modeling Approach, J. Am. Chem. Soc. 131 (2009) 18198-18199.

MOF-177 pore landscape

To convert from molecules per unit cell to mol kg^{-1}, multiply by 0.1089.
The pore volume is 1.968 cm^3/g.

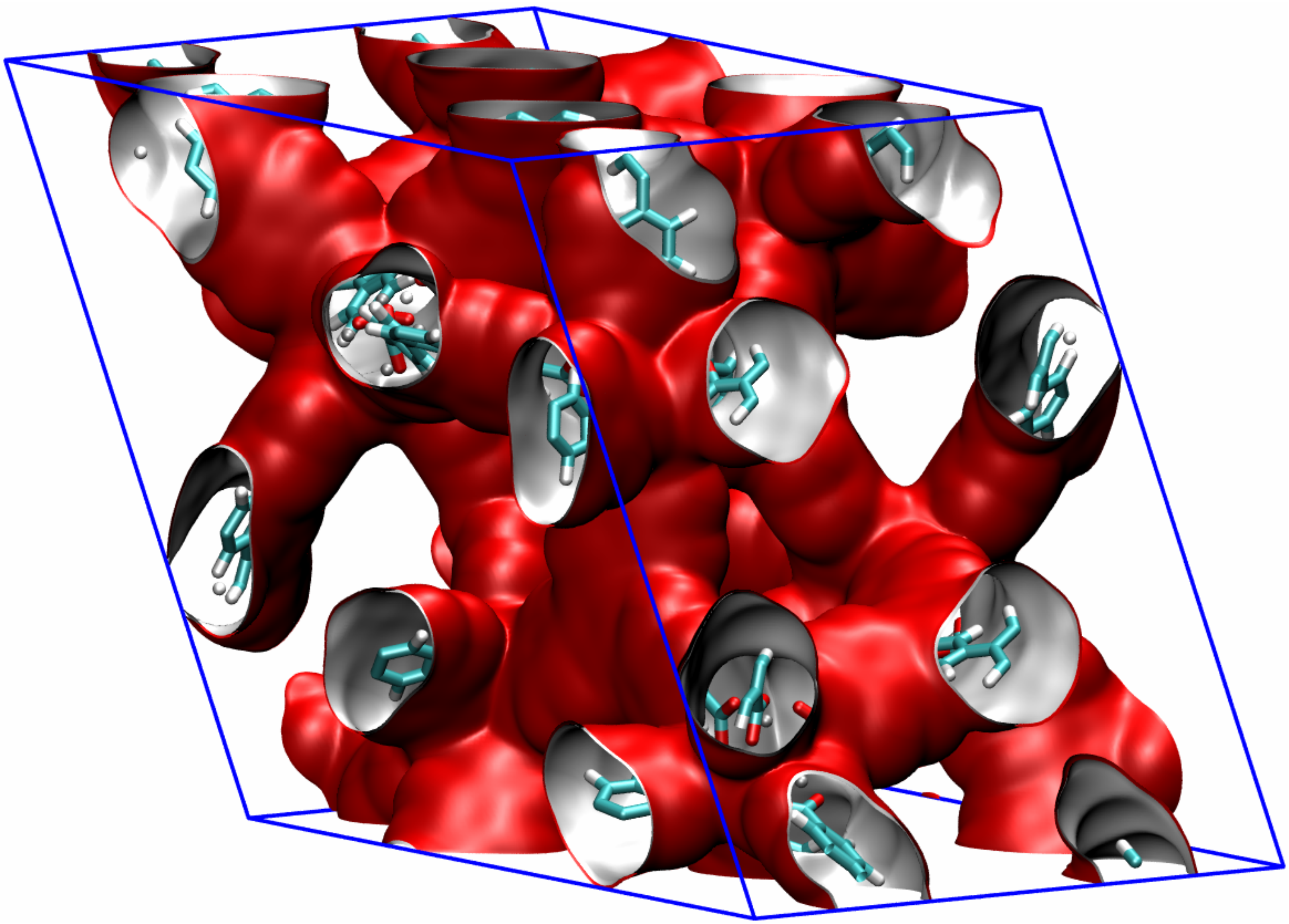

MOF-177 Pure component isotherms: CBMC vs Expt

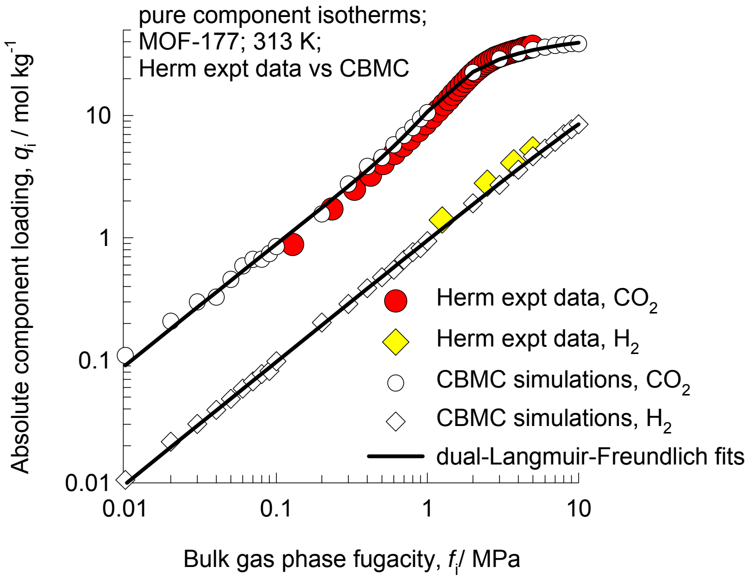

The experimental data for CO_2, and H_2 are from Z.R. Herm, J.A. Swisher, B. Smit, R. Krishna, J.R. Long, Metal-Organic Frameworks as Adsorbents for Hydrogen Purification and Pre-Combustion Carbon Dioxide Capture, J. Am. Chem. Soc. XXX (2011) XXX-XXX. (http://dx.doi.org/10.1021/ja111411q)

MOF-177 CBMC mixture simulations

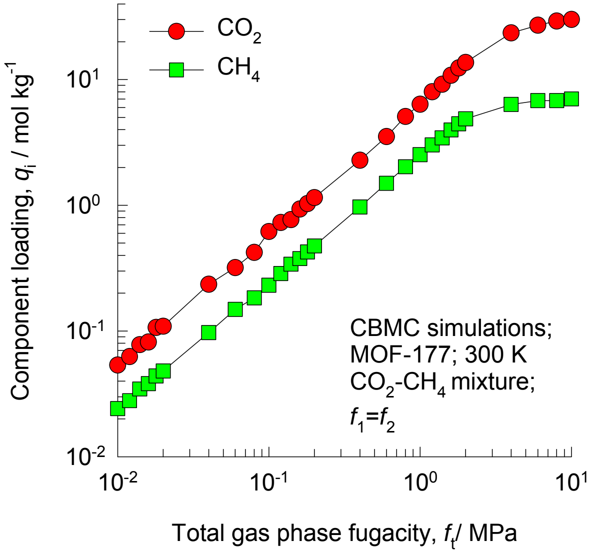

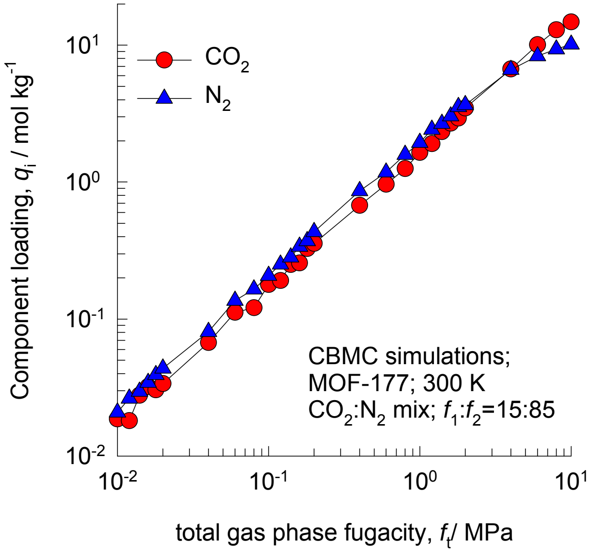

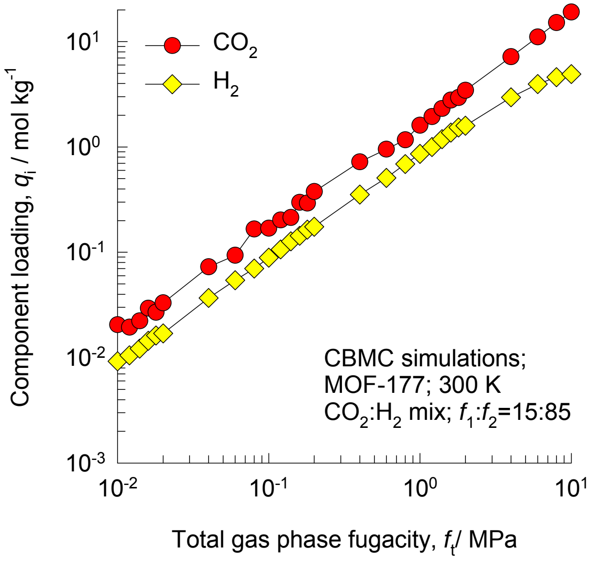

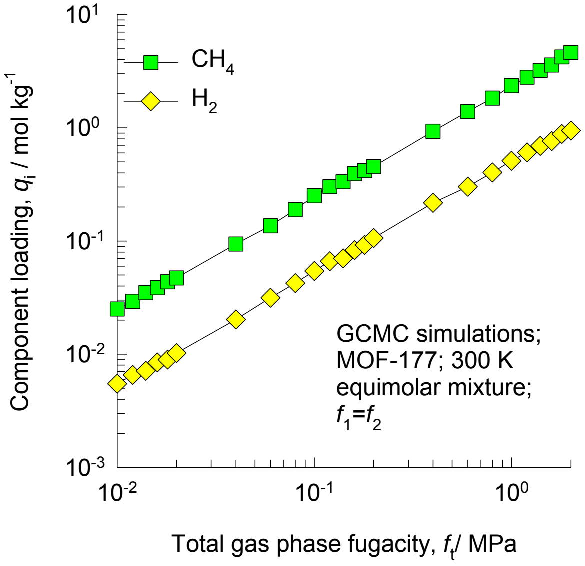

MOF-177 CBMC pentanes mixture simulations

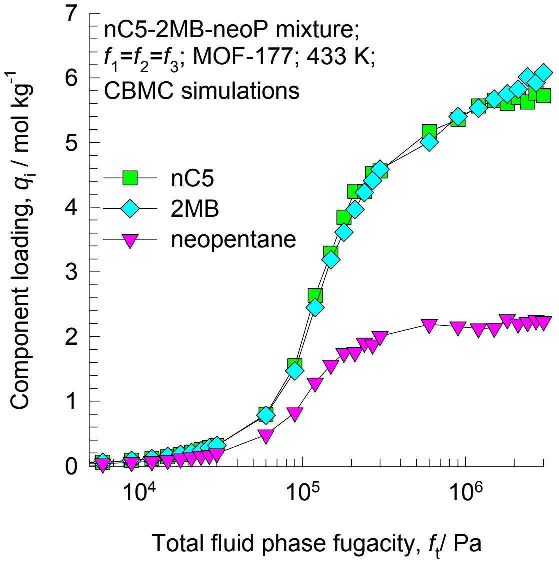

$$S_{ads} = \frac{\dfrac{q_{nC5}}{f_{nC5}} + \dfrac{q_{2MB}}{f_{2MB}}}{\dfrac{q_{neoP}}{f_{neoP}}}$$

Capacity is the total loading of nC5 + 2MB

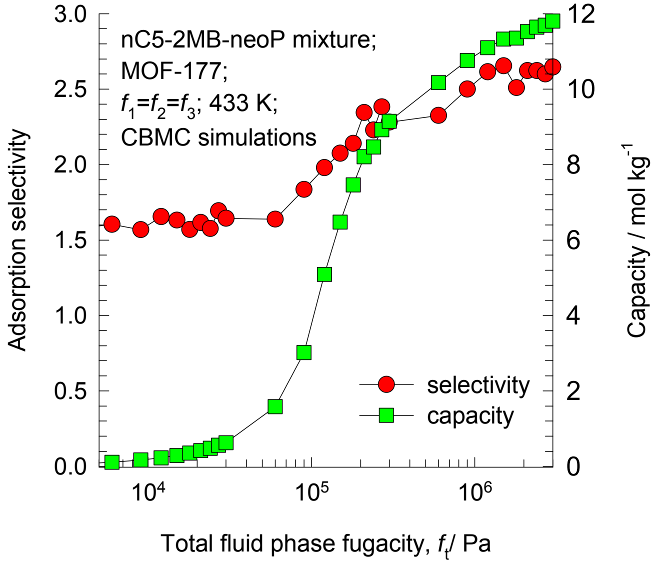

MOF-177 CBMC nC6/3MP/22DMB mixture simulations

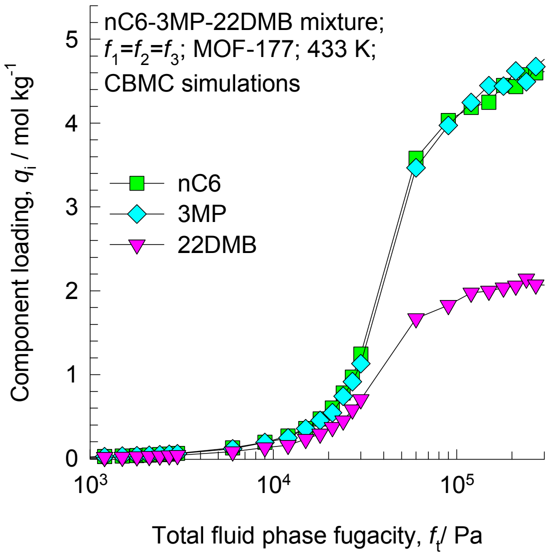

$$S_{ads} = \frac{\dfrac{q_{nC6}}{f_{nC6}} + \dfrac{q_{3MP}}{f_{3MP}}}{\dfrac{q_{22DMB}}{f_{22DMB}}}$$

Capacity is the total loading of nC6 + 3MP

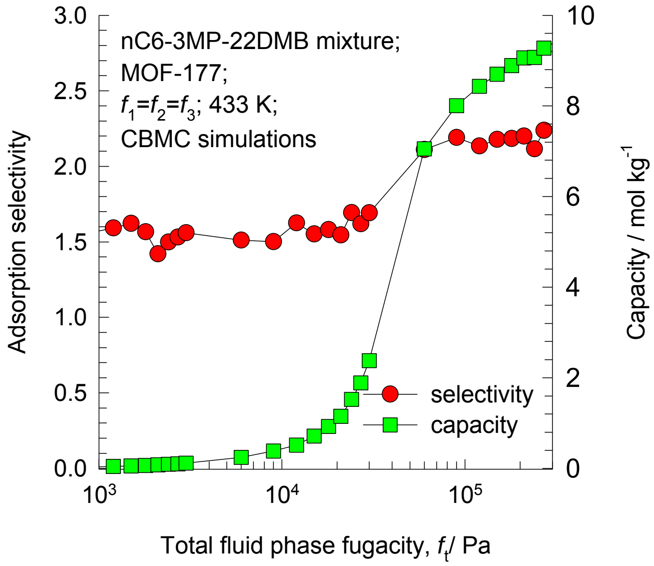

MOF-177 CBMC nC6/2MP/3MP/22DMB/23DMB simulations

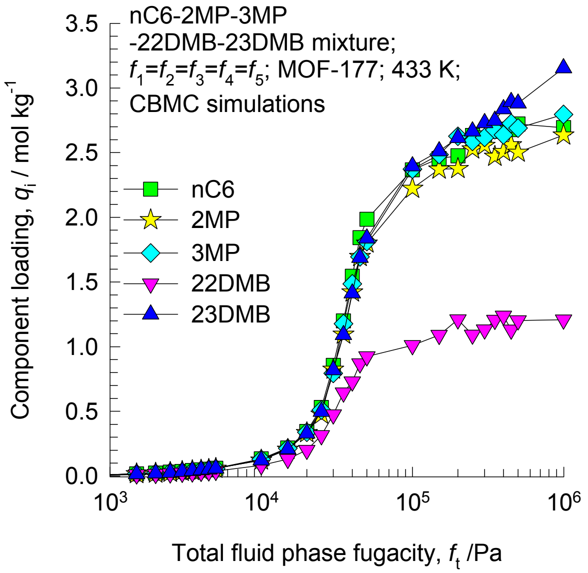

The 5-component mixture simulation shows that 22DMB can be separated from the rest of the mixture. But it is not possible to have clear separation of both the di-branched 22DMB and 23DMB from (linear + mono-branched)

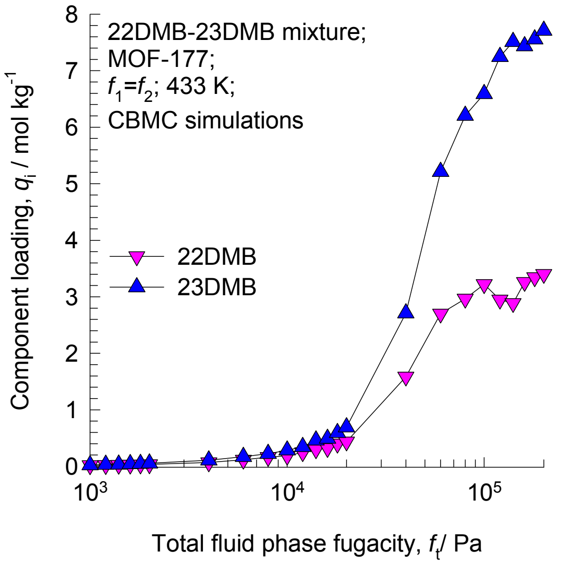

The 22DMB/23DMB binary mixture simulation demonstrates that the flatter 23DMB molecule has better interactions with the pore walls

MOF-177 snapshots of nC66/3MP/22DMB hexane isomers

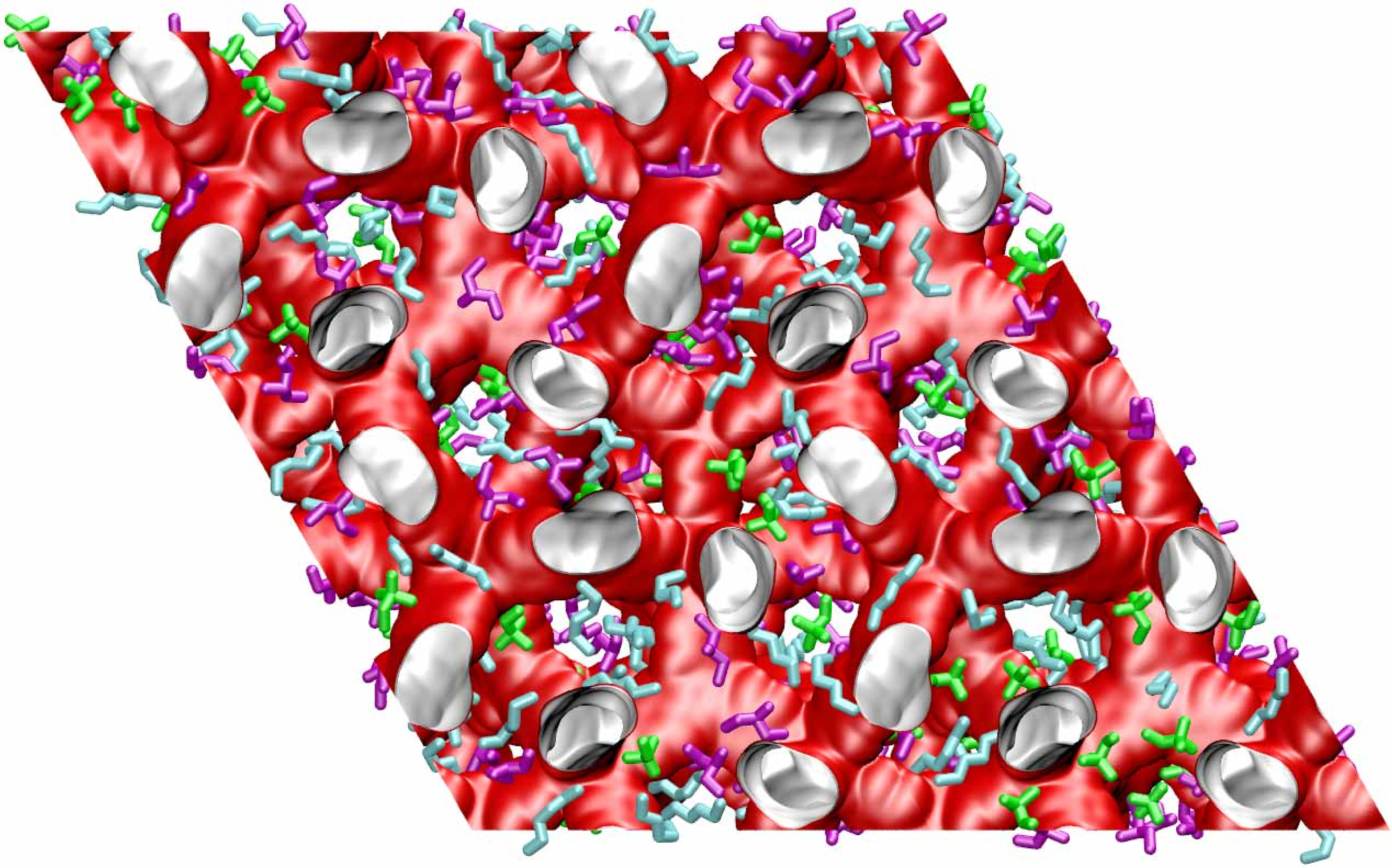

Na-rho-ZMOF pore landscapes

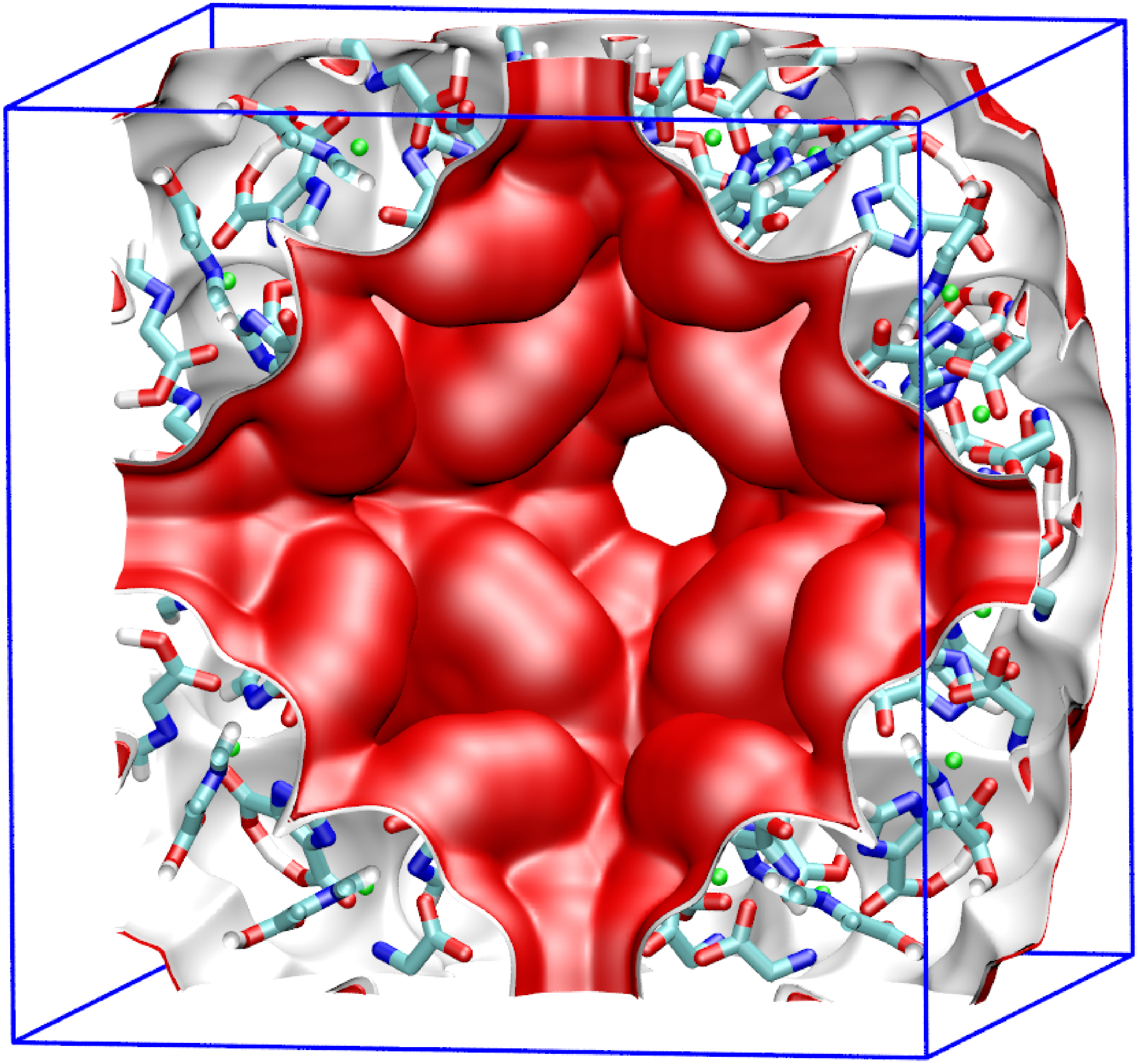

Na-rho-ZMOF pore landscapes

To convert from molecules per unit cell to mol kg^{-1}, multiply by 0.0467.
The pore volume is 0.427 cm^3/g.

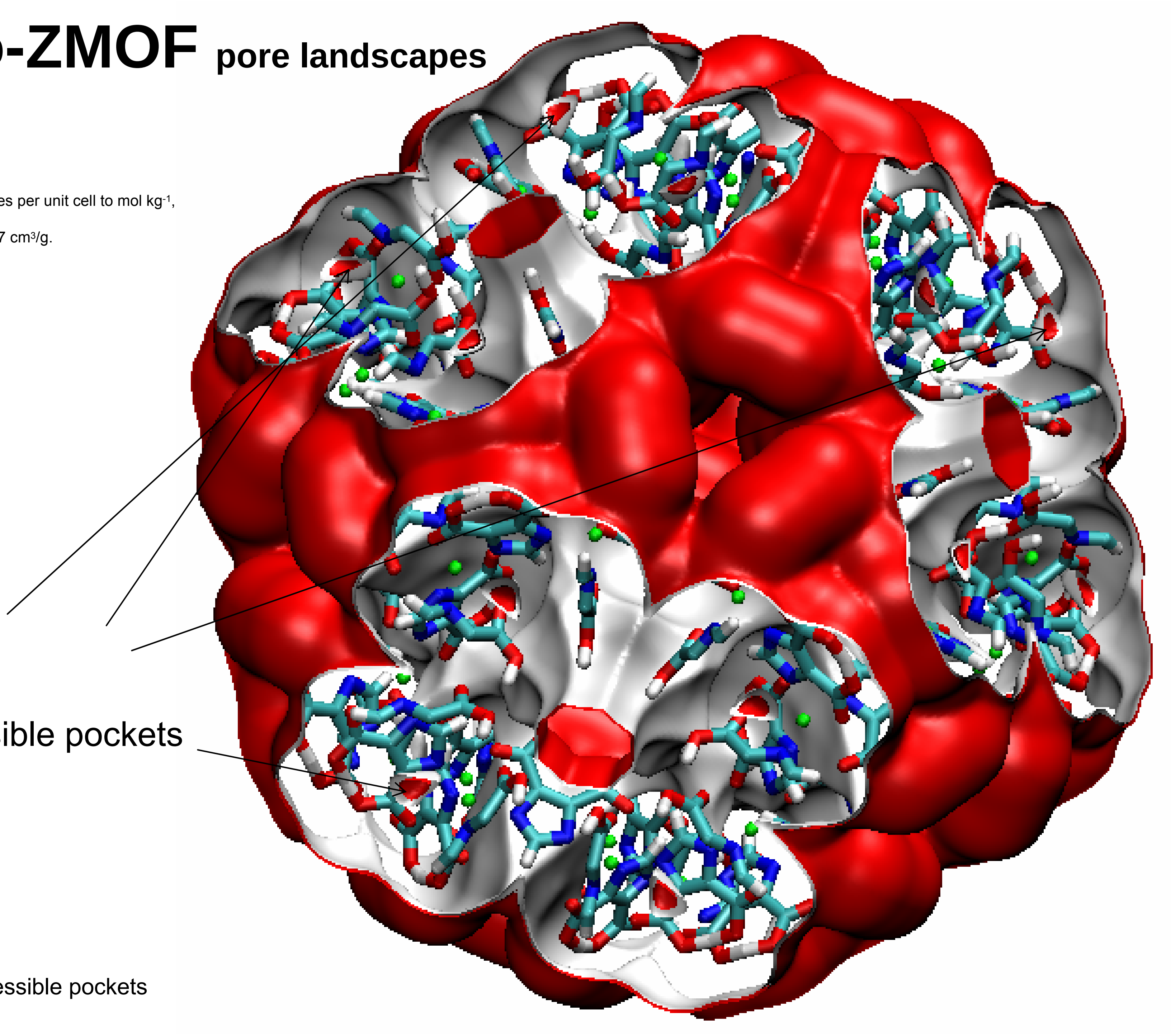

These show inaccessible pockets exist.

Na-rho-ZMOF

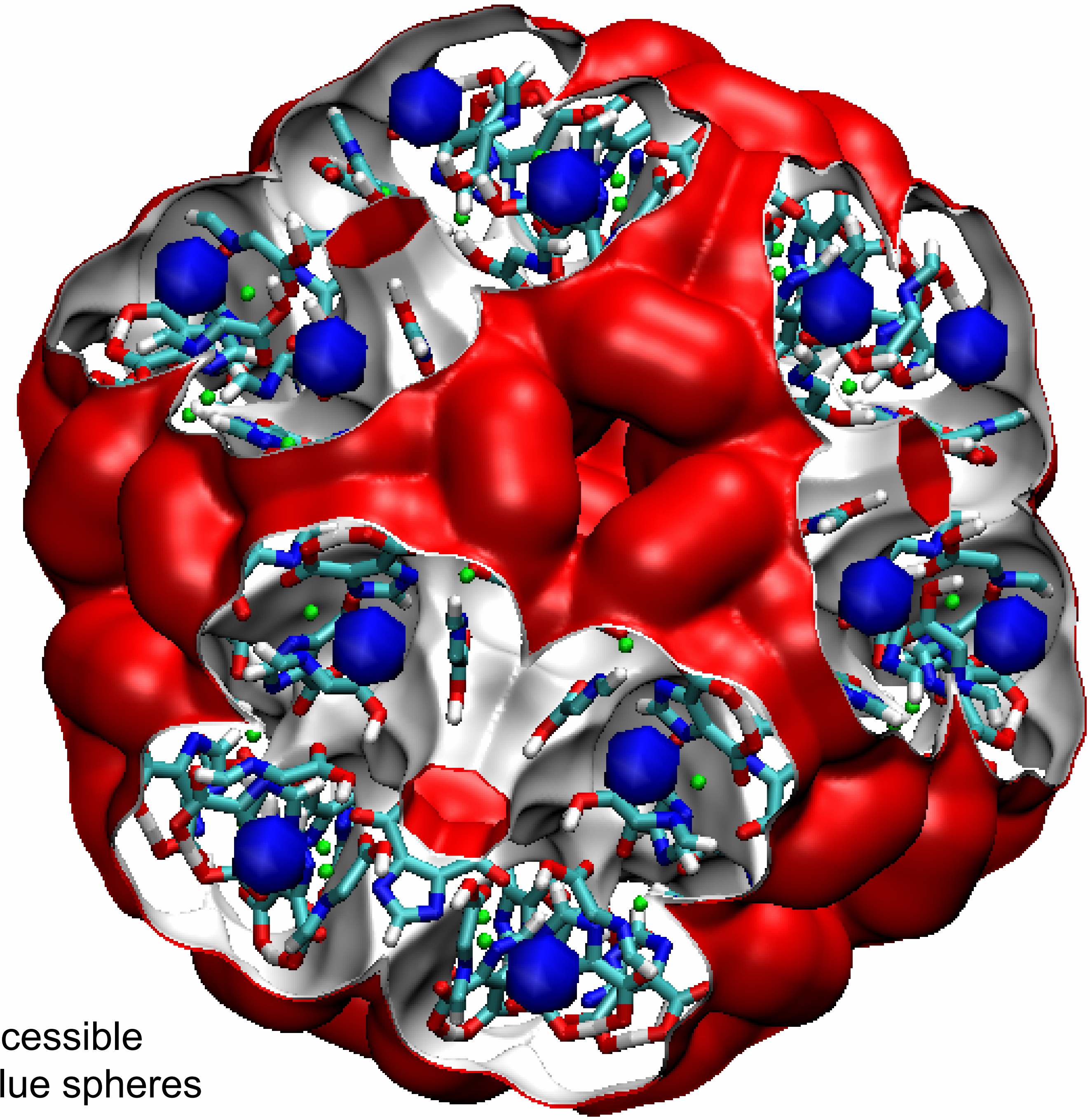

In our simulations the inaccessible pockets indicated by the blue spheres were blocked.

Na-rho-ZMOF CBMC mixture simulations for CO_2 capture

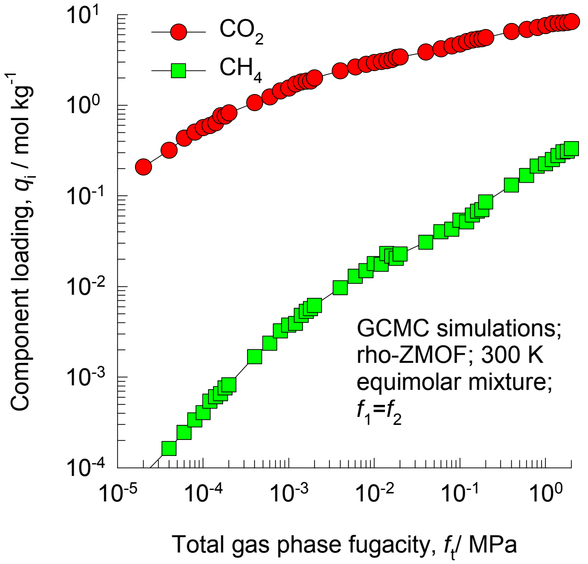

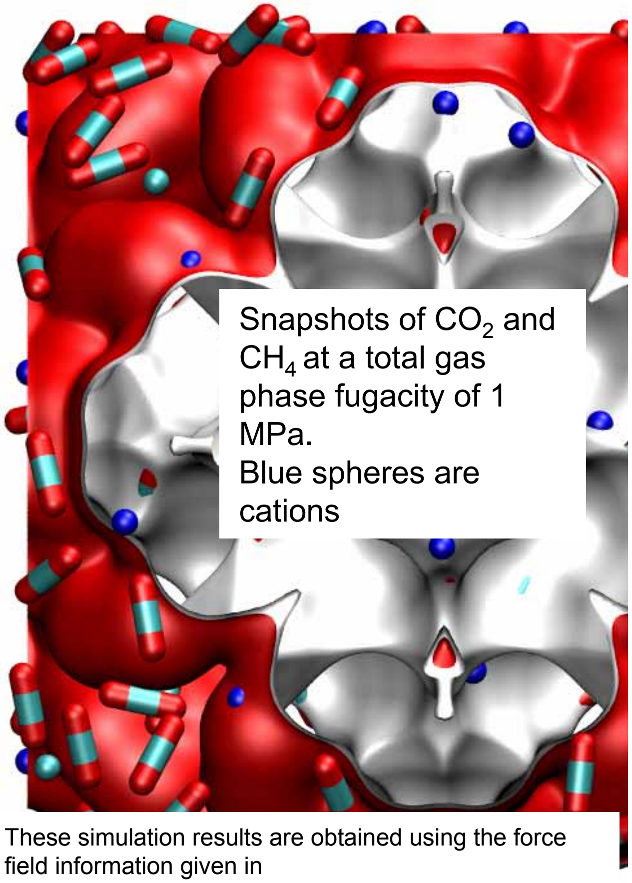

Snapshots of CO_2 and CH_4 at a total gas phase fugacity of 1 MPa.
Blue spheres are cations

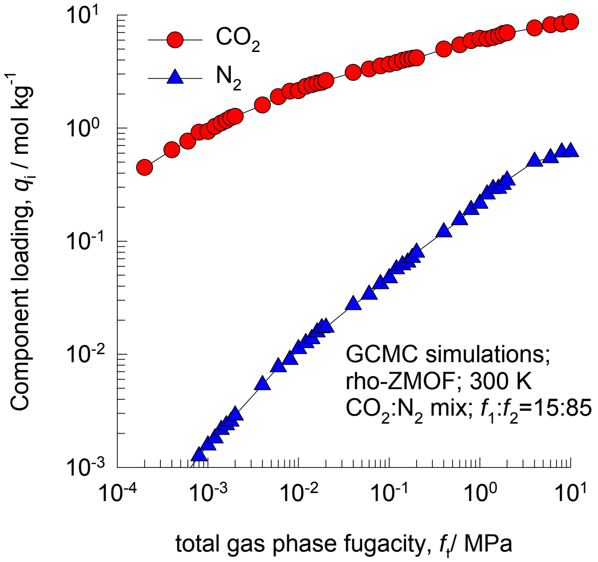

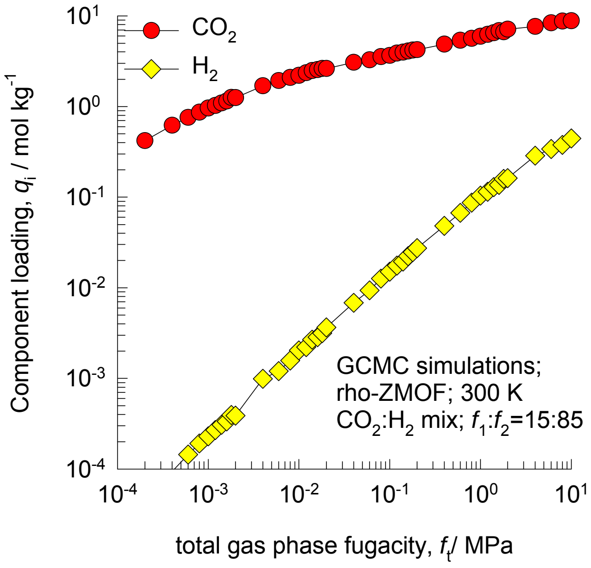

These simulation results are obtained using the force field information given in
R. Babarao, J. Jiang, Unprecedentedly High Selective Adsorption of Gas Mixtures in rho Zeolite-like Metal-Organic Framework: A Molecular Simulation Study, J. Am. Chem. Soc. 131 (2009) 11417-11425.

It must be noted that in the simulations of Babarao and Jiang the inaccessible pockets were neither detected nor blocked. Our simulation results are slightly different from theirs.

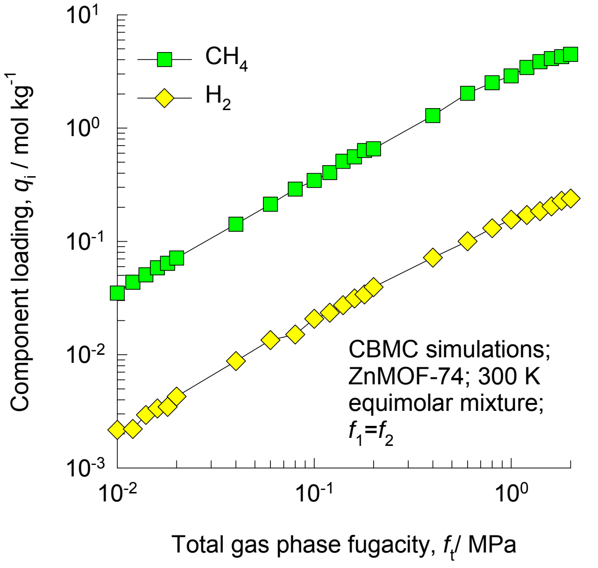

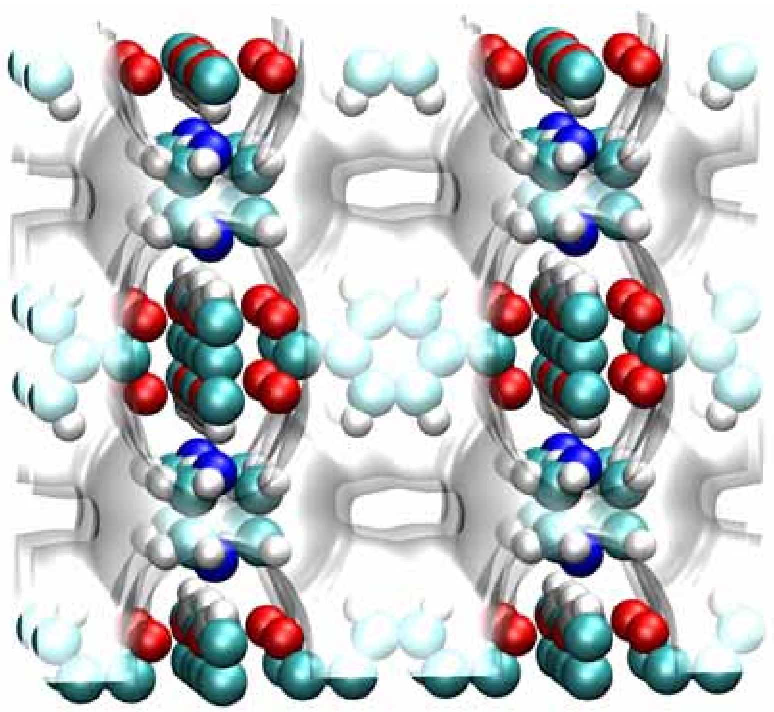

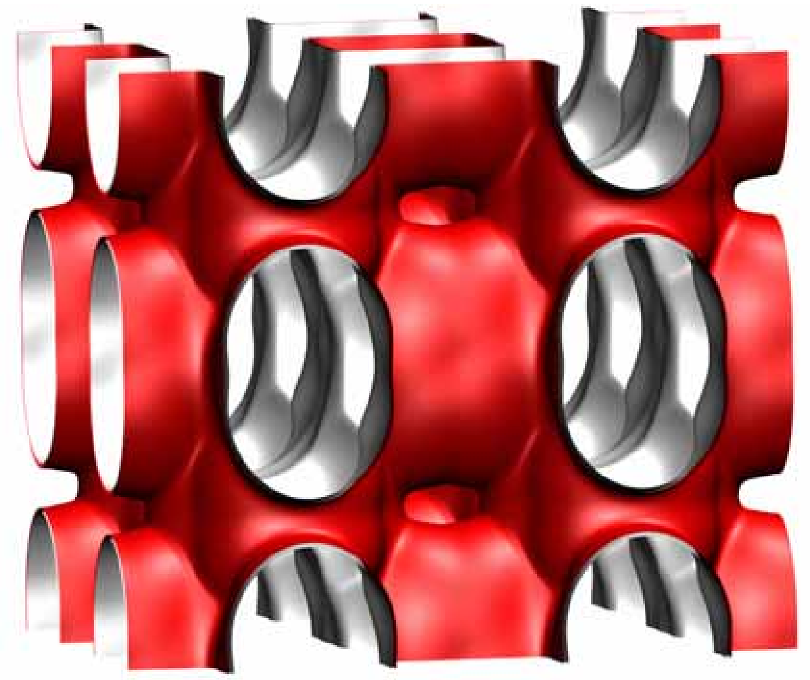

Zn(bdc)dabco landscapes

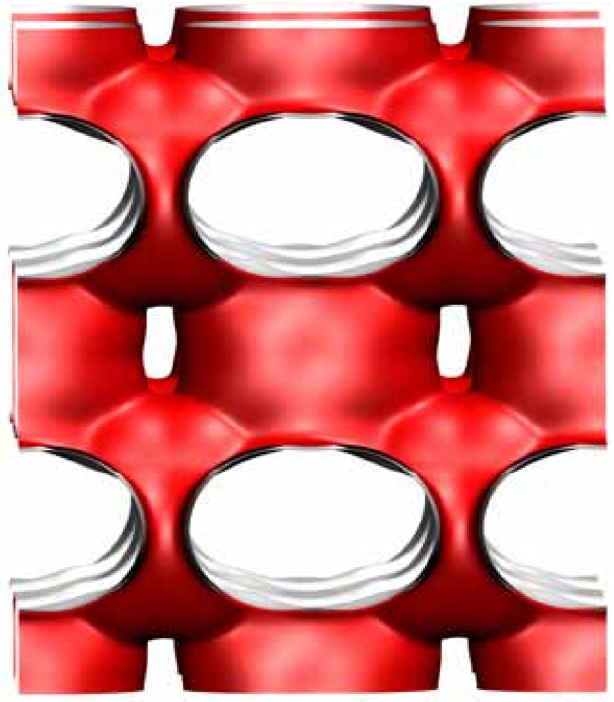

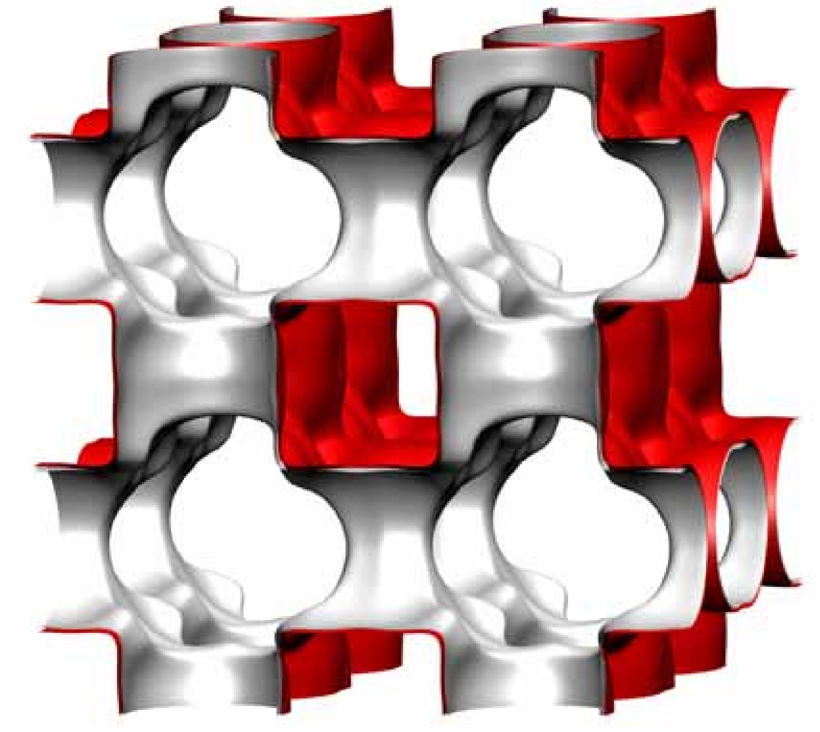

Zn(bdc)dabco landscapes

To convert from molecules per unit cell to mol kg^{-1}, multiply by 1.75.
The pore volume is 0.801 cm^3/g.

3D intersecting channels

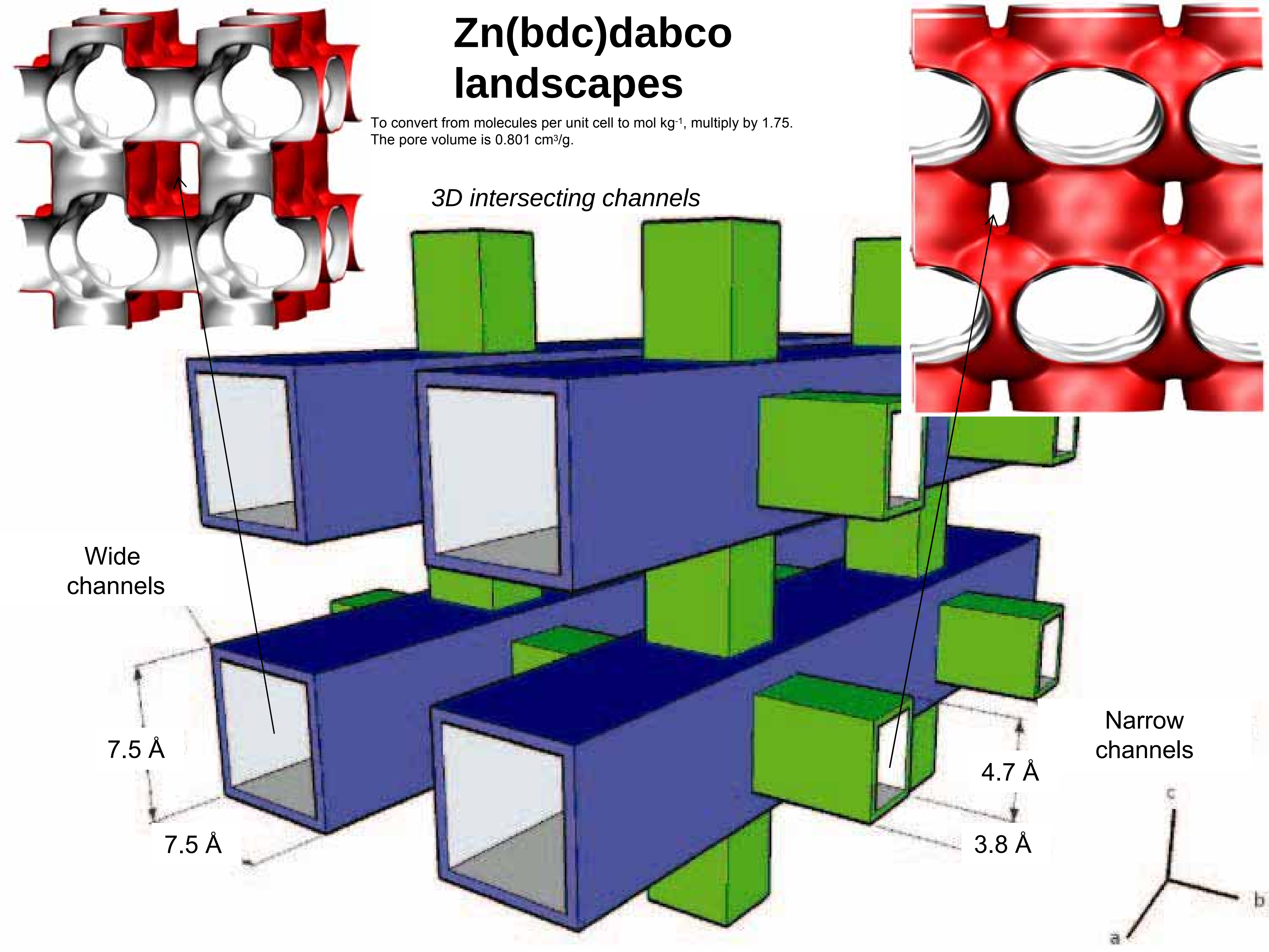

Zn(bdc)dabco CBMC pentanes mixture simulation results

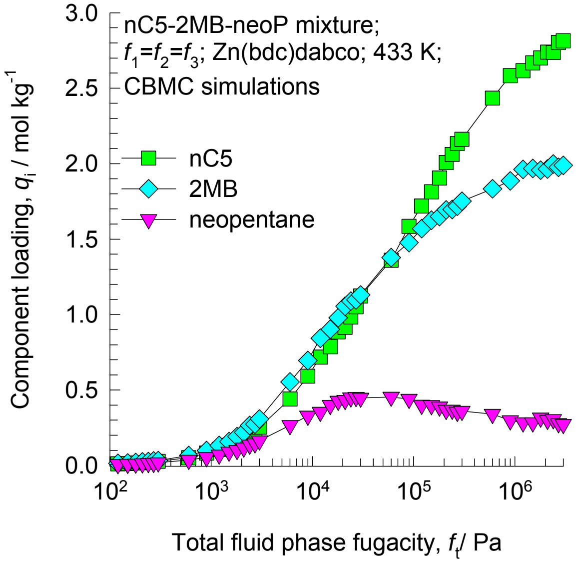

$$S_{ads} = \frac{\dfrac{q_{nC5}}{f_{nC5}} + \dfrac{q_{2MB}}{f_{2MB}}}{\dfrac{q_{neoP}}{f_{neoP}}}$$

Capacity is the total loading of nC5 + 2MB

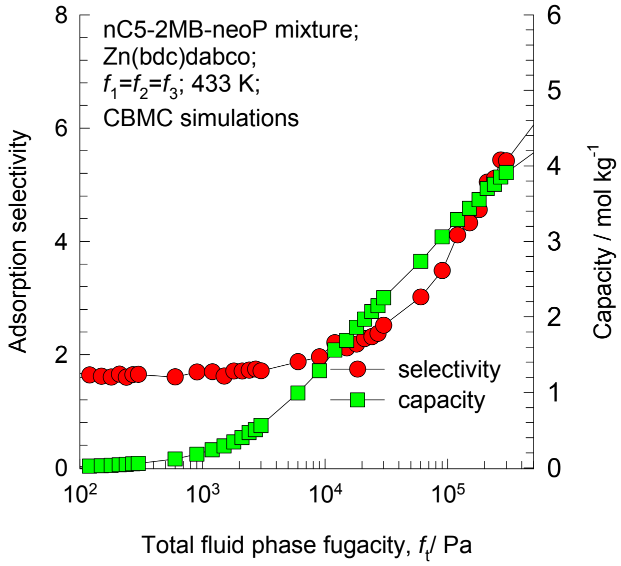

Zn(bdc)dabco CBMC nC6/3MP/22DMB mixture simulation results

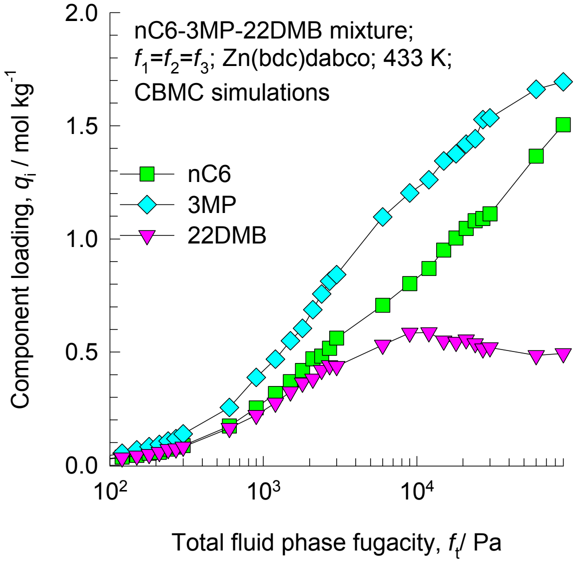

$$S_{ads} = \frac{\dfrac{q_{nC6}}{f_{nC6}} + \dfrac{q_{3MP}}{f_{3MP}}}{\dfrac{q_{22DMB}}{f_{22DMB}}}$$

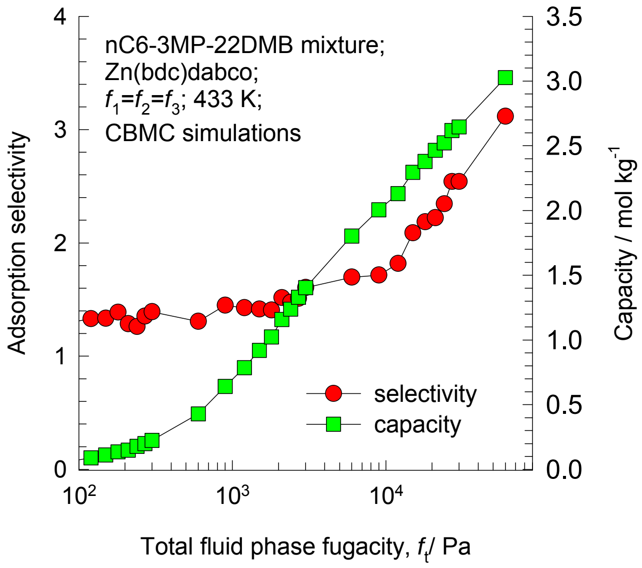

Capacity is the total
loading of nC6 + 3MP

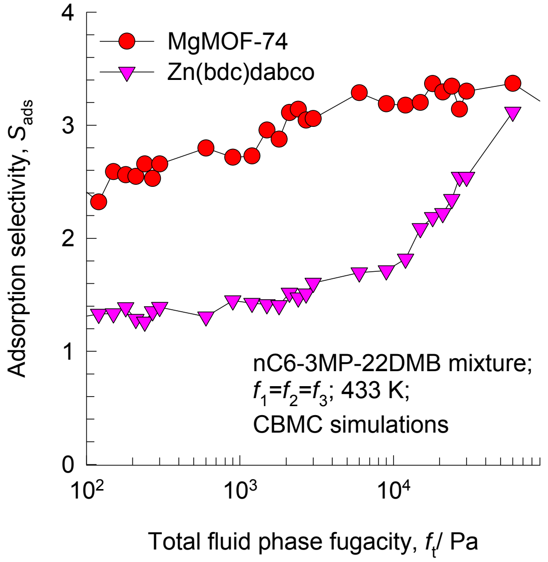

Note that the adsorption selectivity of Zn(bdc)dabco is significantly lower than that of MgMOF-74 for total fugacities lower than 50 kPa. For this reason we do not consider Zn(bdc)dabco to be an attractive MOF for hexane isomer separation when compared to MgMOF-74.

Zn(bdc)dabco Comment on the CBMC nC6/3MP/22DMB experiments of Barcia et al.

Barcia expt

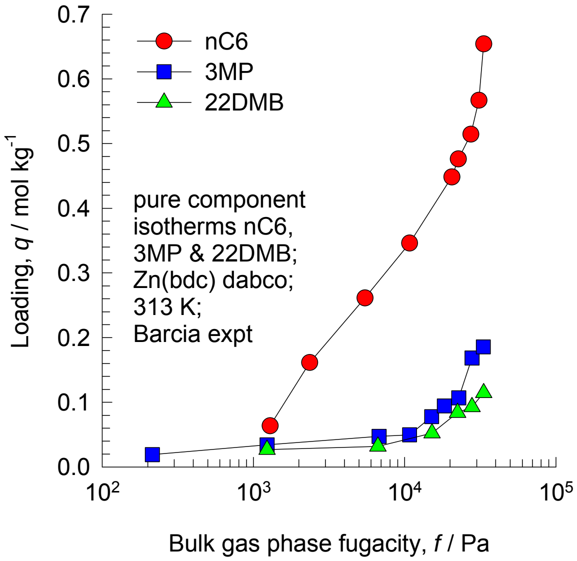

The separation hierarchy obtained in our CBMC simulations is 3MP ≈ nC6 >> 22DMB. This is quite different from the hierarchy nC6 >> 3MP ≈ 22DMB obtained in the experiments of P. S. Bárcia, F. Zapata, J. A. C. Silva, A. E. Rodrigues and B. Chen, J. Phys. Chem. B, 2008, 111, 6101-6103. Their experimental pure component isotherms are plotted on the left. We note that the component loadings are about an order of magnitude lower than those obtained from CBMC (shown on the right). We strongly suspect that that the Zn(bdc)dabco framework used in the experiments had undergone structural changes. This would suggest that their experimental results are not trustworthy.

Our CBMC

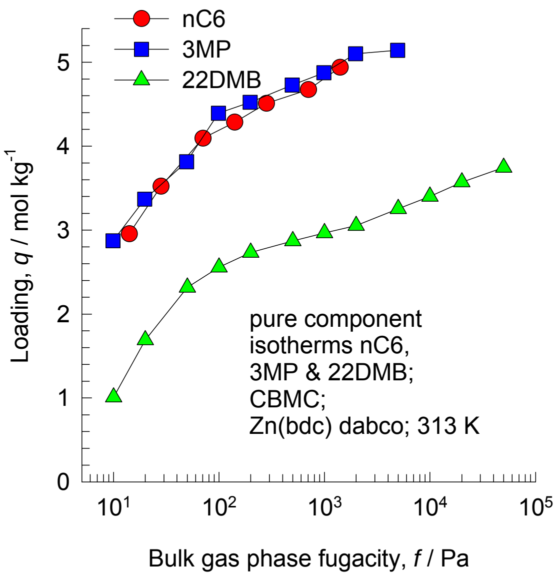

Zn(bdc)dabco snapshots of hexane isomers

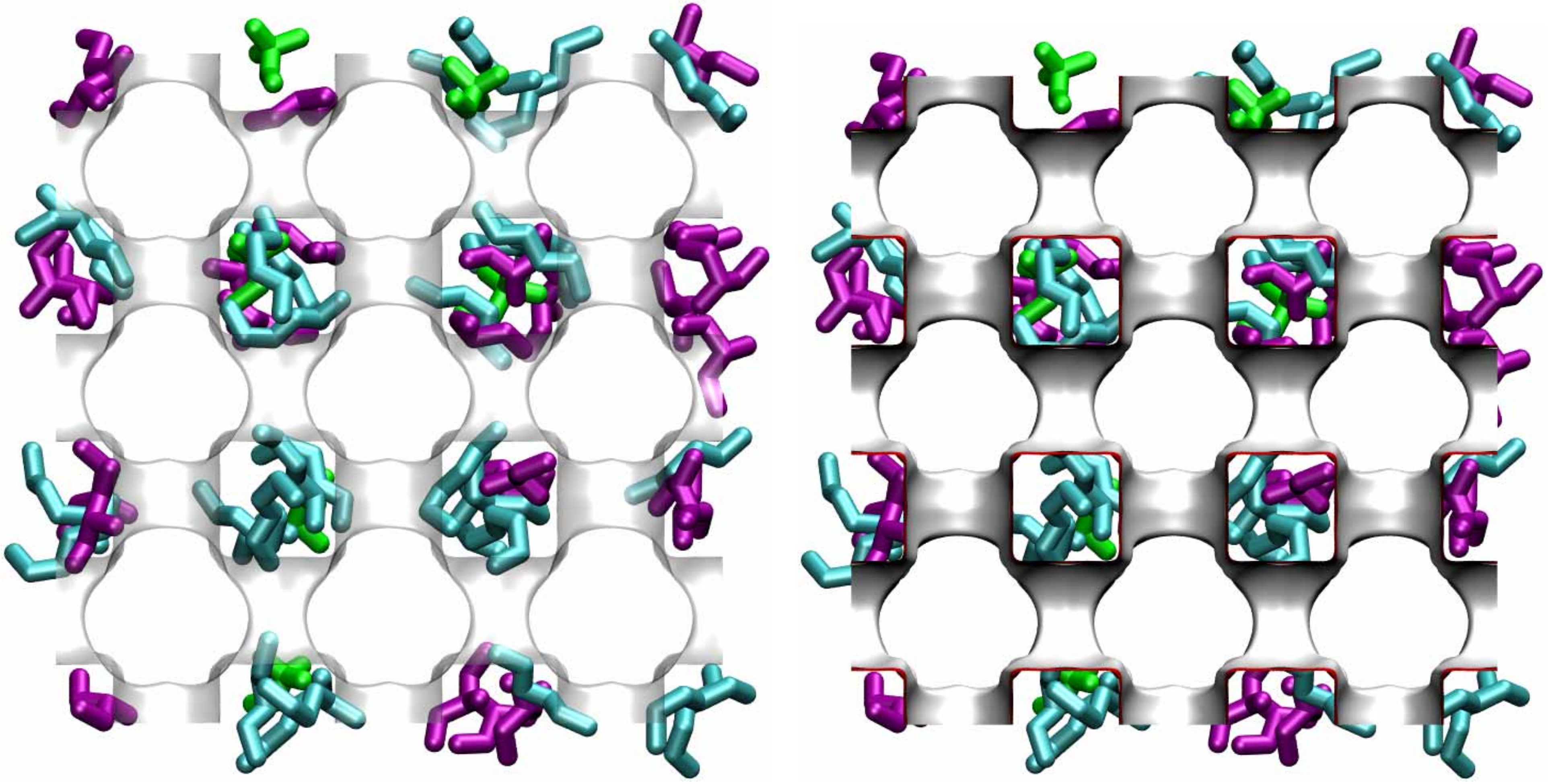

Zn(bdc)dabco CBMC nC6/2MP/3MP/22DMB/23DMB simulations

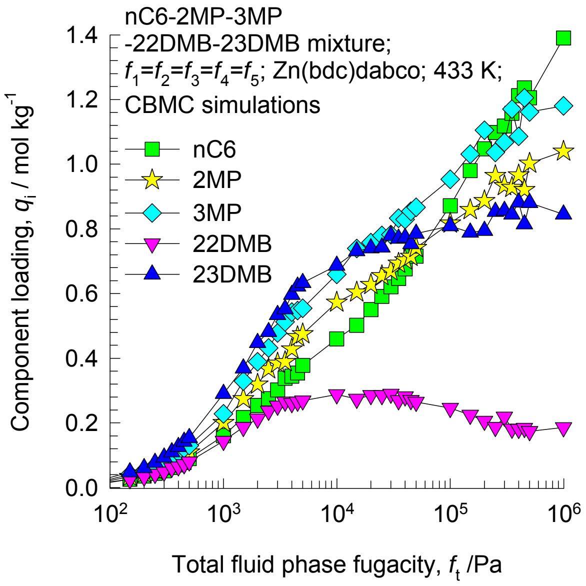

The 5-component mixture simulation shows that 22DMB can be separated from the rest of the mixture. But it is not possible to have clear separation of both the di-branched 22DMB and 23DMB from (linear + mono-branched)

ZIF-8 pore landscapes

To convert from molecules per unit cell to mol kg^{-1}, multiply by 0.366.
The pore volume is 0.518 cm^3/g.

There are 2 cages per unit cell. To convert from molecules per cage to mol kg^{-1}, multiply by 0.7325.

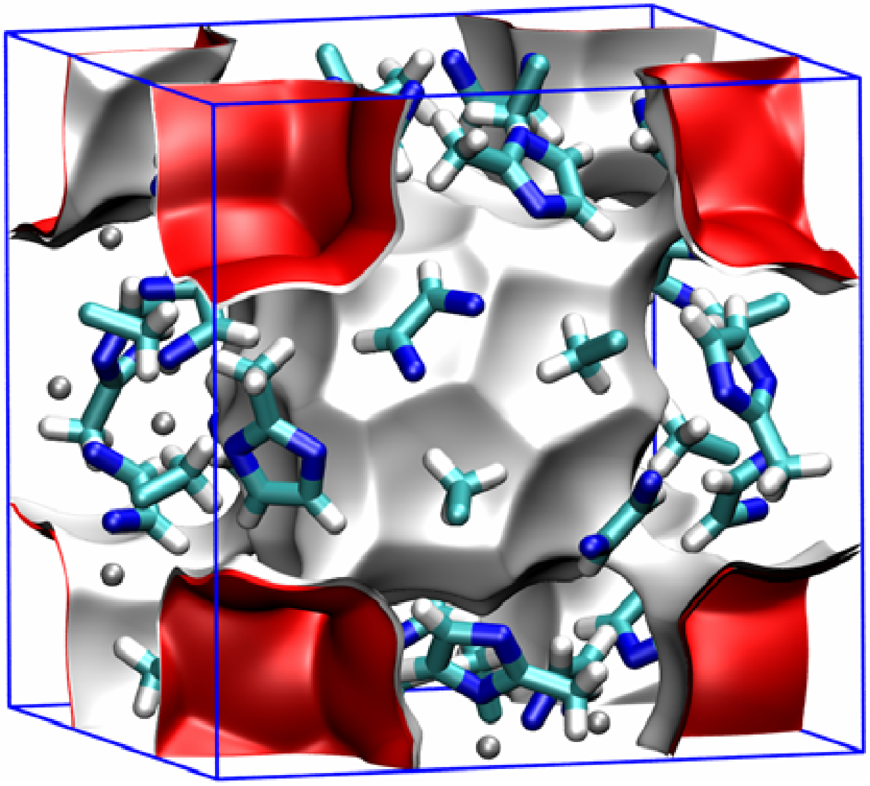

There are 2 cages per unit cell. The volume of one ZIF-8 cage is 1168 Å^3, significantly larger than that of a single cage of DDR (278 Å^3), or FAU (786 Å^3).

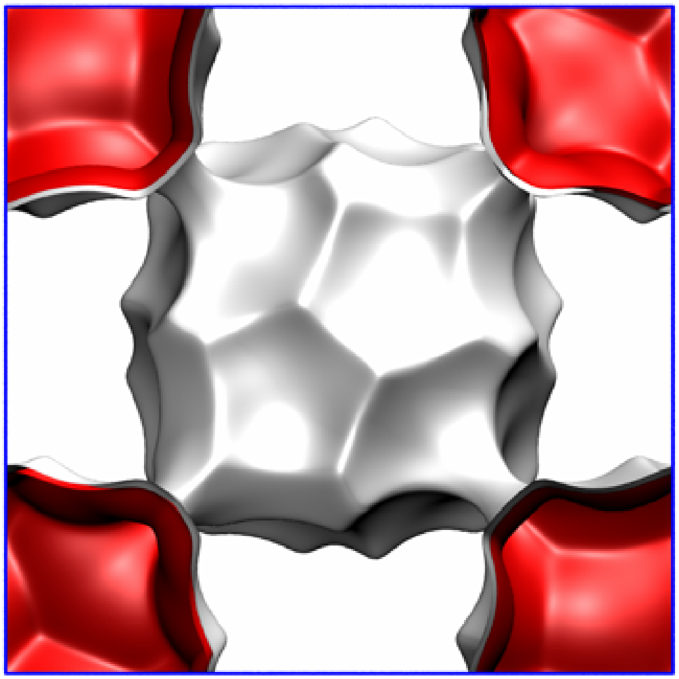

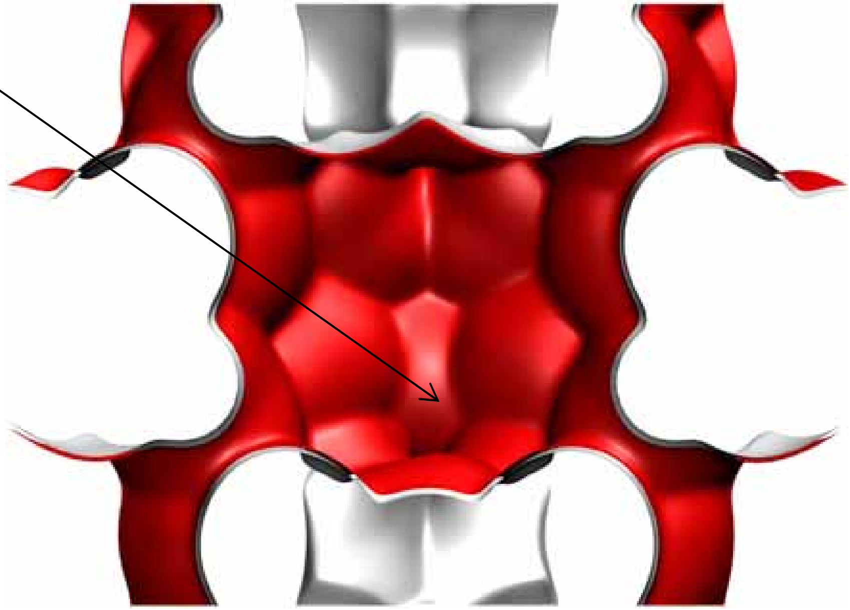

ZIF-8 snapshot of CO_2/CH_4 mixture

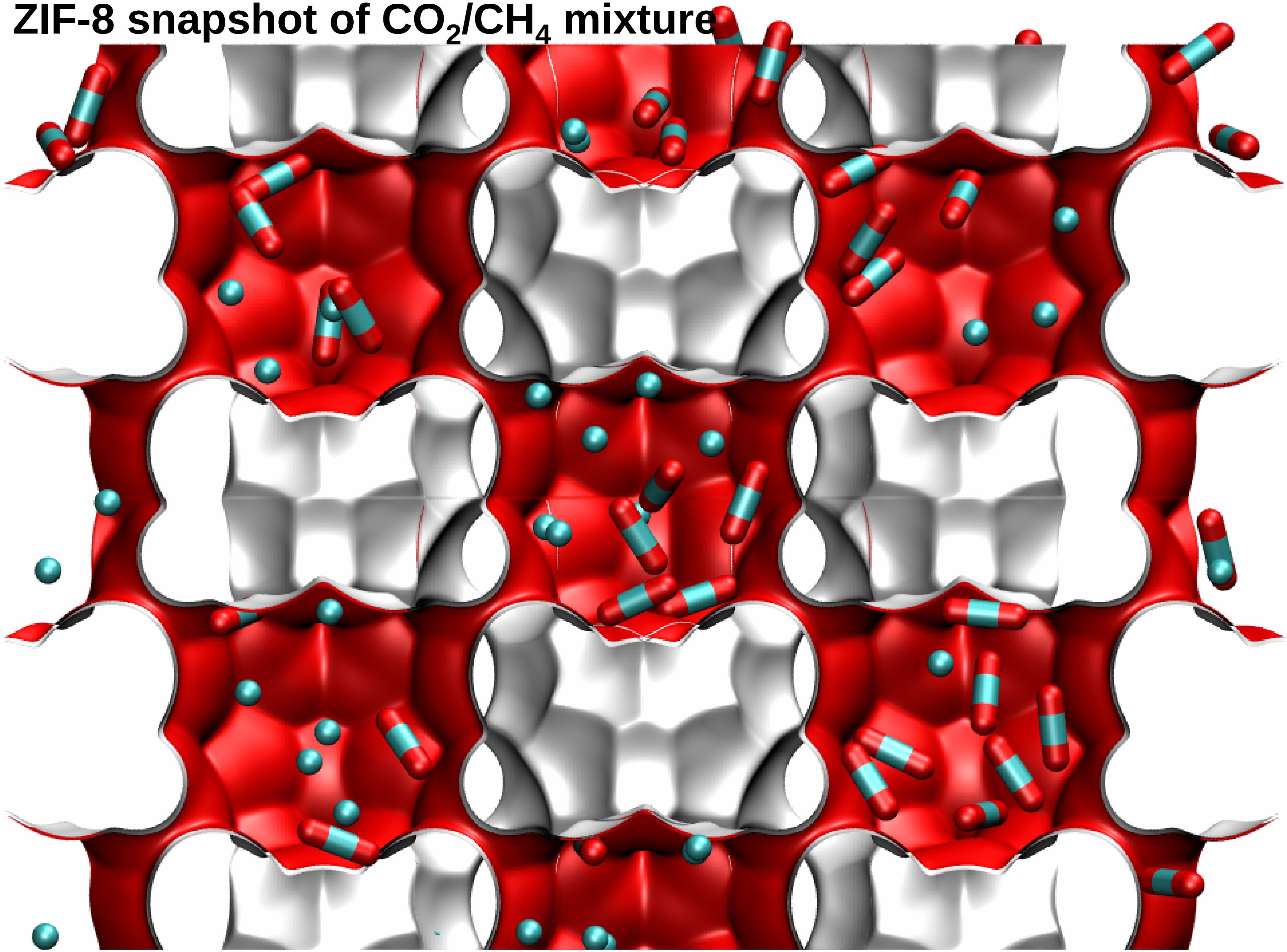

ZIF-8 pure component isotherms; comparison with experiments

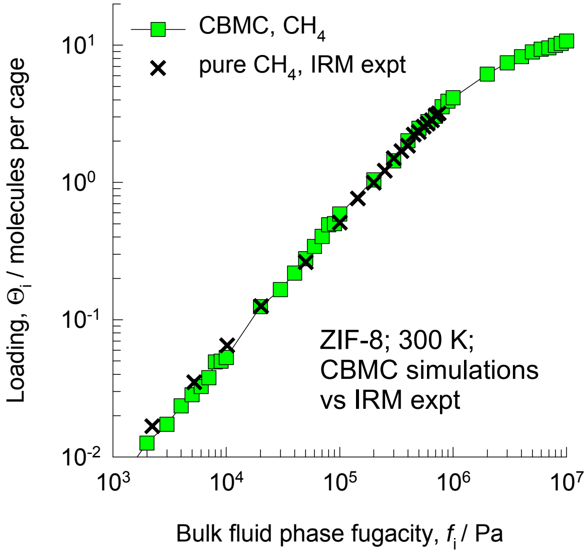

The IRM experimental data is from H. Bux, C. Chmelik, J.M. Van Baten, R. Krishna, J. Caro, Novel MOF-Membrane for Molecular Sieving Predicted by IR-Diffusion Studies and Molecular Modeling, Adv. Mater. 22 (2010) 4741-4743.

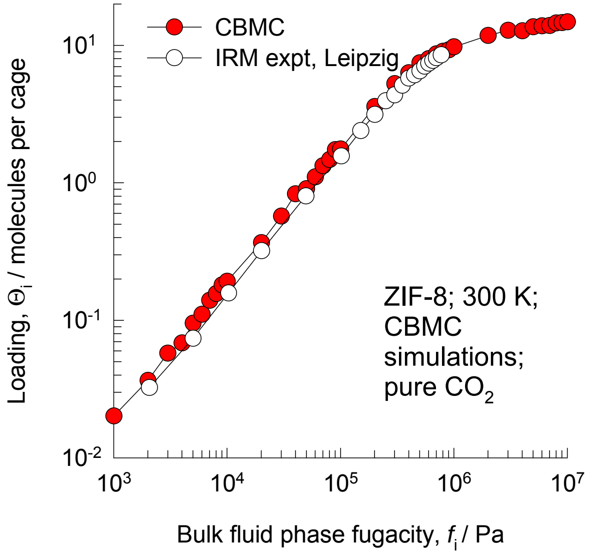

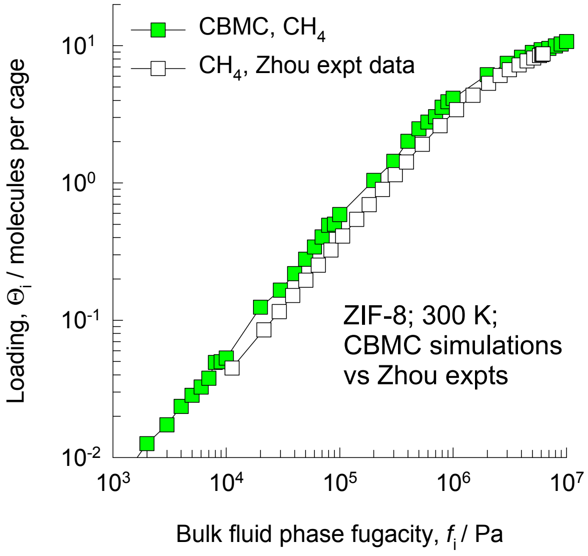

The experimental data is from W. Zhou, H. Wu, M.R. Hartman, T. Yildrim, Hydrogen and Methane Adsorption in Metal-Organic Frameworks: A High-Pressure Volumetric Study, J. Phys. Chem. C 111 (2007) 16131-16137.

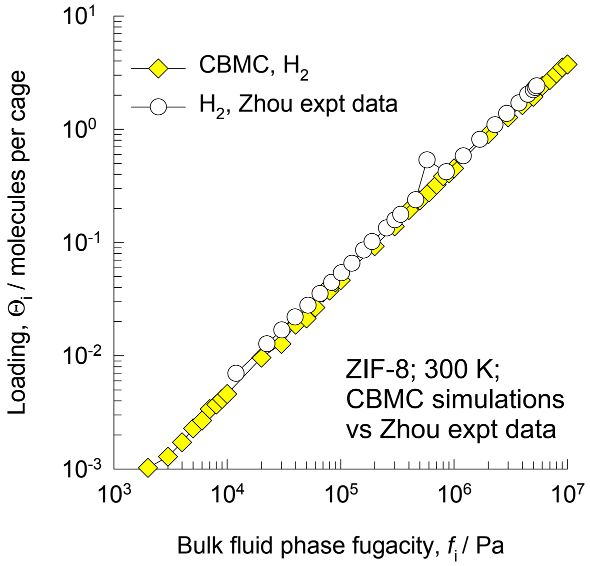

ZIF-8 CBMC mixture simulations for CO_2 capture

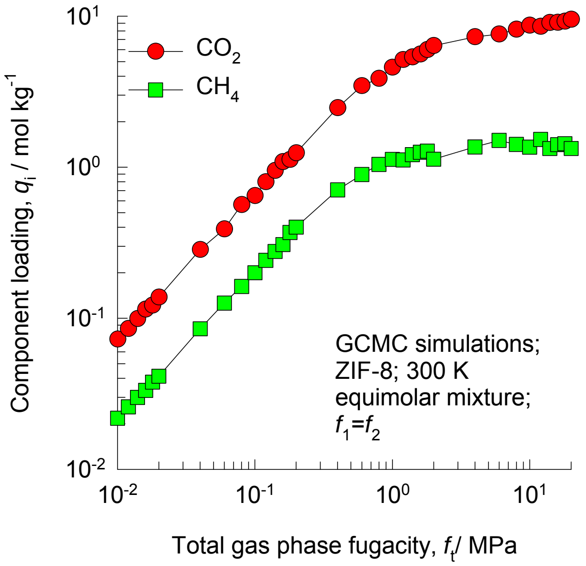

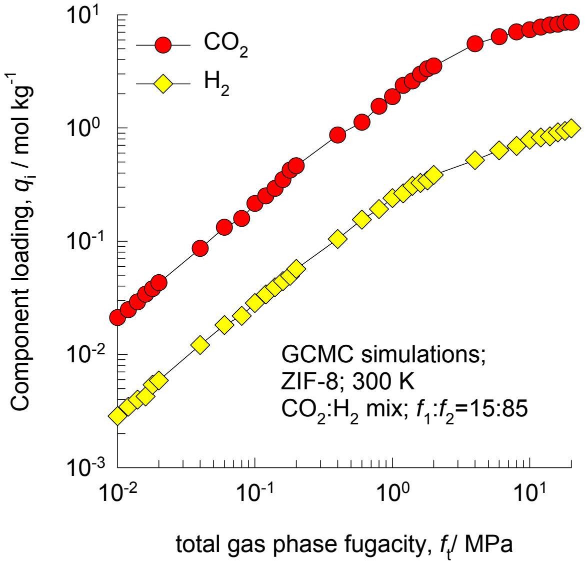

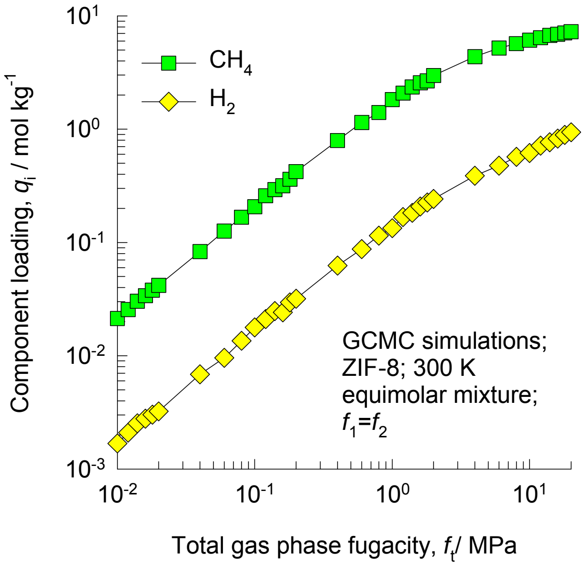

Graphite Slit of four different widths

Graphite slits

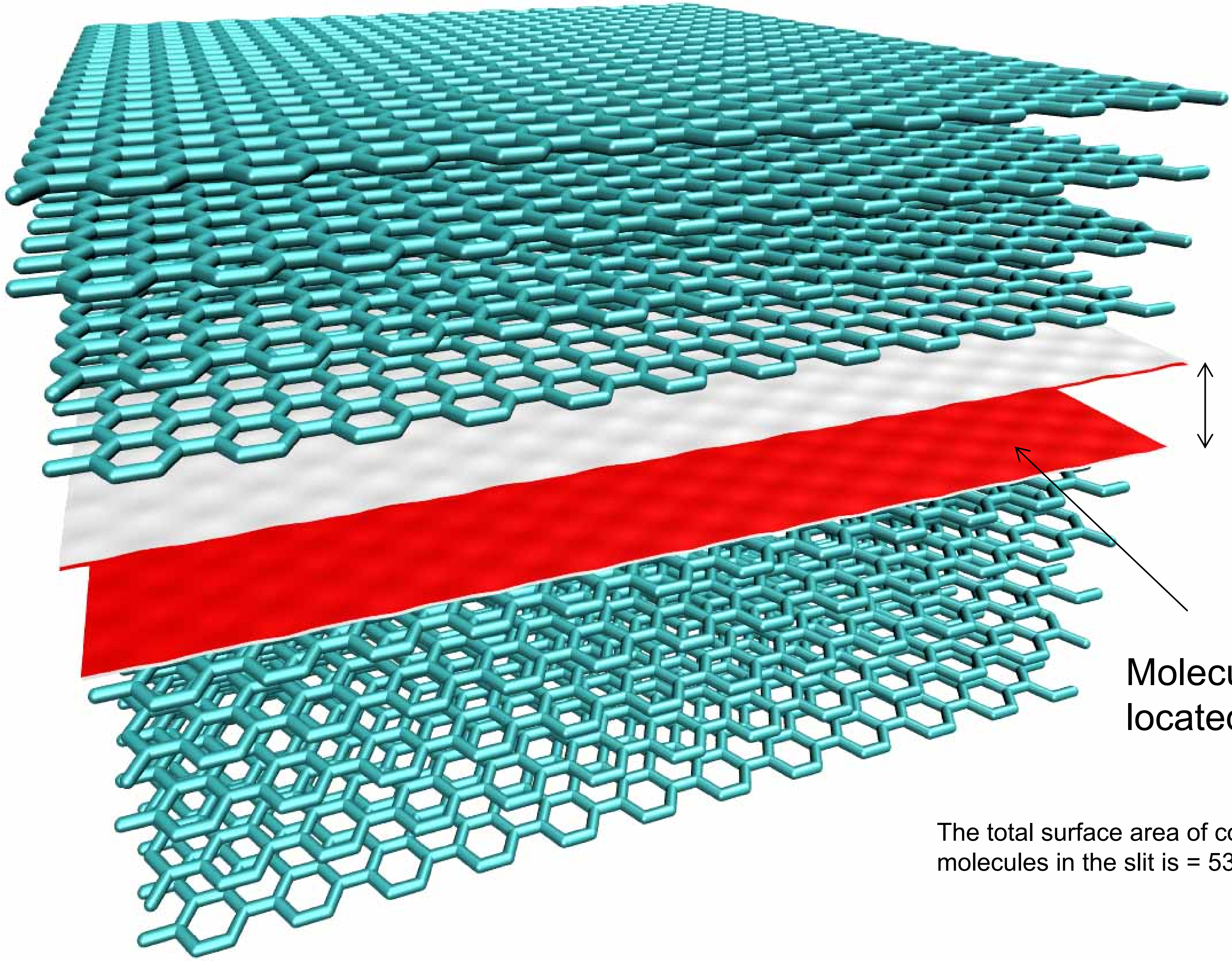

The slit width is obtained by subtracting the L-J sigma

Molecules are located here

The total surface area of contact for the molecules in the slit is = 53.79 nm^2 =5379 Å^2

Slit width = 0.74 nm

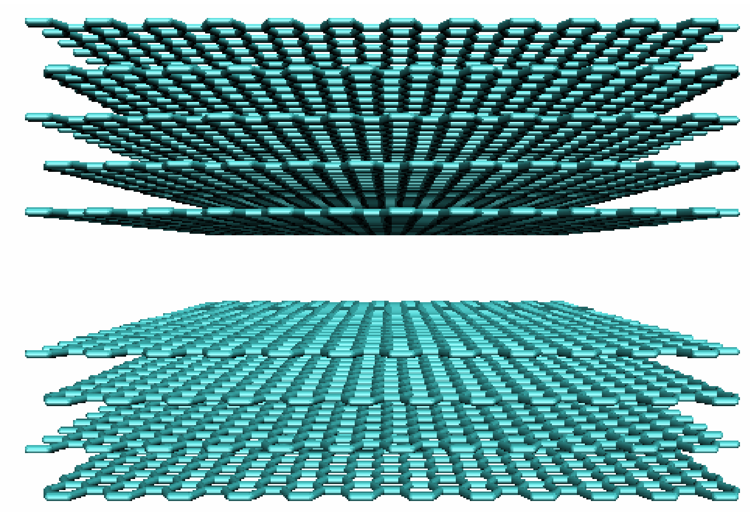

The loadings are expressed in terms of the number of molecules per nm^2 surface area

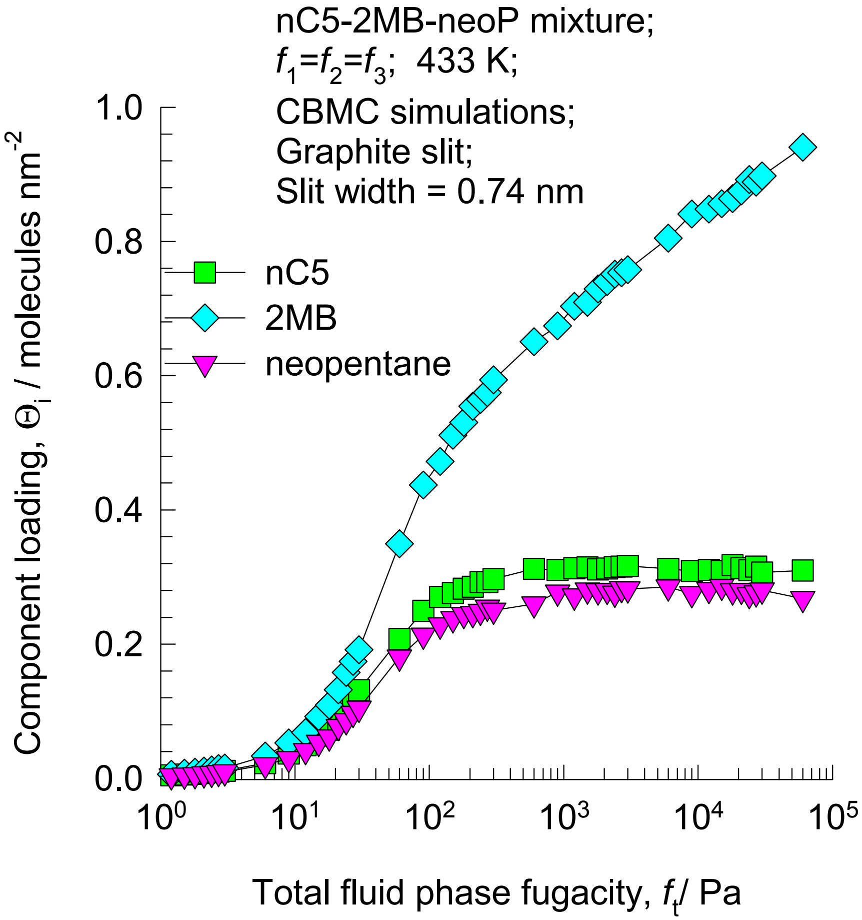
nC5-2MB-neoP mixture;
$f_1=f_2=f_3$; 433 K;
CBMC simulations;
Graphite slit;
Slit width = 0.74 nm

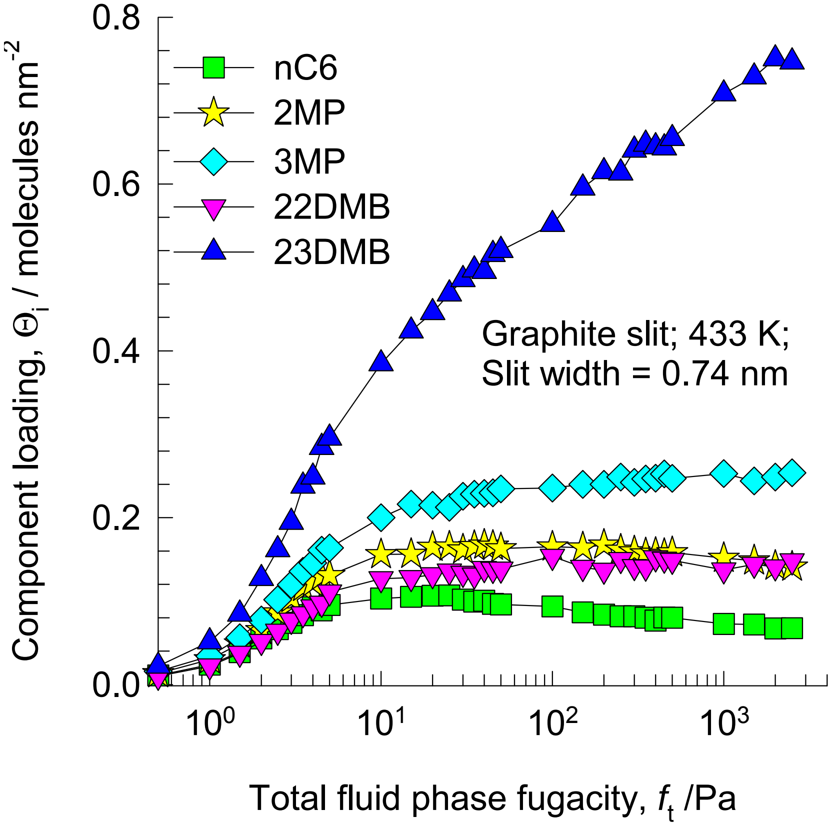
Graphite slit; 433 K;
Slit width = 0.74 nm

Slit width = 0.74 nm snapshots of C5 isomers

Of the C5 isomers, nC5 has the longest footprint and the lowest loading

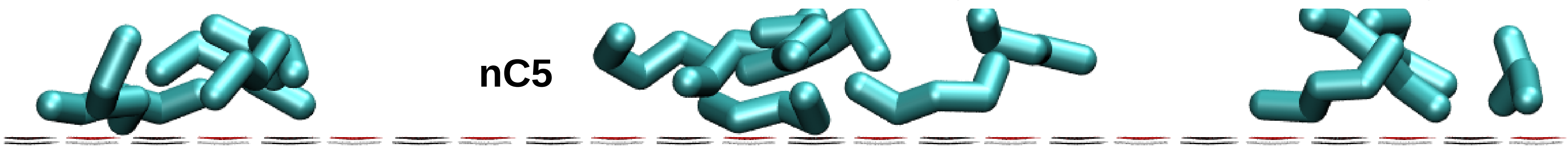

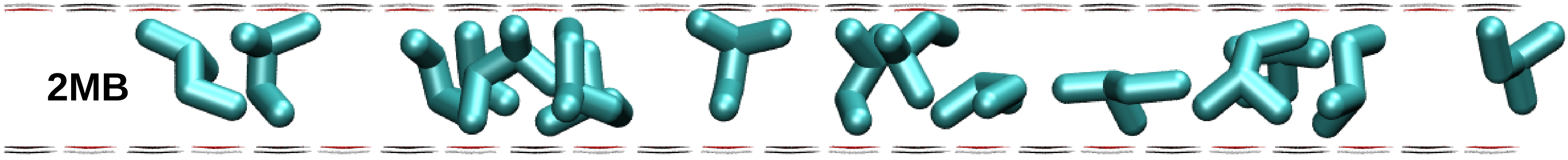

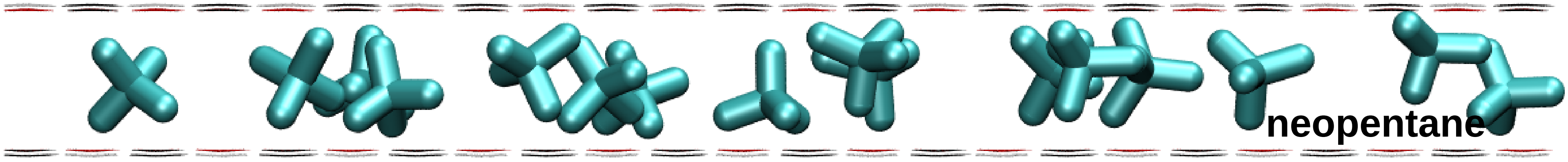

Slit width = 0.74 nm snapshots of C6 isomers

Of the C6 isomers, nC6 has the longest footprint and the lowest loading

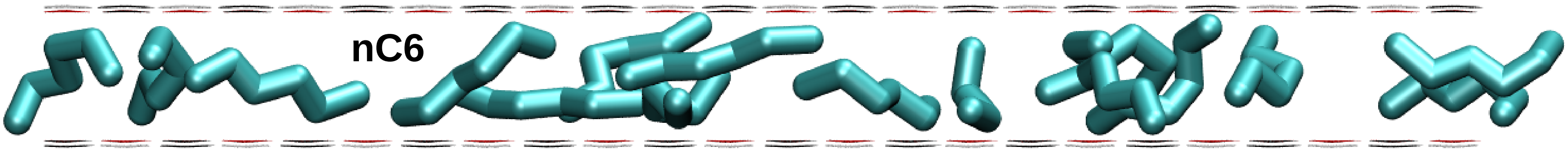

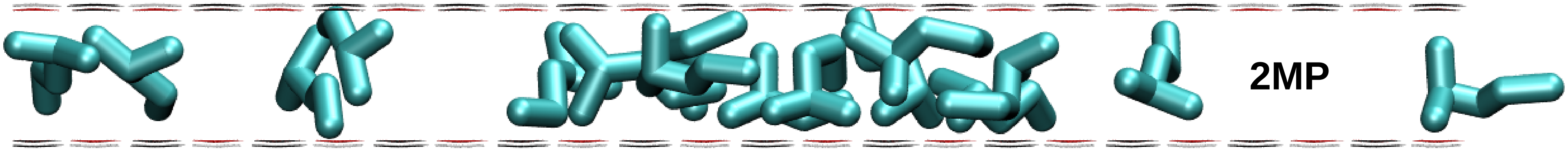

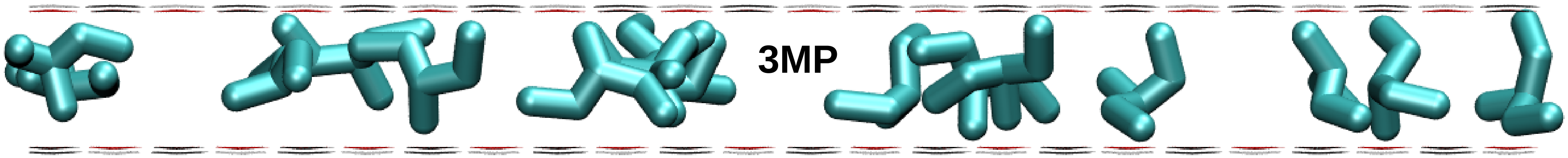

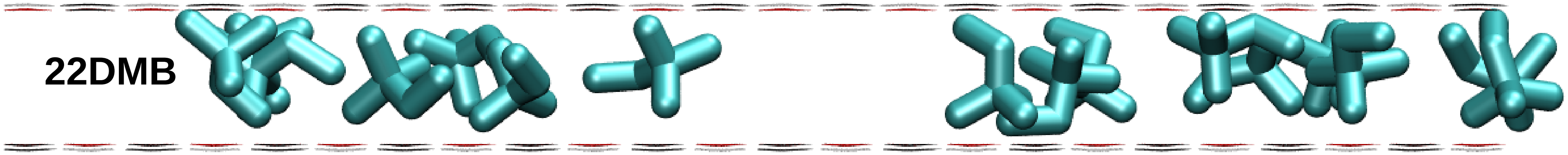

Of the C6 isomers, 23DMB has the shortest footprint and the highest loading

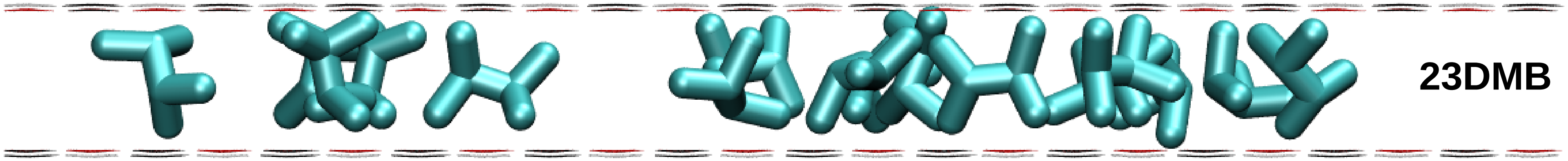

Slit width = 0.94 nm

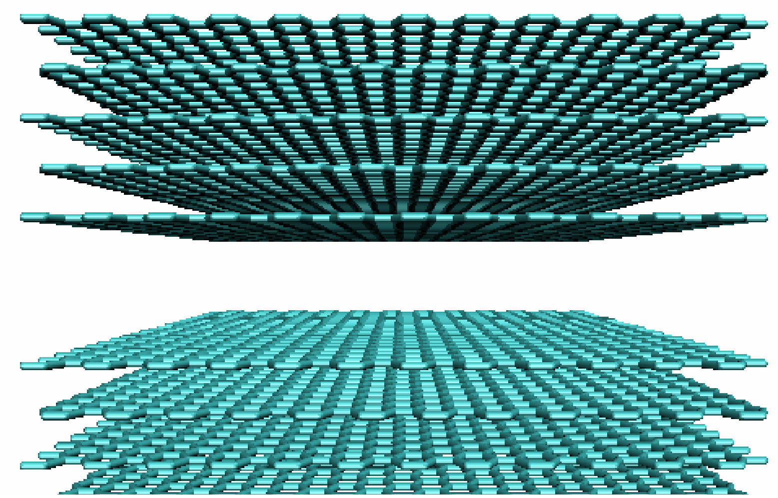

The loadings are expressed in terms of the number of molecules per nm^2 surface area

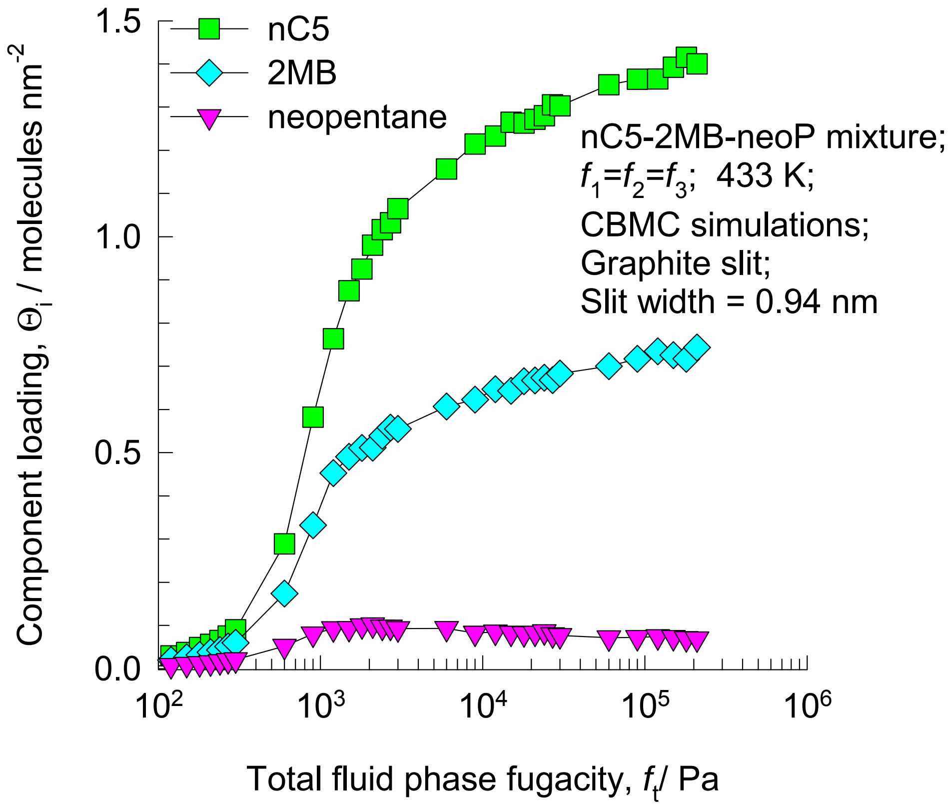

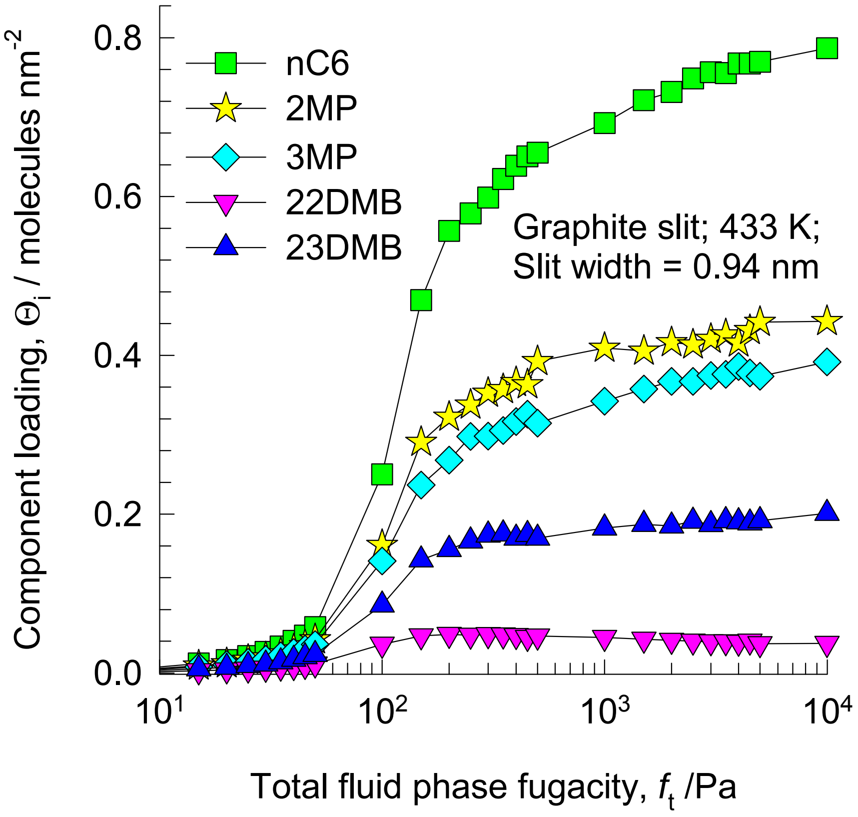

Slit width = 0.94 nm snapshots of C5 isomers

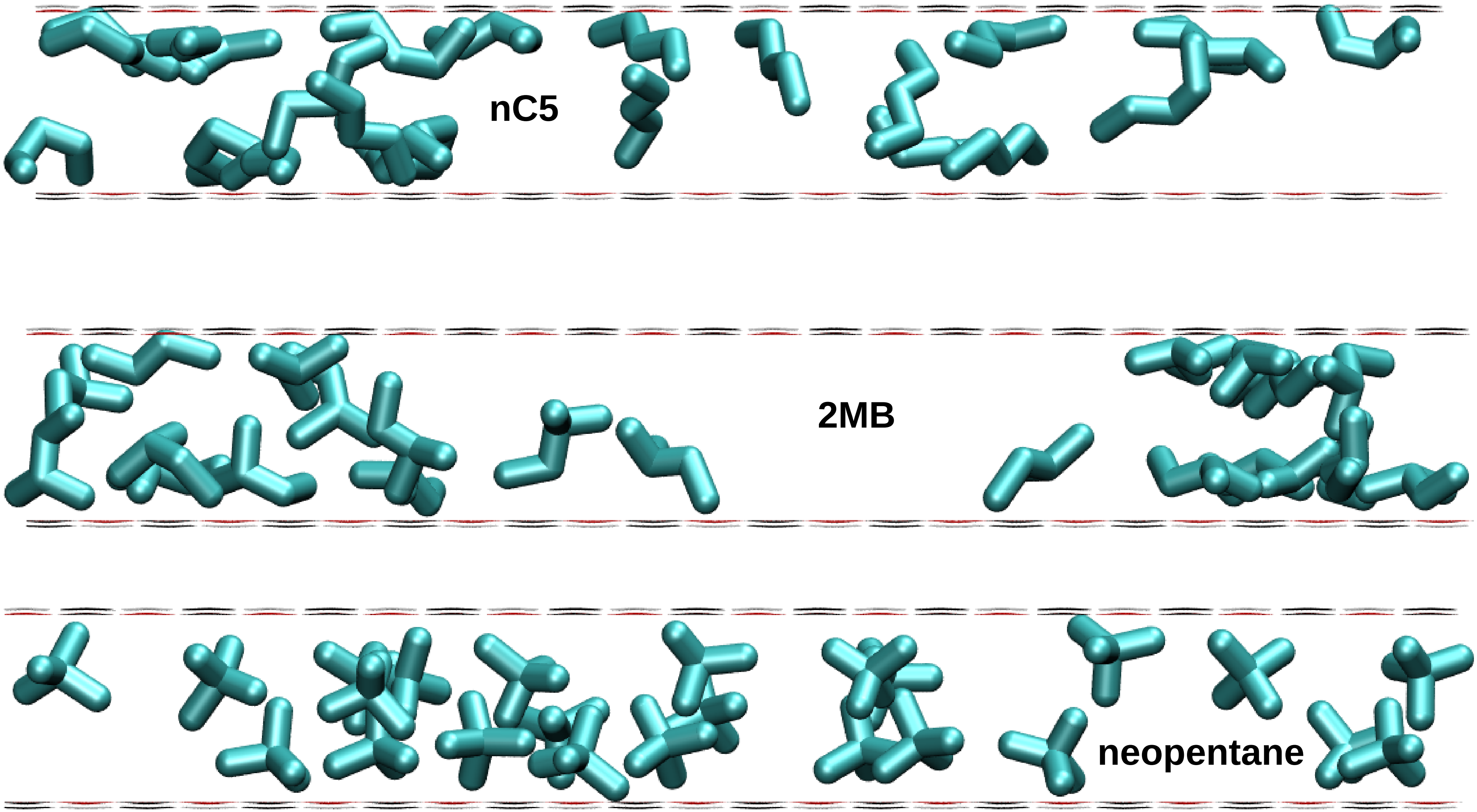

Slit width = 0.94 nm snapshots of C6 isomers

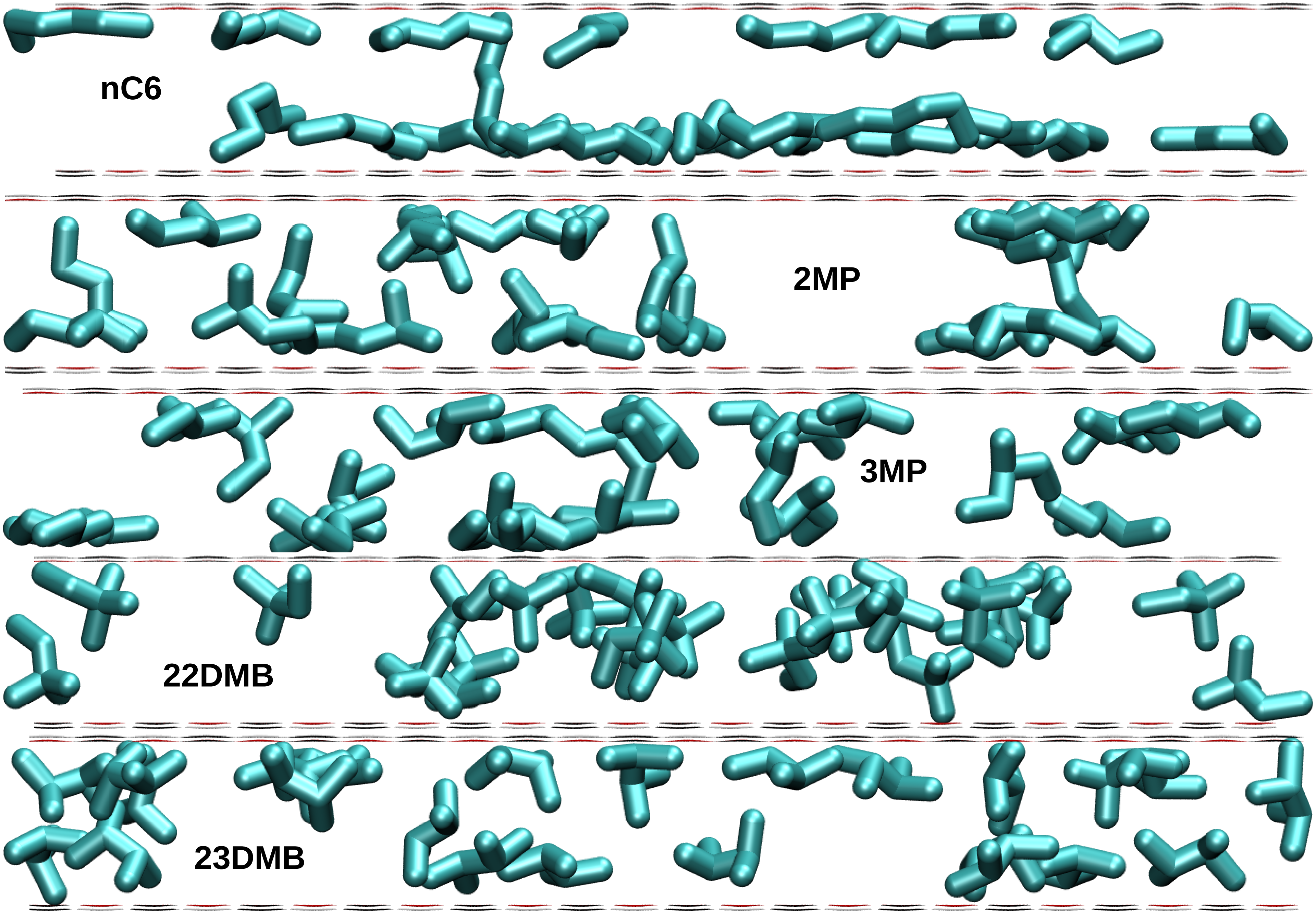

Slit width = 1.14 nm

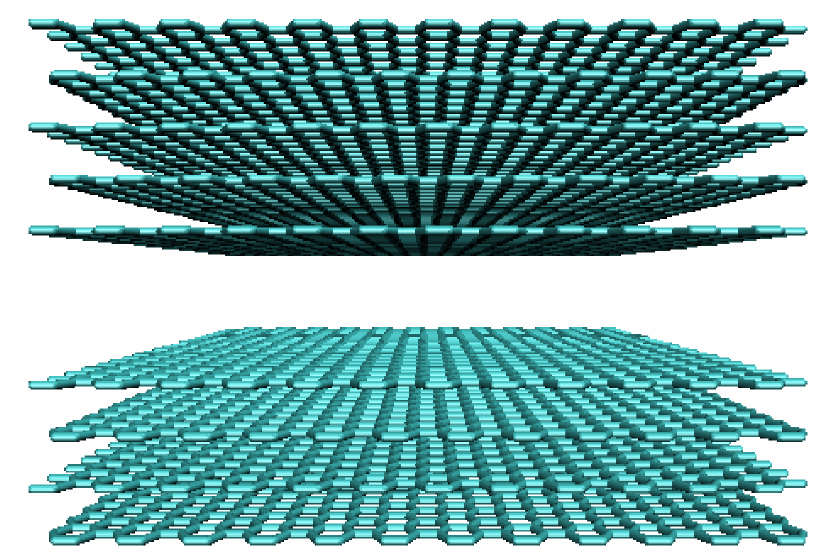

The loadings are expressed in terms of the number of molecules per nm^2 surface area

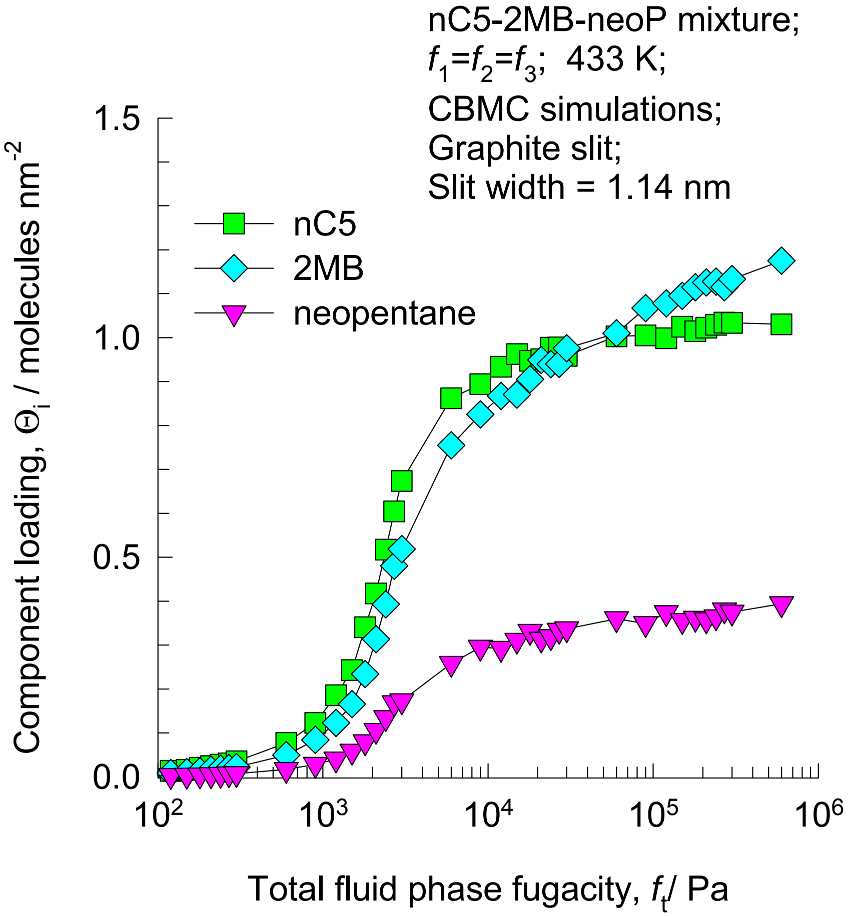

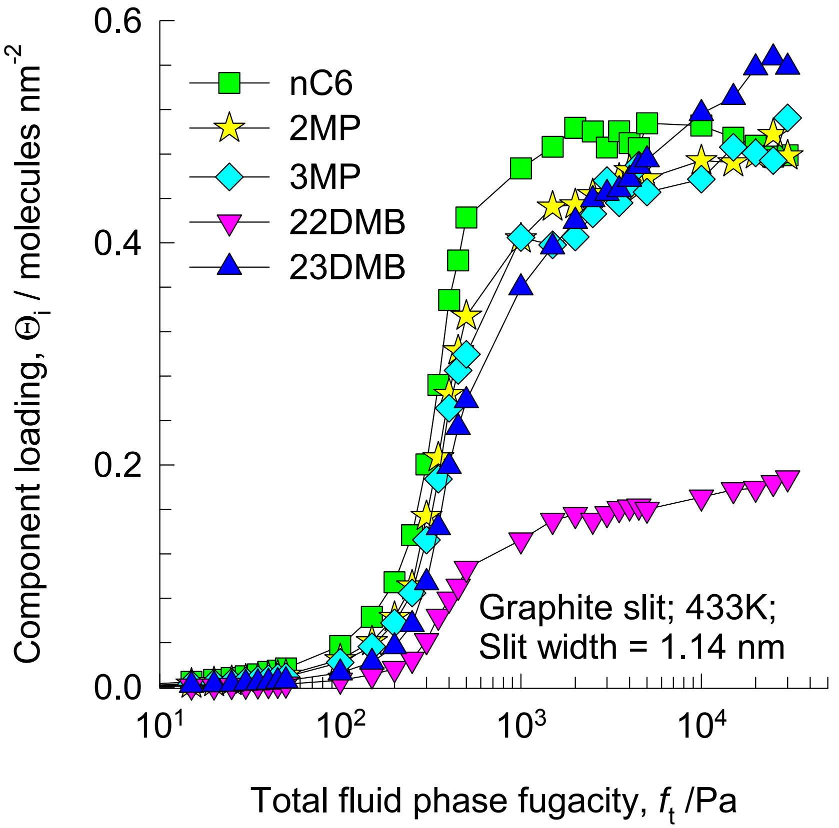

Slit width = 1.14 nm snapshots of C5 isomers

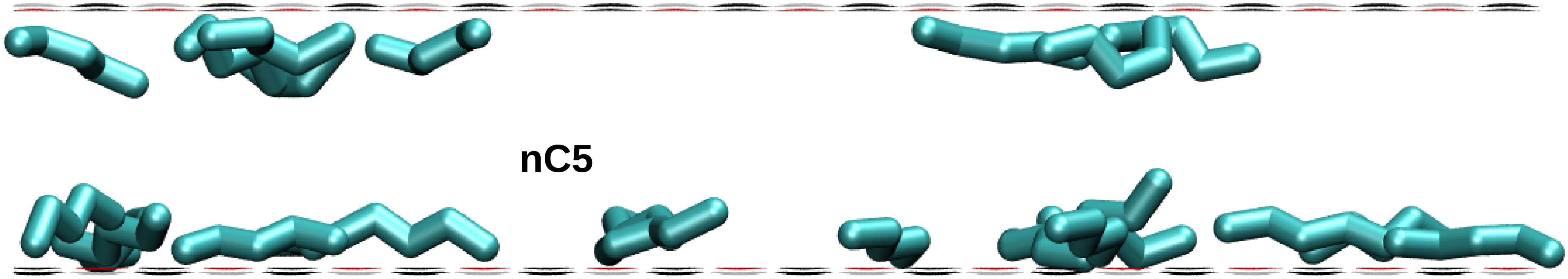

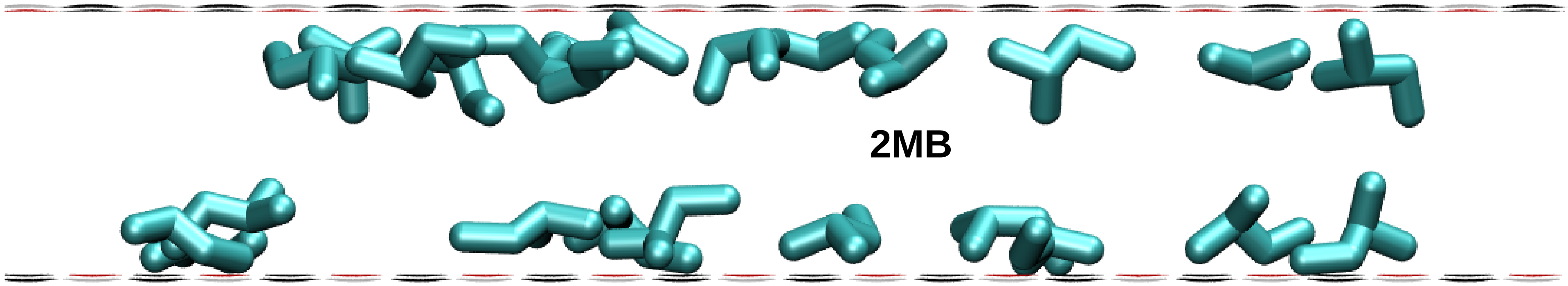

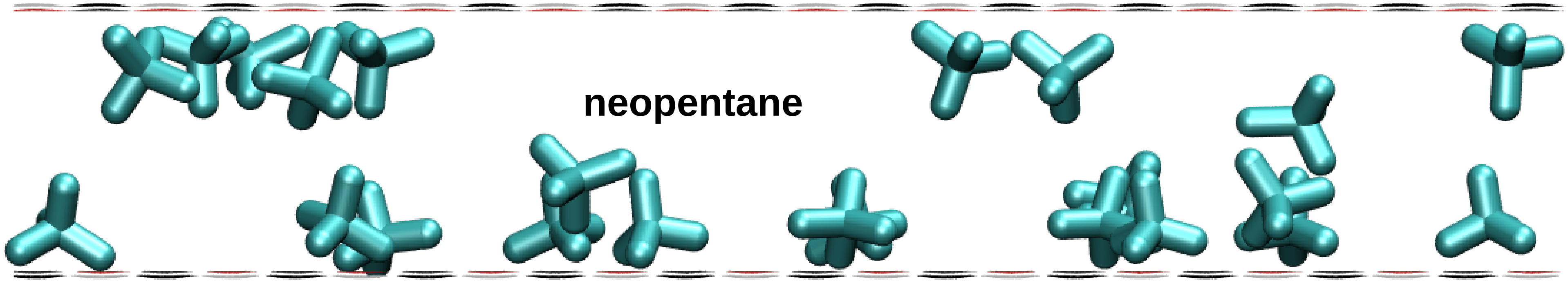

Slit width = 1.14 nm snapshots of C6 isomers

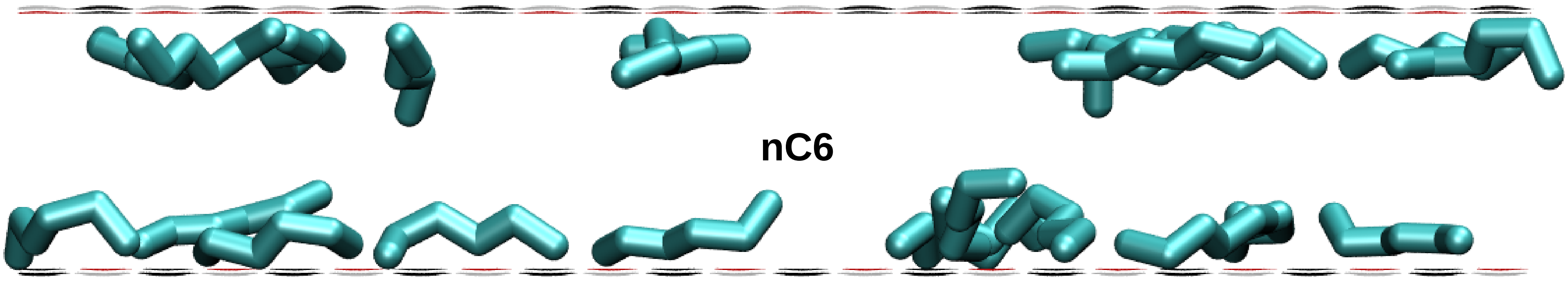

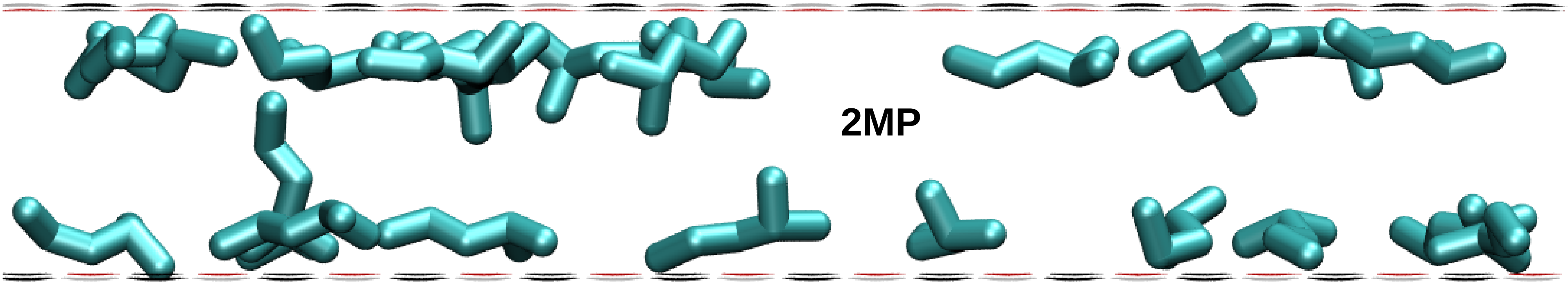

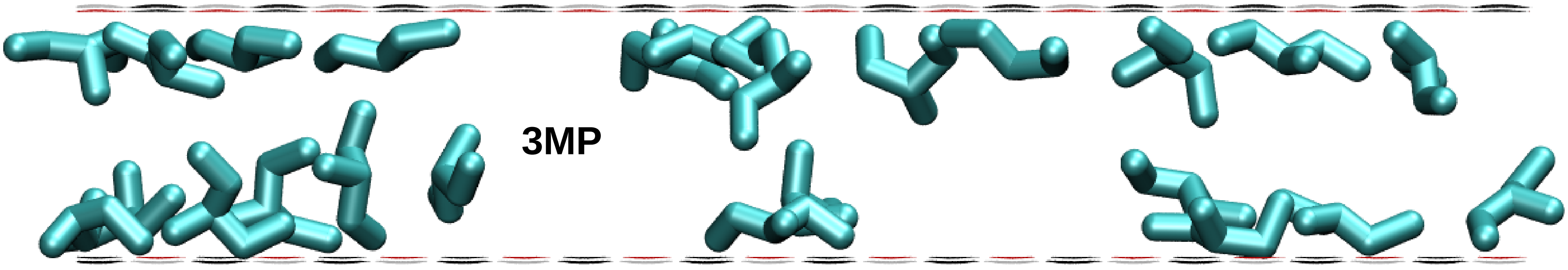

Slit width = 1.14 nm snapshots of C6 isomers

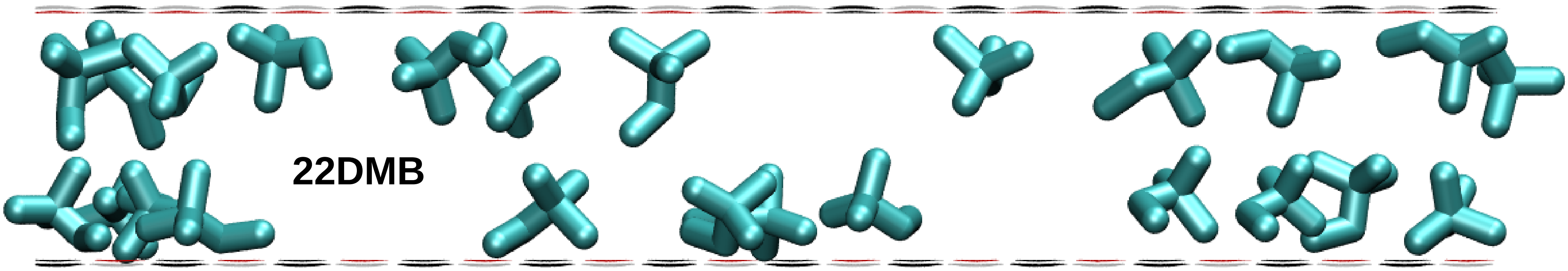

22DMB

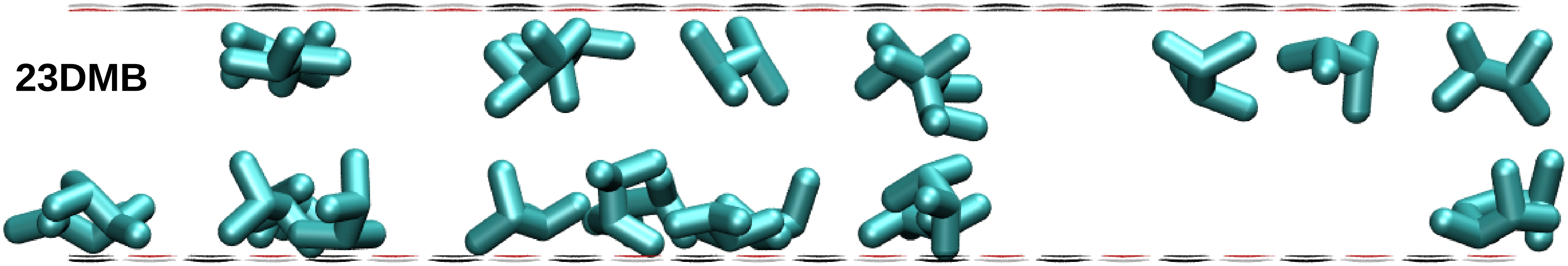

23DMB

Slit width = 1.34 nm

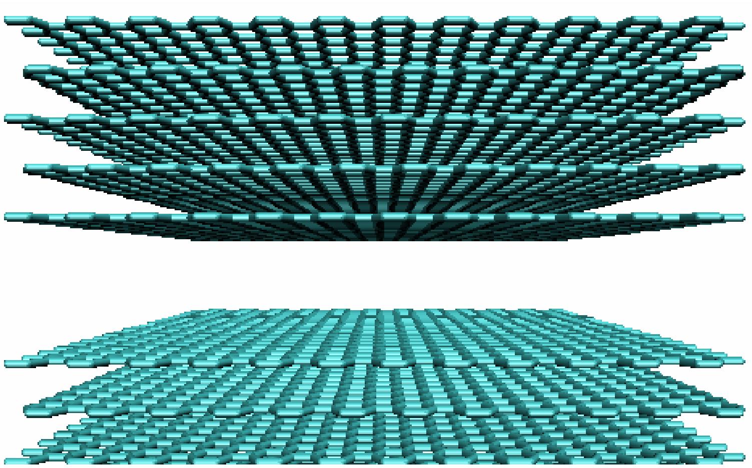

The loadings are expressed in terms of the number of molecules per nm^2 surface area

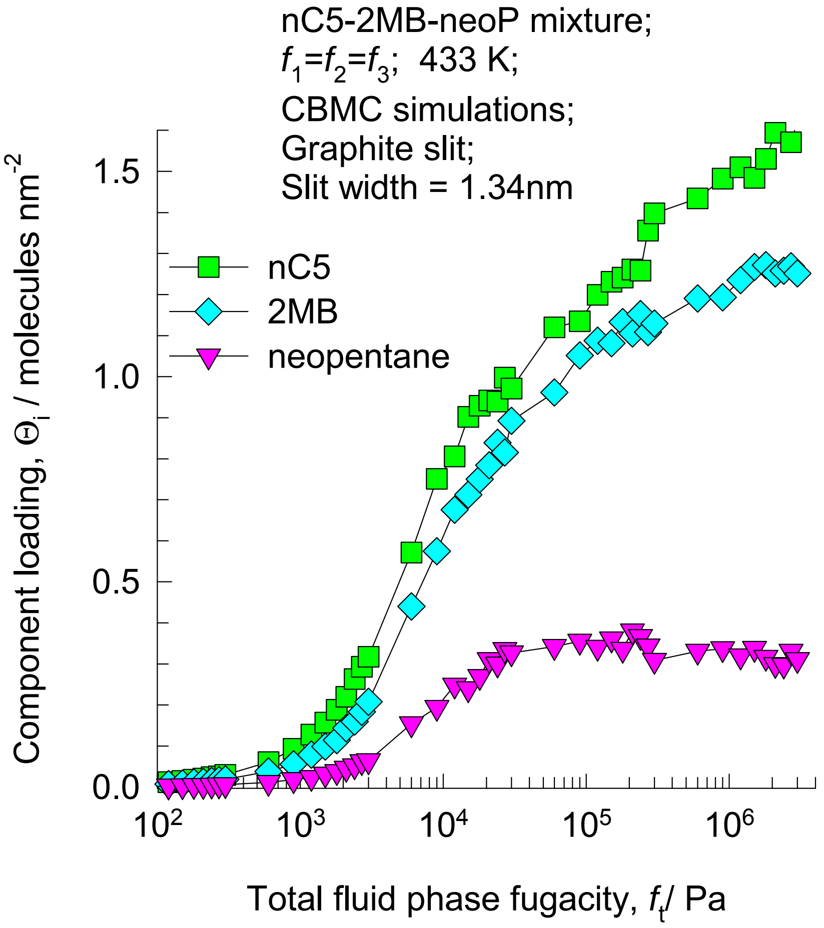

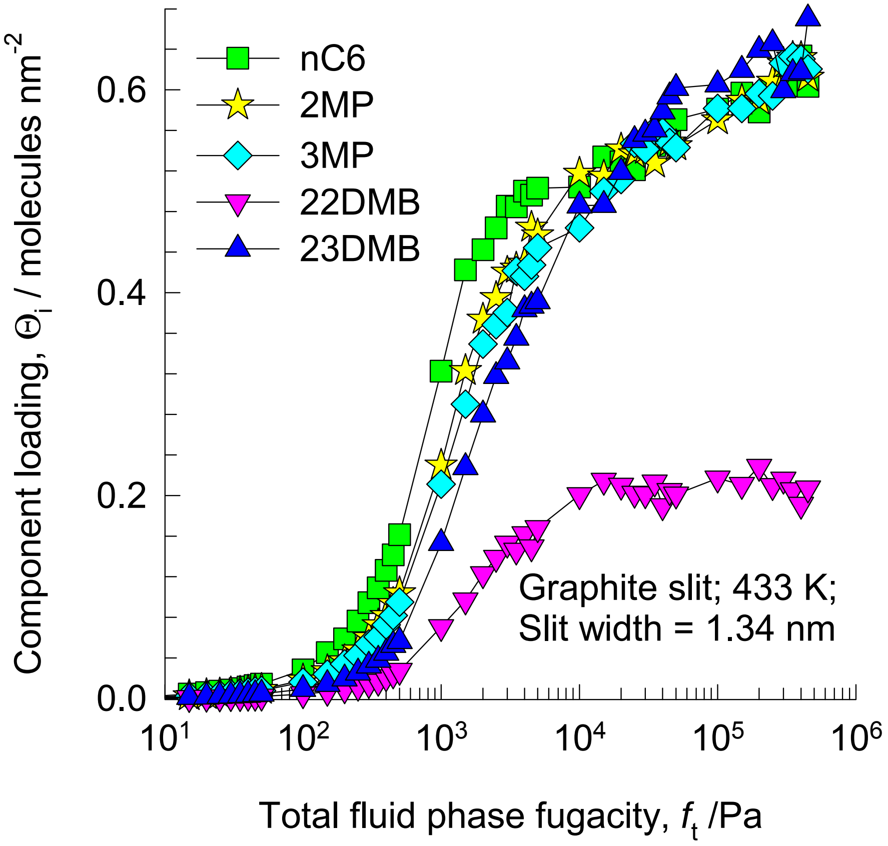

Slit width = 1.34 nm snapshots of C5 isomers

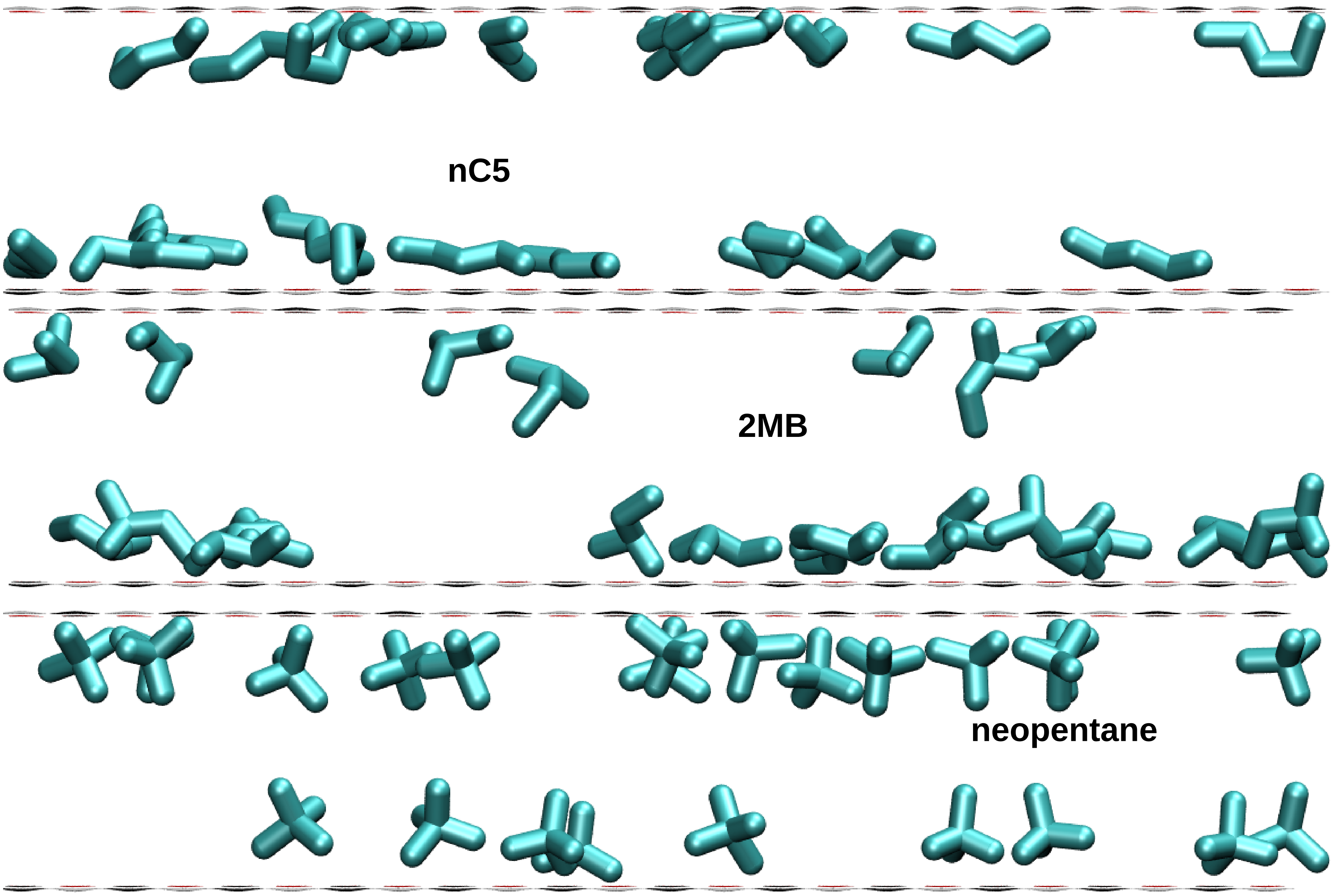

Slit width = 1.34 nm snapshots of C6 isomers

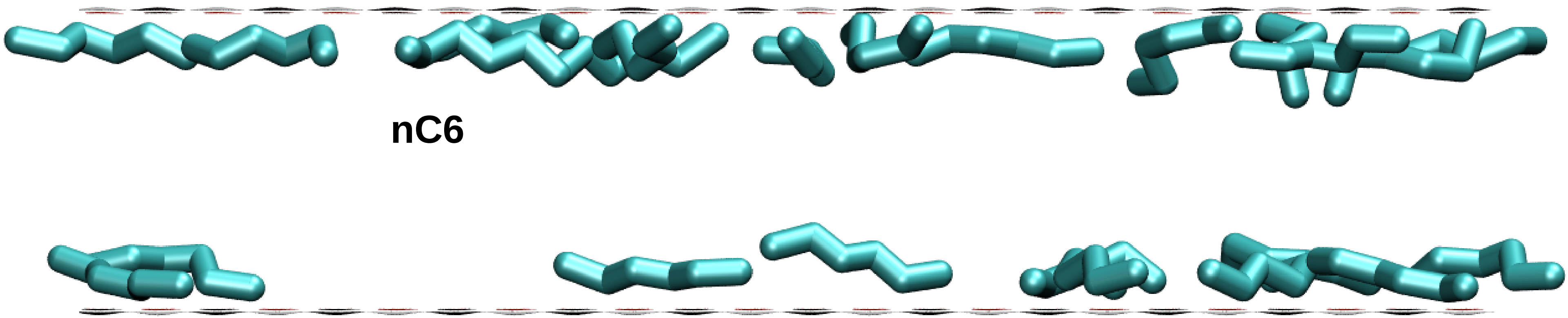

nC6

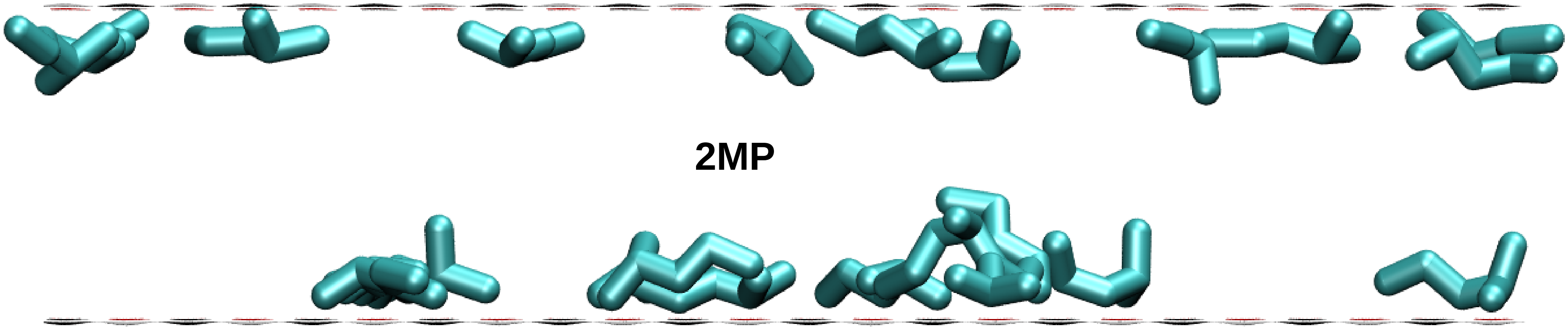

2MP

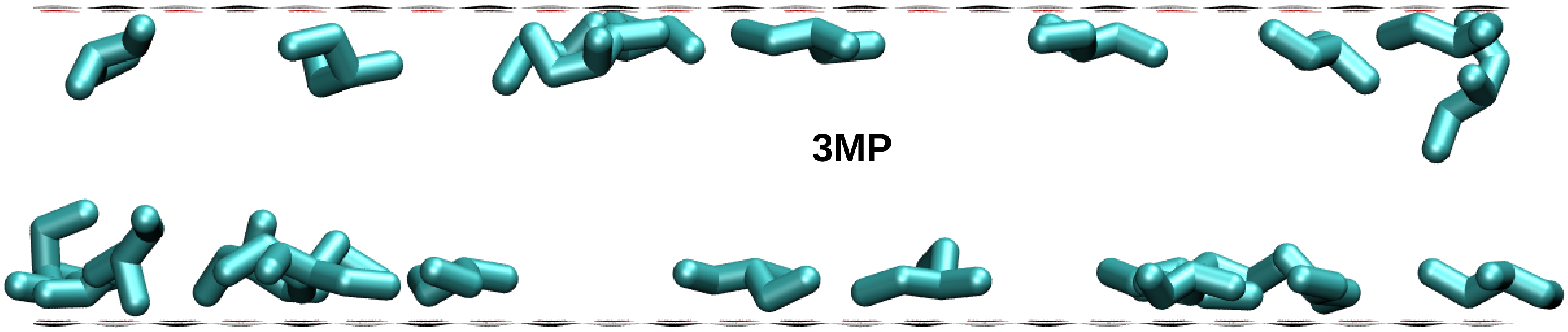

3MP

Slit width = 1.34 nm snapshots of C6 isomers